CRANFIELD UNIVERSITY

MUAMMER ALI AHMED ALSSAYH

Slug Velocity Measurement and Flow Regime Recognition Using Acoustic Emission Technology

SCHOOL OF ENGINEERING

PhD THESIS
Academic Year: 2012 – 2013

Supervisor: Professor David Mba
Co-supervisor: Dr Abdulmajid Addali
July, 2013

CRANFIELD UNIVERSITY

SCHOOL OF ENGINEERING

PhD THESIS

Academic Year: 2012 – 2013

MUAMMER ALI AHMED ALSSAYH

Slug Velocity Measurement and Flow Regime Recognition Using Acoustic Emission Technology

Supervisor: Professor David Mba
Co-supervisor: Dr Abdulmajid Addali
July, 2013

This thesis is submitted in partial fulfilment of the requirements for the degree of Doctor of Philosophy

ABSTRACT

Slug velocity measurement and flow regime recognition using acoustic emission technology are presented. Two non-intrusive and three intrusive methods were employed to detect the slug regime and measure its velocity using AE sensors. For the non-intrusive methods, AE sensors were placed directly on the exterior of the steel pipe section of the test rig with and without clamps. The intrusive method involved using different waveguide configurations with the AE sensors flush with the inner wall of the pipe.

The experimental study presented investigated the application of Acoustic Emission (AE) technology for detecting slug velocity in addition to differentiating flow regime in two-phase (gas/liquid) flow in horizontal pipes. It is concluded that the slug velocity can be determined with acoustic emission (AE) sensors. The results were compared to slug velocities measured using high speed camera (HSC) and Ultrasound Transit Time (UST) techniques with good agreement between the three techniques at low gas void fraction (GVF). However, at high GVF (up to 95%) where the UST technique has limitations in application, the AE and HSC offered a good agreement. Flow regimes were also differentiated by using a combination of AE technology and Kolmogorov–Smirnov test technique. Stratified, slug and bubble regimes were recognised differentiated.

Keywords:

Acoustic Emission, Slug velocity, two phase flow, and flow regimes

ACKNOWLEDGEMENT

My academic goals and my research capabilities could not have been completely realised without contributions from a very wide group of individuals. Too many have made a positive impact in a myriad of ways; some have had a contribution that I would like to mention specifically.

I would like to begin by expressing my deep appreciation to Cranfield University academic staff members responsible for direct oversight of my research. Prof. David Mba who, as my main supervisor, provided me unconditional support, guidance, valuable and continuous advice, thoughtfulness and assistance I needed to successfully complete my research. I would also like to mention my gratitude for Dr. Abdulmajid Addali for the support and wisdom he showed from our first meeting till this day. Dr. Lao Liyun from the Cranfield University Process Systems Engineering team for the technical expertise and training provided to me in operating high speed camera equipment.

My sincere gratitude to the Libyan Government that has availed me the sponsorship to broaden my knowledge in this very challenging albeit interesting field of study.

I would also like to thank Dr. Firoz Khan and Dr. Salem Al-Lababidi. Their experiences and advice was a great benefit to me personally and to my research. For providing me with an environment that allowed me to reach my maximum potential I would like to mention the Cranfield Islamic Society and its continued efforts to provide a central place for all Muslims to complete their religious obligations. I would also like to thank those, whom I have not been able to name that have allowed me to reach this point in my life. I am deeply indebted; words alone can never express my profound appreciation. THANK YOU.

DEDICATION

In the name of Allah, the Most Gracious, the Most Merciful. I dedicate my work to my late parents who encouraged me to achieve the best, to my brothers and sisters and to my wife and children.

TABLE OF CONTENTS

ABSTRACT i
ACKNOWLEDGEMENT ii
DEDICATION iii
LIST OF TABLES xi
LIST OF EQUATIONS xii
LIST OF NOMENCLATURE xiii
Symbol xiii
Denotes xiii
Chapter 1 Introduction 1
1.1 Thesis Aims 2
1.2 Thesis structure 2
1.3 Publications 3
1.3.1 List of journal papers 3
1.3.2 List of conferences 4
Chapter 2 Two-phase flow and flow measurement techniques 6
2.1 Two-phase flow 6
2.1.1 Two-phase flow regimes types 6
2.1.2 Two-phase flow in horizontal pipes 7
2.1.3 Flow regimes in vertical pipes 9
2.2 Multi-phase flow measuring techniques 12
2.2.1 Principles of multiphase measurements 12
2.2.2 Non-invasive techniques 14
2.2.3 Invasive techniques 26
2.3 Chapter conclusion 28
Chapter 3 Acoustic Emission (AE) 29
3.1 Acoustic Emission mechanism 30
3.1.1 Kaiser effect 31
3.1.2 Felicity effect 32
3.2 Acoustic Emission system 32
3.2.1 Acoustic Emission sensors 32
3.2.2 Acoustic Emission preamplifiers 33
3.2.3 Couplants 34
3.2.4 Data acquisition (DAQ) board 35
3.3 Acoustic Emission signals 35
3.3.1 Burst signal: 36
3.3.2 Continuous signal: 37
3.4 Acoustic Emission wave propagation modes 38
3.4.1 Longitudinal, compressional, waves 38
3.4.2 Transverse, shear, waves 38
3.4.3 Surface or Rayleigh wave 39

3.4.4 Plate, Lamb, waves 39
3.5 Wave propagation factors of AE signals 40
3.5.1 Attenuation: 40
3.5.2 Wave velocity: 40
3.6 Dispersion 41
3.7 Acoustic Emission signal parameters 43
3.7.1 Threshold: 43
3.7.2 Arrival Time: 43
3.7.3 Rise time: 43
3.7.4 Amplitude (peak amplitude): 44
3.7.5 Duration: 44
3.7.6 Counts: 44
3.8 Acoustic Emission energy sources 44
3.9 Acoustic Emission: Advantages and disadvantages 45
3.9.1 AE advantages 45
3.9.2 AE disadvantages: 45
3.10 Acoustic Emission in multi-phase flow 45
3.11 Conclusions 54
Chapter 4 Slug flow in horizontal pipes 55
4.1 Slug flow regime 55
4.2 Initiation, growth and dissipation of slug flow 56
4.3 Slug flow types 59
4.3.1 Slug flow benefits 61
4.3.2 Slug flow problems 61
4.4 Slug flow measurements previous work 61
4.5 Flow regime recognition - previous work 67
4.6 Conclusions 73
Chapter 5 Experimental Setup and Methodology 74
5.1 Test rig facilities 74
5.1.1 Water supply system 75
5.1.2 Air supply system 75
5.1.3 50 mm (2 inch) ID closed loop horizontal pipe system 76
5.1.4 Data acquisition system 76
5.1.5 Acoustic Emission (AE) system 76
5.2 Experimental methodology 78
5.2.1 Non-intrusive methods 78
5.2.2 Intrusive method 82
5.3 Comparison of the results with other techniques 89
Chapter 6 Results, observation and discussion 90
6.1 Slug flow velocity 90
6.1.1 Measuring slug velocity using M12 Hexagonal bolts AE waveguide 90

6.1.2 Measuring slug velocity using flush rings as AE waveguides 99
6.1.3 Comparing the measured slug velocity by using M12 and flush-rings waveguides 107
6.1.4 Comparison of Test Results with Results from other Methods 109
6.2 Flow regime recognition 117
6.2.3 120
Chapter 7 Conclusions and recommendations for future work 124
7.1 Conclusions 124
7.1.1 Test-rig design and construction 124
7.1.2 Slug velocity measurement 126
7.1.3 Flow regime recognition 128
7.2 Contribution to knowledge: 129
7.3 Recommendations for future work 130
REFERENCES 131
APPENDICES 143

LIST OF FIGURES

Figure 2-1 Flow regimes for gas/liquid flows in horizontal pipes (Tekna, 2005) . 9

Figure 2-2 Two-phase flow regimes in vertical pipes (Tekna, 2005) 10

Figure 2-3 Inferential method for multiphase flow measurement (Thorn et al., 2013) 13

Figure 2-4 Orifice plate pressure drop recovery (OMEGA, 2001)..... 15

Figure 2-5 Venturi meter (Bertani et al., 2010) 16

Figure 2-6 Pattern of the capacitance probes' electrodes: (a) concave plates, (b) double ring, (c) helical (Ahmed, 2006) 17

Figure 2-7 Common arrangements for electrodes of electrical conductivity probes (a) two full rings, (b) half rings (Ahmed, 2006) 18

Figure 2-8 Wetted sensor arrangement to measure Doppler shift (OMEGA, 2001) 20

Figure 2-9 Clamp-on sensor arrangement to measure Doppler shift..... 21

Figure 2-10 Spool-piece designs (OMEGA, 2001) 21

Figure 2-11 Transit-time Ultrasonic meter (OMEGA, 2001)(OMEGA, 2010)... 22

Figure 2-12 Principle of X- or gamma-rays based flow composition measurement (Tjugum and Mihalca, 2009) 25

Figure 2-13 Single tip optical needle probe (Boyer et al., 2002)..... 27

Figure 2-14 Double tip optical probe (Boyer et al., 2002) 27

Figure 3-1 Kaiser and Felicity Effects..... 31

Figure 3-2 Shape and elements of a regular piezoelectric sensor..... 33

Figure 3-3 Two channel AE data acquisition board (PAC, 2007) 35

Figure 3-4 Principle of Acoustic Emission 36

Figure 3-5 AE burst signal..... 37

Figure 3-6 AE continuous signal..... 37

Figure 3-7 Illustration of longitudinal wave propagation (NDT-ed, 2010)..... 38

Figure 3-8 Illustration of shear wave propagation (NDT-ed, 2010)..... 39

Figure 3-9 Rayleigh wave propagation (NDT-ed, 2010) 39

Figure 3-10 Lamb wave propagation (NDT-ed, 2010) 40

Figure 3-11 Dispersion curves for steel 347 plate (Muravin, 2010) 42

Figure 3-12 Typical Acoustic Emission signal (Hunziker, 2011) 43

Figure 3-13 Experimental set up of water/gas GVF measurement 47

Figure 3-14 AE hit-count map (Yen and Lu, 2002) 49

Figure 4-1 Two Phase Gas/Liquid Slug Profile 55

Figure 4-2 Slug initiation, growth and dissipation (Dukler and and Hubbard, 1975) 57

Figure 4-3 Slug signal captured by conductivity probes (Addali, 2010) 59

Figure 4-4 Schematic of terrain slug (Bratland, 2010) 60

Figure 4-5 Hydrodynamic slug (Bratland, 2010) 60

Figure 4-6 Schematic diagram of the test rig (Andreussi and Bendiksen, 1989) 62

Figure 4-7 Tomographic imaging set up (Reinecke et al., 1998) 64

Figure 4-8 Overall test facility (Al-Safran, 2009) 66

Figure 4-9 . Schematic diagram of gas/liquid two phase flow experimental system (Zhou et al., 2008) 68

Figure 4-10. Schematic diagram of gas/liquid two phase flow experimental system (Kishore et al., 2010) 69

Figure 4-11. Schematic diagram of gas/liquid three phase flow apparatus (Sun et al., 2006) 70

Figure 4-12. Projection geometry of measurement section (Rahiman et al., 2010) 71

Figure 4-13. Schematic view of experimental setup (Ghosh et al., 2012) 72

Figure 5-1 Experimental setup for two-phase slug velocity measurement 74

Figure 5-2 PAC Acoustic Emission System: A- wideband sensor; B- Pico sensor& C- 2/4/6 type preamplifier 77

Figure 5-3 AE system data acquisition system and AE wideband sensors installation on outside surface of steel pipe 78

Figure 5-4 AE wideband sensors clamped to outside surface of steel pipe using clamp type I 79

Figure 5-5 AE wideband sensors clamped to outside surface of steel pipe using clamp type II 79

Figure 5-6 AE waveform for 1.1 V_{SL} and 1.02 V_{SG} sensors placed on the outside of the stainless steel test pipe 80

Figure 5-7AE waveforms at 1.1V_{SL} and 1.02V_{SG} using clamp I stainless steel test pipe 81

Figure 5-8 AE waveforms at 1.1V_{SL} and 1.02V_{SG} using clamp II on stainless steel pipe 82

Figure 5-9 4mm ID Prismatic cylinder waveguide and AE Pico sensor installation..... 83

Figure 5-10 Illustration of the prototype of the contact area between the slug and AE sensors 84

Figure 5-11 AE waveforms at 1.1V_{SL} and 1.02V_{SG} using Prismatic cylinder waveguide 85

Figure 5-12 Waveguides (M12 hexagonal bolts) and AE Pico sensor installation 86

Figure 5-13 AE waveform at 1.1V_{SL} & 1.02V_{SG} using M12 Hexagonal bolts waveguide 86

Figure 5-14 AE Pico sensors on conductivity ring installation 87

Figure 5-15 Schematic of flush mounted circumferential rings acting as AE waveguides..... 88

Figure 5-16 AE waveform at 1.1 V_{SL} and 1.02 V_{SG} using AE Pico sensors on flush circumferential rings 88

Figure 5-17 High Speed Camera (Olympus i-SPEED) 89

Figure 6-1 AE waveform at flow 1.02 V_{SL} and 2.52 V_{SG} using M12 waveguide 91

Figure 6-2 First AE waveform threshold crossing detection for flow of 1.02 V_{SL} and 2.52 V_{SG} using M12 waveguide 92

Figure 6-3 Determination of first threshold crossing for each burst signal for both AE sensors at flow of 1.02 V_{SL} and 2.52 V_{SG} 93

Figure 6-4 Measured slug velocity and mixed flow velocity at 0.7 V_{SL} and 1.02 V_{SG}..... 97

Figure 6-5 Measured slug velocity and mixed flow velocity at 0.7 V_{SL} and 1.52 V_{SG}..... 97

Figure 6-6 Measured slug velocity and mixed flow velocity at 1.52 V_{SL} and 1.52 V_{SG}..... 98

Figure 6-7 Measured slug velocity and mixed flow velocity at 1.52 V_{SL} and 2.52 V_{SG}..... 98

Figure 6-8 AE waveform at flow 1.02 V_{SL} and 2.52 V_{SG} using flush rings as waveguides..... 100

Figure 6-9 First AE waveform threshold crossing detection for flow of 1.02 V_{SL} and 2.52 V_{SG} using flush ring waveguide 101

Figure 6-10 Determination of first threshold crossing for each burst signal for both AE sensors at 1.02 V_{SL} and 2.52 V_{SG} using flush ring waveguide 102

Figure 6-11 Measured slug velocity with mix velocity 0.7 V_{SL} and 1.02 V_{SG} ... 104

Figure 6-12 Measured slug velocity with mix velocity 0.7 V_{SL} and 1.52 V_{SG} ... 106

Figure 6-13 Measured slug velocity with mix velocity 1.52 V_{SL} and 1.52 V_{SG} . 106

Figure 6-14 Measured slug velocity with mix velocity of 1.52 V_{SL} and 2.52 V_{SG} 107

Figure 6-15 test-rig facilities set-up for validation 109

Figure 6-16 Two-phase slug flow images using HSC 110

Figure 6-17 Comparative of slug velocity results at 0.30 V_{SL} 114

Figure 6-18 Comparative of slug velocity results at 0.50 V_{SL} 115

Figure 6-19 Comparative of slug velocity results at 1.03 V_{SL} 116

Figure 6-20 M12 waveguide and AE Pico sensor installation for two phase flow regime recognition 117

Figure 6-21 Original captured AE waveform signals 119

Figure 6-22 KS test CDF of stratified-stratified signals 121

Figure 6-23 KS test CDF of stratified-slug signals 122

Figure 6-24 KS test CDF of stratified-bubble signals 122

Figure 6-25 KS test CDF of slug-bubble signals 123

Figure 7-1Slug signal captured by Acoustic Emission probe 127

Figure 7-2 Two phase flow experimental campaigns map 128

LIST OF TABLES

Table 6-1 Time delay and slug velocity calculation using M12 waveguide at 1.02 V_{SL} and 2.52 V_{SG} 94

Table 6-2 Time delay and slug velocity calculation using M12 waveguide 96

Table 6-3 Time delay and slug velocity calculation using flush ring waveguides at 1.02 V_{SL} and 2.52V_{SG} 103

Table 6-4 Time delay and slug velocity calculation using flush ring waveguides 105

Table 6-5 Measured slug velocity at 0.3 V_{SL} 111

Table 6-6 Measured slug velocity at 0.5 V_{SL} 112

Table 6-7 Measured slug velocity at 0.73 V_{SL} 112

Table 6-8 Measured slug velocity at 0.93 V_{SL} 113

Table 6-9 Measured slug velocity at 1.03V_{SL} 113

Table 6-10 KS test distance and p-value for flow regime recognition 120

LIST OF EQUATIONS

2-1 11
2-2 11
2-3 11
2-4 11
2-5 12
2-6 12
2-7 13
2-8 13
2-9 15
2-10 15
2-11 15
2-12 19
2-13 20
2-14 20
2-15 22
6-1 92
6-2 108
6-3 108
6-4 120

LIST OF NOMENCLATURE

Symbol	Denotes
A	cross-sectional area
AE	Acoustic Emission
α_g	volume fraction of gas
α_o	volume fraction of oil
α_w	volume fraction of water
C_t	velocity of sound inside the medium
DAS	Data Acquisition System
d_T	time differential between upstream and downstream transit time
ECT	Electrical Capacitance Tomography
EIT	Electrical impedance Tomography
EL	Total volumetric flow rate
ET	Electrical Tomography
f_0	transmission frequency
f_1	reflected frequency
GVF	gas void fraction
h	pressure difference
HSC	High Speed Camera
K_o	discharge coefficient of the orifice
K	calibration factor for the volume and time units
L	distance between two AE sensors
M	mass flow rate
NDT	Non-destructive test
PAC	Physical Acoustics Corporation

Sv	Slug velocity
T1	upstream transducer
T2	downstream transducer
TL	zero flow transit time
USTT	Ultrasound Transit Time Technique
v	flow velocity
V_m	Mixture flow velocity
v_g	Volumetric flow of gas
v_o	Volumetric flow of oil
VSG	superficial gas velocity
VSL	superficial liquid velocity
v_w	Volumetric flow of water
Δt	time delay between two AE sensors
μ	mean of slug velocity
ρ	density
ρ_g	Gas density
ρ_o	Oil density
ρ_w	water density
σ	Standard deviation of slug velocity

Chapter 1 **Introduction**

Multiphase flow is the simultaneous flow of two or more materials in different states, phases or chemical properties such as gas/water; water/oil, gas/water/oil, gas/water/sand, etc. The importance of multiphase flow arises because many industrial processes depend on this phenomenon for material transport and processing. Gas and oil transportation, power generation, nuclear technology and chemical reactors are examples of industrial applications that depend on multiphase flow.

The hydrodynamics of multiphase flow is substantially different from single phase flow because of the effect of the secondary flow upon the main flow dynamics, i.e. the flow conditions in the system (the flow regime) may vary significantly based on the relative amounts of each phase present in the flow. In gas/liquid pipeline flow for example, the flow can be classified into different regimes such as stratified, slug, bubble, and annular (Section 2.1.1) depending on flow speed and relative proportions of gas and liquid. Different flow regimes induce different performances of the system. Optimum system performance is where the conduit is full of liquid phase. However, system performance decreases as the gas phase increases, as becomes obvious with the appearance of slug, bubble and annular regimes. The prediction of flow regime transitions is difficult due to the highly non-linear nature of the forces that govern the flow and there is no universal method that can predict the flow regimes under different circumstances. Thus, investigating and studying this phenomenon is necessary to find a technique that can confidently recognise the different regimes.

The most important regime that can cause significant problems, especially in the oil and gas industry, and needs to be controlled, is slug flow. It can create high pressure fluctuations which might damage instruments, uneven flow arriving at the processing facilities can cause flooding, repeated hammering that occurs with slug flow causes fatigue and there is an increase in deposits of hydrates and corrosion because of the density and heat capacity differences

between gas and liquid. Thus the investigation of this phenomenon is important to avoid such problems.

Many commercially available techniques are used to detect and measure the slug characteristics in two phase flow including ultrasonic methods, conductivity probes, and high speed cameras. However, such techniques have limitations. The accuracy of conductivity rings and ultrasonic techniques, for example, decreases as the gas void fraction (GVF - the ratio of the volumetric flow rate of the gas to the total volumetric flow-rate) in the pipe increases. Also, conductivity rings are affected by temperature, i.e., when the temperature increases, the accuracy of conductivity measurements decreases. Thus, there is a need to investigate another technology that overcomes such limitations and measures the slug flow velocity in two phase flow in horizontal pipes. The use of Acoustic Emission technology was investigated in this research.

1.1 Thesis Aims

The main aim of this study is investigation of slug velocity measurements and flow regimes recognition using Acoustic Emission Technology. Its specific objectives include:

- Developing a methodology for applying AE technology to investigate two phase flow parameters in horizontal pipes
- Detecting slug flow regime in two phase flow horizontal pipes
- Measuring slug velocity by using acoustic emission technology
- Recognizing two phase flow regimes by using acoustic emission technology.

1.2 Thesis structure

Chapter II presents an overview of two phase flow: definition and types of two phase flow, two phase flow regimes in horizontal and vertical pipes and two phase flow parameters that will be used in this study. This chapter also presents a brief description of multi-phase flow measurement techniques that are commercially available. It presents the principle of each of these techniques with advantage and disadvantages.

Chapter III discusses acoustic emission (AE) technology. It starts with a brief history of AE followed by describing generation mechanisms and sources, AE technology and system; AE signal types, AE wave propagation, dispersion of phase velocity and group velocity, AE signal parameters and the advantages and disadvantages of using AE techniques. This chapter ends by reviewing previous applications of AE to multi-phase flow.

Chapter IV describes slug flow in two phase flow in horizontal pipes. Initiation, growth and decay of the slug are presented based on previous investigations. It also presents the benefits and drawbacks of the slug regime. This chapter concludes by presenting previous work measuring slug flow parameters, and flow regime recognition in two phase flows.

Chapter V presents the test-rig which was used in this research and describes the research methodology. It describes each part of the experimental facilities such as the water and air supply systems, AE transducers and data acquisition system. This chapter concludes by presenting the research methodology and the design of the test-rig for slug flow detection, slug velocity measurement and flow regime recognition in two phase flows in horizontal pipes.

Chapter VI reports the observations and results of this study. The M12 and flush ring AE waveguides successfully used to detect and measure the slug flow are discussed in detail. These results were validated using ultrasonic transit times and a high speed camera. This chapter concludes by discussing two phase flow regime recognition using AE methods and the Kolmogorov–Smirnov test.

Chapter VII briefly presents the main findings and conclusions of this study and suggests possible relevant future research.

1.3 Publications

1.3.1 List of journal papers

- El-Alej, M., Mba, D., Yan, T.; and Alssayh, M.; Identification of minimum transport condition for sand in two-phase flow using acoustic emission

technology, Applied Acoustics Journal, (Accepted for publication on May, 2013).

- Alssayh, M.; Addali, A., and Mba, D.; Acoustic Emission Measurements for High Speed Two-phase Slug Velocity in Production Pipelines, Flow Measurement and Instrumentation, (Submitted on February, 2013).
- Alssayh, M.; Addali, A., Mba, D.; and El-Alej, M.; Slug Velocity Measurement Using Acoustic Emission Technology, Journal of Mechanical Process Engineering, Part E (IMechE), (Submitted on April, 2013).

1.3.2 List of conferences

- Alssayh, M.; Addali, A., and Mba, D.; (2012). Acoustic Emission Applied to Slug Velocity Determination in Two Phase Flow.15th International Conference on Applied Mechanics and Mechanical Engineering (Amme-15),Egypt, 28-30 May 2012
- Eftekharnejad, B.; Alssayh, M.; Addali, A.; and Mba, D.; (2012). Spectral Kurtosis Applied to Acoustic Emission in Bearings. 25th International Congress on Condition Monitoring and Diagnostic Engineering (COMADEM 2012), UK, 19-21 June 2012.
- Alssayh, M.; Addali, A., and Mba, D.; (2012). Determining slug velocity in two phase flow with Acoustic Emission. 51st Annual Conference of the British Institute for Non-Destructive Testing (NDT 2012), UK, 11-13 September 2012.
- Alssayh, M.; Addali, A., and Mba, D.; (2012). Investigating the Capability of Acoustic Emission Technology to Determine Slug Velocity in Gas/ Water Two phase Flow in Horizontal Pipes. The International Conference on Mechanical & Manufacturing Engineering (ICME2012), Malaysia, 20-21 November 2012.
- Alssayh, M.; Addali, A., Mba, D.; and Naid, A., (2013). Detecting and Measuring Slug Velocity in Two-Phase Flows Horizontal Pipes. 1st Euro-Mediterranean Conference on Structural Dynamics and Vibroacoustics (MEDYNA 2013), Morocco, 23-25 April 2013.

- Alssayh, M.; Addali, A., and Mba, D.; (2013). Two Phase Flow Regimes Recognition by using Acoustic Emission Technology, World Academy of Science Engineering and Technology (WASET), Turkey, 20-21 June 2013.

Chapter 2 Two-phase flow and flow measurement techniques

2.1 Two-phase flow

Two phase flow is a common occurrence in industry. It covers a wide range of flow phenomena combining gases, liquids and solids. Gas/liquid flow can be found in oil and gas transportation, air-conditioning systems, power and process industries. Liquid/solid is commonly found in food processing and slurry transportation. Liquid/liquid flow is encountered in chemical reactors and the petroleum industry.

The behaviour of two phase flow is much more complex than that of single phase flow. Different densities, viscosities and speeds of each phase highly affect two phase flow. In addition to the effects of the physical parameters of the individual components in two phase flow, the geometry and diameter of the flow line and its orientation are very important factors that affect the flow behaviour. For example, if the proportions and properties of liquid and gas in a two phase flow are kept constant but flow line size or orientation is changed, the superficial gas and liquid velocities will change, as will the flow patterns in the line (Tekna, 2005).

2.1.1 Two-phase flow regimes types

Different types of flow regimes can be produced for gas/liquid mixture flows along a pipe, according to such variables as fluid properties, the relative rates of flow and the pipe geometry and orientation (horizontal or vertical). There are common regimes that appear in two phase flows such as Stratified flow, where liquid and gas phases are separated and flow along the bottom and upper portions of the pipe respectively; Bubble flow, innumerable bubbles of gas of small size are present within the liquid; Slug flow, where a large gas mass is formed from the merged individual gas bubbles; and Annular flow, where the gas phase flows in the core of the pipe while the liquid phase occupies the space adjacent to the pipe wall. Generally, flow regimes can be grouped into

dispersed flow, separated flow, intermittent flow or combination of these (Tekna, 2005; Christopher, 2005).

2.1.1.1 **Dispersed flow** is characterized by a uniform phase distribution both radially and axially. It can be further divided into bubble flow and mist flow depending on the relative proportions of gas and liquid.

2.1.1.2 **Separated flow** is characterized by a continuous phase distribution in the axial direction and a non-continuous phase distribution in the radial direction. This flow includes both stratified and annular flows.

2.1.1.3 **Intermittent flow** is represented by being non- continuous in the axial direction. Churn and slug flows are grouped under this type of flow (Tekna, 2005)

2.1.2 Two-phase flow in horizontal pipes

There are large differences in flow behaviour between horizontal and vertical or inclined pipes flow because gravitational forces causes the less dense gas phase to rise (buoyancy). In horizontal pipes, the gas phase tends to occupy the upper part of the pipe.

The gas changes from dispersed phase to continuous phase as the gas-to-liquid ratio increases. The transition between the flow regimes is gradual. In general, seven flow regimes for fully-developed horizontal pipe flow have been identified as shown in Figure 2-1. In order of decreasing ratio of liquid to gas flow rate they are (Mark et al., 2009):

2.1.2.1 **Bubbly flow:** the gas is scattered in the liquid as bubbles which move at a velocity similar to the liquid. This flow regime occurs at high ratios of liquid to gas flow rates, but note that because of gravitational forces the bubbles will tend to concentrate near the top of the pipe. The separation is greater at lower liquid velocities and the distribution of bubbles becomes more homogeneous at higher liquid velocities, due to increased turbulence in the flow.

2.1.2.2 **Annular flow:** gas flows in the core with some entrained droplets of liquid while liquid flows as a film along the pipe walls.

2.1.2.3 **Slug flow:** liquid waves touch the top of the surface of the pipe, forming frothy slugs which move at a velocity much greater than the liquid average velocity. (See Chapter 5)

2.1.2.4 **Spray, dispersed or mist flow:** is similar to annular flow except nearly all the liquid phase is entrained as small droplets.

2.1.2.5 **Elongated bubble flow:** alternate plugs of liquid and gas move along the upper part of the pipe.

2.1.2.6 **Wavy flow:** is similar to stratified flow but waves moving in the flow direction are formed at the gas–liquid interface because of higher relative velocities between the phases.

2.1.2.7 **Stratified flow:** has a smooth interface, the liquid and gas flow along the bottom and top of the pipe respectively.

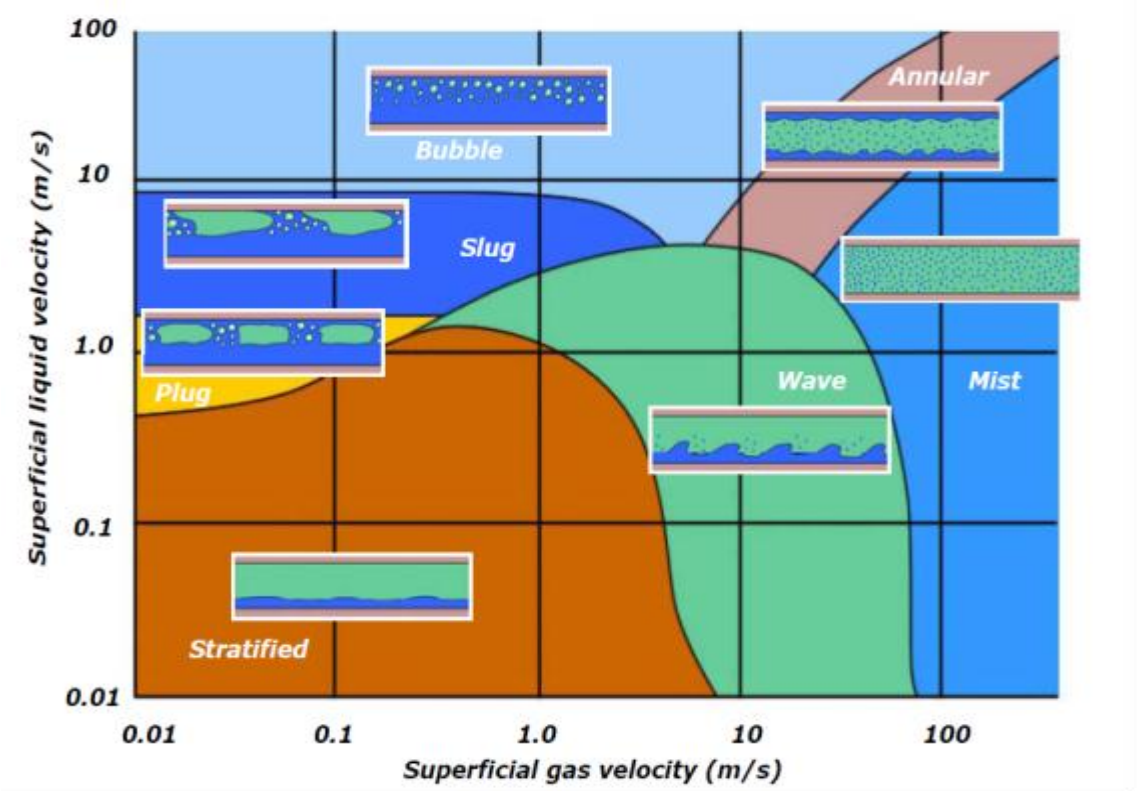

Figure 2-1 Flow regimes for gas/liquid flows in horizontal pipes (Tekna, 2005)

2.1.3 Flow regimes in vertical pipes

In vertical pipe, multi-phase flow has bubble, slug, churn and annular flows determined primarily by the superficial liquid and gas velocities, see Figure 2-2. Because the pipes are vertical there are no stratified or wavy flows.

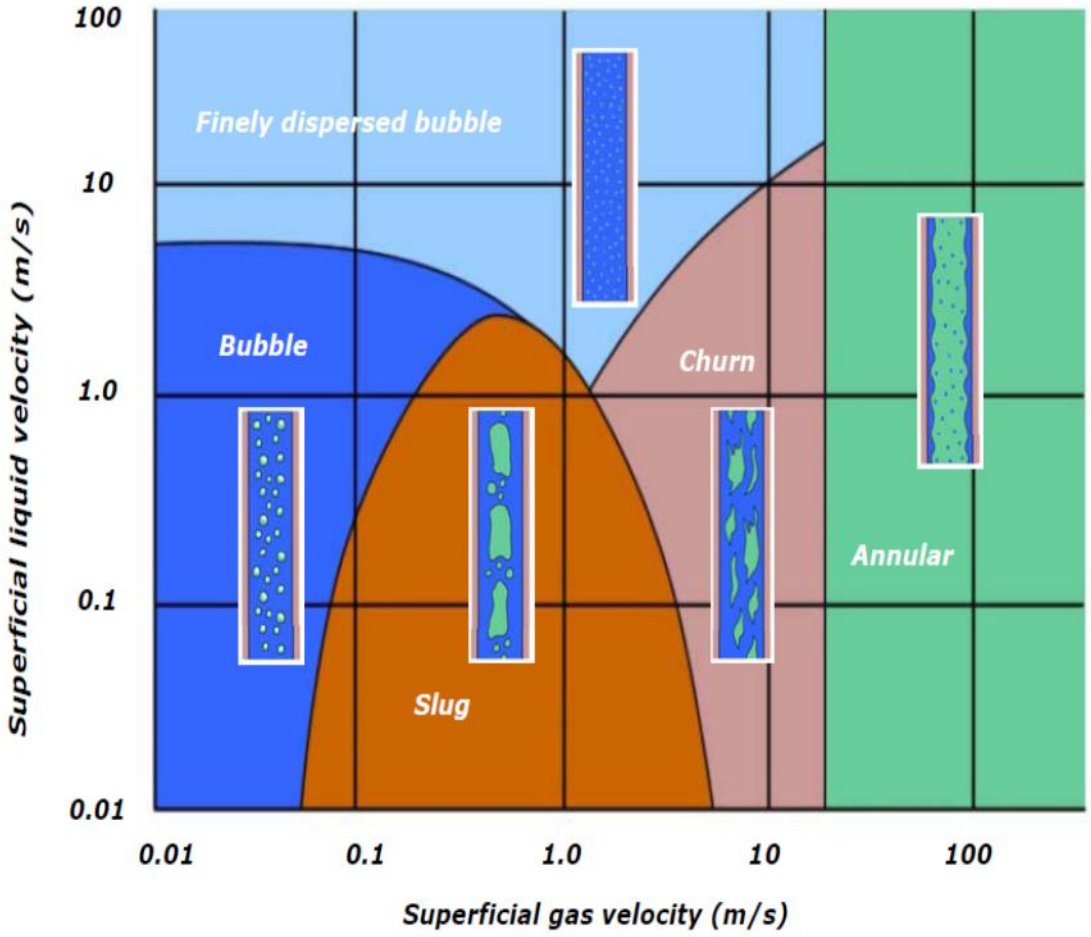

Figure 2-2 Two-phase flow regimes in vertical pipes (Tekna, 2005)

Because of difference in densities the gas phase tends to rise through the continuous liquid as discrete bubbles (bubbly flow) at low gas flow rates. The bubbles begin to combine and form larger bubbles as the gas flow rate increases. These bubbles tend to grow until they become large enough to occupy almost the entire pipe cross section. At sufficiently high gas flow rates the bubbles become large enough (Taylor bubbles) to separate the liquid between them into slugs. Smaller entrained gas bubbles can be carried in these liquid slugs. As the flow rates increase the shear stress between the Taylor bubble and the liquid film increases. This eventually causes a breakdown of the liquid film and a churning motion of the fluid results. At extremely high gas flow rates annular flow occurs, here the entire gas phase flows in the central portion

of the pipe. Some liquid is entrained into the gas flow as droplets, while the rest of the liquid flows along the wall.

2.1.3.1 Two-phase Flow Parameters

Important parameters used to describe two-phase flow are (Clayton, 2005):

Superficial Phase Velocity (V_{st}):

The term superficial phase velocity describes the phase velocity computed from the mass flow rate of each individual phase in the pipe. It assumes the phase fills the entire cross-sectional area and neglects the existence of any other phase in the flow. Thus the definition of superficial velocity, gas or liquid, is the individual volumetric flow rate (v) divided by the cross-sectional area of the pipe (A)

Superficial liquid velocity:

$$V_{SL} = {}^{v_L}/_{A} \qquad 2\text{-}1$$

Superficial gas velocity:

$$V_{SG} = {}^{v_G}/_{A} \qquad 2\text{-}2$$

The algebraic sum of the gas and liquid superficial velocities determines the mixture velocity (V_M) as:

$$V_M = V_{SL} + V_{SG} \qquad 2\text{-}3$$

Gas Volume Fraction (GVF):

The GVF is the ratio of the volumetric flow of gas to the total volumetric flow-rate:

$$GVF = {}^{v_G}/_{(v_L + v_G)} = {}^{V_{SG}}/_{(V_{SG} + V_{SL})} \qquad 2\text{-}4$$

Liquid Hold-up ($\mathbf{E_L}$)

Hold-up is ratio of volumetric flow of liquid to the total volumetric flow-rate:

$$E_L = \frac{v_L}{(v_L + v_G)} \qquad 2\text{-}5$$

Thus

$$GVF + E_L = 1 \qquad 2\text{-}6$$

2.2 Multi-phase flow measuring techniques

2.2.1 Principles of multiphase measurements

In the oil and gas industry, the fundamental purpose of multi-phase measurement techniques is to provide the user with the information needed concerning the mass flow rates of gas, oil and water individually and in combinations. However, to date, there is no measurement technique that gives direct measurement on the mass flow rates of multi-phase flows. However, by simultaneously measuring velocity and the cross-section fraction of each phase, it is possible to calculate the mass flow rates of the individual component and, hence, derive the total mixture mass flow rate (M). This method is termed “inferential” because M is inferred from other measurements (Addali, 2010; Thorn et al., 2013).

Measured multi-phase flow variables can be categorized into primary variables such as phase fraction, velocity and density; and secondary variables which include phase viscosity, phase salinity and flow regime. The measurement or evaluation of primary variables is necessary to successfully apply the multi-phase flow inferential method. Taking into consideration secondary variables provides more accurate measurement. However, if a sensing technique which depends on the flow regime is used to determine the core primary variables, then the flow regime will be a primary variable and has to be evaluated. Figure

2.3 illustrates the principles of the inferential method of multi-phase flow measurement (Thorn et al., 2013)

Information on the density of oil, gas and water ($\rho_o, \rho_g, \rho_w\, respectively$) is readily available from production instrumentation such as densitometers. The other parameters required are the velocities of the gas, water and oil phases ($v_o, v_w, v_g\, respectively$) and volume fractions of gas (α_g) and water (α_w). The oil volume fraction (α_o) can be derived from equation (2-7) and mass flow rate (M) can be deduced from equation (2-8). More details can be found in (Thorn et al., 2013; Thorn et al., 1999).

$$\alpha_o = 1 - (\alpha_w + \alpha_g) \qquad 2\text{-}7$$

$$M = \alpha_g v_g \rho_g + \alpha_w v_w \rho_w + \alpha_o v_g [1 - (\alpha_g + \alpha_w)] \qquad 2\text{-}8$$

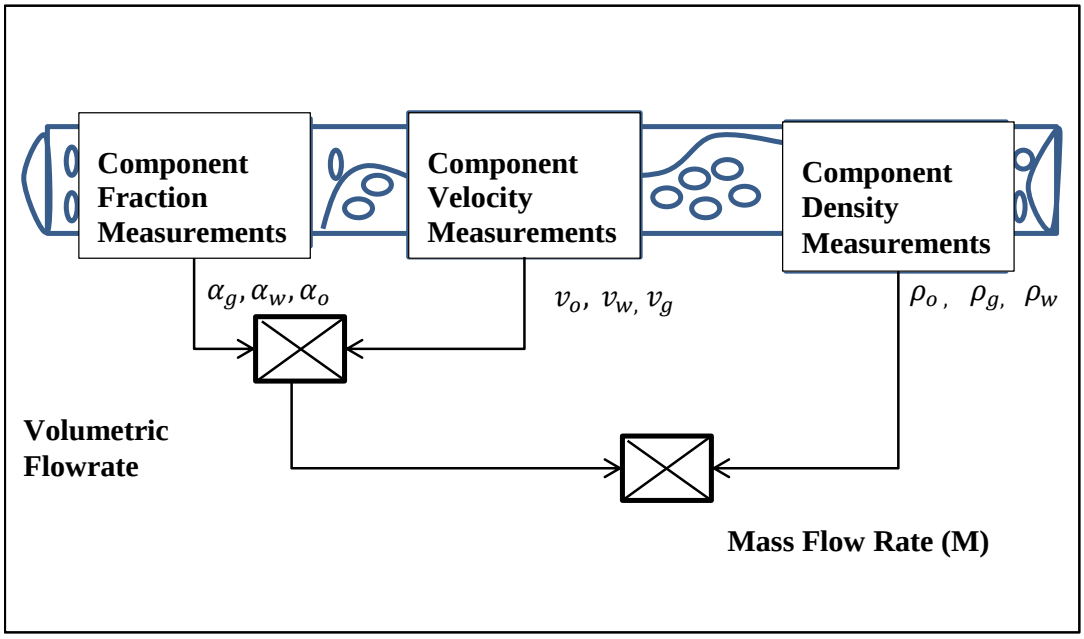

Figure 2-3 Inferential method for multiphase flow measurement (Thorn et al., 2013)

Multi-phase flow measurement utilizes a large number of techniques and technologies to measure volume fraction and velocities of components. These techniques can be classified in different ways. For example, they can be grouped as invasive and non-invasive; or intrusive and nonintrusive, or can be

classified on the basis of the multiphase flow parameter that will be measured or monitored such as phase fraction, velocity or density. In this chapter the classification used is invasive and non-invasive technologies.

2.2.2 Non-invasive techniques

Non-invasive meters are those that can be used to measure multi-phase flow without affecting or disrupting the flow in the conduit. These techniques can be used to determine gas and liquid velocities, bubbles and particle sizes and position, flow regimes patterns, pressure drop, gas void fractions, liquid hold-up etc. The following are some of the commercially available non-invasive techniques.

2.2.2.1 Time- averaged pressure drop

An important variable is the pressure drop between two points in the flow. The main use of pressure drop measurements is to determine flow velocity, gas void fraction and liquid and/or solid holdup (Vallen, 2002). It is also used to identify hydrodynamics and flow regime transitions in multiphase flow (Bendjaballah et al., 1999; Vial et al., 2001).

The best known meters used to measure pressure drop in many two phase flow investigations are orifice and venturi meters. These techniques are utilised to measure mixture flow rate and flow velocity when the multiphase flow is sufficiently mixed. Details of the technical designs of these instruments are given in ISO 5167:2003 (Measurement of fluid flow by means of pressure differential devices inserted in circular-cross section conduits running full).

Orifice meter

The principle of the orifices technique is that the pressure drop increases linearly with the fluid density and the square of the flow velocity. There are a wide variety of orifice plate configurations each with specific application. Figure 2-4 presents orifice plate pressure drop recovery. To calculate the flow velocity (V), for example, a flat plate with a suitable orifice is inserted into the pipe perpendicular to the flow stream. This will cause an increase in velocity and

decrease in pressure as the flow passes the orifice. The pressure difference (h) before and after the plate is used to calculate the flow velocity as in equation (2-9). To calculate the volumetric flow (Q) and the mass flow (M), equation (2-10) and (2-11) are used.

$$V = K(^{h}/_{\rho})^{0.5} \qquad 2\text{-}9$$

$$Q = KA(^{h}/_{\rho})^{0.5} \qquad 2\text{-}10$$

$$M = K_o A(h\rho)^{0.5} \qquad 2\text{-}11$$

Where K_o is the discharge coefficient of the orifice; A is the cross-sectional area of the orifice and ρ is the density of the flow.

Orifices plates are available for all pipe sizes and can be made from different materials based on the diameter of the pipe, the temperature, the material flowing and the differential pressure. Orifices plates are commonly used in clean gas/liquid flow but their flow resistance is a draw-back (Bertani et al., 2010; OMEGA, 2001).

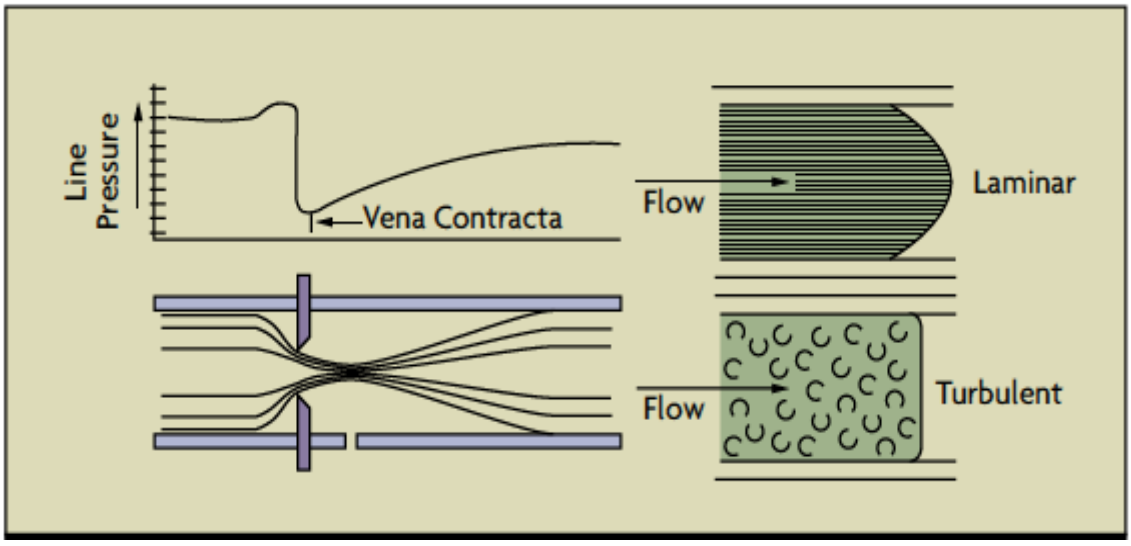

Figure 2-4 Orifice plate pressure drop recovery (OMEGA, 2001)

Venturi meters

Venturi meters are tubular with a relatively long and smooth entry and exit passages as shown in Figure 2-5. It is connected to the existing pipe with the initial and final diameters matching the original pipe diameter. An increased flow velocity produces a decrease in fluid pressure at the downstream pressure tapping as result of change of the flow area of the meter. The small angle of the downstream cone minimizes frictional losses and so aids pressure recovery. Venture meters are currently available with inlet diameter up to nearly 2 metres (72 inches) and pass 25- 50 % more flow than an orifice meter for the same pressure drop. An advantage of the venture meter is that it requires a shorter straight pipe run than do orifices because of its insensitivity to velocity profile effects.

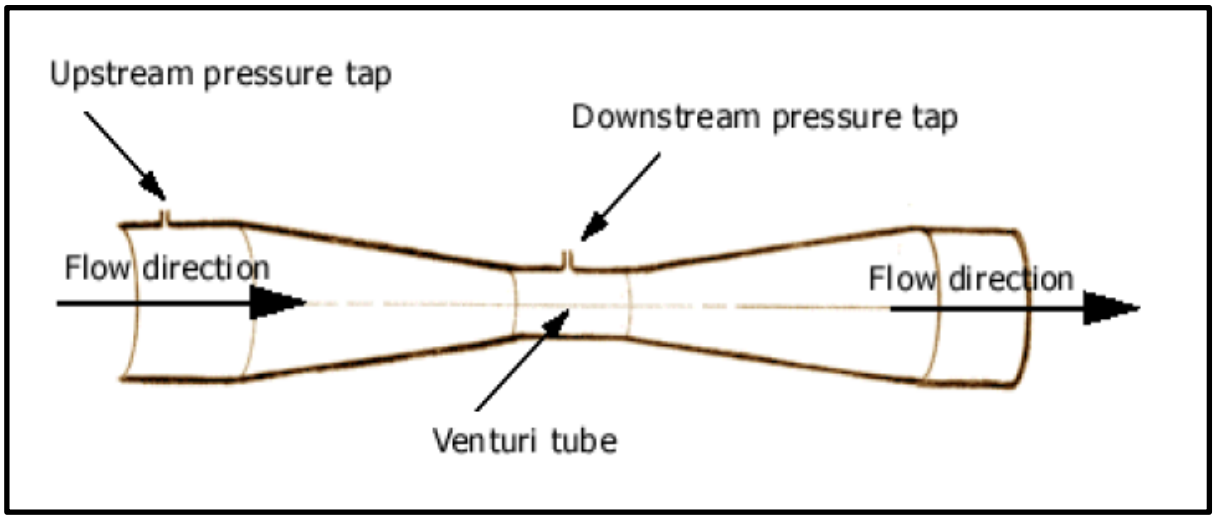

Figure 2-5 Venturi meter (Bertani et al., 2010)

Venturi meters are also resistant to erosion and corrosion and internal scale build up, the pressure flow loss is very low and less affected by up-stream flow distortion. The Venturi meter has a low maintenance cost but its construction and installation are expensive. Other disadvantages are it occupies considerable space and is limited to clean, non-corrosive liquids and gases (OMEGA, 2001).

2.2.2.2 Electric impedance technique

The principle of the impedance technique is the different electrical conductivities and relative permittivity of gases and liquids. This technique is low cost and relatively easy to construct compared to other techniques (Storck et al., 1986). Electrodes are mounted around the circumference of the pipe and the impedance between various pairs of electrodes is measured which allows the void fraction to be found. According to the type of device used and liquid material to be examined, the impedance technique can be divided into electrical conductivity and capacitance.

Capacitance probes can be applied to investigate two phase flow problems if the liquid is nonconductive, e.g. oil. These probes can be a non-intrusive way to measure void fraction and do not need contact between electrodes and fluid (Stott et al., 1985). Assembling the capacitance electrodes can be achieved in different ways. Concave plate, ring and helical sensors, see Figure 2-6, are the most common arrangements of capacitance based measurement systems (Ahmed, 2006).

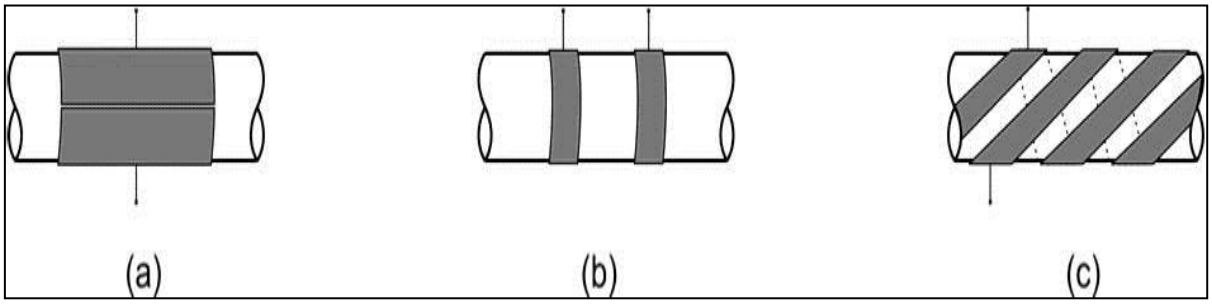

Figure 2-6 Pattern of the capacitance probes' electrodes: (a) concave plates, (b) double ring, (c) helical (Ahmed, 2006)

Electrical conductivity probes have almost the same procedure as the capacitance probes except it has to be in contact with the conducting fluid. The common arrangements of these electrodes are achieved by using two metallic rings (Ma et al., 1991) or a pair of measuring half-rings facing one another (Costigan and Whalley, 1997) in the inner wall of the pipe as shown in Figure 2-7.

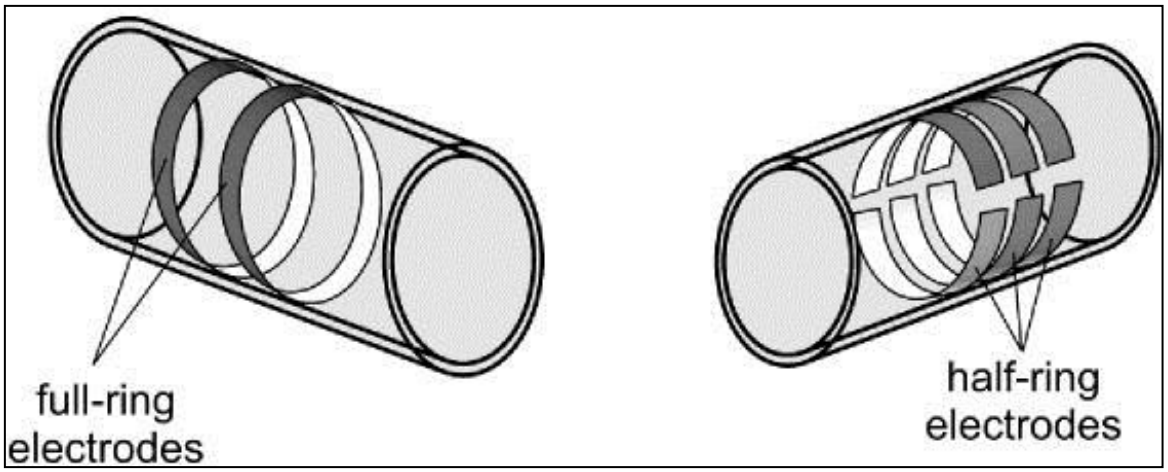

Figure 2-7 Common arrangements for electrodes of electrical conductivity probes (a) two full rings, (b) half rings (Ahmed, 2006)

The impedance technique is cheaper, relatively easy to install and provides a high frequency response, but it has several disadvantages that are occasionally hard to resolve. For example, it is sensitive to void fraction distribution due to the non-uniformity of the electrical field inside the measuring volume, to temperature effects on the electrical properties of the two phase flow and to the noise of electromagnetic fields around the sensor which affect the signal. However, most of these disadvantages can be resolved through better design of the sensors (Ahmed, 2006).

2.2.2.3 Ultrasound Techniques

Whereas electromagnetic flow meters require a minimum electric conductivity of the liquid for operation, ultrasonic flow meters can be applied in nearly any kind of flowing liquid. In addition, cost of electromagnetic flow meters increases drastically with pipe diameter while the price of ultrasonic flow meters is nearly independent of pipe diameter (Ahmed, 2006).

Ultrasound is the sound with a frequency between 20 KHz to about 1 GHz, above the frequency range of the human ear (Hauptmann et al., 2002). Several ultrasonic flow measurement techniques are commercially available today and are commonly used to measure the necessary velocity of both single phase and multi-phase flows for liquids that allow ultrasonic waves to pass. Water, molten sulphur, and cryogenic liquids are examples of such liquids. However, care

must be taken because fluids that rapidly attenuate the ultrasonic signal include many types of slurry (FlowMeters, 2010). Ultrasonic techniques are often divided, in general, into two categories: Doppler flow meters and transit-time flow meters.

Doppler flow meters

Doppler flow meters are named after Christian Johann Doppler (1803–1853), the Austrian physicist and mathematician. He predicted in 1842 that the frequencies of received sound waves depended on the relative motion of source, observer and propagating medium (OMEGA, 2001). Doppler observed and explained why the frequency of a source of sound perceived by a stationary observer increases when the source is approaching the observer and decreases when the source was moving away (OMEGA, 2001; Sanderson and Yeung, 2002).

Doppler flow meter transducers commonly operate at 0.640 MHz in clamp-on designs while wetted sensors tend to be designed to work at 1.200 MHz (OMEGA, 2001). Doppler flow meters detect the velocity of the discontinuities, rather than the velocity of the fluid thus a minimum amount of sonically reflective materials such as entrained air bubbles or solid particles must be contained in the liquid flowing through the pipe. These materials reflect the signals that are emitted by the transmitter to the receiver and allow the flow velocity to be calculated.

To calculate the flow rate, the flow velocity (V) can be determined by (OMEGA, 2001):

$$V = {(f_0 - f_1)\, C_t}\Big/{2f_0 \cos a} \qquad \text{2-12}$$

Where: C_t is the velocity of sound inside the medium.

f_0 is the transmission frequency.

f_1 is the reflected frequency.

a is the angle of the transmitter and receiver crystals with respect to the pipe axis as shown in figure 2-8.

If $K = {C_t}/{(2f_0 \cos a)}$, the relationship can be simplified to:

$$V = (f_o - f_1)K \qquad 2\text{-}13$$

Flow velocity V is directly proportional to the change in frequency.

The flow rate Q is usually measured in the industry in US gallons per minute GPM (3.785 x 10^{-3} m^3/min) for a pipe of inside diameter (ID) the flow rate is given by:

$$Q = 2.45[(f_o - f_1)K](ID)^2 \quad GPM$$
$$= \quad 9.27\ x\ 10^{-3}\ [(f_o - f_1)K](ID)^2 \quad m^3/min \qquad 2\text{-}14$$

Doppler flow meters are typically used to measure raw sewage, sludge, slurries, tar, sands, and oil-water-gas mixtures (Sanderson and Yeung, 2002).

Figures 2- 80 and 2- 9 illustrate the layouts of wetted sensors, Doppler shift and clamp-on designs respectively.

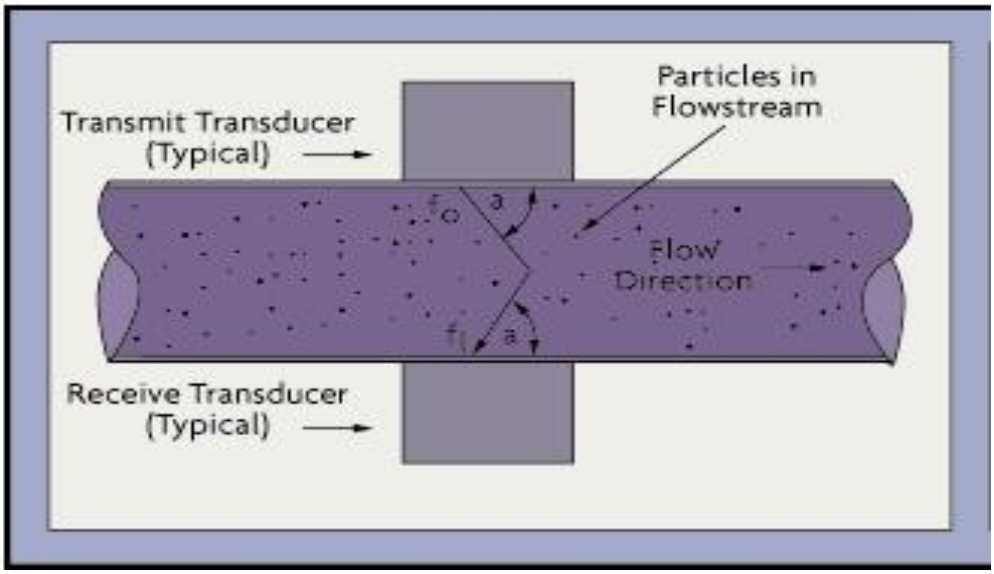

Figure 2-8 Wetted sensor arrangement to measure Doppler shift (OMEGA, 2001)

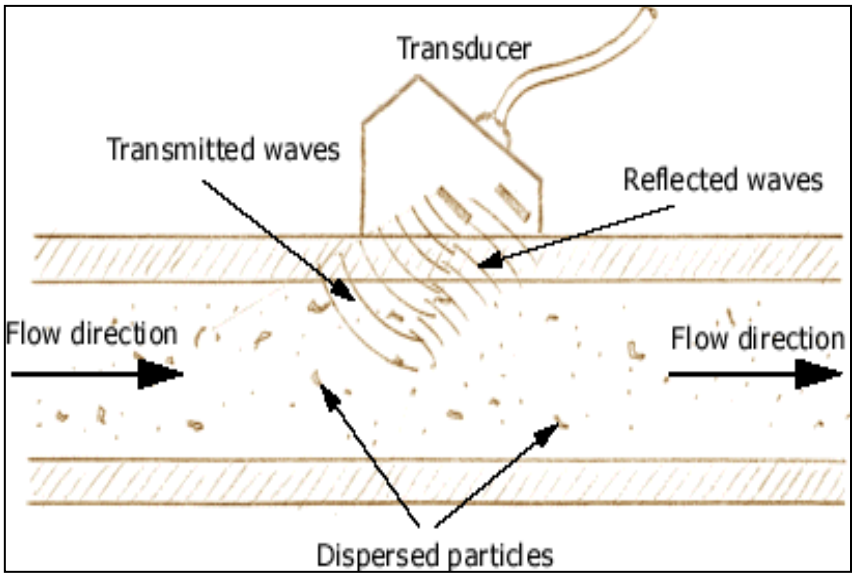

Figure 2-9 Clamp-on sensor arrangement to measure Doppler shift

Transit-time flow meters

This is one of the most commonly used ultrasonic flow metering techniques. Transit Time method is available as a spool piece meter for liquids and gases or as clamp-on design as shown in figures 2-10 and 2-11 respectively.

In this method, the small transit time required for a particle to move a known distance is measured using two ultrasonic pulses one upstream, T1, and the other downstream, T2, as shown in Figure 2-11.

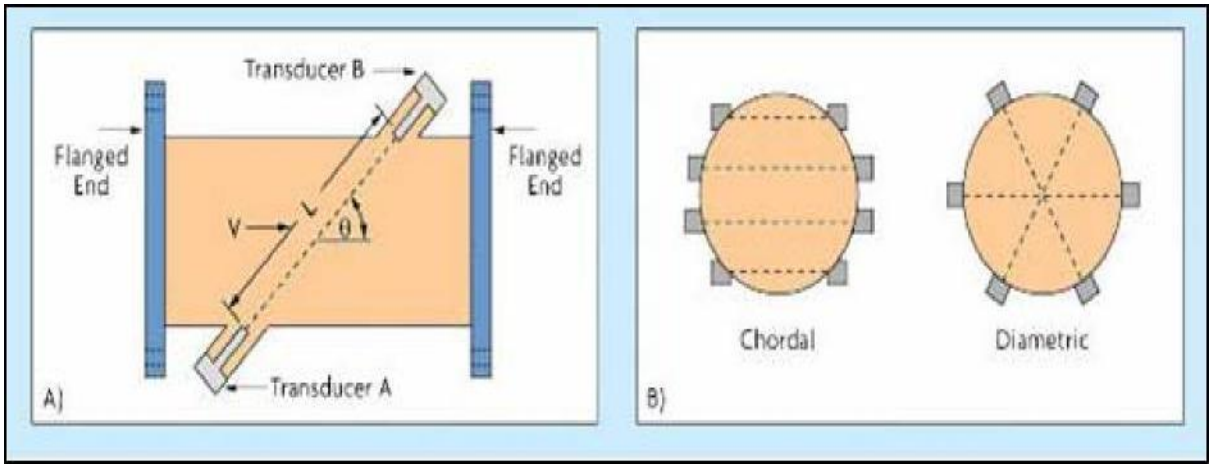

Figure 2-10 Spool-piece designs (OMEGA, 2001)

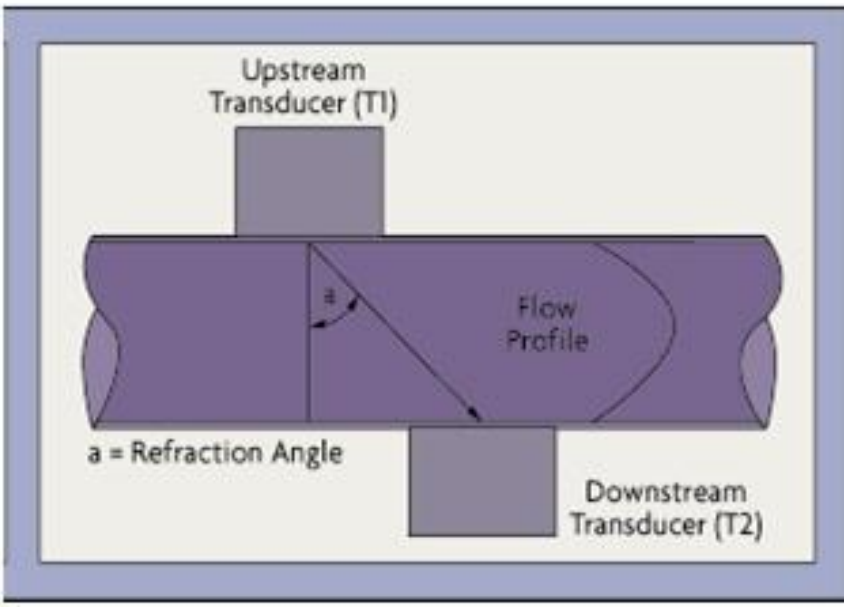

Figure 2-11 Transit-time Ultrasonic meter (OMEGA, 2010)

Provided there is no transverse flow in the pipeline, the signal time transfer from T1 to T2 and vice versa depends only on the longitudinal flow. However, a longitudinal flow increases the signal speed in the downstream direction, while decreasing it in the upstream direction. Equation 2-15 calculates the flow velocity.

$$V = K\left({}^{d_T}/_{T_L}\right) \qquad 2\text{-}15$$

Where (OMEGA, 2001);

V is the flow velocity.

K is a calibration factor for the volume and time units used.

d_T is the time differential between upstream and downstream transit times.

T_L is the zero flow transit time.

Transit time method is counted as one of the most accurate techniques because (i) the ability of the signal processing electronics to determine the

transit time with great precision, and (ii) the speed of sound in the medium is known accurately and is reliably constant if the temperature is maintained constant (OMEGA, 2001).

Transit time flow meters are often used to measure the flow of crude oil and other viscous liquids for laminar flow and provided the Reynolds number is either less than 4000 or greater than 10000. Such techniques have been used to measure cryogenic liquids down to -300º C. However, these techniques are not recommended to measure raw wastewater because such flows are not always clean enough, solids concentration can be too high for transit time measurement, (OMEGA, 2001).

Advantages of ultrasonic meters (Upp, 2002)

1. If meters are the same diameter as adjacent piping, there is no added pressure drop;

2. It can minimize errors from effects of pulsations and fluctuating flow if a high frequency pulse rate is used;

3. No moving parts are in contact with flowing fluid which leads to low maintenance cost; and

4. It is easy to check accuracy using a simple mechanical calibration.

Disadvantages of ultrasonic meters (Upp, 2002)

1. High initial cost;

2. Higher set up cost; and

3. It needs power for operation.

2.2.2.4 Visualisation techniques

Bubble shape and size can be measured by using visualisation techniques. Photographic and radiographic techniques are example of methods that can be grouped under this heading.

The photographic techniques depend on being able to take pictures through the wall of the pipe and to observe the flow behaviour; a transparent wall and transparent liquids are required. Thus it is limited to the vicinity of the pipe walls with high gassing rates. These techniques have been used to determine flow regimes and bubble size, quantity and shape (Camarasa et al., 1999). Also, they have been used to investigate three phase fluidised beds (Peterson et al., 1987).

As an extension of the photographic technique, is to use other forms of radiation such as X-rays to observe bubbles shape and position (Heindel, 2000). The advantage of this technique is it can yield results even in presence of a non-transparent fluid.

2.2.2.5 Polarographic technique

This technique is based on the fast electrochemical reduction of reagent dissolved in the moving medium. It is used to yield information on the flow behaviour (e.g. velocity fluctuations) in the immediate vicinity of the wall. The major disadvantage of polarographic techniques is that a conductive liquid is required. This technique can sometimes lead to changes in the coalescence behaviour of the liquid (Boyer et al., 2002; Nicol and Davidson, 1988).

2.2.2.6 Tomography techniques

The general principle of the tomographic technique is the measurement through vessels or pipelines of physical properties that can be related to the phase fraction. There are different kinds of tomographic methods that have been developed such as tomography by using attenuation measurement, γ or X – ray; Electrical tomographic system and ultrasonic tomography (Boyer et al., 2002).

Transducers are placed at different angular positions on the pipe carrying the flow, measurements of phase properties are performed. To do this a reconstruction algorithm is used. This analyses the acquired signals and provides the phase fraction image over a cross section of the pipe. Time and

space resolution may differ widely according number of transducers and physical properties of the flow.

X- and gamma-ray attenuation measurement technique

This method of the non-invasive tomography technique has the capability of measuring the phase distribution inside multiphase flows without affecting normal operations. It is based on measuring a narrow beam X- or γ- ray attenuation coefficients as shown in Figure 2 -12. The attenuation coefficient depends mainly on X- or γ-ray energy, flow composition and flow density. A number of different 2-dimensional projections at various angles around the pipe are combined mathematically through filtered back-projection software to create the distribution of attenuation coefficients in the material as a 3-dimensional image. The flow parameters such as volume fraction can be then extracted from these 3D images. This technique has been used to measure gas void fraction in two phase flow (Thiyagarajan et al., 1991; Bieberle et al., 2009), two phase flow regime recognition (Chunguo and Qiuguo, 2009). However, X- and γ-ray attenuation techniques have some limitations; the X- ray system is limited to low density materials or small pipe diameters due to its low source energy. In γ-ray systems, the spatial resolution is low and measurement time relies mainly on source activity which means that it can be used only with stationary or very slow flows (Boyer et al., 2002; Tjugum and Mihalca, 2009)

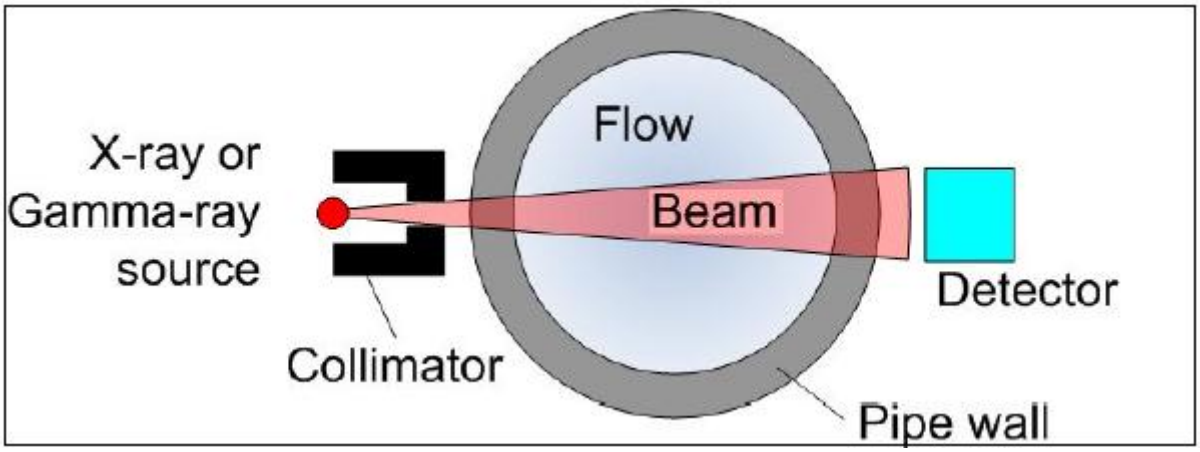

Figure 2-12 Principle of X- or gamma-rays based flow composition measurement
(Tjugum and Mihalca, 2009)

Electrical tomography (ET)

ET is a non-invasive technique to acquire quantitative and qualitative data in multi-phase flows. It can provide data about velocities and cross-sectional profile of phase distributions in pipelines and vessels. ET is divided into two types: electrical impedance tomography (EIT) and electrical capacitance tomography (ECT). EIT produces images based on conductivity and ECT produces images based on variation in permittivity. Both EIT and ECT can be applied on-line or off-line and are used mainly as research tools to monitor dynamic processes such as fluidised beds, hydraulic transportation etc. They have been used to measure two phase flow (Hervieu and Junior, 1999; Huang et al., 2003; Kim et al., 2003; Faia et al., 2012). The ET is low cost and relatively fast and simple to operate, however it has low spatial resolution and requires a non-conductive liner or process wall material (Rasteiro et al., 2011).

2.2.3 Invasive techniques

For industrial operations many non-invasive techniques are ineffective for a number of reasons. For example, images analysis techniques cannot be used because of opaque walls. High gas hold up is very difficult to measure by non-invasive methods. Additionally, non-invasive techniques are sometimes difficult to apply and much more expensive than invasive techniques. Thus, invasive techniques are still important for some applications in the industrial field (Boyer et al., 2002).

Before the development of hydrodynamic non-invasive techniques, needle and heat transfer probes were developed for local measurements in multi-phase flow. These are sufficiently successful to still be in use today (Boyer et al., 2002).

2.2.3.1 Needle probes

Needle probes were designed and are still used to study high gas void fraction systems, and have been used to measure gas void fractions (Nicol and Davidson, 1988), bubble velocity and bubble distribution in gas, liquid or gas-

liquid-solid flows (Yu and Kim, 1991). Needle probes need to be sharp and the end designed to face flow direction to pierce as many bubble as possible.

Optical needle probes and impedance probes are the two main types of needle probes. These probes are used either as a single-tip system (Figure 2-13) to measure gas fraction and bubble frequency, or as double-tip system (Figure 2-14) to measure bubble velocity. This method is not effective with all organic liquids because the difference between refraction indices of the liquid and gas phases is too small. Similarly, if the conductivity of the organic liquid is too small impedance probes cannot be used (Boyer et al., 2002).

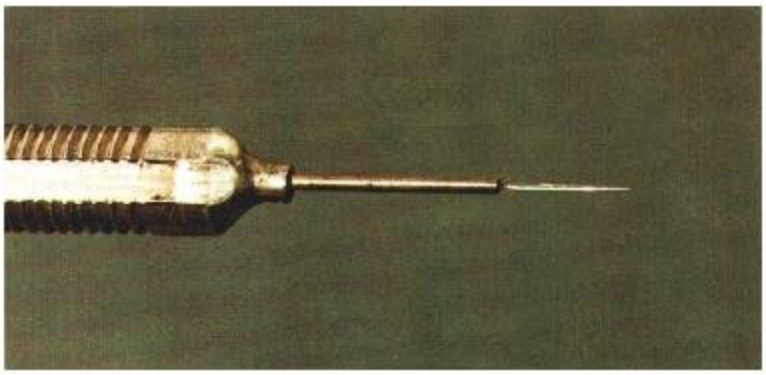

Figure 2-13 Single tip optical needle probe (Boyer et al., 2002)

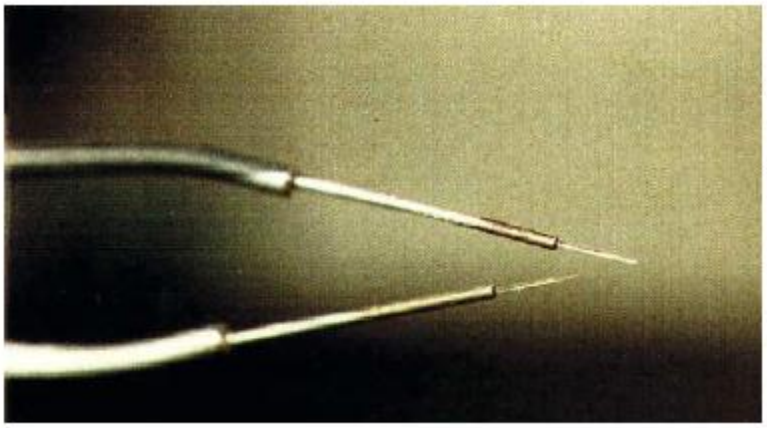

Figure 2-14 Double tip optical probe (Boyer et al., 2002)

2.2.3.2 Heat Transfer Probes

Heat transfer probes are mainly applied to gas-liquid flows and sometimes to gas-liquid-solid flows to measure gas void fraction (Farrar et al., 1995) and liquid phase velocity (Utiger et al., 1999). The principle of this method is the interaction between the probe and the adjacent flow. With hot film anemometry the heat loss depends on the heat exchanged between an electrically heated probe and the surrounding flowing liquid medium, and is a function of flow velocity. Hot film anemometry is low-cost technique and gives accurate results as long as bubbles can be distinguished. However, accuracy is considerably reduced for very turbulent conditions. More details can be found in (Boyer et al., 2002).

2.3 Chapter conclusion

Several non-invasive and invasive techniques to measure multi-phase flow behaviour have been briefly reviewed in this chapter. Some of these techniques do not affect the flow such as ultrasonic and tomography probes, while others such as needle probe do disturb the flow.

Flow measurements with non-invasive technique have been used with multi-phase flow for many years. However all these techniques are subject to some limitations. Ultrasonic techniques, γ-ray and conductivity probe, for example, give inaccurate results at higher gas void fractions. Conductivity probes are also highly sensitive to the flow temperature. Photographic techniques are limited to transparent conduits and transparent liquids.

Thus, there is still a need to develop the capability of an improved technique that can overcome at least some of these limitations.

Chapter 3 **Acoustic Emission (AE)**

(Muravin, 2009) summarized Acoustic Emission history and divided it into two main eras: pre-technological and technological. From beginning of humankind people have noticed AE from cracking stones, bone fractures and wood crackling in the fire, etc. Early peoples also used Acoustic Emission to control quality of production. Since about 6500 BC potters used to listen for audible sounds signifying structural failure during the cooling of their ceramics and this helped to adjust the pottery making process. Around 3500 BC, the term “tin cry” was coined by tin smelters as a result of sound emission due to plastic deformation of mechanical twinning of pure tin. The first documented case of audible Acoustic Emission was in the 8th century, when the Arabian alchemist Jabir ibn Hayyan wrote in his book that Jupiter “tin” gives off a harsh sound or crashing noise while Mars “iron” sounds much during forging (Miller and McIntire, 1987; Drouillard, 1996). Tin cry was commonly discussed and found in textbooks and handbooks on chemistry during the last half of the 19th century. This information and other examples of AE in history can be found with more details in Drouillard, 1996.

The AE technological period started at the beginning of 20th century when researchers started to investigate and report audible sounds of material deformation (Czochralski, 1916; Portevin and Le Chatelier, 1923). In 1936 Forester and Schell built the earliest known AE system to convert mechanical vibration induced from martensite transformations into electrical voltages but this area of research was not progressed until the ground-breaking work of Joseph Kaiser at Munich University in the 1950s who demonstrated the usefulness of AE and set it on scientific foundation. For the next twenty years researchers investigated AE fundamentals, developed specific instrumentations and characterised the AE behaviour of many materials.

The first use of the term “Acoustic Emission” was by Schofield when he developed Kaiser’s work and published it in 1961. Since that time AE has been used as a non-destructive test (NDT) method to monitor dynamic processes. It

has commonly been used for stressed structures and components to detect and locate faults long before failure. In the 1980s the computer became a basic part for both AE instrumentation and its data analysis and gave greater flexibility of AE applications (Drouillard, 1996).

Authors and researchers have defined the Acoustic Emission differently. For example, (Kohn, 1995) defined Acoustic Emission as “Acoustic waves generated by the release of energy from localized sources in a material subjected to an externally applied stimulus”. (Sarfarazi, 1992) defined it as “a transient elastic wave generated as an outcome of a material deformation”. (Muravin, 2009) said that “Acoustic Emission is a phenomenon of sound and ultrasound wave generation by materials that undergo deformation and fracture processes”. From these definitions and others, AE can be scientifically defined as: In different materials there are unique sources that generate transient elastic waves due to the energy released from the deformation process, which spread within the material and can radiate from the material’s surface. The frequency range of Acoustic Emission is generally taken to be 100 kHz – 1 MHz and the time domain waveform signal of AE can be burst and/or continuous.

Unlike most of other non-destructive, active techniques, Acoustic Emission is a passive method, listening to the energy released from the object instead of applying it to the object under examination. Also, Acoustic Emission works only with dynamic processes in a material produced by crack growth, fibres breaking and various other modes of active damage in the stressed material (Hellier, 2001).

3.1 Acoustic Emission mechanism

Acoustic Emission is a passive NDT method that tests or monitors dynamic materials or components in real time and so is effective only when the material being tested is loaded or stressed. Depending on the stress level, Acoustic Emission occurs only at the locations that have high enough stress to cause permanent deformation. The material emits energy after its deformation and that tends to relieve the high local stresses. Frequently, these stresses are

transferred to other parts of the structure. Kaiser and Felicity investigated and described loaded material behaviour (Miller and McIntire, 1987; Hellier, 2001).

3.1.1 Kaiser effect

Wilhelm Kaiser, in 1995, investigated and described the “Kaiser effect”. He found that acoustic waves are released from a loaded material only after any previous maximum load level is exceeded. When the material is reloaded, it behaves elastically until the preceding maximum load is reached after which AE may occur. That means; Acoustic Emission is missing or not easy to interpret in the unloaded phase.

Figure 3-1 illustrates this phenomenon. Acoustic Emission events are plotted directly against load, first the load is increased, then reduced, then increased again to a higher level, again reduced and then finally increased to its highest level. The first load, increases from A to B, generates an emission but there is no emission when the load is reduced, from B to C. The load is increased again, from C to B during which there is no emission. At B, the preceding maximum load emission starts again – this is the Kaiser effect (Miller and McIntire, 1987; Hellier, 2001).

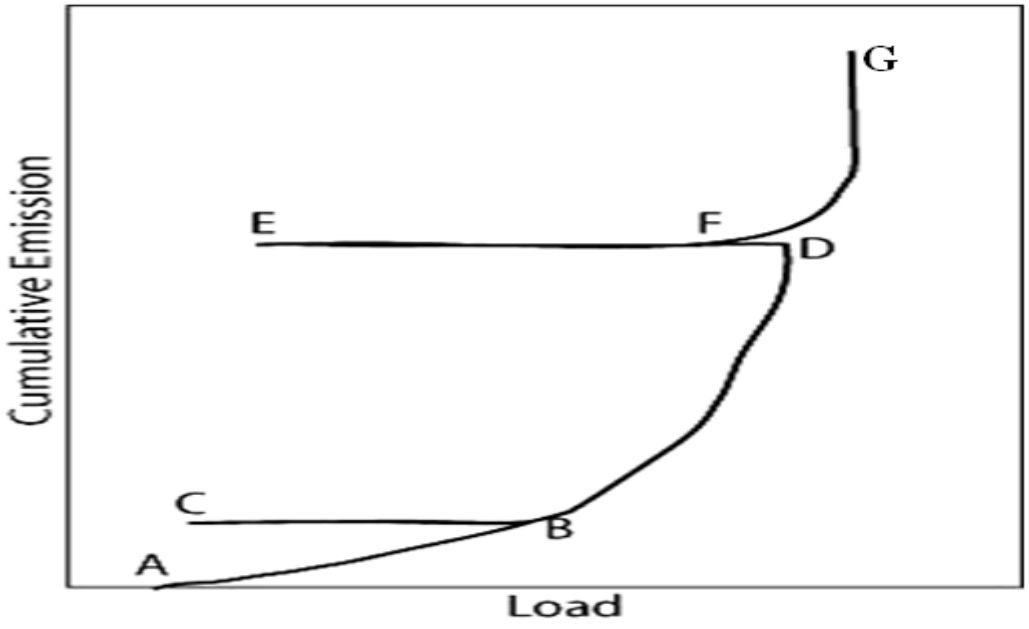

Figure 3-1 Kaiser and Felicity Effects

3.1.2 Felicity effect

It can be seen from Figure 3-1 that when the load is decreased from D to E there is no emission, and when the load is increased there is no emission up to the load F – where F is less than D – where emission begins again. The emitting of Acoustic Emission at a stress level below the preceding maximum load is known as the Felicity effect (Hellier, 2001).When the load is further increased from F to G emission continues.

3.2 Acoustic Emission system

An Acoustic Emission system typically consists of sensors, preamplifiers, cables and data acquisition. These devices will be described briefly in the following subsection.

3.2.1 Acoustic Emission sensors

AE sensors are the devices mounted on the surface of materials to be tested to record and transform mechanical elastic waves into electrical signals. There are several types of AE sensors; electromagnetic, capacitive and the most popular, the piezoelectric transducer. This is because of ease of installation, high sensitivity, and tough enough for use in industrial applications. These sensors have piezoelectric material as a thin disk which can transform mechanical deformation into electrical voltage. For electrical contact, this thin disk is coated with metal on both faces, and mounted in a metal cylinder to provide electromagnetic interference shielding. The piezoelectric ceramics commonly used in AE sensors are made from crystals such as titanates and zirconates (PZT). Figure 3-2 shows the shape and elements of a regular piezoelectric sensor. The diameter of piezoelectric element defines the area over which the sensor averages surface motion.

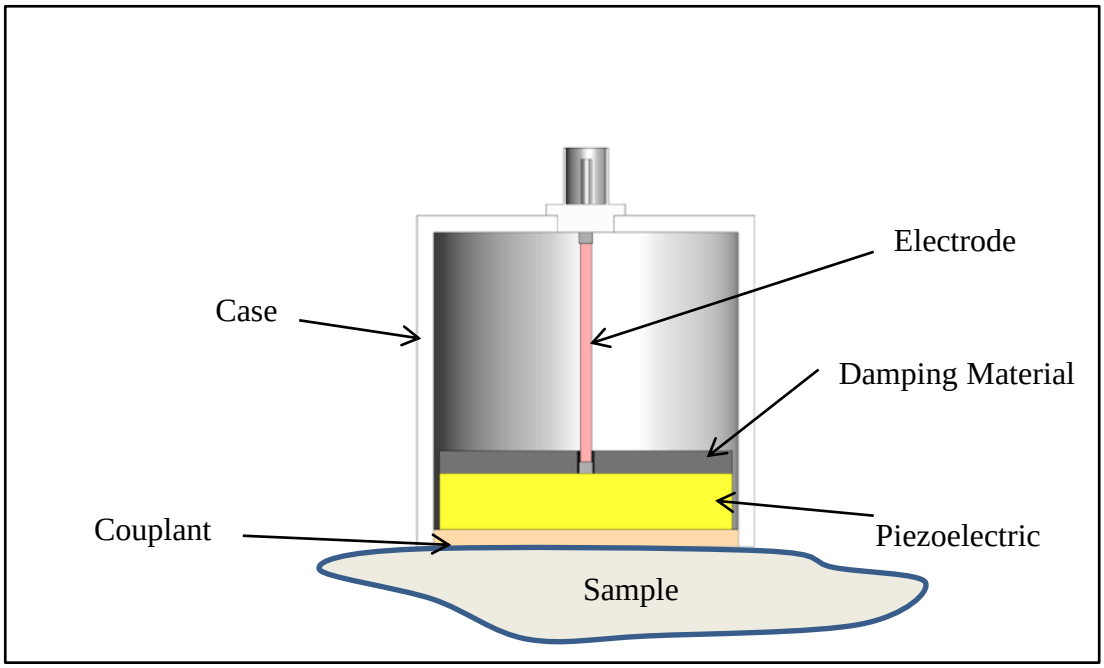

Figure 3-2 Shape and elements of a regular piezoelectric sensor

Based on the application, sensitivity and background noise among other factors, specific AE sensors are selected. AE sensors can be classified into two qualitative types based on the frequency response characteristics: wideband and Pico sensors. The resonant frequency of sensor is described by the thickness of the piezoelectric element. Also, AE sensors can be categorized into passive and active sensors: active sensors have an integral preamplifier, while passive sensors are without integral preamplifiers (Vallen, 2012). To maximise sensitivity piezoelectric sensors must be attached to the monitored material carefully to avoid loss of AE energy at the transducer-material interface. This can be achieved by using a thin film of grease, oil or epoxy adhesive between sensor and material surface (Muravin, 2009; Vallen, 2012; PAC, 2007).

3.2.2 Acoustic Emission preamplifiers

The preamplifier is used to boost the initial AE signal, filter out any unwanted background noise and transform the high impedance signal of the sensor into a low impedance signal which can drive long cables. A preamplifier should be

linked closely to the sensor by short and shielded cables to avoid any electro-magnetic noise and minimize interference. Preamplifiers can be external or integral. An external preamplifier has a separate housing and is connected to the sensor by a cable usually 1 m long, whereas integral preamplifier is part of the sensor within the housing.

There is a wide range of preamplifiers commercially available that can be used with AE systems. This variety of preamplifiers is needed as a result of different applications, specific environmental needs and cost constraints. A 2/4/6 preamplifier, for example, means 20 dB, 40 dB and 60 dB gain ranges. It is provided with three selectable gain settings and is designed to be used with most available AE laboratory systems. Both single-ended and differential sensors can be used with this preamplifier. PAC (2007) and Vallen (2012) have more details of AE preamplifiers.

3.2.3 Couplants

The existence of air between AE sensors and a measurement surface interface seriously attenuates the transmitted AE energy. This is because of impedance mismatching, the big difference in magnitude of acoustic impedance of air and of the two contacting surfaces. To remove any air due to surface roughness and microstructure of the two contacting surfaces and avoid attenuation, a thin layer of couplant material fills any air gaps between AE sensor and monitored material. The couplant improves the quality and quantity of AE energy transmission. Examples of couplants that can provide bonding of measurement surface and AE sensor include silicone oil and propylene glycol, silicone grease, Ultrasonic gel or Cyanoacrylate adhesive and Dental cement.

Factors that have to be considered in the selection of couplants are type of AE measurement or monitoring applications, removal and re-application of AE sensor, measurement surface shape or condition, measurement surface temperature, etc. Both measurement surface and AE sensor need to be smooth and clean before contacted to each other to maximize bonding. The most common couplant is Cyanoacrylate adhesive glue (super glue). However, this

material has a drawback for temporary applications, i.e. it is difficult to remove and AE sensor is at risk of being damaged. Special care must be taken when removing AE sensor when using this type of couplant material (Theobald et al., 2012; Colombo et al., 2005).

3.2.4 Data acquisition (DAQ) board

The key hardware of AE DAQ system is the data acquisition card which converts analog signals to digital signals, analyses and charts data. The acquisition board has more than one channel, see Figure 3-3, and is attached to the computer through the PCI bus. Every channel is connected to a preamplifier and an AE sensor through cables. After the threshold crossing, the acquisition card starts to collect analog data and transform it into a digital signal. After analysing the AE digital signal, information such as event rise time, duration, arrival time, count, RMS value, and peak amplitude can be collected.

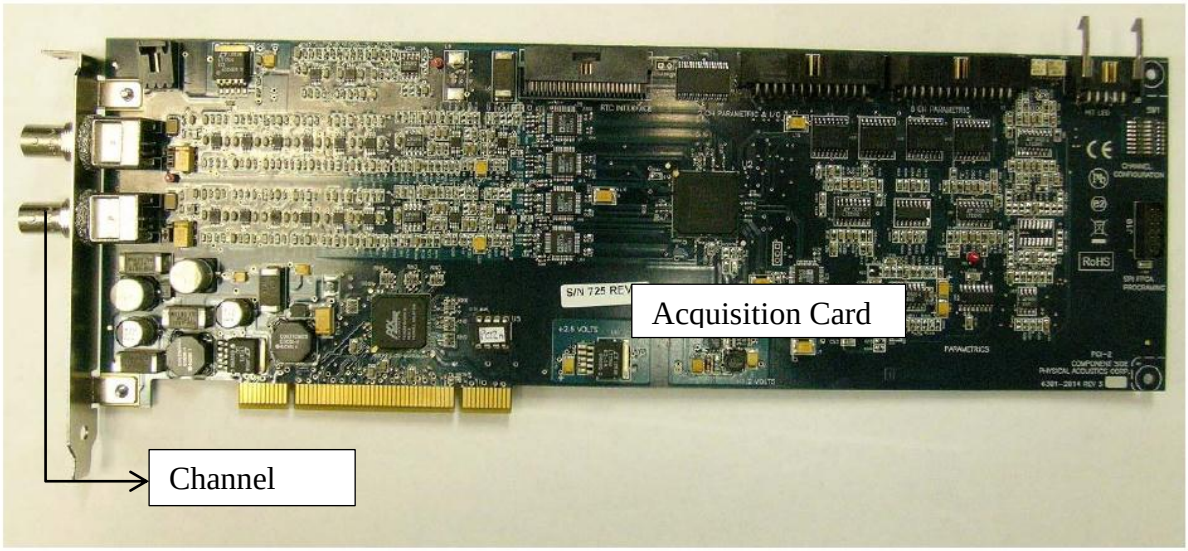

Figure 3-3 Two channel AE data acquisition board (PAC, 2007)

3.3 Acoustic Emission signals

The release of elastic energy within a material as result of inelastic material deformation radiates as mechanical waves and is detected by sensors mounted on the surface of the material, as illustrated in Figure 3-4. Depending on the

nature of the flaw and the dynamics of the source process, the amplitude and energy of the stress pulse created can vary radically.

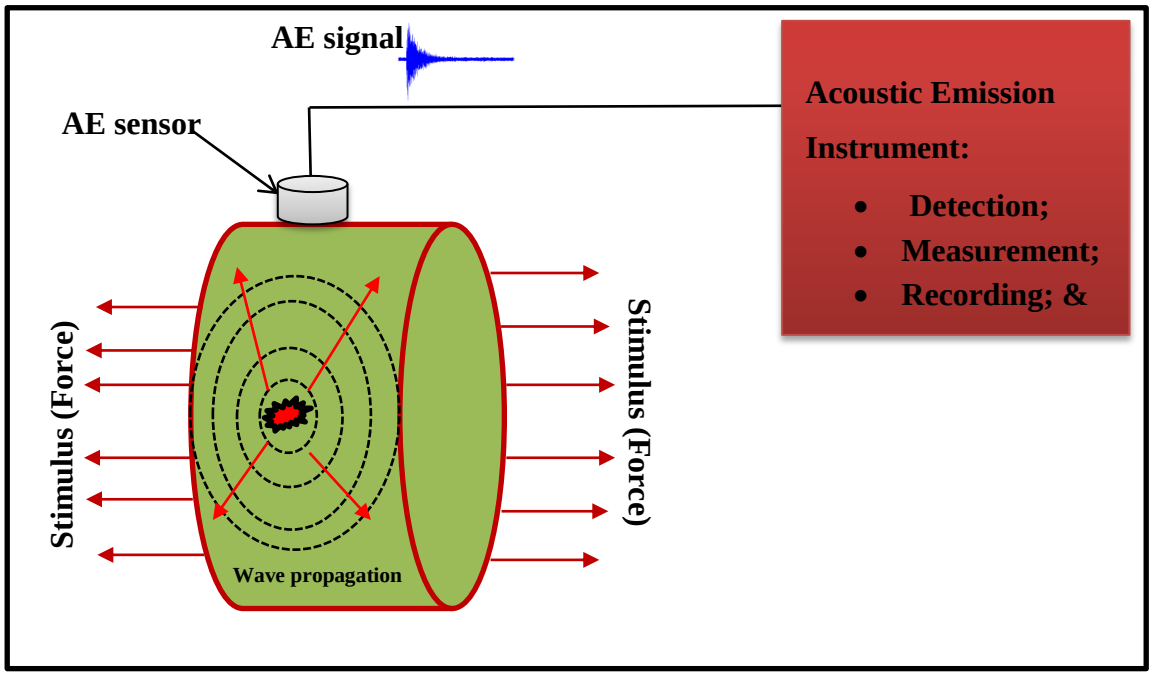

Figure 3-4 Principle of Acoustic Emission

An Acoustic Emission signal can be classified into:

3.3.1 Burst signal:

As seen in Figure 3-5; this type of signal has definite starting and ending points, discrete transients, deviating clearly from surroundings noise.

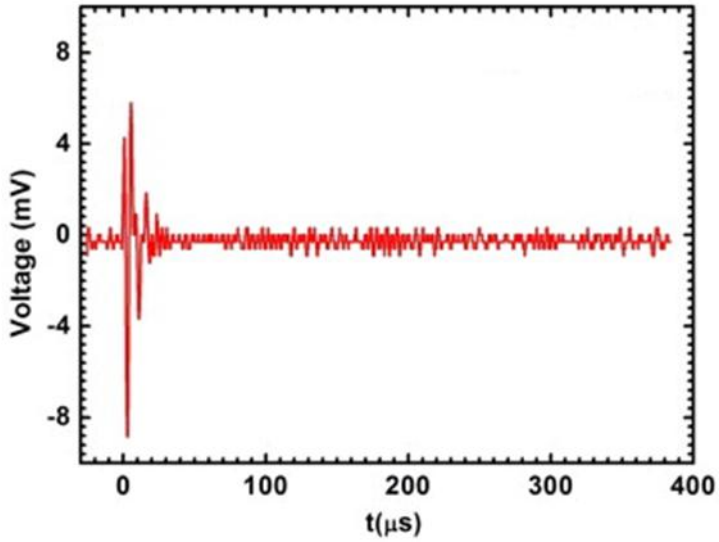

Figure 3-5 AE burst signal

3.3.2 **Continuous signal:**

It is a continuous wave that has frequency and amplitude variations but never ends, whilst is operation, as shown in Figure 3-6. Of course a continuous signal is a series of burst signals sufficiently overlapping to appear continuous.

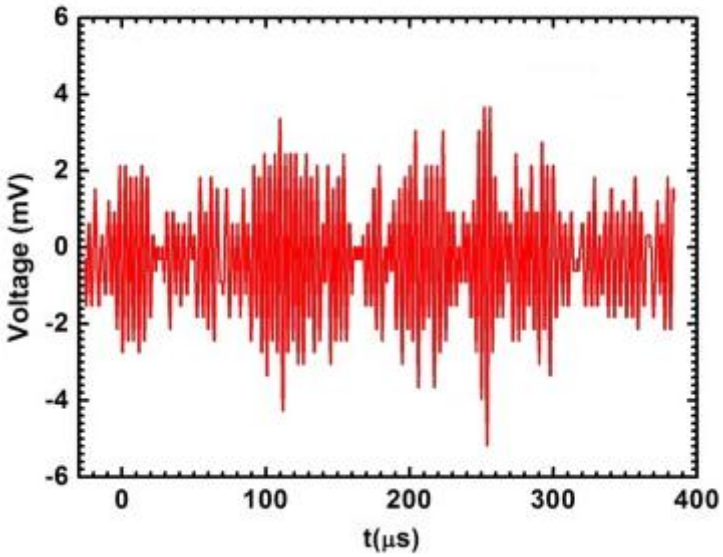

Figure 3-6 AE continuous signal

3.4 Acoustic Emission wave propagation modes

AE energy can propagate in a manner based on the way the particles oscillate: longitudinal waves, shear waves, surface waves and plate waves.

3.4.1 Longitudinal, compressional, waves

The oscillations, particle displacements, occur in the longitudinal direction of the wave propagation as show in Figure 3-7. The energy travels through the atomic structure as a series of compressions and rarefactions.

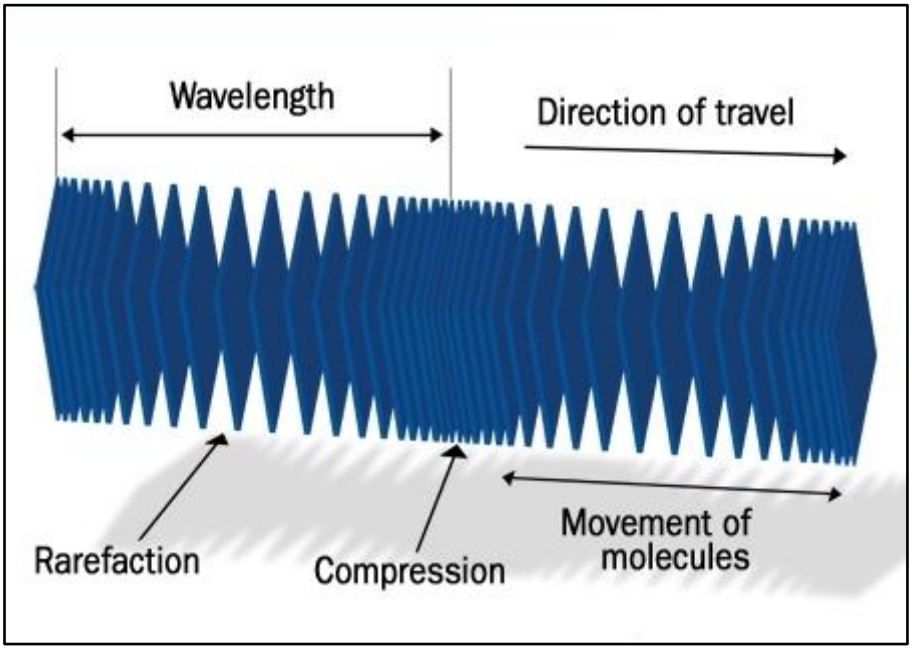

Figure 3-7 Illustration of longitudinal wave propagation (NDT-ed, 2010)

3.4.2 Transverse, shear, waves

In these waves the oscillations are perpendicular to the direction of the wave propagation as can be seen in Figure 3-8. Transverse waves need an acoustically solid material for effective propagation, and therefore do not propagate in liquids or gases. Shear waves are relatively weak compared to longitudinal waves, (NDT-ed, 2010).

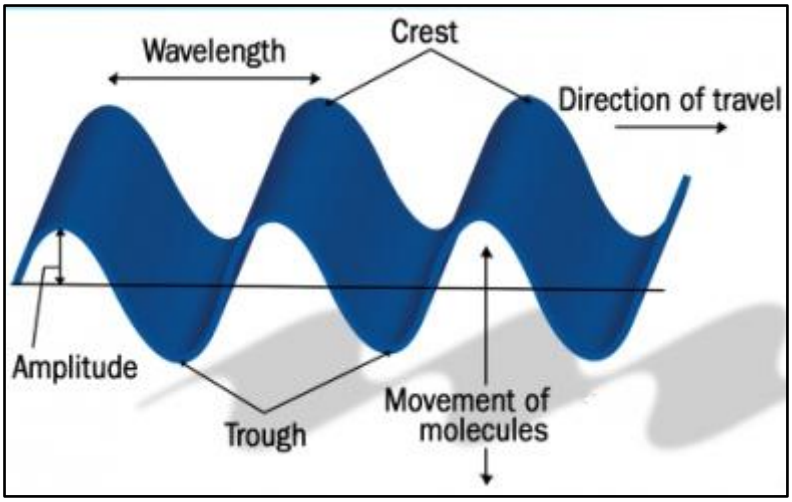

Figure 3-8 Illustration of shear wave propagation (NDT-ed, 2010)

3.4.3 Surface or Rayleigh wave

With this wave the particle motion is a combination of both longitudinal and transverse oscillations so that they move in elliptic “orbits” in planes normal to the surface and parallel to the direction of the wave propagation, see Figure 3-9. Because they are very sensitive to surface defects and they follow the surface around curves, Rayleigh waves can be used to inspect areas that other waves might have difficulty reaching.

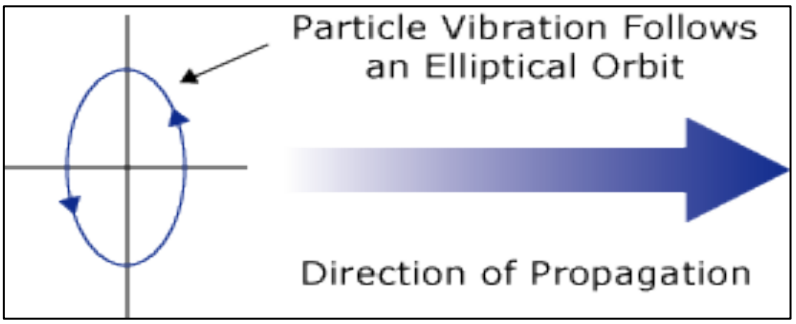

Figure 3-9 Rayleigh wave propagation (NDT-ed, 2010)

3.4.4 Plate, Lamb, waves

They are the waves that propagate parallel to the test surface of a thin plate and are known as plate modes. Lamb wave velocity depends strongly on frequency as well as plate thickness. These waves can be classified as symmetric, where

both surfaces pinch together, and anti-symmetric, where both surfaces deflect at the same time in the same direction, as shown in Figure 3-10.

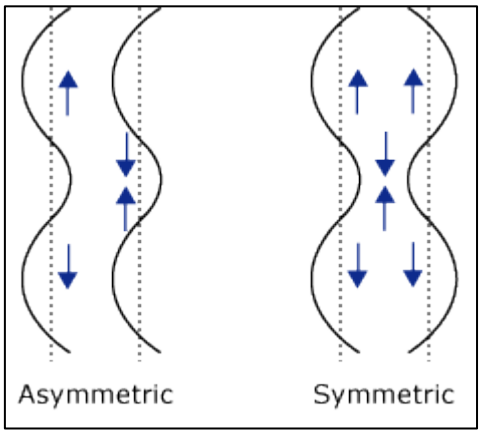

Figure 3-10 Lamb wave propagation (NDT-ed, 2010)

3.5 Wave propagation factors of AE signals

Important wave propagation factors in Acoustic Emission signals include attenuation and wave velocity.

3.5.1 Attenuation:

It is the gradual decrease of intensity of the wave as it travels through the medium outward from the source. This happens as a result of material damping, of increase in area of the wave front and geometrical factors such as scattering and absorption. Attenuation is a vital aspect especially when detecting waves from distant sources (Hellier, 2001).

3.5.2 Wave velocity:

It is calculations of source location are based on the wave arrival times at the sensors, which are dependent on the wave velocity between the sensors (Vallen, 2002; Hellier, 2001; NDT-ed, 2010).

In addition to attenuation and wave velocity many other factors that can impact AE waves: stress loading rate applied to the material, and material properties

and geometry are example of the factors that effect on the generation and behaviour of AE waves.

3.6 Dispersion

The wave velocity is known as the phase velocity, the velocity at which the waves travel through the medium. In general, acoustic waves propagating through solids have multiple frequencies. In bounded media the phase velocity is a function of frequency. Therefore, different frequencies propagate at different speeds; this is called dispersion. Dispersion has little effect on continuous waves; however, Acoustic Emissions are packets of waves which can be thought of as a superposition of continuous waves of different frequencies. If each wave train making up the packet travels at a different velocity, the wave packet will change as it travels through the medium. The result is that the same Acoustic Emission produces a different response when detected in different positions.

For Lamb waves the velocity cannot be found as easily as for longitudinal and transverse waves. It depends not only on the elastic constants of the material, but also on the plate thickness and on the frequency. The symmetric mode (S_0) generally travels at the highest velocity and is non-dispersive in nature, meaning that all frequency components of this mode travel at the same velocity. The antisymmetric mode (A_0) travels at a lower velocity and is dispersive with the square root of frequency, meaning that the higher frequency components propagate faster than the lower frequency components. In practice, this leads to a gradual decrease in the amplitude of A_0 as it propagates, owing to the spatial separation of the different frequency components (Surgeon and Wevers, 1999).

The values of the group velocities, the velocity at which a group of waves travel at a similar frequency, for the different Lamb modes are generally given in dispersion curves such as those in Figure 3-11, presented as a plot of group velocity versus the frequency times thickness product of the structure. These curves can be simulated with dedicated software. The numerical values presented in Figure 3-11 will not coincide exactly with those of other laminates,

these must be calculated according to the specific geometry. Figure 3.11 shows that for values of 0.1 MHz or below, only the S_0 and A_0 modes are observed, higher modes are not observed. The figure also indicates that the symmetric mode is much faster and so arrives at the sensor before the anti-symmetric one; nevertheless, the AE system can be triggered by the anti-symmetric mode if it happens that the symmetric mode has an amplitude below the triggering threshold. Generally, dispersion curves are used to accurately predict the location of an AE source. For example, to improve location accuracy, Acoustic Emission waveforms are filtered at the frequency of the triple point, where all the modes have a similar speed, and the threshold at all sensors will be triggered by the same wave mode as shown in Figure 3-11. Dispersion curve can be constructed for all kinds of structures such as plates, pipes, rods …etc (NDT-ed, 2010; Surgeon and Wevers, 1999; Muravin, 2010).

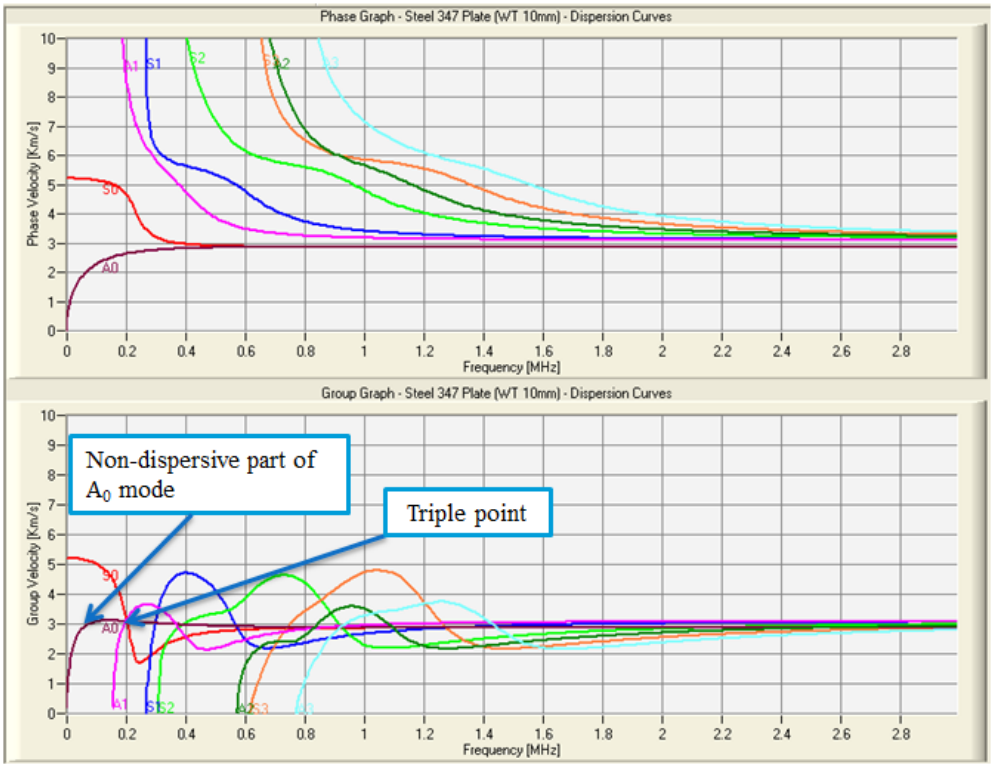

Figure 3-11 Dispersion curves for steel 347 plate (Muravin, 2010)

3.7 Acoustic Emission signal parameters

To understand an Acoustic Emission signal, knowledge of certain basic terminology, is essential to interpret and analyse the AE signal. Figure 3-12 presents the typical Acoustic Emission signal and its parameters. The most widely features used to analyse the AE signal are:

3.7.1 **Threshold:**

It is a voltage level signal, only signals with amplitudes larger than this will be recognized.

3.7.2 **Arrival Time**:

It refers to the time of the first crossing of signal. This parameter is used to calculate source locations.

3.7.3 **Rise time:**

It is the time duration between the first threshold crossing of the burst signal and the peak amplitude. This feature is determined by wave propagation between the sensor and the Acoustic Emission source.

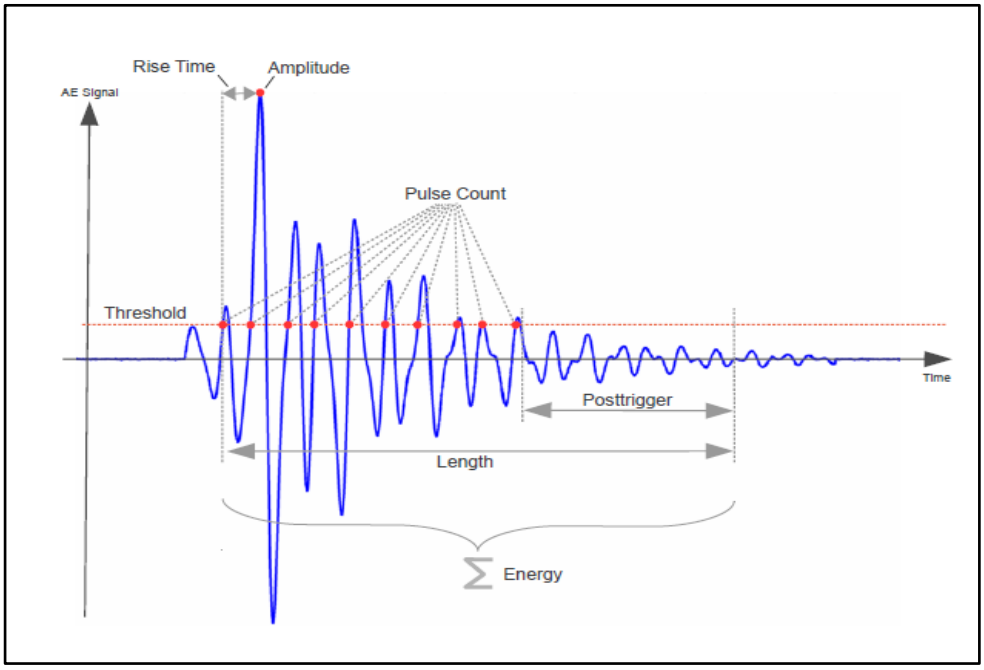

Figure 3-12 Typical Acoustic Emission signal (Hunziker, 2011)

3.7.4 **Amplitude (peak amplitude):**

It is the largest voltage within the duration of the signal. It is considered as one of the most important parameters in the AE signal.

3.7.5 **Duration:**

It is the time interval between first and last threshold crossing in the burst signal. It is useful to filter out noise and to identify different types of sources.

3.7.6 Counts:

It is the number of pulses that cross the predetermined threshold. Note only an increasing signal is counted. Depending on size, shape and frequency of the signal among others, one hit may produce one or hundreds of counts. This feature needs to be combined with amplitude and/or duration to give suitable information about the signal shape (Hellier, 2001; Holroyd, 2000).

3.8 Acoustic Emission energy sources

The ability to understand and determine the interconnection between measured AE characteristics and generating sources is the cornerstone in the AE research development. Acoustic Emission users in industrial applications aim to detect and locate flaws in structures made of metal, composites or concrete from the release of energy due to facture and crack propagation which are the primary sources of AE. A rapid release of stress waves is generated as a result of plastic deformation in metals, breakages in fibre composites, and fracture of aggregate in concrete, etc. Non-material secondary source of AE energy include leaks, friction, cavitation, solidification and liquefaction (Addali, 2010; Muravin, 2009). Air bubble formation, oscillation and collapse are a good Acoustic Emission energy source in multi-phase flow (Longuet-Higgins et al., 1991; Manasseh, 2004; Husin, 2011; Chen et al., 2012).

3.9 Acoustic Emission: Advantages and disadvantages

3.9.1 AE advantages

Acoustic Emission has a number of advantages more than other non-invasive techniques. Acoustic Emission receives a signal instead of transmitting it as most other NDT do. AE testing has many other advantages such as:

- It can be used as a pre-service and in-service testing;
- It is a global monitoring system which means sensors can detect acoustic signals from large distances;
- It can reduce costs by allowing immediate inspection; shutdown is not needed;
- It can detect a flaw at an early stage;
- It is insensitive to typical background noises in the environment; and
- It can be used, simultaneously with other invasive and non-invasive techniques (Hellier, 2001; Holroyd, 2000; Envirocoustics., 2010).

3.9.2 AE disadvantages:

As any other technique, Acoustic Emission has some limitation and disadvantages such as:

- AE cannot be replicated because each loading is different and has its unique stress signature;
- The Acoustic Emission waves will be attenuated within the structure under test.
- Other ultrasonic sources may be present such as turbulence in fluid flows and crushing, which are very effective AE sources;
- It has need for special sensors and signal processing; and
- Its signals are weak compared to the vibration signals.

3.10 Acoustic Emission in multi-phase flow

Acoustic Emission technology has widespread applications as a measurement and monitoring method in many industrial fields such as petrochemical, civil

engineering, nuclear power, aerospace, automotive industries, and also in industrial and academic research. It is used to detect cracks, leaks or corrosion damage in piping inspection (Ai et al., 2010; Sun et al., 2010; Dunegan, 2004), condition monitoring of concrete bridges (Kalicka, 2010), fatigue and crack propagation in materials (Roberts and Talebzadeh, 2003), etc. In some application, the only applicable and effective non-destructive test method is Acoustic Emission. For example, test of composite overlap pressure vessels and detection of micro structural damage (Muravin, 2009).

The first study of bubble behaviour was in 1917 when Lord Rayleigh investigated the effect of cavitation damage of ship propellers. In 1933, Minnaert confirmed experimentally that bubbles can emit a natural frequency with small amplitude as a result of oscillations. Since then a significant amount of research has been undertaken to understand bubble behaviour (Longuet-Higgins et al., 1991; Husin, 2011; Chen et al., 2012; Strasberg, 1953; Manasseh et al., 2008). From their studies, it can be concluded that bubble formation, oscillation and collapse generate sound and acoustic energy. AE technologies have been used for decades to monitor and measure multiphase flow. This section focuses on previous work applying acoustics and Acoustic Emission to monitor multi-phase flow.

(Ajbar et al., 2009) predicted flow regimes transitions in an air/water column using acoustic measurement techniques. A miniature hydrophone (Bruel& Kjaer type 8103) was placed in the centre of the column at 40 cm above the gas injector to record sound pressure fluctuations. Sound measurements were collected at different superficial gas velocities up to 6.6 cm/s with a sample rate of 20 kHz and 10 second of a recording time. The researchers used a combination of chaos-based and spectral techniques to analyse the collected data to predict the transition point and recognise the flow regimes of the column. Power spectra analysis was to identify the transition stage between homogenous and churn-turbulent regimes. The chaos-based analysis was to identify the bubble and heterogeneous transitions stage. Ajbar et al., concluded

that the acoustic measurement technique is able to identify the flow regime with air bubbles in water.

(Addali, 2010) used AE to monitor and measure gas void fraction of water/gas two phase flow. A test rig was designed and built up as shown in Figure 3-13. Ten different superficial liquid velocities and twenty-four superficial gas velocities were used in this experiment. All twenty-four gas velocities were investigated at each liquid velocity; so 240 test conditions were used. The range of superficial liquid velocity was from 0.3 - 1.2 m/s at 0.1 m/s increment; and the superficial gas velocity ranged from 0.1 - 4.0 m/s using a 12.5 mm diameter air supply pipeline, to supply gas velocity from 0.0 - 2.0 m/s at 0.1 m/s increment, and 25 mm diameter air supply pipeline, to supply gas velocity from 2.5 - 4.0 m/s at 0.5 m/s increment. Addali presented his results for the AE signal as a function of its absolute energy and RMS amplitude.

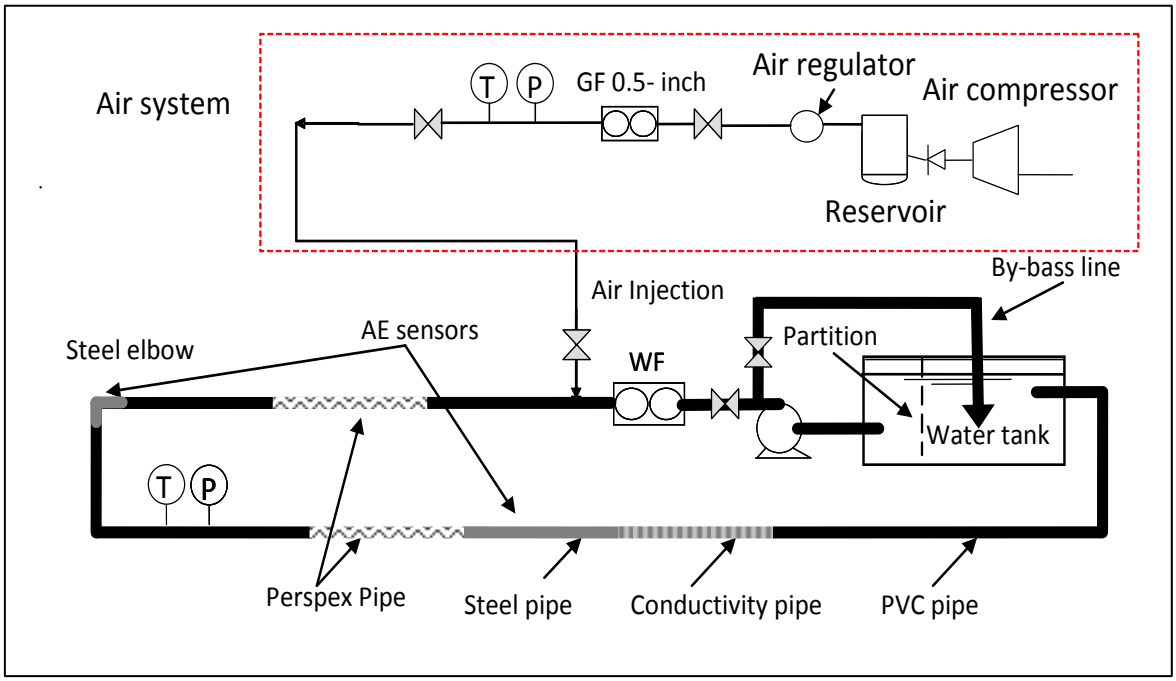

Figure 3-13 Experimental set up of water/gas GVF measurement

Addali investigated AE sensor type; internal surface roughness of the pipe; gas and liquid velocities; liquid viscosity; liquid temperature; straight pipes and pipes with elbows. As shown in Figure 3-13, a 50 mm diameter Acrylonitrile-

Butadiene-Styrene (ABS) pipe with total length of 22.5 meter was used in this experiment to allow flow stabilization and to ensure that the flow regime was completely developed before the flow entered the test section; three different 50 mm ID stainless steel pipes each with length 750 mm and wall thickness 10 mm were used as a test section to investigate the surface roughness effect. A $4m^3$ fibreglass tank was used to supply water through the 50 mm ID closed loop system using a centrifugal pump with capacity of 40 m^3/hr and a pressure of 5 bar. Two domestic electric heaters with input power of 2700 W each were fitted in the water tank to increase the temperature of the circulated water to investigate the temperature effect. Sensors were mounted on a stainless steel test section; these sensors can be on top or on the bottom by rotating the test section. Addali used conductivity rings (electric impedance technique) to validate the results.

This study concluded that an increase of superficial liquid and gas velocity will cause an increase in the level of Acoustic Emission; the correlation between liquid velocity and Acoustic Emission suggest the possible applicability of use of AE for in-situ monitoring of changes in fluid viscosity. Addali concluded his study by introducing a new non-invasive gas void fraction measuring technique for two phase water/gas flows that gives quantitative and qualitative values.

(Yen and Lu, 2002)applied an Acoustic Emission detection system and synthetic neural network techniques to distinguish four main regimes (bubbly, slug, churn and annular) in an air/ water two phase flow in a vertical column. They attached two piezoelectric sensors on the pipe: one to detect AE signals generated in the flow, and a second one located near the first to detect the background noise. In this experiment, a continuous regime-changing process was designed. It included twelve steady states, about thirty second of typical air and water flow rate, and eleven transient states, unstable phase flow rate, for twenty minutes data acquisition time. All steady and transient states were recorded to generate a reference map, The authors did not mention how and what type of technique they used to record steady and transient states. For every second of the processes the AE count and hit numbers were measured

and stored. By drawing an AE hit-count map, the annular regime was clearly separated from the other regimes. Churn and slug regimes were also well separated but with a small overlap between them. The overlapping area between bubbly and slug regimes was not small so they could not be linearly separated.

It was concluded that it was possible to use a two-hidden-layer neural network with the AE sensors to separate and classify the flow regimes as show in Figure 3-14. It was concluded that AE events and ring-down counts density can be combined as a stable and excellent flow regimes identifier.

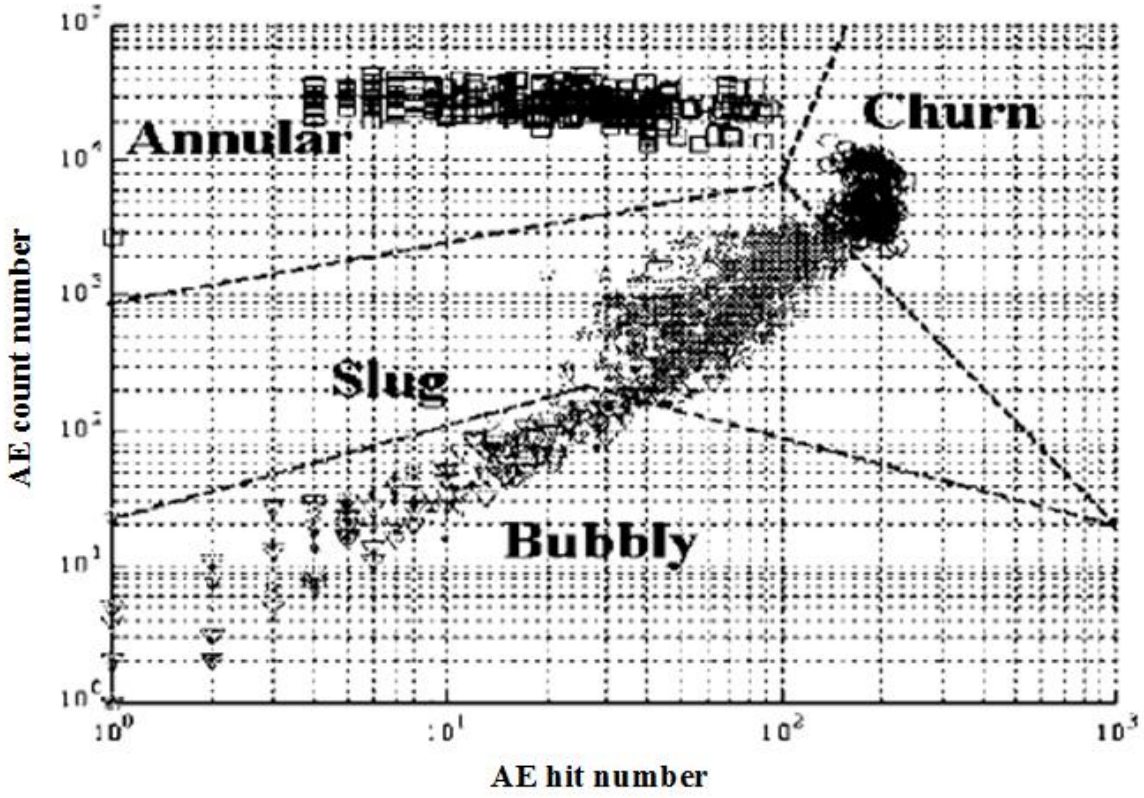

Figure 3-14 AE hit-count map (Yen and Lu, 2002)

(Hou et al., 1999) used an AE technique to monitor the pumping of fine silica particle suspensions in a 44.5 mm diameter pipeline network. A positive displacement pump, circulating tank and ball valves were used to construct the experimental rig. The experimental material was silica flour product, HPF-2 from Hepworth Minerals and Chemicals. A 190 KHz piezoelectric sensor was

mounted, using epoxy adhesive, on the pipeline in the vicinity of the pump outlet to obtain the highest signal-to noise ratio. Preamplifiers, signal conditioning unit, computer with conversion card and data storage facilities were used as the signal processing system. After running the experiment many times at different solid concentrations and volume flow rates at room temperature, Hou and his colleagues noticed that signal characteristics are very sensitive to solid concentration and volume flow rate changes. They used a stepwise regression analysis method to find quantitative relations between signal features and the physical properties of the flow. A quantitative model to infer solid concentration, mass flowrate, and volume flowrate was built utilizing spectral and statistical characteristics of collected AE signals at different conditions of the experiment. Hou and his group concluded that passive acoustic signal has the capability to be used for on-line monitoring of slurry flows.

(Betteridge et al., 1981) investigated whether or not certain chemical reactions emitted sound. They placed piezoelectric transducer underneath a laboratory glass beaker to receive any acoustic signals during the chemical reaction. A low noise amplifier was selected to amplify the acoustic signals. The RMS converter was used to transmit the signal and act as a high pass filter retaining only the 100-300 kHz ultrasonic components. Betteridge and his colleagues examined 43 chemical reactions and separated the reactions into eight groups according to the duration of the Acoustic Emission, the highest intensity of the Acoustic Emission and a heterogeneity factor of both reactants and products. The study demonstrated that the criteria used did not provide clear differences between the groups and the researchers recommended further work such as analysing the acoustic signals statistically.

(Al-Masry et al., 2005) conducted an investigation using acoustic analysis to determine bubble characteristics (radius, size, distribution and void fraction) in bubble columns. A 150 mm diameter vertical bubble column of height 660 mm was used to produce a stable bubbly flow regime at atmospheric pressure and room temperature. To introduce the gas, a ring sparger with 85 holes was used. A hydrophone recorded the emitted sound pressure from bubbles. Two

statistical methods were used, based on the zero crossings phenomenon, to analyse the acoustic sound parameters. One investigated whether the zero crossings were due to random trends or due to oscillatory behaviour. The other measured the oscillation period regularity. To distinguish oscillatory signals from random noise and to determine the frequency of oscillation, the two methods were combined. The researchers claimed excellent results such as bubble pulsation and frequency can be detected and the number of pulsations can be counted. As a result, dominant bubble radius was obtained, and bubble size distribution was found. The bubbling rate calculated from the bubble count varied linearly with superficial gas velocity while the RMS of the measured sound pressure varies monotonically with superficial gas velocity. The authors developed a correlation to estimate the gas void fraction directly from the RMS of the Acoustic Emission. They found excellent agreement between the measured and estimated void fraction.

(Manasseh, 2004) used a passive bubble acoustic technique as a part of feedback loop, to control and optimise a chemical aeration process in a 2000 litre bioreactor tank. A hydrophone was placed into the bioreactor tank in the vicinity to the wall. Because the lowest frequency of interest was 700 Hz, high pass with lower limit 400 Hz was used to remove unwanted background noise. The data was collected continuously over 24 hours while the tank was operating at full production. Manasseh noticed that the typical bubble diameter was 4 mm and generated sound at a frequency of about 1500 Hz. The study concluded by providing a new sensing technique that can be used to increase bubble dispersion and improve aeration in industrial processes.

(Duclos et al., 2004) employed an Acoustic Emission technique to monitor the rate of erosion in pipes due to particulate impacts. They were able to separate particulate impact signals from Acoustic Emission signals generated from gas bubbles and fluid flow. Two AE sensors were located on a sharp 90º bend made from stainless steel, 26.7 mm diameter and 3.1 mm thick. A 60 ml syringe was placed 2 m upstream of the bend, to inject a controlled quantity of sand particles and bubbles into the flow. The researchers found that (i) AE

waveforms of air bubbles could be clearly distinguished from particle impact signals; (ii) AE event duration for air bubbles was much longer and emission intensities were much lower compared to those of particle impacts; and (iii) AE increased as the number of air bubbles increased, and as the number of sand particles in the flow increased regardless of the particle size.

(Albion et al., 2007) studied the flow regimes of powder in horizontal pipes using an Acoustic Emission technique. Their test rig used a 100 mm inner diameter stainless steel pneumatic transport pipe; a compressor controlled by a regulator to supply air; two AE sensors, one mounted on the top and the other underneath the pipe. A high speed video camera was also used to record the flows under various operation conditions. Albion and his colleagues concluded that the analysis of the frequency spectrum and various statistical parameters such as signal average and standard deviation of the acoustic measurements recorded from the experiment provided a reliable means of identifying dilute phase and settled solids flows.

(Al-lababidi et al., 2009) used an Acoustic Emission technique to monitor slug flow and measure gas void fraction in two phase gas/liquid flow. Their test rig used a 50 mm diameter pipe of total length 22.5 m (long enough for the formation of fully developed slugs) made from three different materials (ABS pipes, Perspex for visual observation and stainless steel on which to place the AE sensor); centrifugal pumps supplied water to the flow loop; AE sensors with 150 - 750 kHz frequency range were placed on the steel pipe; a 60 dB preamplifier was used with the AE acquisition system. The experiment was run with a superficial water velocity (VSL) range from 30 cm/s to 200 cm/s in incremental steps of 10 cm/s, and superficial gas velocity range from 20 cm/s to 140 cm/s in incremental steps of 20 cm/s at each VSL. The duration of each run was 120s. Al-lababidi and his colleagues developed a correlation of gas void fraction for gas/liquid flow as a function of slug velocities and the absolute Acoustic Emission energy. They concluded that the average percentage error and standard deviation of the developed correlation were smaller than for previous reports of this correlation.

(Pandit et al., 1992) studied sound emanating from two types of bubbly two-phase flow: firstly for different fluid void fractions and velocities using a horizontal pipeline located downstream of a centrifugal pump, where a hydrophone was mounted onto the pipe to measure the sound. The second was by using an axi-symmetric gas-liquid jet immersed in a rectangular Perspex tank where the same hydrophone was located in front of the gas-liquid jet. A spectrum analyser was used to resolve the pressure pulse into an amplitude/ frequency spectrum by performing a Fast Fourier Transform. Pandit and his group concluded that bubble size distribution can be determined from the amplitude and frequency of the measured pressure.

(Crowther et al., 1991) investigated Acoustic Emission signals from an electrolytic cell with the formation of oxygen and hydrogen bubbles at the electrodes. The cathode and anode were both 120 mm long and 7mm diameter circular rods and made from nickel and stainless steel respectively. The electrolyte was Sodium hydroxide, NaOH, solution with varied strength between (0.1- 2.1) M. a piezo-electric transducer was mounted onto the working electrode. (1.4- 5.0) voltage range was applied. The experiment was concluded by bubble formation coincided with Acoustic Emission bursts at up to 800 KHz of frequencies. Also the Acoustic Emission signal strength depended on the electrolyte concentration.

(Shuib et al., 2010a) explored the correlation between Acoustic Emission and single bubble formation, motion and collapse. The test rig was built up by using a 150 mm ID column with a height of 1500 mm filled with a fluid. Three Acoustic Emission sensors were mounted on the column; one was located near to the bubble inception; the second was mounted mid-way along the column; and the third was located immediately beneath the free surface of fluid. Three broadband piezoelectric transducers, each with an operating frequency of 100 - 750 kHz and pre-amplification at 60 dB were used to measure any Acoustic Emission. A syringe with different sized nozzles diameters, 1.4, 4.4 and 8.4 mm was placed in the middle of the bottom of the water column to create single bubbles. Two cameras were used to record the motion of every bubble

throughout the test. Fifty tests were undertaken for each nozzle diameter. AE rise time; AE amplitude; AE absolute energy; and AE burst duration were measured. This study concluded that AE technology has the capability to detect single bubble formation and collapse.

(Shuib et al., 2010b) investigated single bubble dynamics in a liquid-filled column using an Acoustic Emission technique. The test rig was designed to investigate the viscosity effect on AE emitted from a bubble on its formation and burst. A syringe was used to produce single bubbles in the column. Three AE sensors were used; one near to the nozzle at the bottom; one mounted next to the water free surface and the third one located mid-way between the two sensors. All sensors were submerged in the liquid. The sensors were all broadband piezoelectric transducers with frequency range of 100 - 750 kHz and pre-amplification at 60 dB. Shuib and his colleagues concluded that Acoustic Emission technology has the capability of detecting single bubble formation and burst at the free surface. Also, Acoustic Emission levels associated with burst at the free surface increased as liquid viscosity increased.

3.11 Conclusions

A brief description of Acoustic Emission systems and parameters has been presented in this chapter. Acoustic Emission wave propagation modes and characteristics, energy sources, advantages and disadvantages have also been presented. This chapter concluded by reviewing previous work describing Acoustic Emission technologies applied to multi-phase flow: such as monitoring gas void fraction in horizontal pipes, flow regime recognition in vertical columns and studying single bubble characteristics in a liquid filled column. However, to date no one has investigated slug flow velocity in two phase (gas/water) flow in horizontal pipes. On the basis of the literature review this study will focus mainly on detecting slugs in gas/water flow and measuring their velocities using Acoustic Emission technology. The study will also investigate the capability of Acoustic Emission for regime recognition in two phase (gas/water) flow regimes.

Chapter 4 Slug flow in horizontal pipes

4.1 Slug flow regime

The definition of slug in multiphase flow is a liquid mass travelling in a pipe being driven by the difference in the dynamic pressure between the gas content ahead of and behind the liquid mass. This liquid mass covers the entire cross-section of the pipe. In vertical pipelines, slug flow is symmetrical and bullet-shaped of liquid with dissolved bubbles, but in inclined and horizontal pipes the slug is in the upper part of the pipe with a liquid film below it with some dissolved bubbles in the liquid forming the slug. Generally, the shape of the slug constitutes a front (Region 1-2), body (Region 2-3) and a tail (Region 3-4) as shown in Figure 4-1.

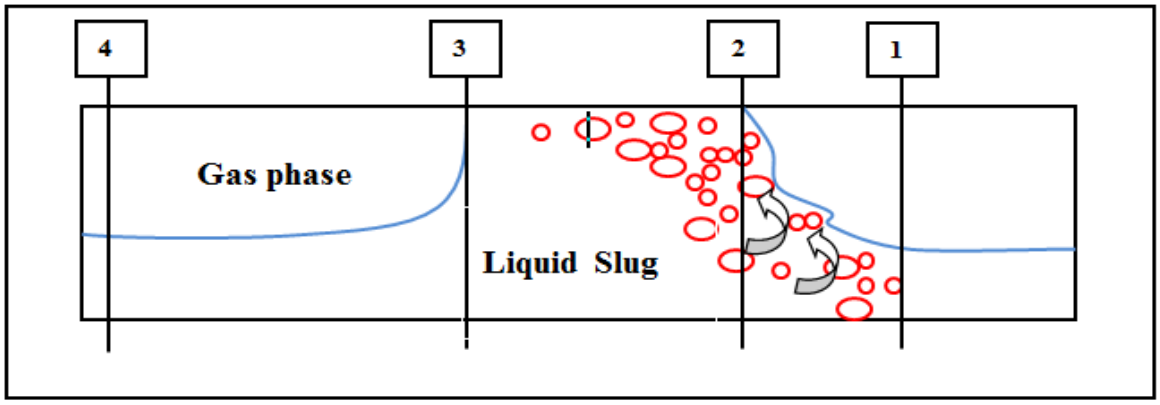

Figure 4-1 Two Phase Gas/Liquid Slug Profile

Slug flow occurs for the whole range of pipes diameters and lengths, and over a wide range of gas and liquid flow rates. It is characterised by a complex dynamic structure of liquid slugs separated from one another by a relatively large gas pockets or stratified flow. Slug flow is commonly observed in many industrial applications such as oil wells and transporting pipelines, chemical and nuclear reactors. Slug is flow considered to be the most severe regime that can occur in any production line. Slugs create significant pressure fluctuations; cause flooding at the receiving end; induce severe mechanical vibrations in the pipeline; and increase deposits of hydrates and corrosion.

4.2 Initiation, growth and dissipation of slug flow

Attempts to predict the occurrence of slugs based on classical stability criteria for stratified flow have been made by a number of researchers. Kordyban and Ranov, (1970) examined horizontal co-current flow using the classical Kelvin-Helmholtz instability (waves are generated by a velocity difference across the interface between the gas and liquid - gas pressure fluctuations are greater than the forces of gravity and surface tension). Mishima and Ishii, (1980) extended the work of Kordyban and Ranov and showed that slug formation is governed by the finite amplitude wave with the largest rate of growth. Graham et al., (1973) investigated the growth of linearly unstable disturbances on a flowing liquid in two phase flow in a horizontal pipe. Taitel and Dukler, (1976b), and Fan et al., (1993) considered how a slug could evolve from a finite amplitude wave, and based on a balance between gravity and Bernoulli forces and found stable slug flow if the wavelength was in a range that would be stable according to the Kelvin Helmholtz mechanism.

Ruder et al., (1989), Taitel and Dukler, (1976a) and Dukler and and Hubbard, (1975) investigated the development and stability of slugs in two-phase gas/liquid flow in horizontal pipe using visual observations. Near the pipe entrance, the gas and liquid flows were quite distinct and the gas clearly flowed above a moving stratified liquid layer. However, the liquid layer decelerated because of shear forces experienced at the pipe wall and its depth changed gradually towards an equilibrium depth which was governed by gravitational, shear and pressure forces. During this process small disturbances or perturbations on the surface of the liquid layer could develop and grow into distinct waves.

Figures 4-2 (a), (b) and (c) show how a “suction effect” can be generated by the gas flow over one of these perturbations which increases the size of the disturbance which can then grow into a distinct wave. In time one of these waves could grow to a sufficient size to fill the pipe, even if only momentarily. Should the wave block the gas flow in this way, see Figure 4-2 (c), there will a

sudden increase in the thrust on the wave due to the upstream pressure and this will cause the blockage to accelerate.

As the blockage accelerated (and it appeared to accelerate more or less uniformly over its cross-section) it pushed the slower moving liquid ahead of it and grew in volume to become a slug, see Figure 4-2 (d).

At the front of the slug, gas may be entrained into the slug as small bubbles. These will be subject to the combined effect of turbulent shear forces generated by velocity differences between the slower moving liquid and the faster slug front, and buoyancy forces. Thus, a dispersion of small bubbles was observed which were transported through the body of the liquid slug.

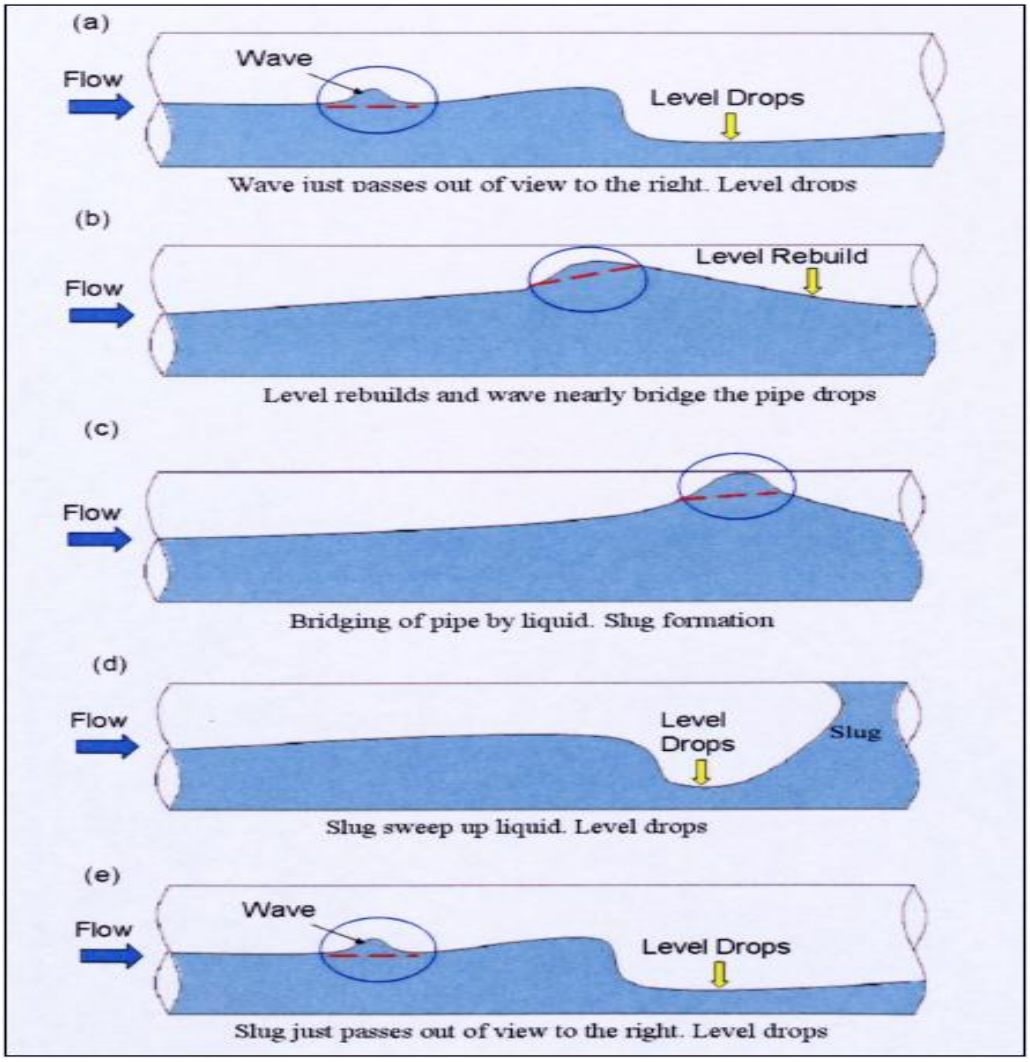

Figure 4-2 Slug initiation, growth and dissipation (Dukler and and Hubbard, 1975)

At the tail of the slug, liquid and gas are shed from the slug body. The shed liquid returns to the stratified layer, see Figure 4-2 (e) A small proportion of the shed gas remains within the liquid, but the majority of the gas returns to the gas layer above the liquid though, with the formation of slugs, this will be in the form of an elongated bubble. So long as the slug "picks-up" liquid at a faster rate than it "sheds" the liquid, it will grow. Eventually the slug gains liquid at the same rate as it "sheds" it, the slug stabilises (is “fully developed”) and its length remains constant. Obviously, if the “pick-up” rate is greater than the “shedding rate”, the slug grows; If the “pick-up” rate equals the “shedding" rate, the slug is fully developed with a stable length; If the "pick-up" rate is less than the "shedding" rate, the slug will dissipate.

As gas flow velocity increase slug dissipation occurs. With increase in gas velocity the degree of aeration of the slug increases until the gas forms a continuous phase through the slug at which point the slug no longer fully blocks the gas flow so the flow characteristics change. This point marks the beginning of "blow-though" and the commencement of the annular flow regime.

Nydal et al., (1992) found experimentally that the slug development distance, the pipe length necessary to attain quasi-stable flow, was between 300 and 600 pipe diameters. Once quasi-stable conditions were attained, the slug length had a mean value of between 12 to 15 pipe diameters.

Generally, the measured parameters for slug flow can be divided into four main categories: slug frequency, the number of slugs passing a specific point in a pipeline over a certain period of time; slug velocity, slug hold up and slug lengths. Figure 4-3 shows time and liquid holdup for flow regime identification using acoustic emission technology

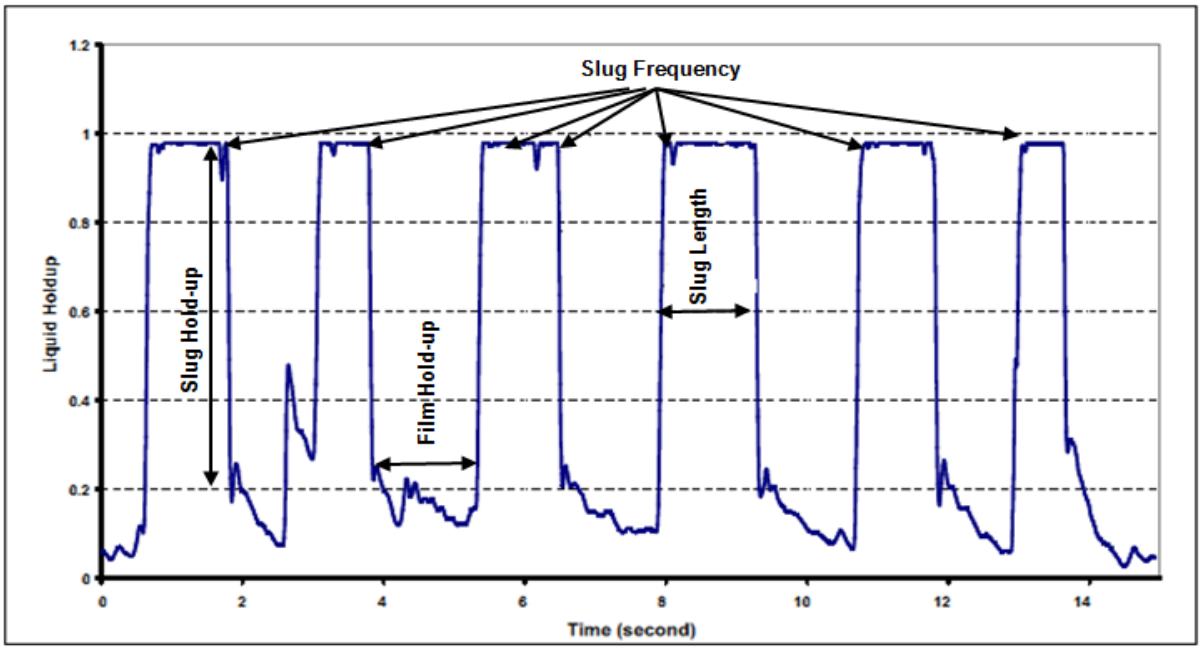

Figure 4-3 Slug signal captured by conductivity probes (Addali, 2010)

4.3 Slug flow types

Slug flow is commonly classified into two main types; terrain slug and hydrodynamic slug. Terrain slug is characterized by liquid accumulation at low points in the system. The upstream pressure builds up until the force it exerts is greater than the gravitational head of the liquid, thereby creating a long liquid slug that is pushed in front of the expanding gas upstream, see Figure 4-4. This type of slug occurs where there are low gas and liquid flow rates in downward inclined pipes before low points as can occur in a pipe line, riser or well (Yehuda, 1986).

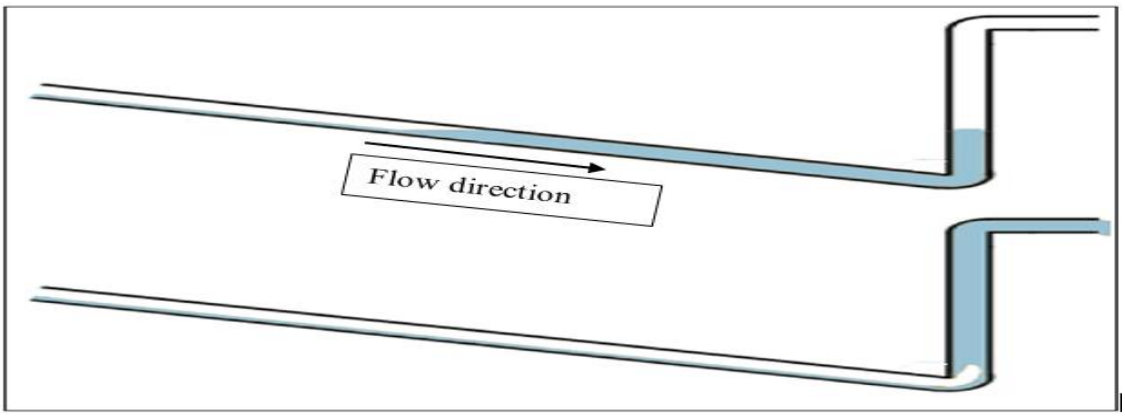

Figure 4-4 Schematic of terrain slug (Bratland, 2010)

Hydrodynamic slug for horizontal pipes has been discussed above. It is due to waves forming and growing at the gas/liquid interface and attaining an amplitude sufficient to completely fill the cross sectional area of the pipe. In vertical pipes, the hydrodynamic slug is associated with Taylor bubbles, (long gas bubbles) as shown in Figure 4-5. The hydrodynamic slug is relatively short compared to the terrain slug, but can occur over a wide range of flow conditions.

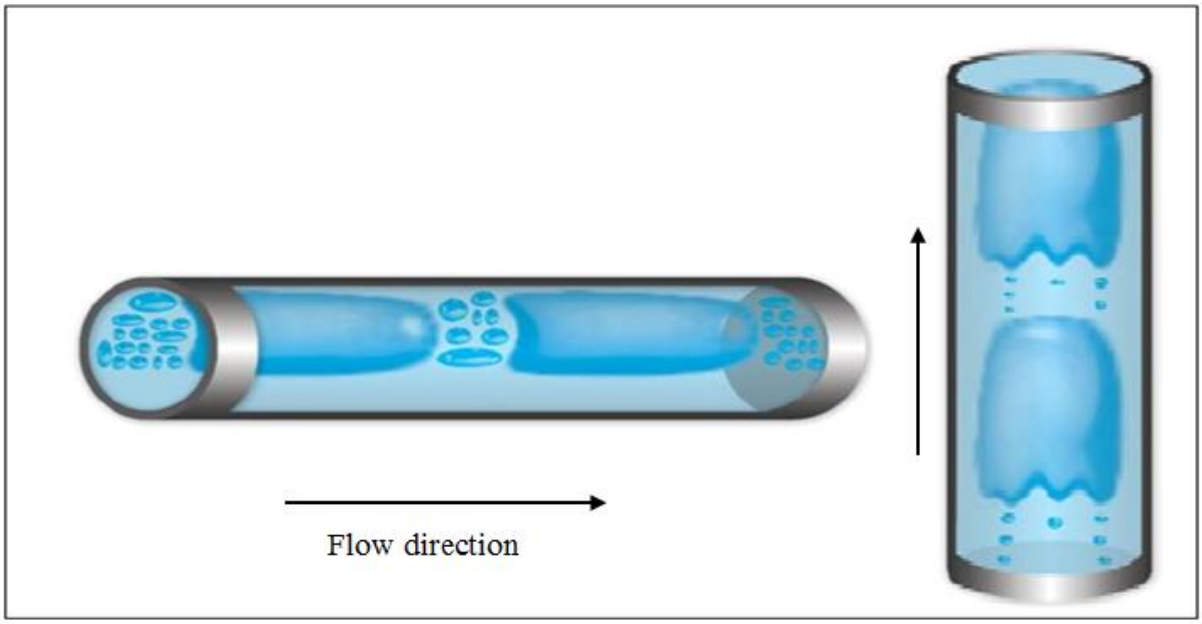

Figure 4-5 Hydrodynamic slug (Bratland, 2010)

In general, in the early and the late stages of production slug flow would be expected because of low flow rates, terrain, hydrodynamic slug flow would be expected for the rest of the time.

4.3.1 Slug flow benefits

Slug flow can play an important role in oil and gas industry in terms of production rate. With slug flow it is often possible to move larger amounts of liquids in smaller lines than with two phase flow. High convective heat and mass transfers resulting in very efficient transport operations. This is because of the very high liquid velocities in slug flow (Fabre and Line, 2010). Also, when high concentrations of sand exist in multiphase flow slugs can offer better sand movement in the pipeline.

4.3.2 Slug flow problems

Generally, slug flow is an unwanted phenomenon in oil and gas industry. Slug flow creates: high pressure fluctuations which might damage instruments; the flow arrives at the processing facilities unevenly causing flooding; fatigue is caused by the repeated hammering and impacts that occur with slug flow; there is an increase in deposits of hydrates and corrosion because of the density and heat capacity differences between gas and liquid.

Also, the intermittent behaviour of slug flow makes it difficult to measure and control which are undesirable phenomena for oil and gas operators.

4.4 Slug flow measurements previous work

Andreussi and Bendiksen, (1989) measured the void fraction for liquid slugs in two phase flow for two different diameter pipes both horizontally and inclined using a conductance probe. The test section was two 17 m lengths of transparent pipe of 50 mm and 90 mm diameters which could be interchanged. These sections could be fixed to an inclinable bench as shown in Figure 4-6. Water was circulated by using two different size centrifugal pumps. A high

pressure line was connected to supply air to the pipe, Two sets of rotameters were used to meter air and water, Two sets of conductivity rings were flush-mounted to measure void fraction of the liquid slug, and a PC was used to record and analyse captured signals.

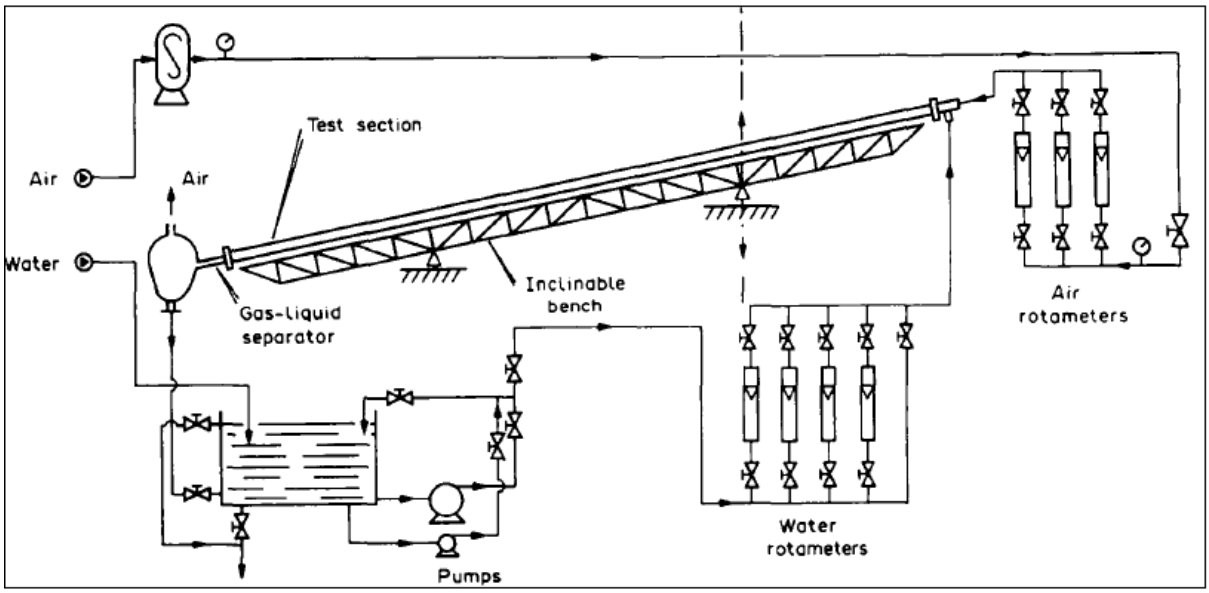

Figure 4-6 Schematic diagram of the test rig (Andreussi and Bendiksen, 1989)

After running the experiment at different pipe inclinations with different superficial liquid and gas velocities, the authors concluded that an empirical correlation could be developed which predicted the effect of fluid properties, pipe diameter and inclination on the void fraction in liquid slugs.

Nydal et al., (1992) used the conductance method to determine the mean slug characteristics (hold up, length and velocity) for a large range of gas and liquid velocities in horizontal pipes. They installed two conducting rings 1.32 m apart on a 17 m long and 52.9 mm internal diameter horizontal pipe. Tap water and air were circulated using a centrifugal pump and a compressor at a controlled pressure of 6 bar respectively. Calibrated rotameters were installed before the mixing section to measure single phase flow rates. Two quarters of rigs were positioned on the rings as triggers to monitor the flow condition. This test rig was linked to a data acquisition and analysis system. Nydal et al., conducted

the experiment at superficial liquid velocities (VSL), 0.6 - 3.5 m/s and superficial gas velocities (VSG) 0.5 - 20 m/s at standard conditions (1 bar, 20° C). They concluded that the developing slugs were shorter and more aerated than regular slugs due to shorter pipes or higher gas velocities; the initial developing length of slug flow increased when the gas velocity increased and decreased when the liquid velocity decreased. In most cases the slug length and slug hold up were log-normally distributed, and the measured slug bubble velocity was somewhat higher than single bubble velocity in pure liquid flow.

Reinecke et al., (1998) used an electrical tomographic imaging technique to measure the phase distribution of two phase slug flow in horizontal pipelines, see Figure 4-7. The test-rig includes a closed loop of transparent horizontal pipe with 59 mm internal diameter and length 48 m. Two nozzles were installed to inject air and water into the pipe. Orifices were equipped to measure the volumetric flow rates of the individual phases. A tomographic sensor was installed onto the pipeline. The gas and liquid flow rates were controlled for the range of aerated slug flow up to 3 m/s. The images were recorded for 1.8 second with a sample rate of 110 pictures/second. By using tomographic sensors, Reinecke et al., measured the conductance between the pairs of parallel wires of the sensors. This conductance was found to be proportional to the liquid holdup between the wires. They concluded that at different gas and liquid superficial velocities, slugs are formed with different lengths. They also noticed that the slug front is the area of dispersion of the gas phase, and the gas bubbles travels at the top of the pipe to coalesce with the bubble pocket following the slug.

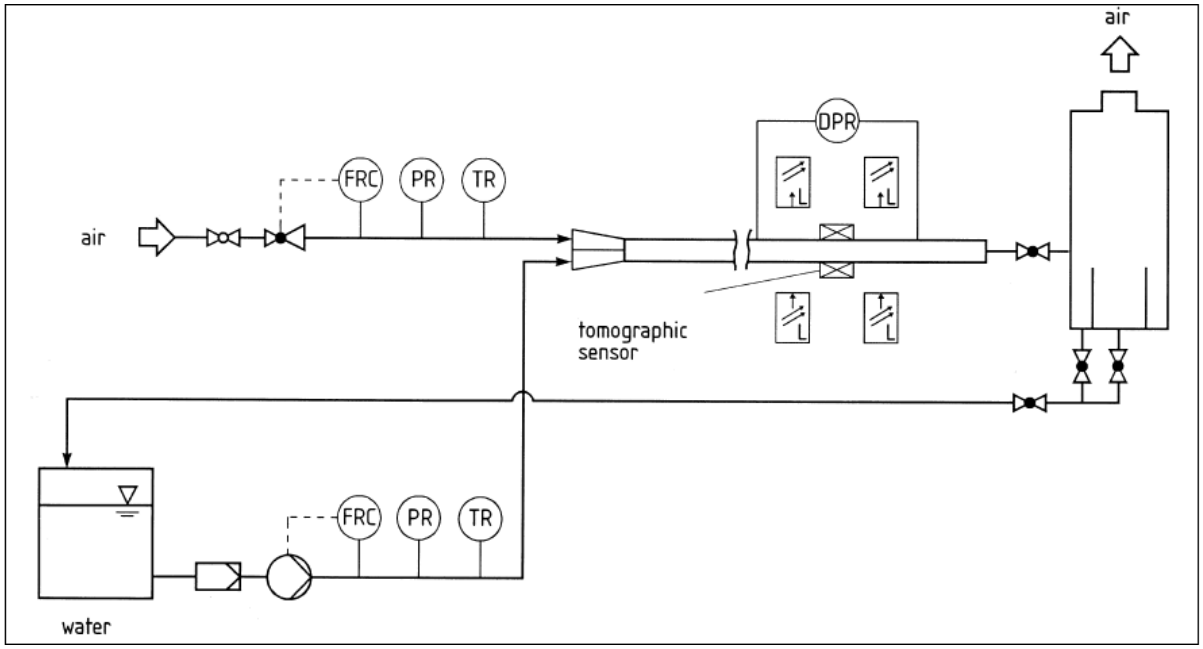

Figure 4-7 Tomographic imaging set up (Reinecke et al., 1998)

Emerson and Leonardo, (2005) measured the slug velocity of two phase flow in horizontal pipe using the capacitive technique. They measured the capacitance between two thin electrodes located on external surface of a dielectric pipe. The two sensing electrodes were mounted on two separate capacitance transducers circuits. One source electrode was connected to a sinusoidal signal source. Emerson and Leonardo calculated the mean bubble transitional velocity of the slug using the cross-correlation between the two signals from the transducers. The calculated mean slug velocities were compatible with the empirical correlation of Bendiksen (1984). The observed variance was attributed to the discontinuities of velocity along gas liquid flow. This led to determination of time delay using a cross-correlation method. They concluded that this technique has the capability to study the behaviour of gas-liquid flow in pipes.

Al-Lababidi and Sanderson, (2006) used ultrasonic technique to measure the slug transitional velocity in two phase, gas/liquid, flows in a 22 m long horizontal plastic horizontal pipe with an inner diameter of 50 mm. Two pairs of 1 MHz ultrasonic transducers were mounted on the pipeline separated by a distance of 180 mm. A conductivity probe was used to validate the results. After running the

experiment with different liquid and gas velocities through the range of slug regime (up to 1.03 VSL and 2.02 VSG), they used cross-correlation to calculate the time delay between the two ultrasonic transducers signals, and between the conductivity probe signals. This study concluded with the decision that the ultrasonic technique has the capability to determine the slug transitional velocity with a percentage error in the range 2.3 -18 % relative to the conductivity probes results.

Gu and Gue, (2008) carried out an experimental investigation of slug development using horizontal two-phase flow. They connected a centrifugal pump to supply tap water to a 50 mm internal diameter and 16 m long horizontal pipe. Compressed air at 1.0 MPa was fed using a screw compressor to a buffer vessel. An orifice plate was used to filter out the compressed air. Five entry points were used to introduce stable liquid and air flows to prevent large hydraulic gradients downstream of the entry. Twenty pairs of parallel wire conductivity probes were mounted at 10 different locations on the horizontal pipe to track slug initiation and evolution. The sample frequency of each pair of probes was varied from 0.5 - 2.0 kHz. This experiment was conducted at the superficial liquid velocity range of 0.1 - 2.3 m/s and superficial gas velocity range of 0.5 - 8 m/s. Cross correlation was used to calculate slug velocities from adjacent pairs of probes. Gu and Gue found that the slug initiation mechanism depended only on superficial gas velocity (V_{SG}). When V_{SG} < 3.0 m/s, the interfacial waves of the stratified regime grow and bridge the pipe near the entrance. Increase of V_{SL} led to the fully developed slug frequency. The slug frequency along the pipe also increases when V_{SL} increases with V_{SL} < 3.0m/s and V_{SG} > 3.0 m/s, the slug initiation is stochastic.

Al-Safran, (2009) investigated slug frequency in two phase flow in horizontal pipes using capacitance sensors. He used a test rig shown in Figure 4-8 which included: a 50.8 mm internal diameter pipe in the form of a flow loop 420 m long, a centrifugal pump to feed the liquid phase from a storage tank, a two-

stage compressor to supply air, micro-motion mass flow meters to measure gas and liquid flow rates. Pressure transducers and temperature transmitters were fitted to measure pressure and temperature respectively at different points in the flow as shown in Figure 4-8. Three transparent test sections (B, C and D) were used to measure slug frequency, liquid hold-up, and length by the mounted capacitance sensors as seen in Figure 4-8. The length of the pipe used in this study gives the opportunity for the slug to be initiated at three different slugging mechanisms, hydrodynamic, terrain and severe slugging. Al-Safran concluded that the mechanism of slug initiation has a significant effect on slug frequency which is dependent on pipe length and decreases for two phase slug flows.

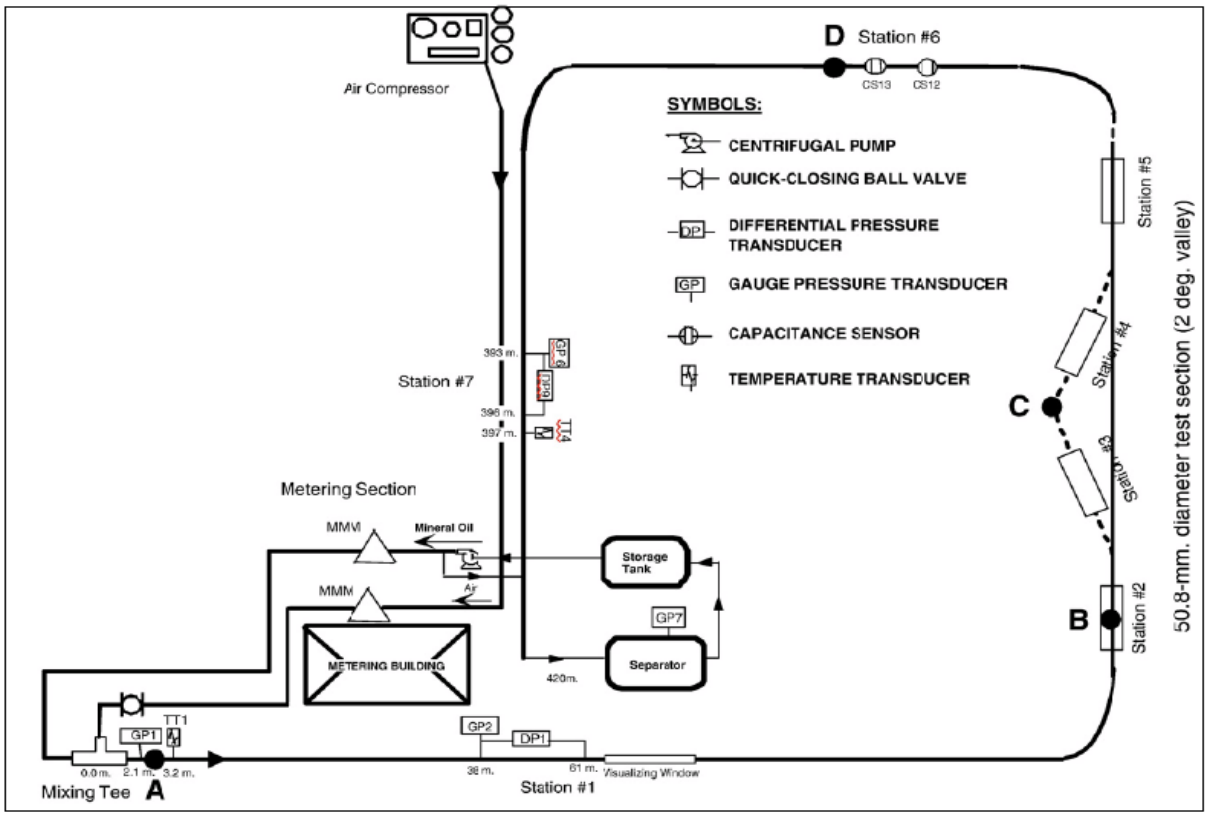

Figure 4-8 Overall test facility (Al-Safran, 2009)

Fusheng and Feng, (2010) used a local cross-correlation method to determine slug flow velocity for gas/liquid flow in a horizontal pipe. A 20 m of stainless steel pipe with an inner diameter of 50 mm was used. An organic glass window

to observe the flow regimes was located at the backend of the stainless steel pipe. A cross-section information system was installed downstream of the pipe to make sure that the flow rate of water and gas was stable and the regime was well developed. Based on the positions at which the cross-correlation was performed, the electrodes were sorted into three kinds; electrodes in water, electrodes in gas and electrodes at the interface of water and gas. To record the flow rate stage of the slug regime, a high speed camera was used.

On the basis of the behaviour of the electrode voltage cross-correlation the researchers concluded that cross-correlation of the second kind (electrodes in gas) was more accurate than the other two. This was because gas slug occupies the upper pipe whereas the water phase occupies the bottom. Therefore, gas area electrodes were more sensitive to the phase distribution changes. Fusheng and Feng summarised their research by saying that the experimental error was within 10% on the whole but this error increases when the mixed velocity increases.

4.5 Flow regime recognition - previous work

Zhou et al., (2008) identified the flow regimes in gas/liquid two phase flow in horizontal pipes by using a digital high speed camera system. The experimental facilities were installed as shown in Figure 4-9 which included: a transparent pipe section of 50 mm diameter and 2 m length inserted 3 m downstream of the gas/liquid mixture point. The fluid flow control system included a water tank and centrifugal pump, an air compressor and two phase flow mixer. An electromagnetic flow meter and orifice flow meter fitted into the two phase mixer were used to measure water and gas flow rates respectively; a high speed video camera (with maximum resolution of 1536 x 1024 and highest frame frequency of 10000 Hz) was fixed opposite the test section. The researchers performed the experiment at different liquid flow rates (0.1 - 15) m^3/h and air flow rate (0.5 - 48) m^3/h. The experiment was conducted at pressure of 1.01 x 105 Pascal and temperature of 20 C˚. The captured images of the different flow regimes were acquired at 512 x 192 resolution and 125 frames per second.

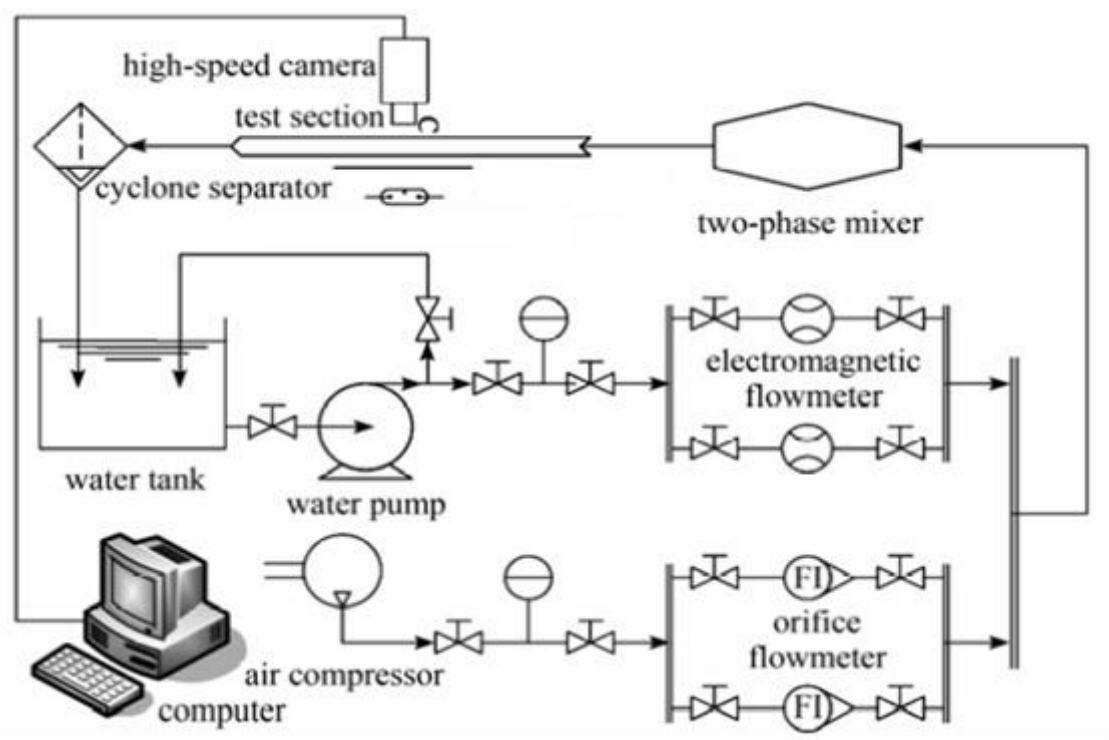

Figure 4-9 . **Schematic diagram of gas/liquid two phase flow experimental system** (Zhou et al., 2008)

Three hundred and fifty groups of images were acquired which covered the whole range of flow regimes. Zhou and his colleagues used image processing to extract the images invariants and grey level co-occurrence matrix texture features. A multi-feature fusion and support vector machine was used to reduce any non-essential factors and the dimension of flow regime samples to differentiate and classify flow regimes. They concluded that the combination of high speed camera, multi-featured fusion and the support vector machine could identify two phase flow regimes in horizontal pipes.

Kishore et al., (2010) used digital signal processing techniques to identify flow regimes in horizontal pipes. The test-rig shown in Figure 4-10 has transparent Perspex pipes (P1 and P2) each of length 2 m and 25.4 mm and 12.7 mm diameters respectively, connected to the water tank as a1 and a2. A centrifugal pump supplied water and an air compressor fed air into the pipeline; water and gas flow rates were controlled by Rotameters upstream of the test sections.

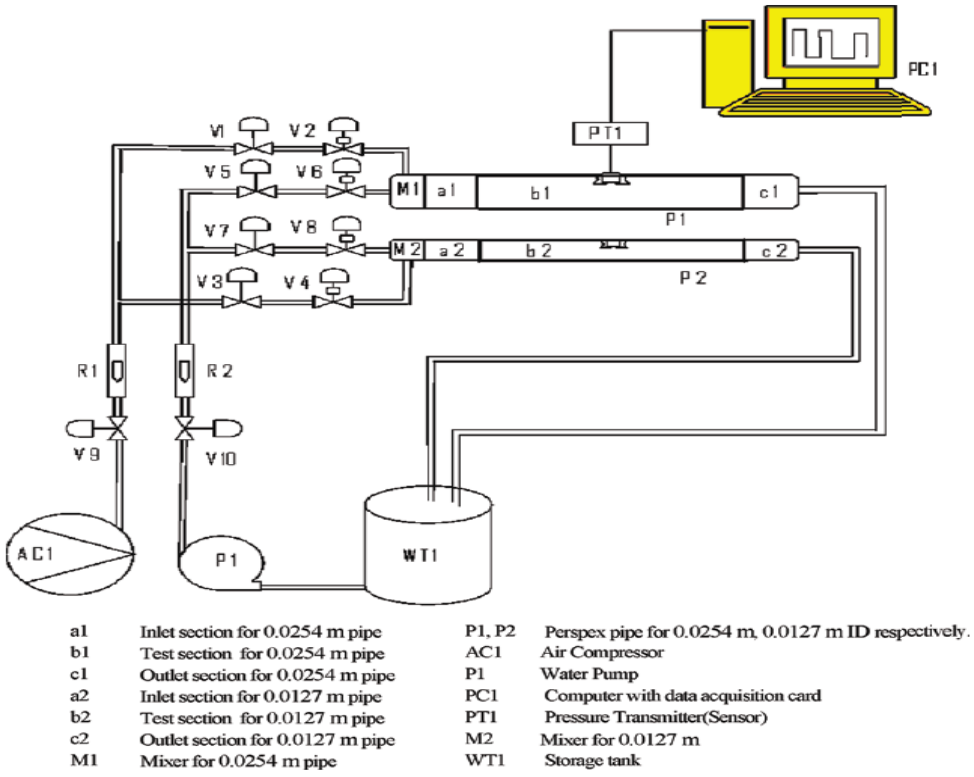

Figure 4-10. **Schematic diagram of gas/liquid two phase flow experimental system** (Kishore et al., 2010)

Kishore and his colleagues installed valves to control the gas and liquid flow rates (when the 25.4 mm diameter pipe is used to collect data, the valve to the 12.7 mm diameter pipe was closed and vice versa). Unfortunately, the authors did not explain why they chose the given Perspex test sections. A pressure transmitter was connected to the test section to measure the pressure inside the pipe and capture signals continuously. These signals were acquired for analysis and flow regimes differentiation using a National Instrument (PCI-6221) data acquisition card. The results showed that when the superficial gas velocity was increased at constant superficial water velocity, different flow regimes were generated in the pipe. By determining the type of flow regime in the pipe based on the flow velocity, the adjusting and separation efficiency can be increased. This is because different flow regimes have different separation efficiencies. A matlab code was generated to show which type of flow regime was present in the pipe so that separation efficiency can be easily controlled. Kishore et al.,

concluded that two phase flow regimes can be identified using digital signal processing techniques such as cross correlation.

Sun et al., (2006) identified gas/liquid flow regimes using a Venturi meter. The experiment was conducted using the multifunctional flow equipment shown in Figure 4-11.

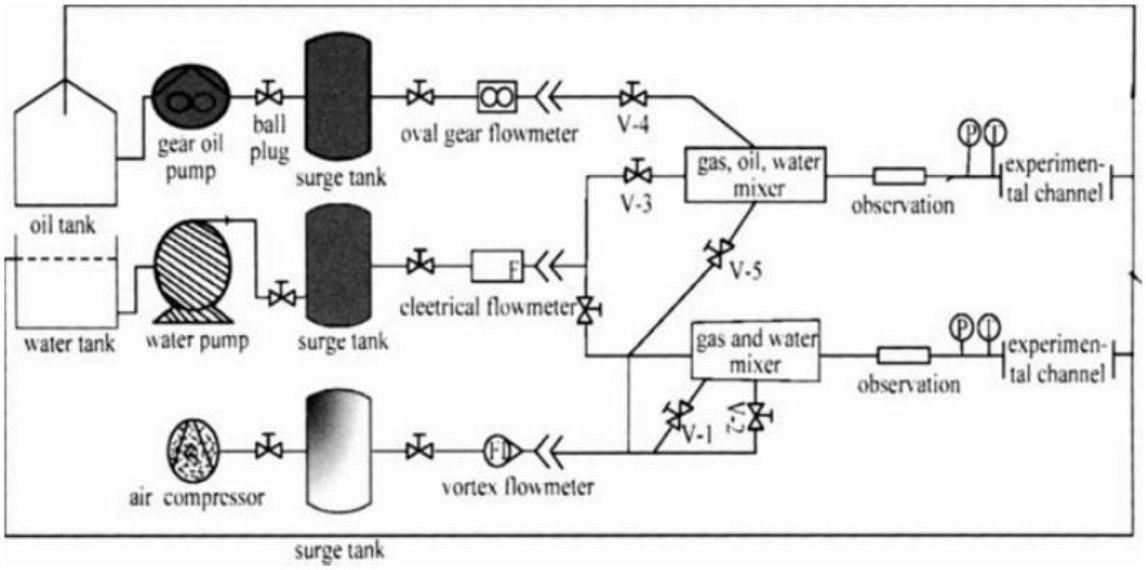

Figure 4-11. **Schematic diagram of gas/liquid three phase flow apparatus** (Sun et al., 2006)

A 4 m length of 50 mm diameter horizontal pipe was used upstream of the test section to ensure fully developed flow. Air and water were supplied through standard flow meters. A venturi meter with 0.5501 and 0.5768 ratios of throat diameter to tube diameter was used. The differential pressure was measured using a Keller differential pressure cell and the output signals were collected using an Advantech Company PC-104 data acquisition card. The experiment was conducted at superficial liquid flow rate of (0.5 - 10.5) m^3/h and gas flow rate of (0 - 15) m^3/h. The collected differential pressure signals were processed by using a Hilbert Huang Transform (HHT). These signals were decomposed into different intrinsic modes to determine the energy fraction. The authors found a correlation between the energy fraction, mean residual value and two phase flow regime. They concluded that the energy fraction of slug and plug

regimes are distinguishable but bubbly flow and single phase flow regimes are very small and difficult to identify. However, the mean residual value function can be used to identify bubbly flow and single phase flow.

Rahiman et al., (2010) used ultrasonic computerized tomography to identify two phase flow regimes. An acrylic pipe of 115 mm outer diameter and 6mm wall thickness was used as the experimental vessel. Sixteen pairs (transmitters and receivers) of ultrasonic transducers with a resonant frequency of 40 kHz were placed non-invasively on the experimental vessel surface as shown in Figure 4-12.

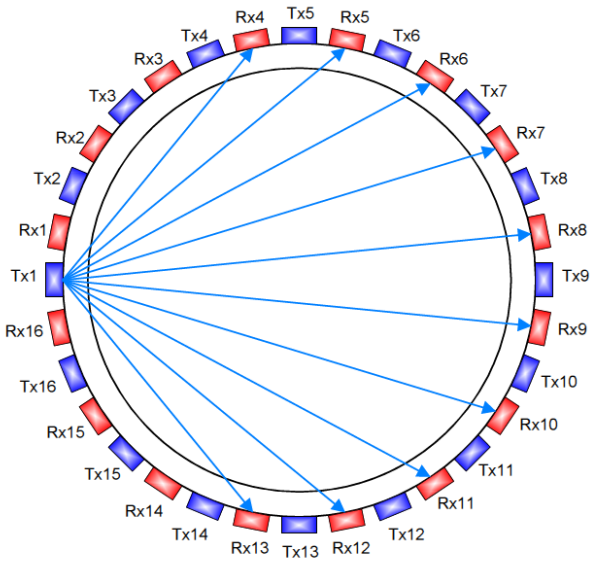

Figure 4-12. Projection geometry of measurement section (Rahiman et al., 2010)

The electronic measurement system includes a signal generator, signal conditioning circuit and data acquisition system to the control ultrasonic transducers. Tx1, …Tx16 represent the transmitters and Rx1, … Rx16 represent the receivers. At each scan, a total of 16 observations were made. So that 160 independent measurements were obtained. They used a Linear Back Projection (LBP) algorithm to combine projection data from each sensor with its computed sensitivity maps and Hybrid Reconstruction (HR) algorithm to determine the condition of the projection data and improve the reconstructed

images. Rahiman et al., concluded that ultrasonic computerized tomography is a feasible and effective way to identify liquid and gas flow regimes.

Ghosh et al., (2012) identified two phase flow regimes by using conductivity probes. A vertical pipe loop of 25.4 mm diameter was constructed as shown in Figure 4-13.

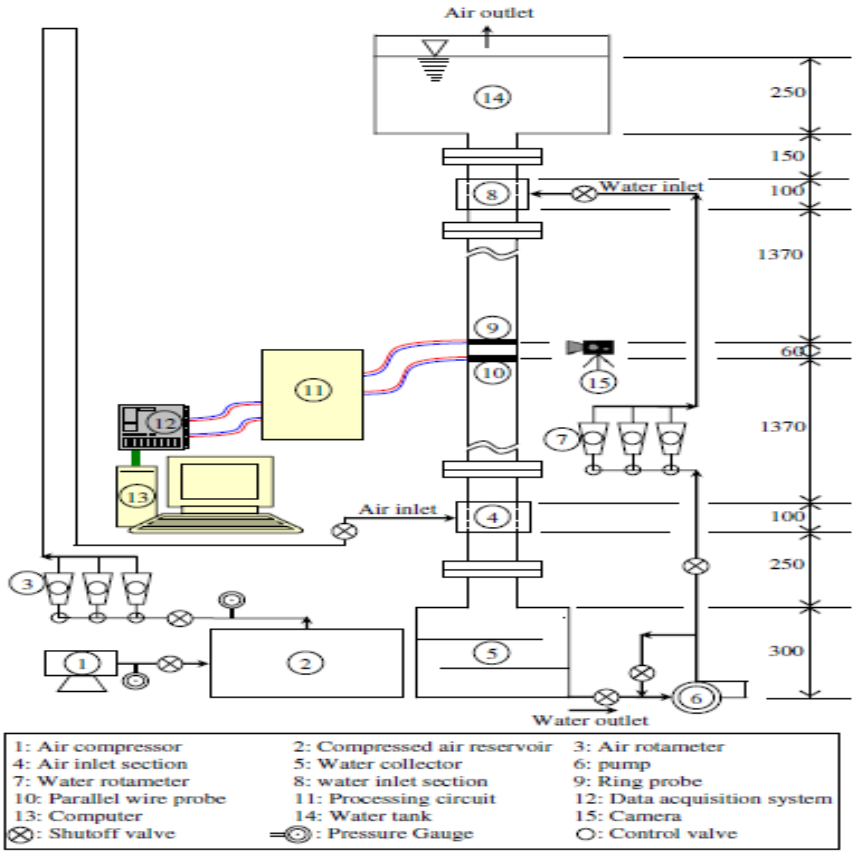

Figure 4-13. **Schematic view of experimental setup** (Ghosh et al., 2012)

The test section was a non-conducting Perspex pipe to allow visual observation of the flow and simultaneously convenient to install the probes. A water tank was connected to the top inlet of the test section via a water Rotameter and valves to meter and control the flow. The air system was supplied by an air compressor with an air reservoir, shut-off and control valves, and pressure gauges. The air passed through an air Rotameter to the bottom of the test section. Two conductivity rings and parallel wire conductivity probes designed to characterise the flow regimes were mounted on the test section and connected

to the data acquisition system. A Sony DSC camera fixed on an adjustable stand was used to photograph and film the flow regimes at different water and air flow rates.

The superficial water velocity was increased at constant superficial air velocity and reading taken for each run. The superficial air velocity was then changed to another value and the procedure repeated. The superficial water velocity range was from 0.1974 to 5.2627 m/s and superficial gas velocity range was from 0.0066 m/s to 0.1447 m/s. For each run, conductivity probe signals were recorded using a data acquisition system; and photos and films were recorded using the digital Sony camera. Three different neural network functions (a multi-layer feed-forward neural network, a multi-layer radial basis function; and a GA-tuned multi-layer radial basis fuction) and probability density function were used to identify the flow regimes. Ghosh et al.; concluded that the designed ring probe could not distinguish the flow regimes adequately due to the variations in ring probe signals for the different flow regimes. The data density was always more for higher normalised voltage and there was no data for lower normalised voltage in the ring probe signals. The parallel wire probe signals were sufficient to distinguish and identify the flow regimes.

4.6 Conclusions

The techniques employed by the above researchers to investigate the slug flow parameters have limitations. The accuracy of conductivity rings and ultrasonic techniques, for example, decreases as the gas void fraction (GVF - ratio of the volumetric flow rate of the gas to the total volumetric flow-rate) in the pipe increases. Conductivity rings are affected by temperature, i.e., when the temperature increases, the accuracy of conductivity measurements decreases. Thus, there is a need to investigate another technology that overcomes such limitations and accurately measures the slug flow velocity in two phase flow in horizontal pipes. This research investigates the capability of acoustic emission technology to detect and measure the slug flow velocity of two phase flow in horizontal pipes.

Chapter 5 Experimental Setup and Methodology

This chapter describes the test rig facilities employed in this research project to recognize flow regimes, detect and measure slug flow velocity in two phase, water/gas flow. It also presents the methodology used.

5.1 Test rig facilities

The test rig has to be suitable for an investigation into the applicability of AE technology to the recognition of two phase flow regimes, to detect slug regime in two phase flow (gas/water) and measure slug velocity in horizontal pipes.

Figure 5-1 shows the general facilities and arrangement of the test rig. Modifications will be discussed in the next section, Section 5.2 Methodology of experimental work. The core of the test rig was the 50 cm (2 inch) ID horizontal PVC pipe and a supply system designed to provide different velocities of water and air in a two phase. The following subsections describe the main facilities of test rig in detail.

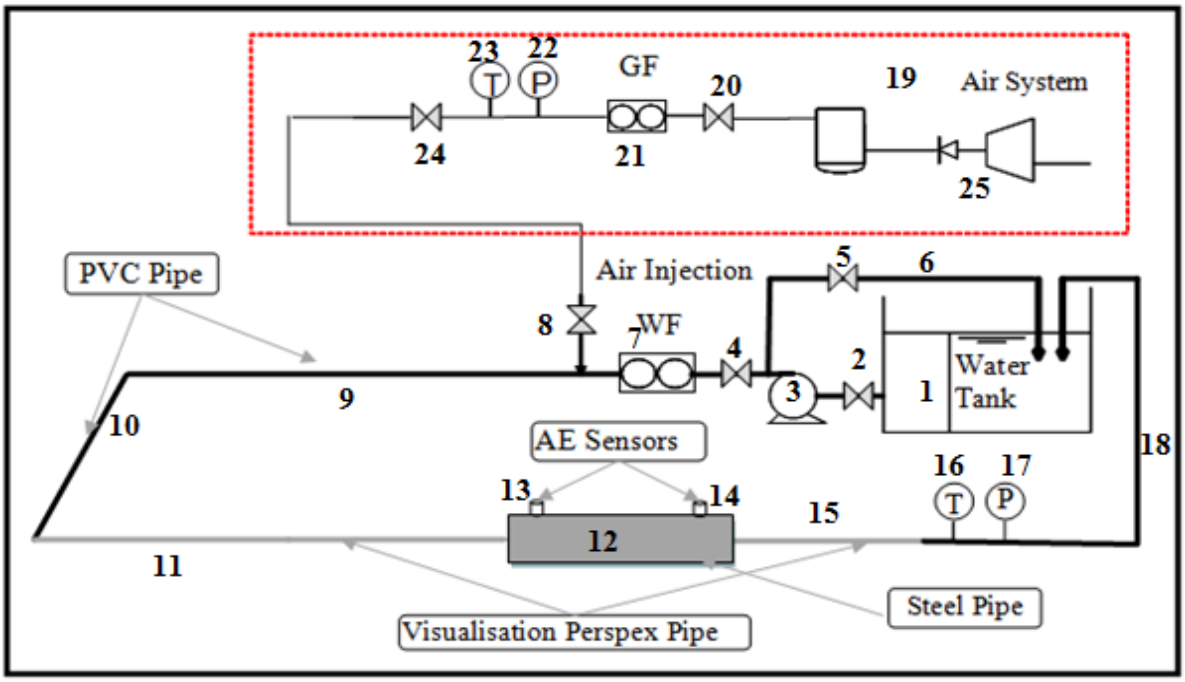

Figure 5-1 Experimental setup for two-phase slug velocity measurement. (WF = Water flow meter; GF = Air flow meter; T = Thermocouple; P = Pressure measurement)

5.1.1 Water supply system

A 2 m^3 fiberglass tank (1 in Figure 5-1) was used to store the water that feeds the test rig and collect return flow from the closed loop through a PVC pipe (18). The tank was physically separated into two (suction and return sides), to ensure bubbles and debris from the return flow did not enter the pump. This tank was connected to the test rig through a Worthington Simpson centrifugal pump (3) with a maximum capacity of 40 m^3/hr and 5 bar discharge pressure. To avoid solids and debris that had settled at the bottom of the tank entering the flow, the suction side of the pump was 20 cm above the tank bottom.

A throttling valve (4) was used to control the water flow rate which was metered using a Krohne Altoflux electromagnetic flow meter (7) with capacity of 20m^3/hr. This was placed upstream of the air/water mixing point. A by-bass line (6) was inserted, to recycle any extra flow produced as a result of the high capacity of the centrifugal pump, to the tank through a controlling valve (5). The valve was adjusted to ensure smooth working of the pump and minimise hydraulic noise.

5.1.2 Air supply system

An Ingersoll Rand compressor unit with maximum of 10 bar output and an integrated air tank of 500 litre capacity and maximum of 12 bar working pressure was used to supply air to the test rig (25).

The air tank was connected via a 25 mm (1”) ID pipe and settling tank (19) to an isolating valve (20) and then to an Endress and Hauser Proline Prowirl type 72F25 air flow meter (21) with a flow range of 3-100 m^3/hr at 9 bar. The air pressure was measured using a pressure transducer (22) and the air temperature was measured using a thermocouple transducer (23) and the air then passed through a second isolating valve (24). A brass gate type valve (8) was installed downstream of the gas flow meter to control the air flow. The metered air flow was injected into the closed loop pipe through the 2” PVC pipe.

5.1.3 50 mm (2 inch) ID closed loop horizontal pipe system

A total length of 22 m of 50 mm ID pipe was used to form a closed loop system. The water tank (1) and air supply (8) were connected to the test section via a 17.4 m length of 50 mm ID PVC pipe (9, 10 and 11). This length of the pipe was sufficient to give a fully developed flow regime before the test section (12) which was a 600 mm length of 50 mm ID steel pipe. Immediately before and after the test section there were lengths of transparent Perspex pipe. This allowed visual observation of the flow for a distance of 2.5 m before (11) and 1.5 m after the test pipe (15).

A thermocouple was installed to monitor the water flow temperature (16) and the water pressure was measured using a pressure transducer (17).

The AE sensors of the first stage of the experimental work were installed at the ends on the stainless steel test section (13 and 14).

5.1.4 Data acquisition system

All measured data such as temperatures, pressures, gas flow rate and liquid flow rate were acquired using a Data Acquisition System (DAS) of a 12 channel PC. The data were collected by means of 4-20 mA HART (Highway Addressable Remote Transducer Protocol) from the flow meters and transduces via a 32 channel parallel port multiplexer (SCB-68) after being converted to an appropriate digital signal. A runtime 10.0.1 version of LabVIEW 2010 ‘National Instrument’ was used to collect the data which was displayed on a computer monitor after being converted to engineering units, for example m^3/hr. to m/s in the case of air and water flow rates. A 2.8 GHz Pentium processor, 250 GB hard disc capacity and the Windows 7 operating system of the personal computer was used to run the Labview software.

5.1.5 Acoustic Emission (AE) system

A two channel Physical Acoustics Corporation (PAC) AE system fitted with a PCI-2 data acquisition card was used for monitoring and acquiring AE data by running AEwin of PCI-2 software. 2.4 GHz, 180 GB hard disc capacity and

windows XP operating system was used to run the AE system. Two types of AE sensors, wideband (WD) (Figure 5-2 A) and Pico (Figure 5-2 B) sensors, supplied by the PAC were used in this experiment. Wideband sensors with 18 mm diameter, 17 mm high and frequency range of 100-1000 MHz were used to detect the flow by mounting them on the stainless steel pipe section. Pico sensors with 5 mm diameter, 4 mm high and frequency range of 150-750 MHz were used to detect the flow. These were mounted on a prismatic cylinder, M12 hexagonal bolts and flush rings waveguides as shown in figures 5-10, 5-13 and 5-15.

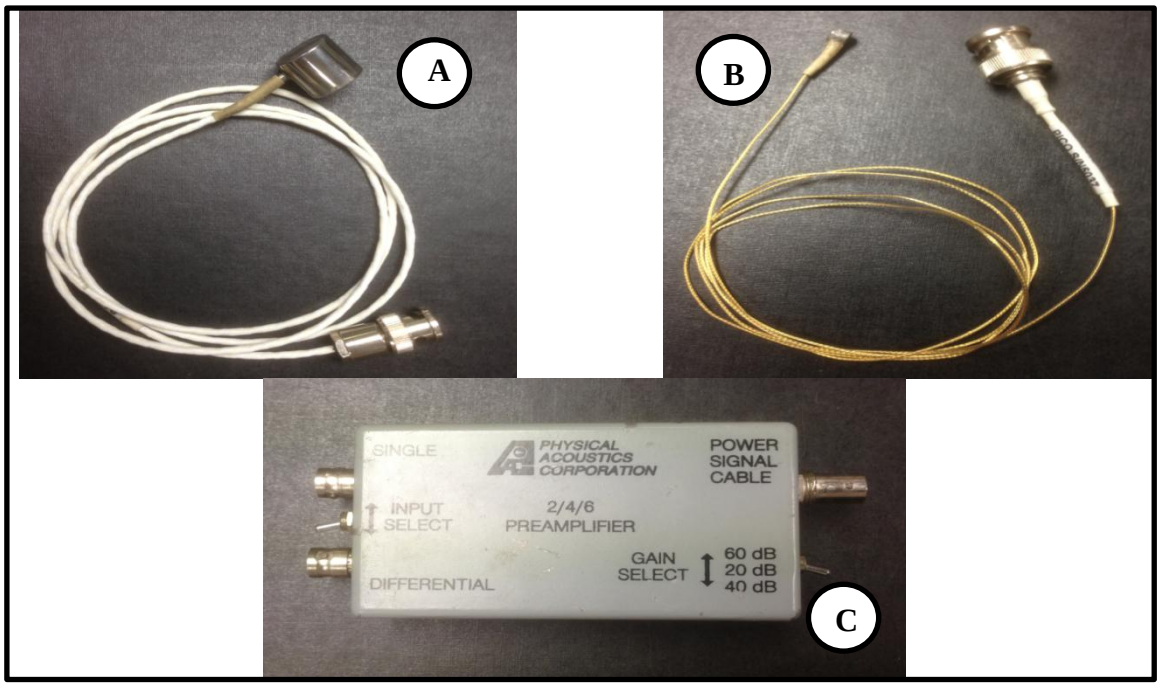

Figure 5-2 PAC Acoustic Emission System: A- wideband sensor; B- Pico sensor& C- 2/4/6 type preamplifier

The AE sensors were connected by coaxial cables to the two channels of the PCI-2 data acquisition card through PAC Preamplifiers (2/4/6 type as shown in Figure 5-2 C) adjusted to magnify signals to 40 dB. The AE signal parameters were sampled at 2 MHz for 30 seconds for each superficial air and water velocities. Also, AE streamed waveforms were captured for every crossing of a

32 dB threshold for a duration of 3 seconds throughout the entire test run for all air and water two-phase flows.

5.2 Experimental methodology

5.2.1 Non-intrusive methods

In determining slug flow velocity using AE sensors, two approaches were explored. The first method was non-intrusive and the AE sensors were placed 40cm apart on the outside surface of the steel pipe using three different fixing systems, see Figures (5-3), (5-4) and (5-5).

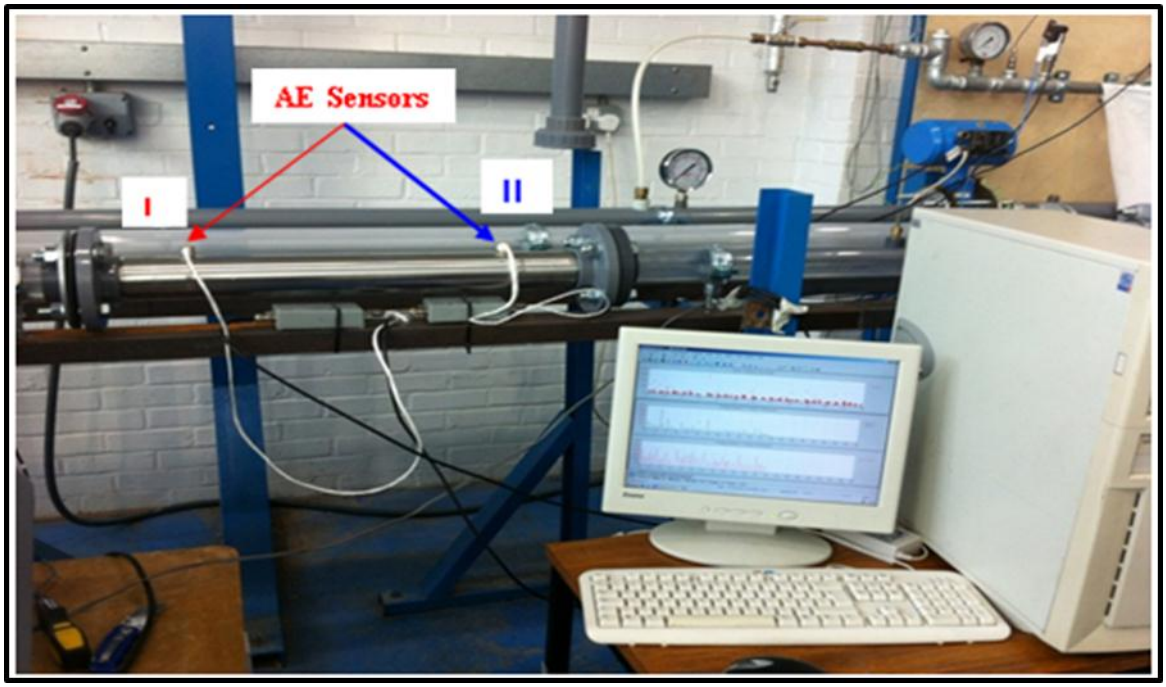

Figure 5-3 AE system data acquisition system and AE wideband sensors installation on outside surface of steel pipe

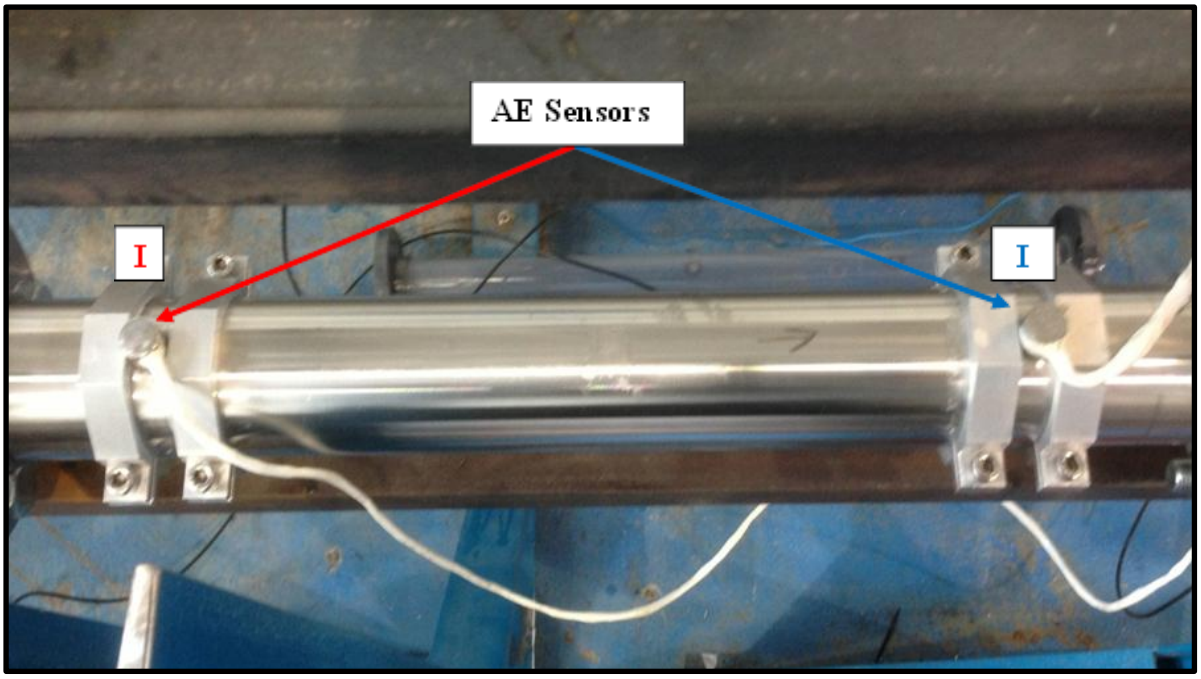

Figure 5-4 AE wideband sensors clamped to outside surface of steel pipe using clamp type I

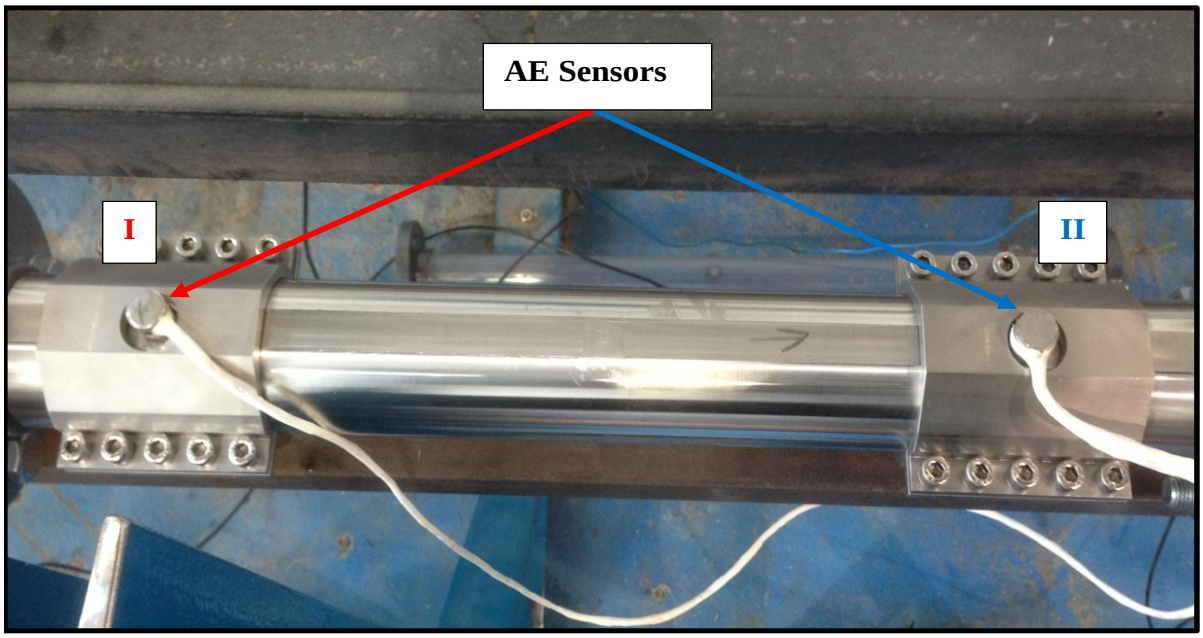

Figure 5-5 AE wideband sensors clamped to outside surface of steel pipe using clamp type II

Two AE broadband sensors were mounted on the outside surface of the stainless steel section 40cm apart as shown in Figures (5-1) and (5-3). After

processing the signals detected by the AE system for different superficial gas and liquid velocities, it was clear that the signals were noisy and it would be difficult to measure slug velocity. The start and end of each burst signal could not be distinguished. This can be seen clearly in Figure (5-6) which represents the waveforms of AE signals detected using broadband transducers for flows of 1.1 V_{SL} and 1.02 V_{SG}.

Normally, AE technique has been used to determine the energy released from static (fixed) source locations. However, the energy source (slug) in this experiment is not stationary but moving through the pipe and at each stage (upstream, underneath and downstream AE sensors) will be transferring AE energy into the pipe which will be transmitted by the steel walls. Consequently, the AE sensors capture signals from the entire length of steel test section through which the slugs are moving. This leads to the difficulty of defining the start and end of each burst signal and, in fact, the arrival time for each burst signal cannot be detected with this simple design of the test rig.

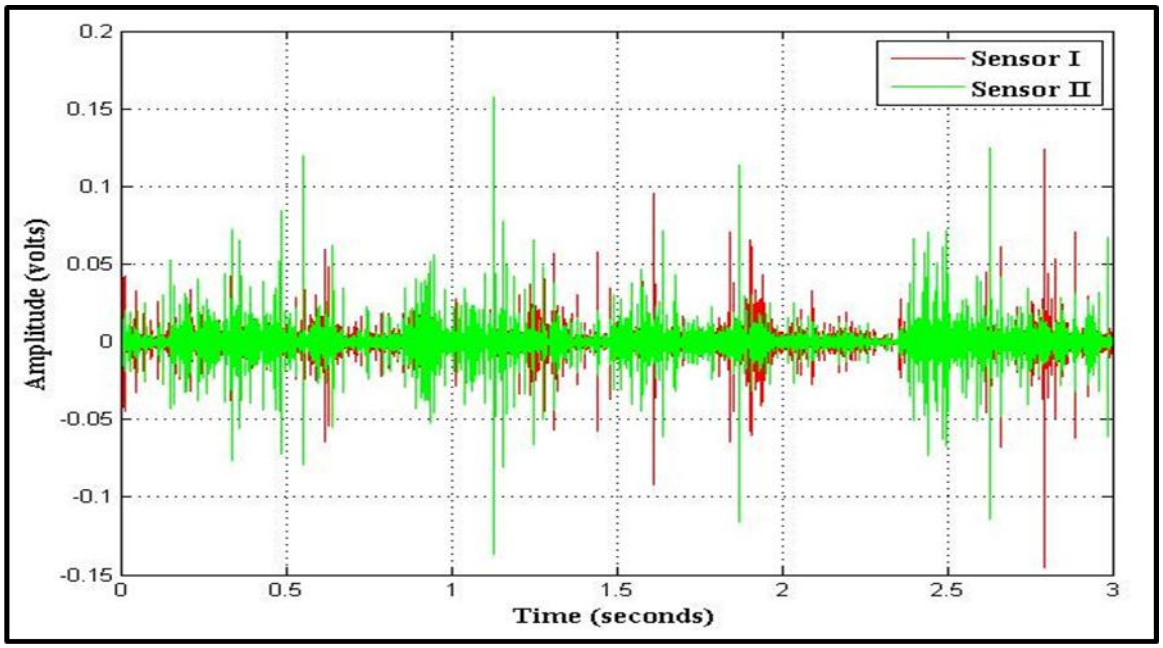

Figure 5-6 AE waveform for 1.1 V_{SL} and 1.02 V_{SG} sensors placed on the outside of the stainless steel test pipe

5.2.1.1 Mounted AE sensors on a clamped steel pipe

To avoid detecting travelling AE generated signal through the pipe and capturing only signals that pass underneath AE sensors, two types of clamp-on were designed, constructed and fitted onto the steel pipe section, see Figures (5-4) and (5-5) to attenuate the AE signals being transmitted through the material of the pipe wall (upstream and downstream of AE sensors).

After positioning the first set of clamps as shown in Figure (5-4) the recorded AE signals at 1.1 V_{SL} and 1.02 V_{SG} are as presented in Figure (5-7). The background noise was reduced in terms of the amplitude compared to the previous experiment but not sufficiently. A further attempt with a larger clamp was made, see Figure (5-5) and the recorded AE signals at 1.1 V_{SL} and 1.02 V_{SG} are as presented in Figure (5-8). Unfortunately the AE waveform signals of two sensors cannot be distinguished and it was decided that this modification was not successful and slug flow and its velocity could not be detected by using such designs.

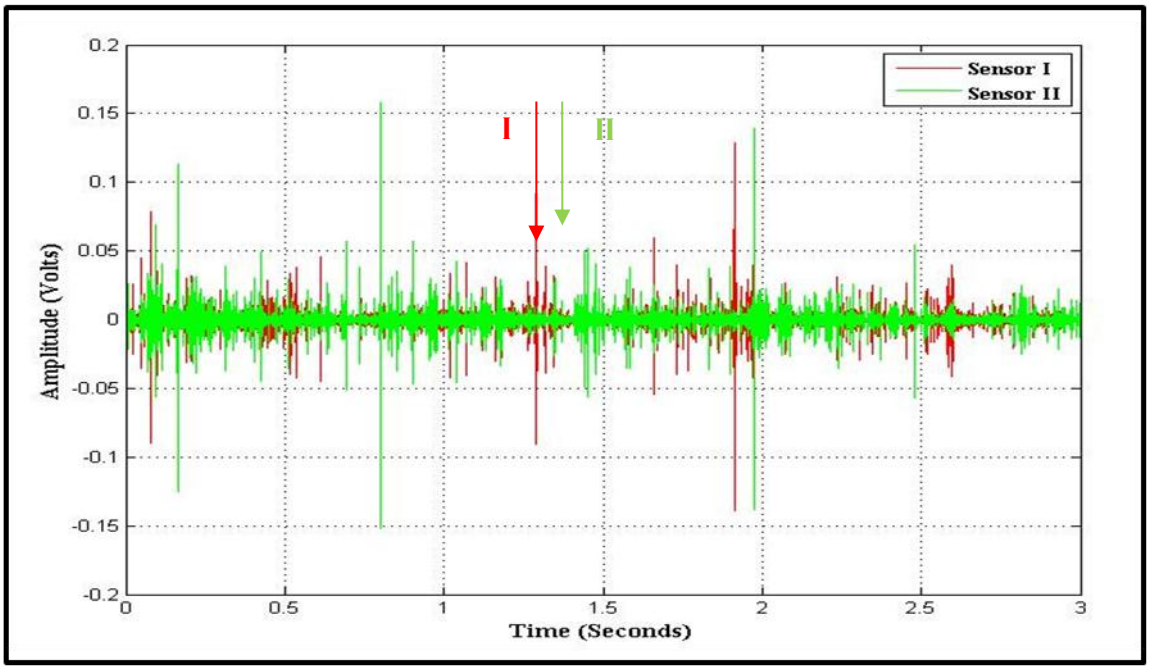

Figure 5-7AE waveforms at 1.1V_{SL} and 1.02V_{SG} using clamp I stainless steel test pipe

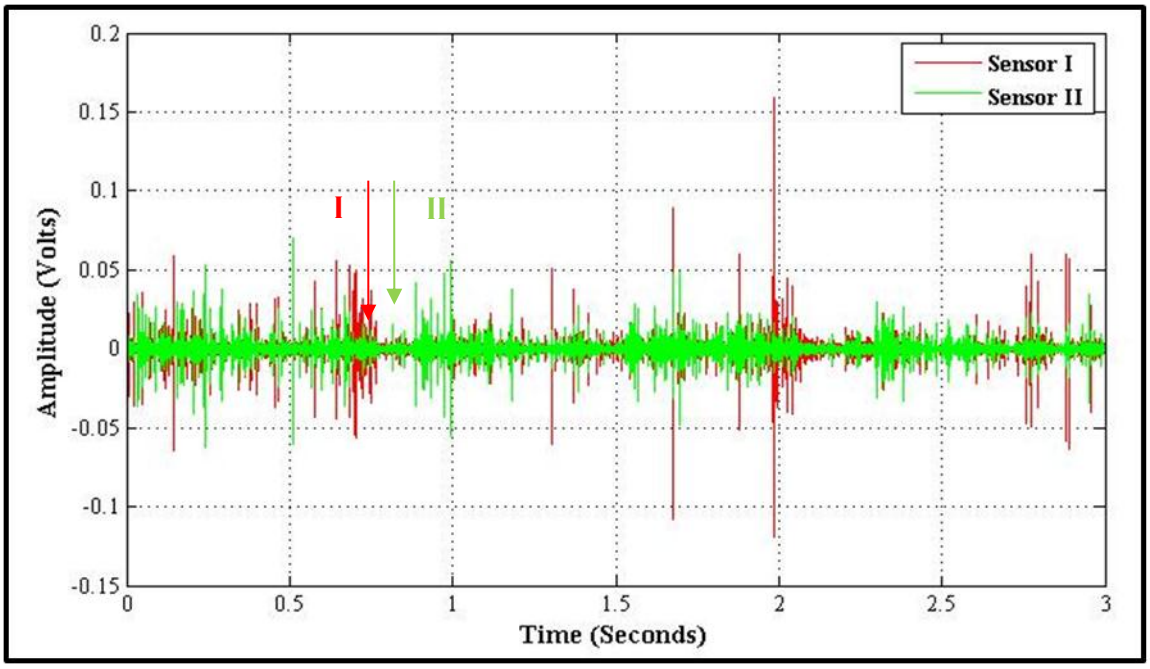

Figure 5-8 AE waveforms at 1.1V_{SL} and 1.02V_{SG} using clamp II on stainless steel pipe

5.2.2 Intrusive method

The second method involved replacing the steel test pipe with a Perspex pipe of the same diameter. The Perspex will attenuate the AE waves as they travel through the pipe walls thus reducing background noise and, effectively, enhancing the slug signal as it passes the sensor. Because Perspex is such an effective attenuator of high frequency elastic waves; the AE sensors are attached to wave guides which pass through the Perspex wall, in this case bolts and flush rings. This ensures direct contact between the AE sensors on the outside of the Perspex pipe and the flow inside the pipe as shown in Figures (5-9), (5-12) and (5-14). The ends of the bolts and rings on the inside of the pipe were profiled to match the pipe curvature, i.e., they were flush with the internal wall of the pipe so that the flow was not affected.

Three modifications were introduced into the test rig; a Prismatic cylinder, M12 hexagonal bolts, and flush mounted rings as waveguides.

5.2.2.1 Prismatic cylinder

For this experiment, two steel prismatic cylinders, studs, of 4mm diameter and 20cm apart were fitted onto the Perspex pipe section in a specifically designed housing and used as AE waveguides. This housing was constructed to allow for direct contact between the waveguides and the fluid passing through the pipe. The studs were placed such that the flow was not affected as the ends of the steel Prismatic cylinders were profiled to match the internal pipe curvature. Two AE Pico sensors were mounted on the waveguides. Figure (6-10) illustrates the test set-up for this stage of work. Figure (6-10) illustrates the prototype of the contact area between the slug and AE sensors.

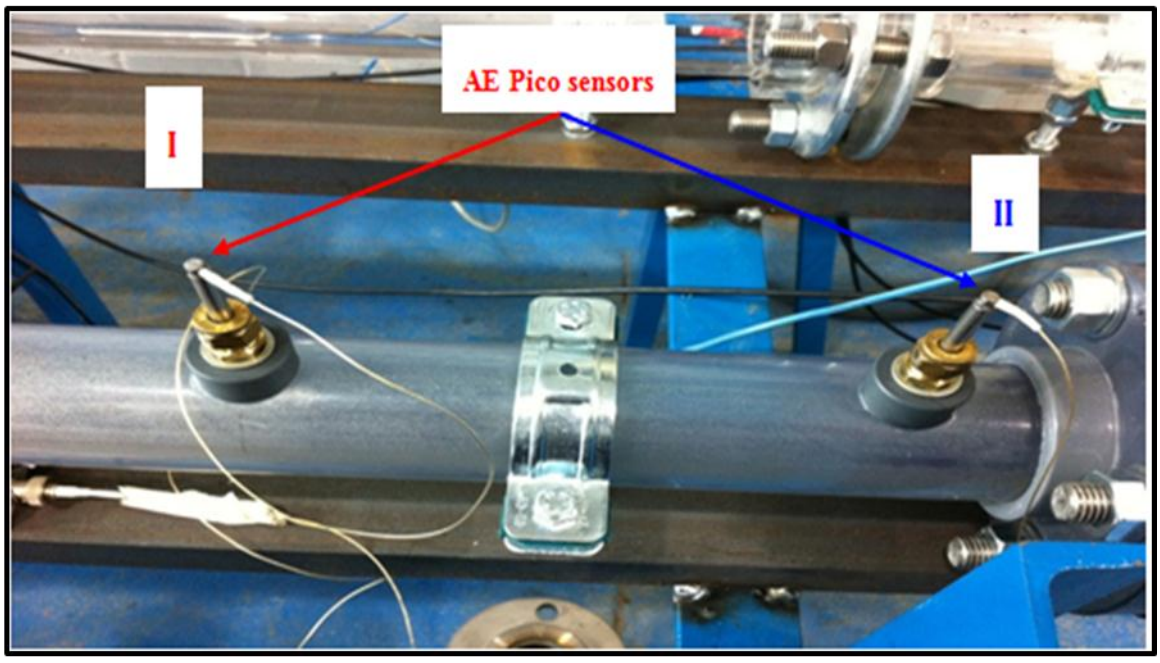

Figure 5-9 4mm ID Prismatic cylinder waveguide and AE Pico sensor installation

The experiment was run at the same superficial gas (V_{SG}) and liquid (V_{SL}) velocities as the previous stage. It was observed that the signals that travel through the material of the pipe wall are almost totally attenuated except signals from directly underneath the steel studs; see Figure (5-11). It can be seen that the waveform signal is almost zero till the slug passes underneath AE sensors. At that moment, the signals amplitude suddenly increases.

This experiment suggests that the energy source location can be detected by using AE method as an intrusive technique. Note that the signal rise time is very short with a very clear and distinct peak, which helps to determine the arrival time precisely. However, because of very small contact area of the AE sensors and the larger area of the slug the energy source may not release the AE energy directly underneath AE sensor.

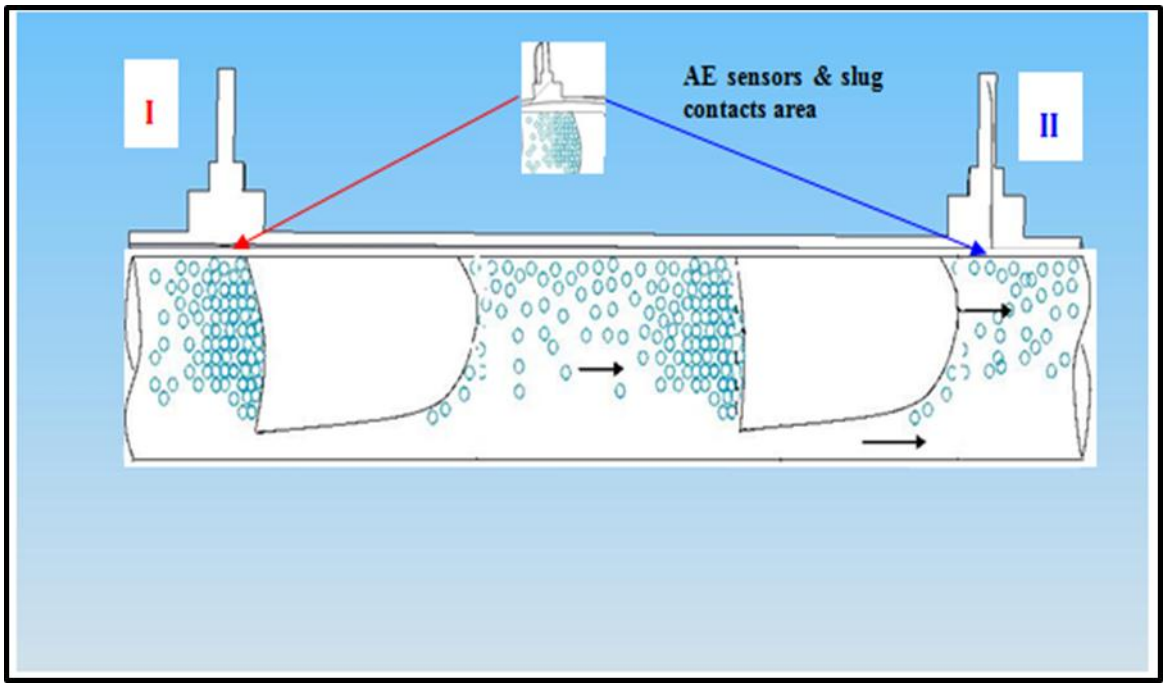

Figure 5-10 Illustration of the prototype of the contact area between the slug and AE sensors

Due to this, it may be difficult to ensure that the slug will be detected as soon as it passes underneath AE sensors. Since the sensor occupies only a fraction of the pipe surface, the energy released by the nose of slug which is further away from the sensor might not always be captured, see Figure (5-11) where the difference between the arrival times of the two signals is not very consistent. See encircled region and the rest of the waveform single. Increasing contact area between AE sensors and flow should improve the AE waveform signals.

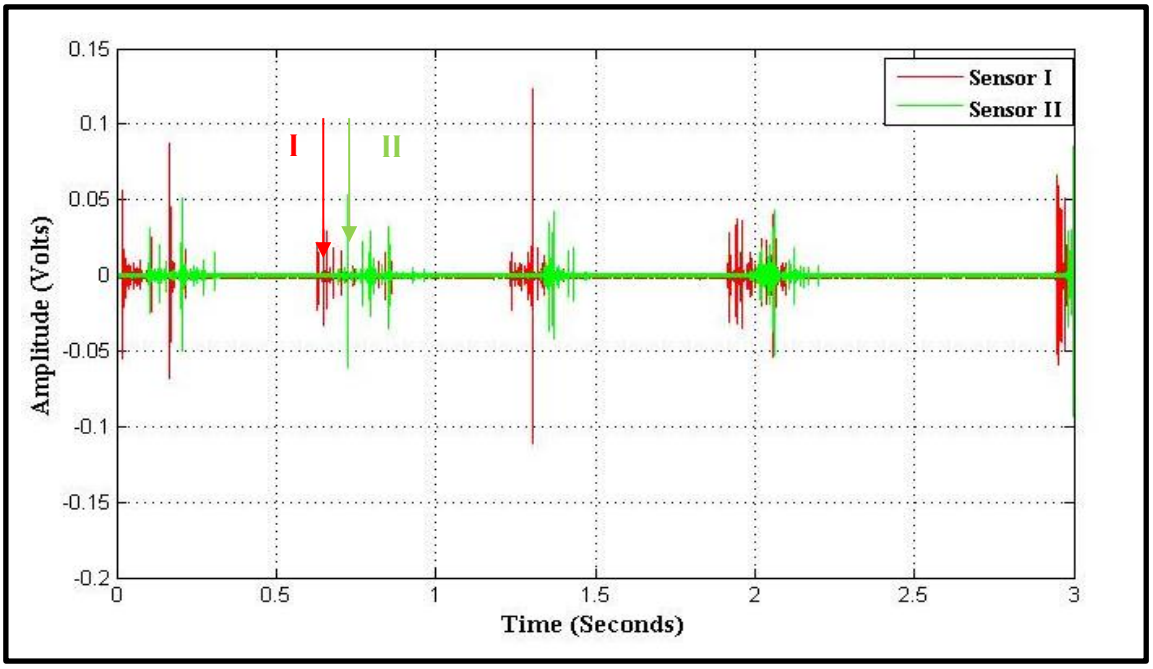

Figure 5-11 AE waveforms at 1.1V_{SL} and 1.02V_{SG} using Prismatic cylinder waveguide

5.2.2.2 M12 Hexagonal bolts waveguides

As a result of the previous experiment, a larger stud (M16 hexagonal bolt) of 12 mm diameter was used as the AE waveguide; see Figure (5-12). This gave a larger contact area between AE sensors and the flow. As previously the waveguides ends where they met the flow were profiled to match the internal pipe curvature.

The signal quality improved sufficiently that the arrival time of each waveform burst signal could easily be identified. Figure (5-13) shows signals recorded using M12 waveguide signals at 1.1 V_{SL} and 1.02 V_{SG}. It can be seen that increasing the stud cross-sectional area significantly improved the amplitude of the signals detected and the differentiation between the signals from sensor I and sensor II. The waveform peaks can be consistently detected with a very short rise time.

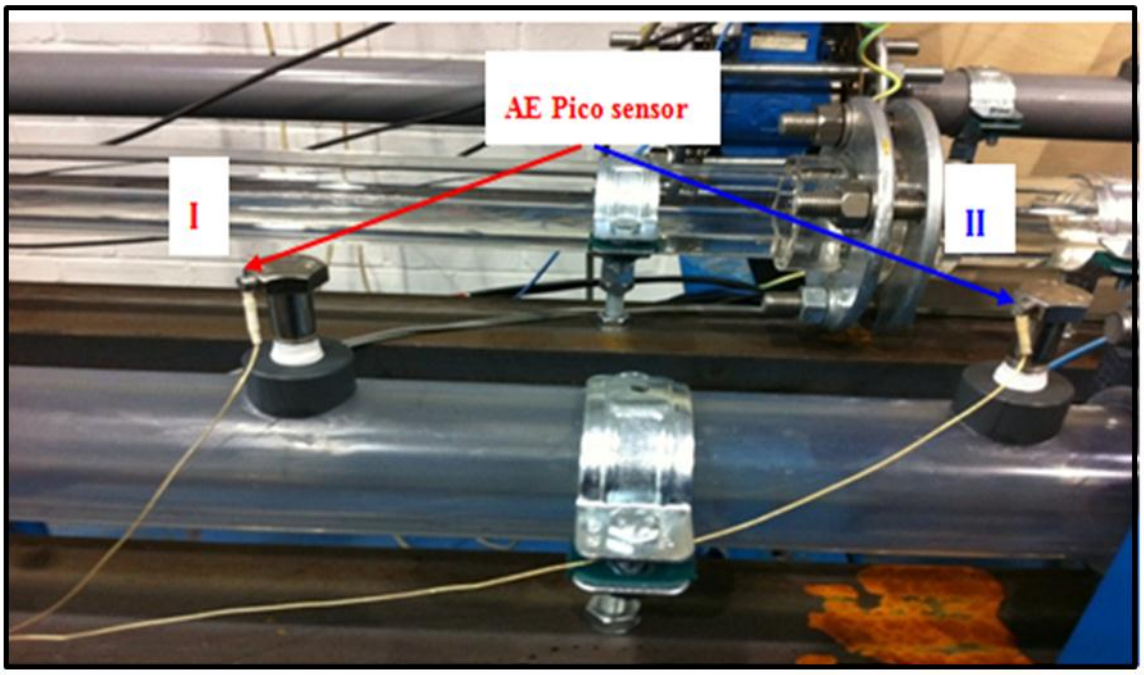

Figure 5-12 Waveguides (M12 hexagonal bolts) and AE Pico sensor installation

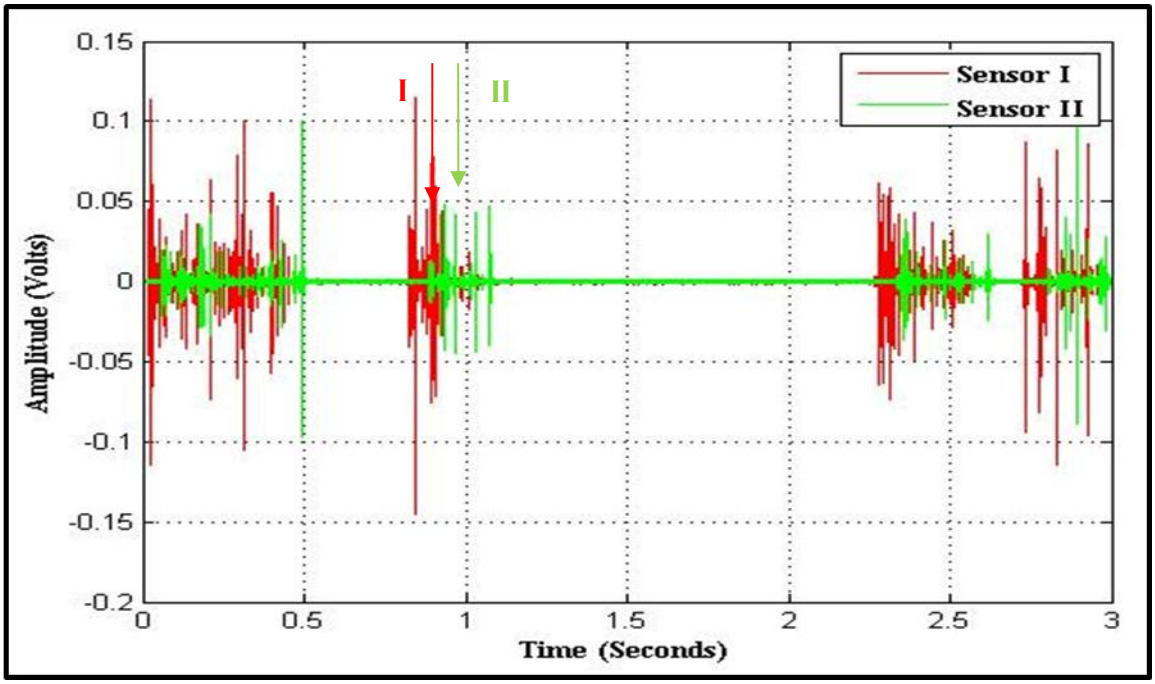

Figure 5-13 AE waveform at 1.1V_{SL} & 1.02V_{SG} using M12 Hexagonal bolts waveguide

5.2.2.3 Flush ring AE waveguide

To test whether further increase in contact area would significantly improve the AE signal above that obtained by the M12 Hexagonal bolt, another experiment was undertaken. Two AE Pico sensors were each mounted on a circumferential ring on the inside of the Perspex pipe, to be used as an AE waveguide. The rings were of steel, 12 mm thick, 50 mm wide and 210mm apart as seen in Figure (5-14). Figure (5-15) illustrates the prototype of the contact area between the slug flow and flush mounted rings of AE waveguides.

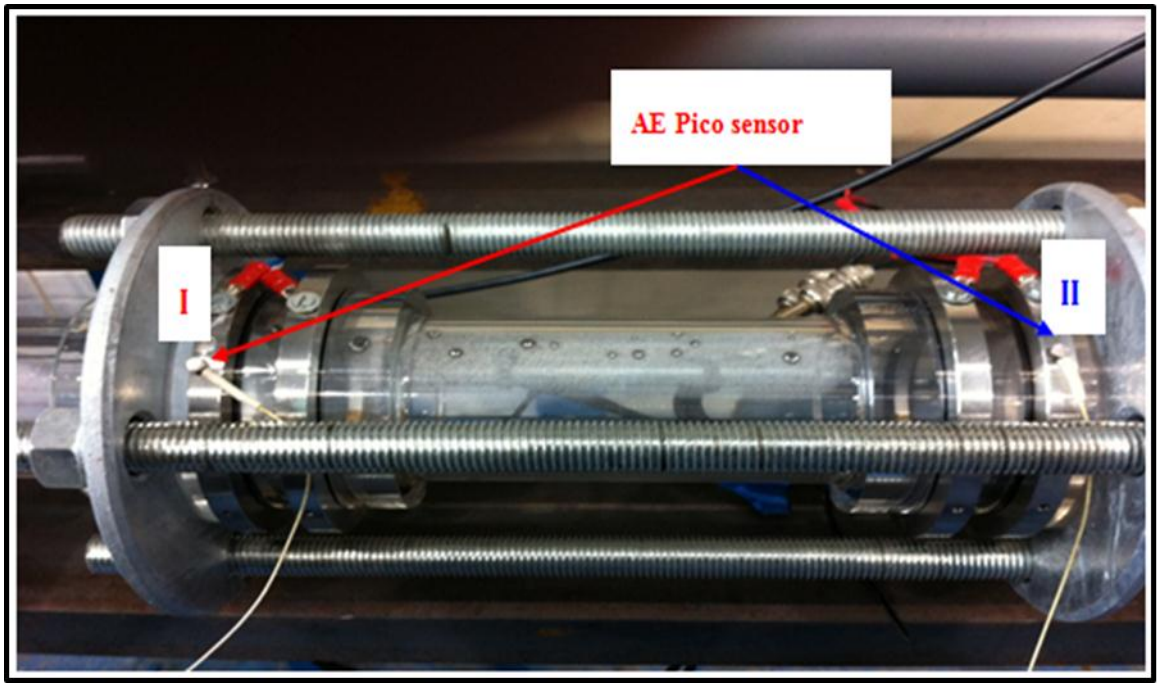

Figure 5-14 AE Pico sensors on conductivity ring installation

This experiment was to make sure that the nose of the slug is captured as soon as it passes through the waveguide. Under identical test conditions as the previous tests (V_{SL}=1.1 and V_{SG}=1.02), the recorded waveform signals were as shown in Figure (5-16). It is clear that the signal quality is superior to that of the previous tests, with distinct peaks and improved consistency in slug detection. However, the rise time in this method is not as quick as with Prismatic cylinder and M12 bolts. This leads to the difficulties of determining the precise arrival time of the slug at each AE sensor. A possible reason for loss of precision is

that the ring will perform a kind of attenuation. Detected emitted energy on the other side of circumference of the flushed rings, opposite AE sensors, will be attenuated due to traveling before being captured by AE sensors.

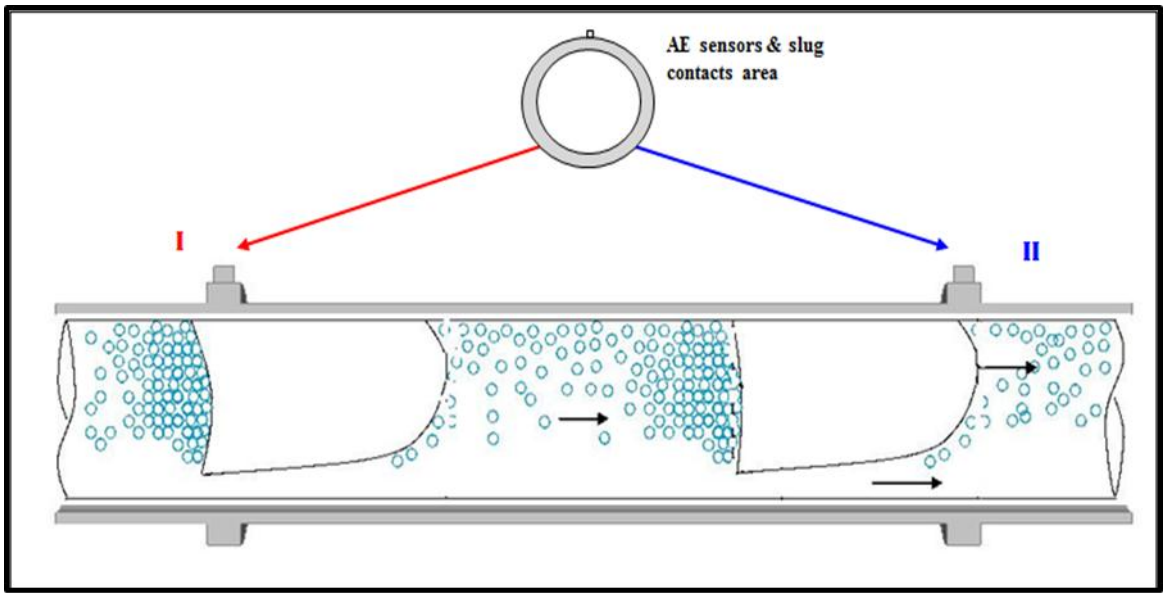

Figure 5-15 Schematic of flush mounted circumferential rings acting as AE waveguides

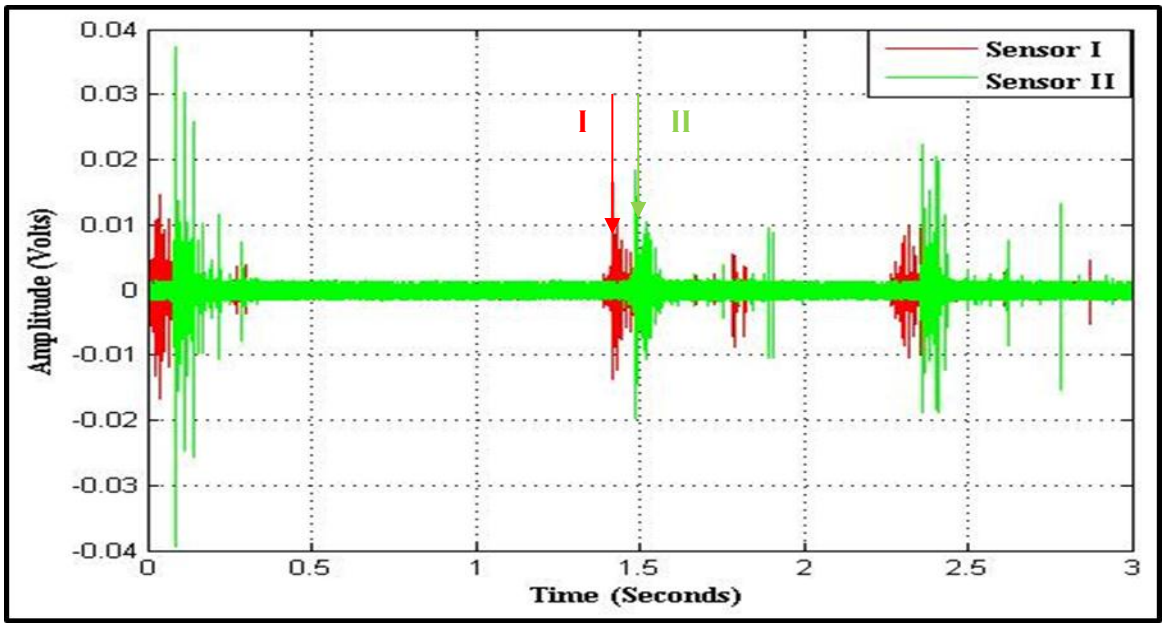

Figure 5-16 AE waveform at 1.1 V_{SL} and 1.02 V_{SG} using AE Pico sensors on flush circumferential rings

5.3 Comparison of the results with other techniques

The determination of slug velocity using acoustic emission technology will be validated by comparing it with previous work of measured slug velocity using ultrasonic technique on the same test rig, and measured slug velocity by using a high speed camera (HSC).

An Olympus i-SPEED high speed video camera (Figure 5-17) was used with full sensor resolution of 1000 frames per second (fps) and a maximum frame speed of 33000 fps. The duration of the recording time at full resolution was 4 second. In this work the slug travelled two marked positions 21 cm apart (the distance between the AE sensors) so the HSC was programmed to capture slugs at 3000 fps for a duration of 3 seconds to ensure the whole range of slugs could be captured.

Figure 5-17 High Speed Camera (Olympus i-SPEED)

Chapter 6 Results, observation and discussion

This chapter discusses the results that have been achieved in detecting the presence of a slug, measuring its velocity and recognizing the flow regimes of two phase gas/water flow. As discussed in the preceding chapter, the slug cannot be detected by mounting AE sensors externally on the steel pipe, even when the steel pipes were clamped in an attempt to eliminate the transmission of unwanted AE waves within the steel. However, using acoustic emission sensors on the internal face of the pipe ("intrusively") via waveguides but not projecting into the flow ("noninvasively") gives the possibility of detecting the presence of slugs and measuring their velocity.

Three approaches were investigated in this study: Prismatic cylinder AE waveguides, M12 Hexagonal bolts as AE waveguides, and flush rings as AE waveguides. Prismatic cylinders AE waveguide were rejected as a slug detection method because of the waveform of the AE signals which resulted from the small contact area between AE sensors and the flow. The use of M12 Hexagonal bolts and flush rings as AE waveguide is discussed in this chapter as is the data captured by both of them. The results were validated using a high speed camera (HSC) and previous data of ultrasound technology (Al-lababidi; 2006). Flow regime recognition will also be discussed in this chapter

6.1 Slug flow velocity

6.1.1 Measuring slug velocity using M12 Hexagonal bolts AE waveguide

From the modifications made on the test rig by using the M12 waveguide signals, the waveform signals were highly improved in terms of identification of the start and end of each burst signal as shown Figure 6-1.

With the M12 waveguide signals the rise time was sharp enough to easily detect the first threshold crossing for each burst signal. The average rise time of the AE burst signal for a flow of 1.02 V_{SL} and 2.52 V_{SG} was 0.178 millisecond,

with 0.697 millisecond standard deviation. The arrival time of each AE sensor was clear with distinct burst signals.

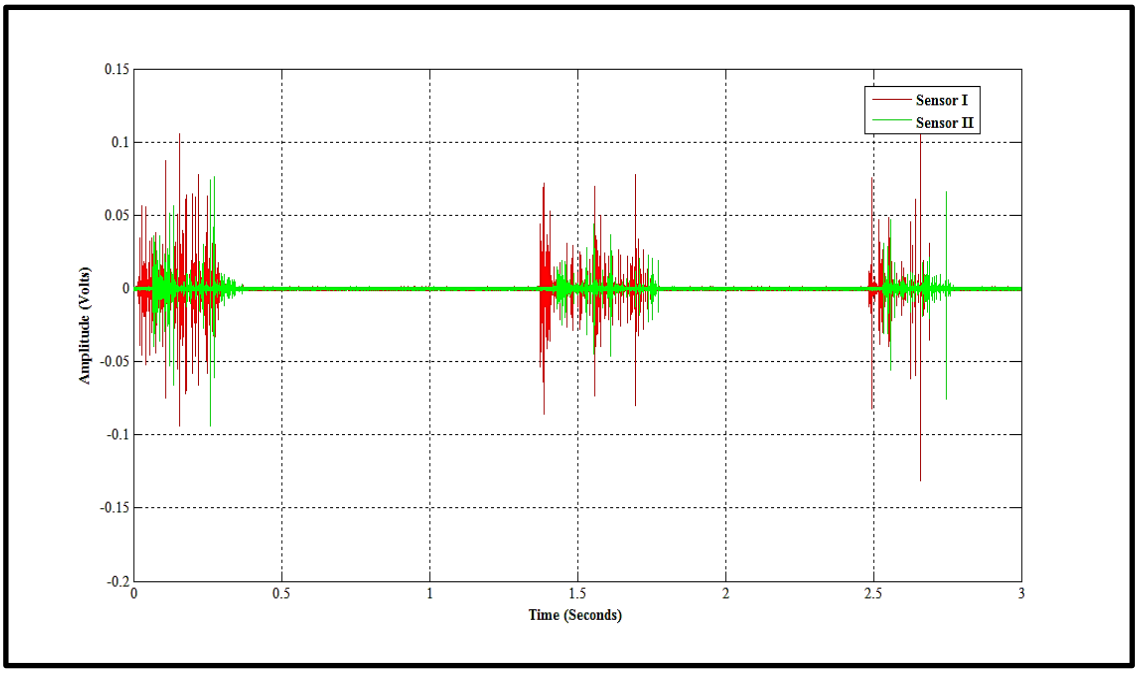

Figure 6-1 AE waveform at flow 1.02 V_{SL} and 2.52 V_{SG} using M12 waveguide

To determine the time delay for flow to proceed between two AE sensors, the AE signals were acquired continuously and used to calculate the slug velocity for the gas/liquid flow. Four superficial liquid velocities, V_{SL} (0.70, 1.02, 1.52 and 2.02) m/s, were used. At each V_{SL}, four superficial gas velocities, V_{SG} (1.02, 1.52, 2.02 and 2.52) m/s, were used; giving a total of sixteen combinations of velocities.

The difference in detection times between both sensors was found by determining the exact times when the AE signals exceeded a pre-defined threshold crossing. To facilitate these calculations, MATALAB code was generated and used to detect the first threshold crossing of each burst signal as shown Figure 6-2. The circled areas on the AE signal for sensors I and II show the first threshold crossings.

Figure 6-3 shows the circled areas in Figure 6-2 magnified. Also shown in the red circles are the exact points of the first threshold crossing of each burst

signal. The average time delay (Δt) of each pair of AE waveform signals was calculated. The times of the crossings for each pair of burst signals of both sensors were determined (three crossings in this case), and the times between crossings determined by simple subtraction. Afterward the average time delay between crossing points was found. The associated slug velocity (S_V) was determined by the following equation:

$$S_V = {}^{L}/_{\Delta t} \qquad 6\text{-}1$$

S_V : Slug velocity (m/s); L: the distance between the two AE sensors.

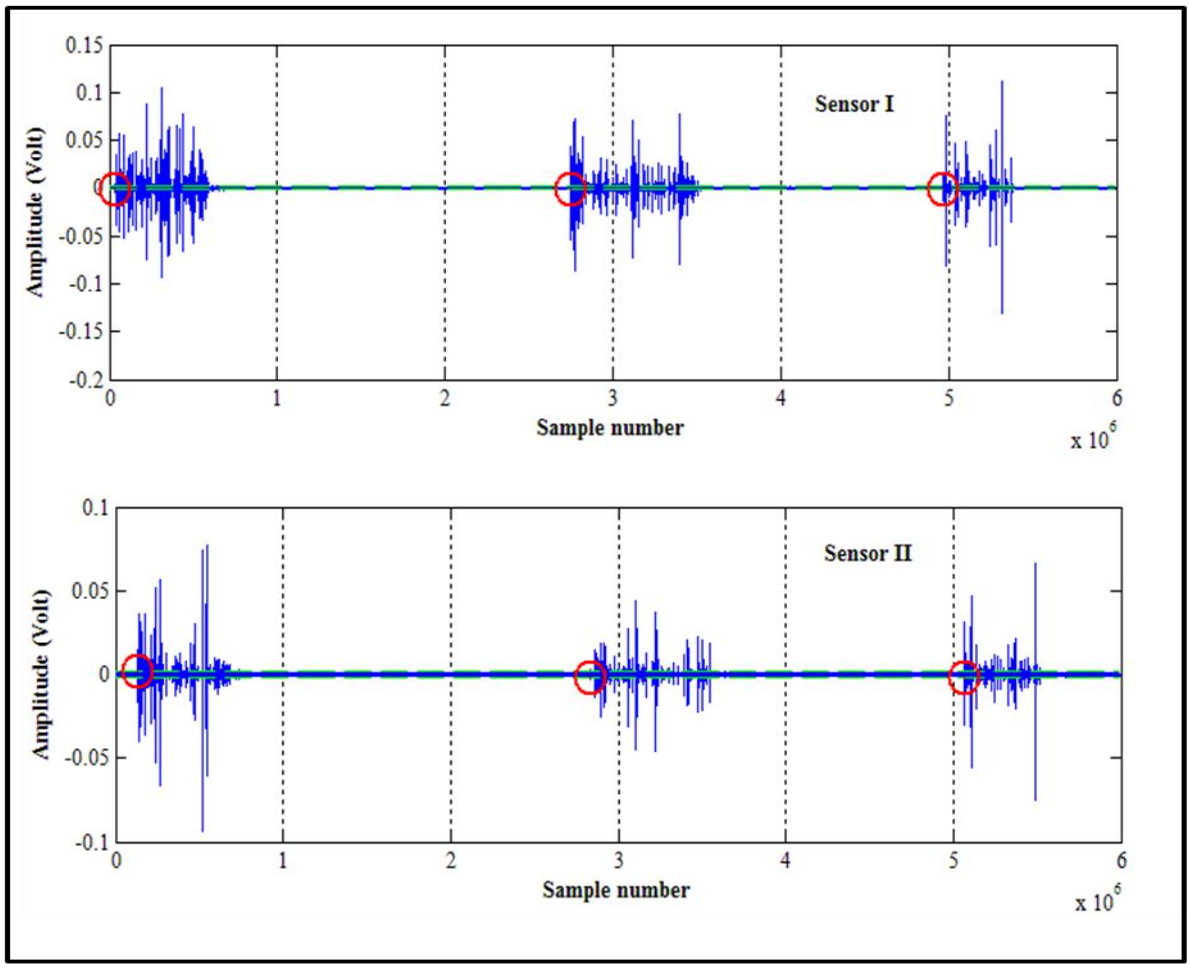

Figure 6-2 First AE waveform threshold crossing detection for flow of 1.02 V_{SL} and 2.52 V_{SG} using M12 waveguide

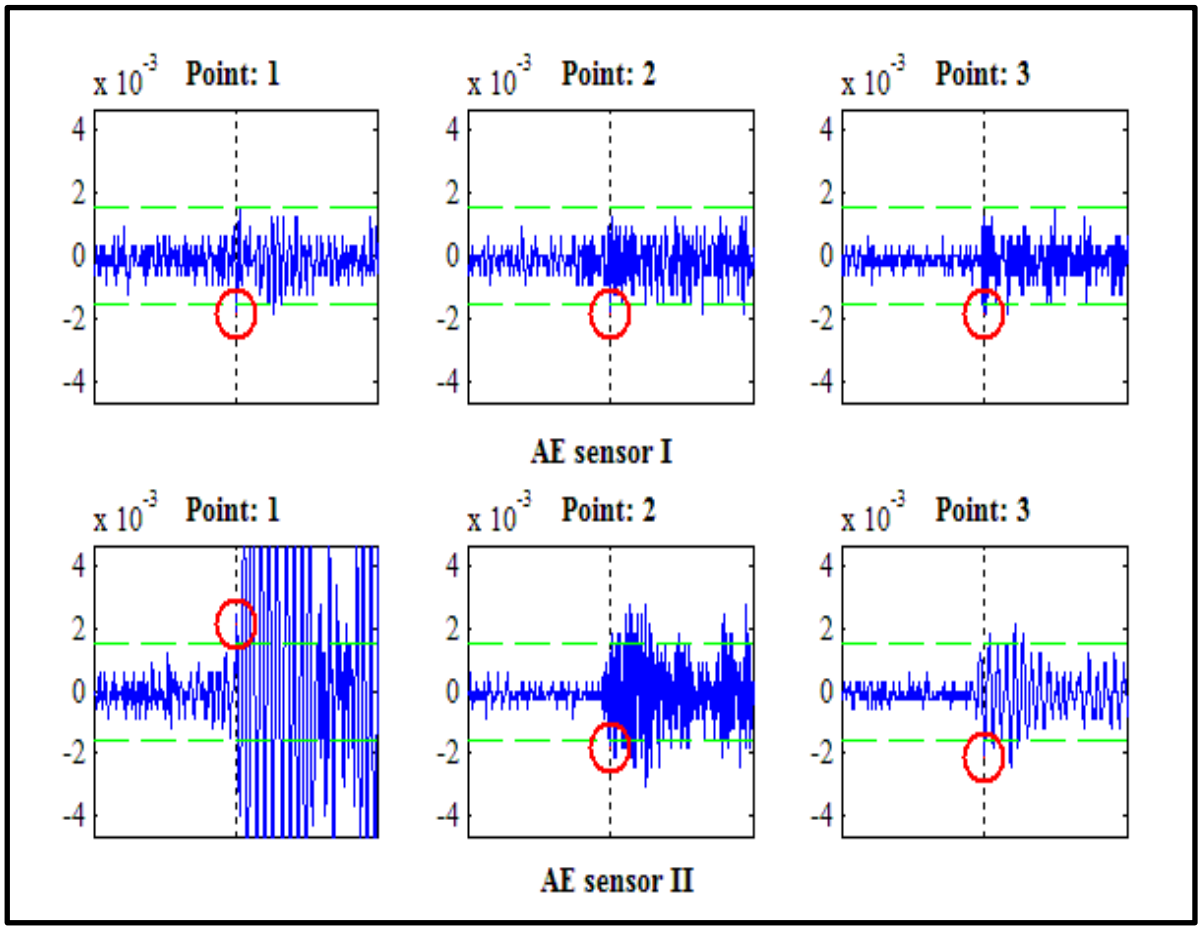

Figure 6-3 Determination of first threshold crossing for each burst signal for both AE sensors at flow of 1.02 V_{SL} and 2.52 V_{SG}

The slug velocity was determined for a defined longitudinal length of 21 cm between sensors and difference in detection time. The AE system was programmed for a 32 dB threshold to avoid background noise. Above this threshold, the AE system captured waveform signals at 2 MSPS sample rate. A total of thirteen randomly selected data files from each test condition were used to determine time delay and consequently calculate the slug velocity of each run. This amount of burst signals was chosen based on a statistical sample size of (10 – 30) % which can describe the whole population (Connor, July 17, 2011). Table 6-1 shows an example of time delay and slug velocity calculation at 1.02 V_{SL} and 2.52 V_{SG}. Similar calculations for other measured slug velocities are in tables A-1 to A-15 in the appendix (A). The slug velocity was seen to vary

between 3.5 m/s to 4.3 m/s with an average of about 3.89 m/s and standard deviation of 0.20 m/s. This average was 10% higher than the mixture flow velocity, which was taken as the sum of superficial liquid and gas velocities.

Table 6-1 Time delay and slug velocity calculation using M12 waveguide at 1.02 V_{SL} and 2.52 V_{SG}

Burst Signal Number	Mixture Velocity (m/s)	Time Delay (ms)	Measured Slug Velocity Sv (m/s)
1	3.54	51.32	3.897
2	3.54	53.74	3.722
3	3.54	49.80	4.016
4	3.54	52.30	3.824
5	3.54	51.42	3.890
6	3.54	51.88	3.855
7	3.54	50.52	3.959
8	3.54	54.53	3.668
9	3.54	55.74	3.588
10	3.54	49.40	4.049
11	3.54	50.54	3.957
12	3.54	45.50	4.396
13	3.54	52.89	3.782
Average of measured Slug Velocity (Sv)			3.89
Mixture Flow Velocity Vm (m/s)			3.54
Standard deviation of Sv (m/s)			0.20
% difference between SV and Vm (m/s)			9.96%

This procedure was repeated for values of V_{SL} and V_{SG} used and a summary of the results is given in Table 6-2. On average, the slug velocity was always greater than the calculated mixture flow velocity by between 7% and 26%. The standard deviations of the measured slug velocity at each V_{SL} and V_{SG} varied from 0.11 to 0.41 m/s. This variation of the slug velocity could be attributed to

the small contact area between the slug and the AE sensors. Similar slugs will not always release equivalent energy levels directly underneath the sensors because of the uncontrollable variation of energy in the moving slug in addition to the natural instability of slug velocities. When slug front and tail travel at different velocities, the slug velocity will be greater or less than for a stable slug (stable slug obtained when front and tail of the slug travel at the same velocity). All these events take place at different times in real flow which lead to different slug velocities (Issa, R., 2009). This can be seen clearly in Figures 6-4, 6-5, 6-6 and 6-7. The slug velocity will vary even for the same gas and liquid flow rates. I.e., the arrival time of the AE signal varies; leading to differences in the time of travel of the slug between AE sensors. Similar obtained results are in figures B1to B12 in appendix B.

In addition to the reasons mentioned above, there were minor variations in liquid and gas flow rates as controlled by the throttling valve and brass gate respectively (see Figure 5 - 1). There were observed variations in the throttling valve of the order of 0.01-0.3 m/s and in the brass gate of the order of 0.1-0.6 m/s. Despite these variations, it has been demonstrated that the AE technique has the potential to determine the slug velocity in gas/liquid two phase flows using M12 AE waveguide signals. It was decided that measurement accuracy could be enhanced by enlarging the contacting area between the slug and AE sensors. The next section discusses an enlarged contact area between AE sensors and the slug flow using flush rings as waveguides for the AE signals.

Table 6-2 Time delay and slug velocity calculation using M12 AE waveguide

Superficial Liquid Velocity (V_{SL}) (m/s)	Superficial Gas Velocity (V_{SG}) (m/s)	Calculated Mixture Velocity (m/s)	Measured Slug Velocity Using AE (m/s)	% Difference Between Measured Slug and Calculated Mixture Velocities	Standard Deviation in slug velocity (m/s)
0.70	1.02	1.72	2.17	26.3%	0.20
0.70	1.52	2.22	2.73	23.1%	0.24
0.70	2.02	2.72	3.14	15.5%	0.41
0.70	2.52	3.22	3.87	20.3%	0.29
1.02	1.02	2.04	2.47	21.1%	0.11
1.02	1.52	2.54	3.01	18.5%	0.13
1.02	2.02	3.04	3.45	13.5%	0.14
1.02	2.52	3.54	3.89	9.9%	0.20
1.52	1.02	2.54	2.96	16.5%	0.20
1.52	1.52	3.04	3.40	11.8%	0.22
1.52	2.02	3.54	3.80	7.3%	0.18
1.52	2.52	4.04	4.57	13.1%	0.25
2.02	1.02	3.04	3.56	17.1%	0.17
2.02	1.52	3.54	3.92	10.7%	0.13
2.02	2.02	4.04	4.46	10.4%	0.22
2.02	2.52	4.54	4.97	9.5%	0.25

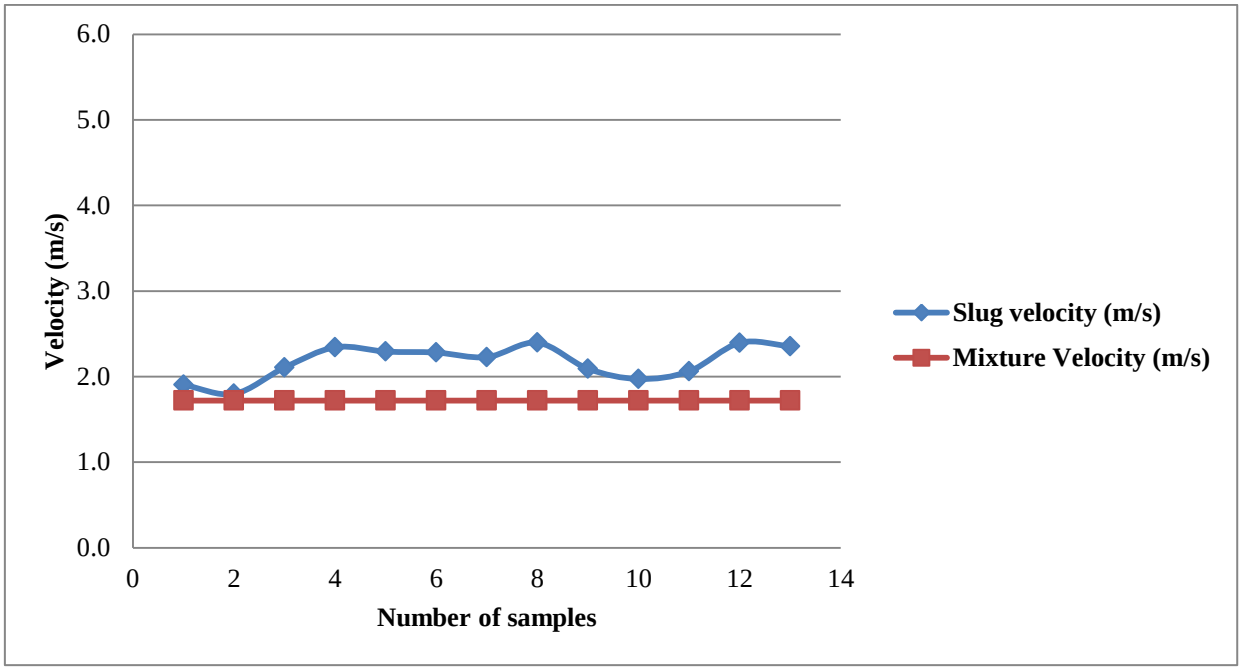

Figure 6-4 Measured slug velocity and mixed flow velocity at 0.7 V_{SL} and 1.02 V_{SG}

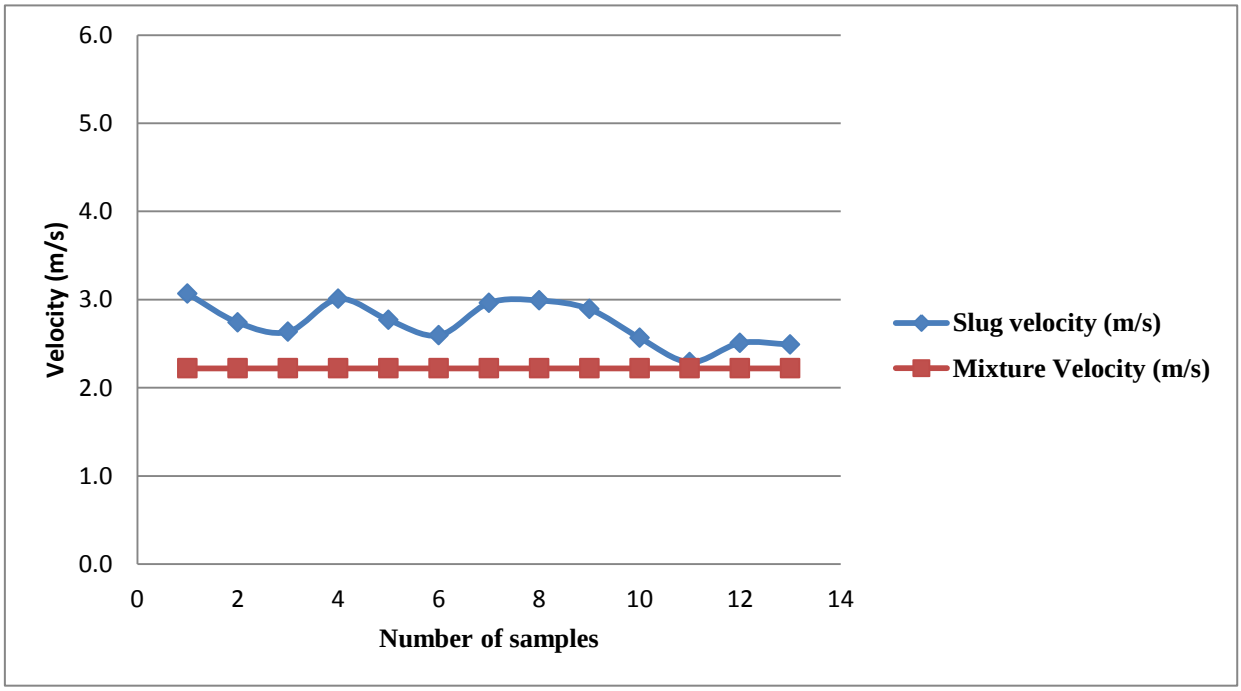

Figure 6-5 Measured slug velocity and mixed flow velocity at 0.7 V_{SL} and 1.52 V_{SG}

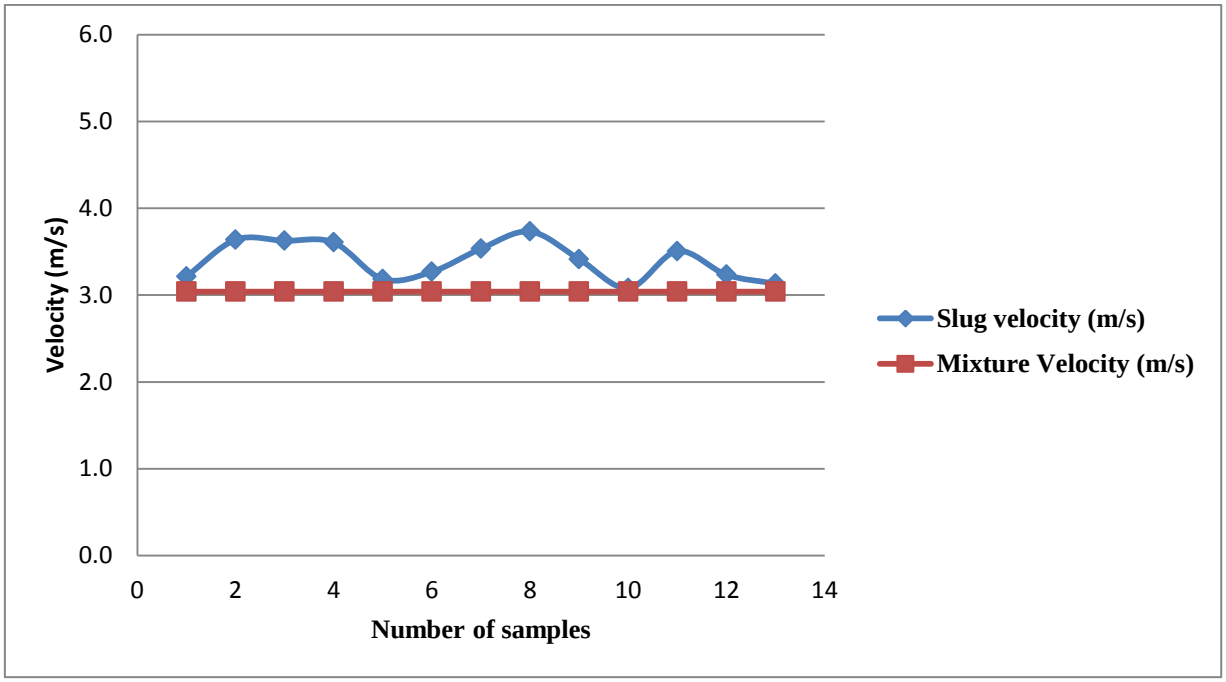

Figure 6-6 Measured slug velocity and mixed flow velocity at 1.52 V_{SL} and 1.52 V_{SG}

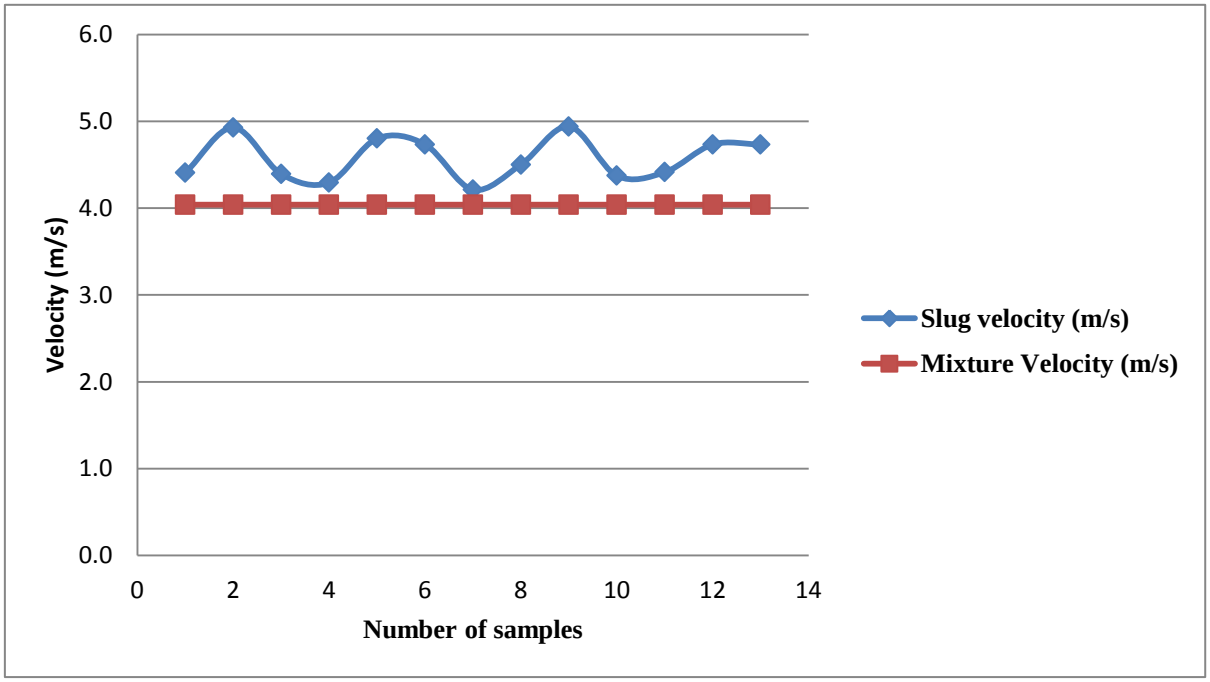

Figure 6-7 Measured slug velocity and mixed flow velocity at 1.52 V_{SL} and 2.52 V_{SG}

6.1.2 Measuring slug velocity using flush rings as AE waveguides

The attempt to improve the AE waveform signals was to use internal flush rings within the pipe as AE waveguides, see Figure 5-14. This enlarged the contact area between AE sensors and slug flow and improved the results obtained using the M12 waveguides. Using flush rings as waveguides for the energy released from the slug gives a higher probability that any energy released will be captured by the AE sensors as soon as it reaches these waveguides.

Figure 6-8 shows the AE waveform signals at a flow of 1.02 V_{SL} and 2.52 V_{SG}. It can be seen that the rise time of each burst signal is more gradual than with the M12 waveguide where the rise time was sharper (Figure 6-1). The average rise time of AE burst signals at 1.02 V_{SL} and 2.52 V_{SG} was 0.377 millisecond with 1.418 millisecond standard deviation. The average rise time was about two times longer than that obtained using the M12 waveguides at the same flow rates.

The AE signal from a slug can be captured at any point on the circumference of the pipe and sometimes the slug will be very close to the AE ring sensor which gives a sharp rise time (third burst signal of sensor II in Figure 6-10).

Sometimes it can be captured at the other side of the ring circumference which leads to having longer rise time of the waveform signal as in the second burst signals of sensors I and II in Figure 6-10.

Additionally, the amplitude of AE signals using this method is lower than that obtained using the M12 waveguides, (compare Figures 6-1 and 6-8). It is 0.12 volts in M12 waveguide method and 0.05volts in flush rings waveguide method. This can be explained by the attenuation of AE signals due to the larger size of the flush rings waveguide. Also, the distance between captured signals and AE sensors is larger than that for the M12 waveguide.

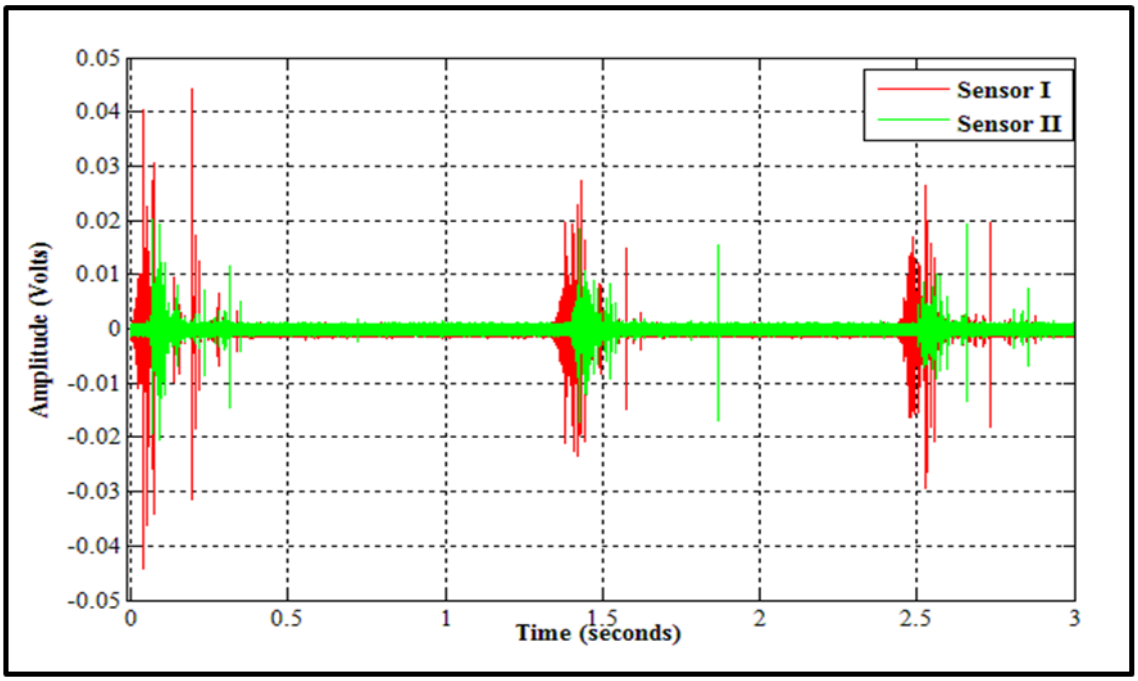

Figure 6-8 AE waveform at flow 1.02 V_{SL} and 2.52 V_{SG} using flush rings as waveguides

To compare the results between the two approaches, the experiment was conducted at the same operating conditions as with the M12 sensors. Again, thirteen burst signals have been taken at random to determine arrival time of the waveform signals and then to calculate the mean slug velocity and standard deviation. The same MATALAB code was used to detect the first threshold crossing of each burst signal as shown Figure 6-9. The circled area of each burst signal of AE sensors I and II shows the first threshold crossing of each burst signal. The circled areas in Figure 6-9 which show each burst signal for AE sensors I and II have been magnified and are shown in Figure 6-10. The crossing points of the first threshold crossing are circled in red for each burst signal. The average of time delay (Δt) for each pair of AE waveform signals was determined by simple subtraction and the associated slug velocity (S_V) was determined using Equation 6-1.

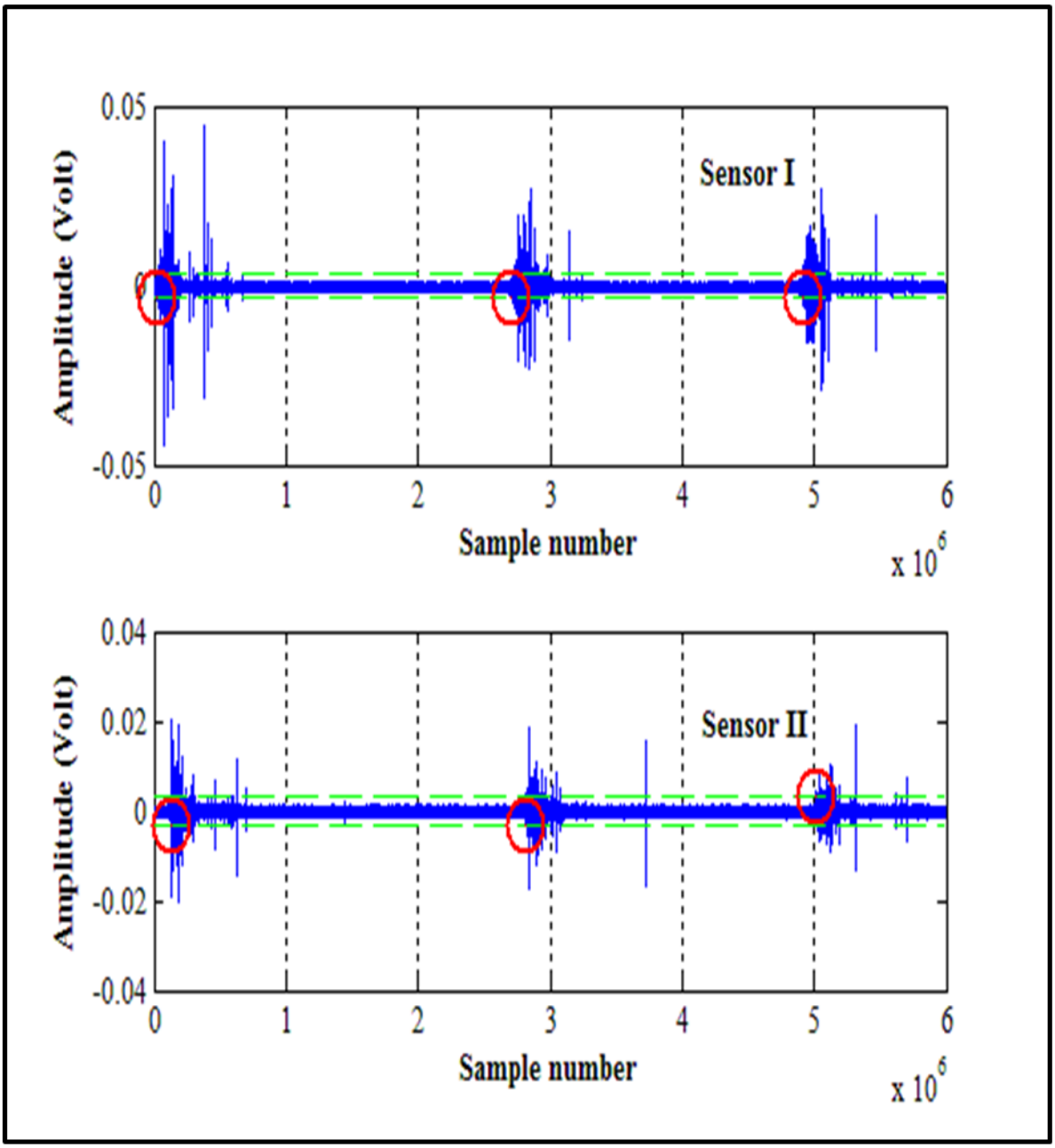

Figure 6-9 First AE waveform threshold crossing detection for flow of 1.02 V_{SL} and 2.52 V_{SG} using flush ring waveguide

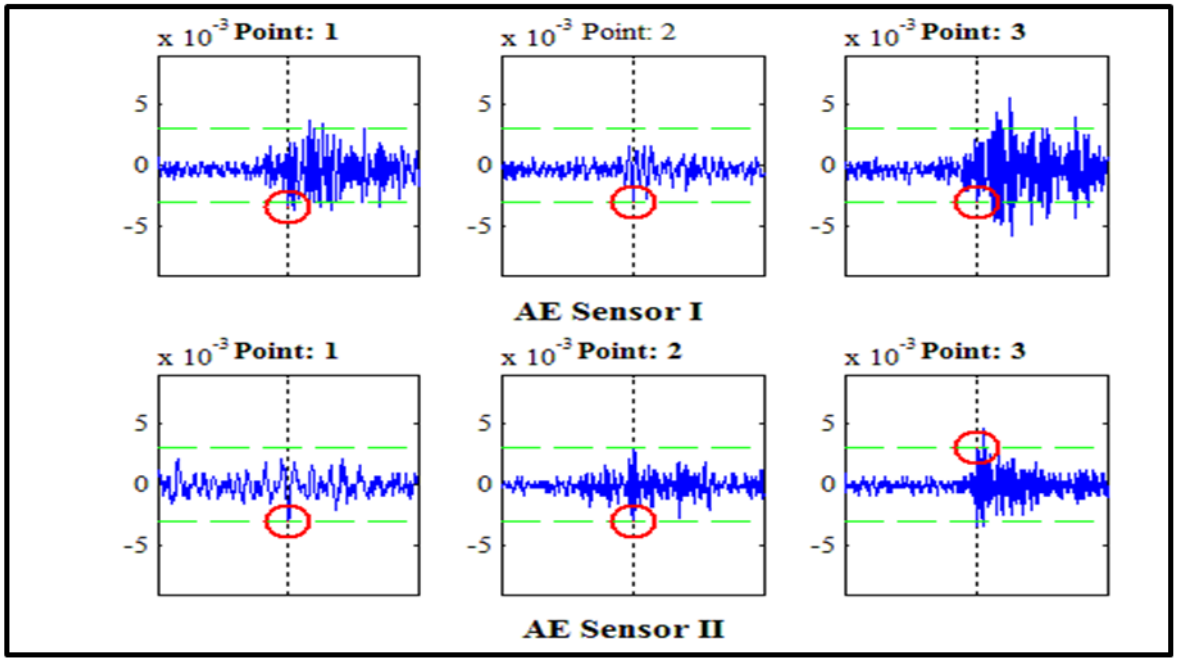

Figure 6-10 Determination of first threshold crossing for each burst signal for both AE sensors at 1.02 V_{SL} and 2.52 V_{SG} using flush ring waveguide

Table 6-3 shows an example of time delay and slug velocity calculation at 1.02 V_{SL} and 2.52 V_{SG}. From this table, time delay between corresponding burst signals varies from 49.43 to 56.93 milliseconds, and the slug velocity is between 3.7 m/s and 4.2 m/s with an average of about 4.01 m/s and a standard deviation of 0.15 m/s from the average slug velocity. This average velocity was 12% higher than the mean velocity of mixture flow (V_{SG} + V_{SL}). Similar calculations for other measured slug velocities are in tables C-1 to C-15 in the appendix (C).

Table 6-3 Time delay and slug velocity calculation using flush ring AE waveguides at 1.02 V_{SL} and 2.52 V_{SG}

Number of burst signals	Mixture Velocity (m/s)	Time delay (ms)	Slug velocity (m/s)
1	3.54	52.74	3.982
2	3.54	51.53	4.076
3	3.54	51.98	4.040
4	3.54	53.53	3.923
5	3.54	52.80	3.977
6	3.54	56.93	3.688
7	3.54	49.43	4.248
8	3.54	50.73	4.140
9	3.54	51.45	4.081
10	3.54	51.41	4.085
11	3.54	53.03	3.960
12	3.54	50.83	4.132
13	3.54	55.28	3.799
Average of measured Slug Velocity Sv (m/s)			4.01
Mixture Flow Velocity Vm (m/s)			3.54
Standard deviation of Sv (m/s)			0.15
% difference between SV and Vm (m/s)			13.28%

Table 6-4 summarises the test results for the full ranges of superficial liquid and gas velocity that was conducted. On average the slug velocity was greater than the mixture flow velocity by between about 9% to 24%. The standard deviation in calculated slug flow varied from 0.13 m/s to 0.25 m/s. It appears that for the same operating conditions the variation in slug velocity is less than that obtained using the M12 waveguide method. This suggests that enlarging the contact area between AE sensors and the flow can give more accurate results.

However, the first threshold crossing for each AE signal burst was more difficult to detect with the flush rings because of the gradually increasing rise time and lower amplitude of the entire AE waveform. The average rise time obtained with the M12 waveguide method is less than that of flush rings waveguides method. This overcomes the smaller contact area of the M12 method comparing to flush rings method. Much the same variation in slug velocity were observed, see Figures 6-11 to 6-14, over the range of flows used as for the M12 waveguide. Similar obtained results are in figures D1to D12 in appendix D. In spite of the differences found in the measured AE signals the average slug velocities were not significantly different for the two methods over the range of flows used. This indicates that either of these methods (M12 or flush ring waveguides) can be used to detect and measure velocity of the slug in two phase flow.

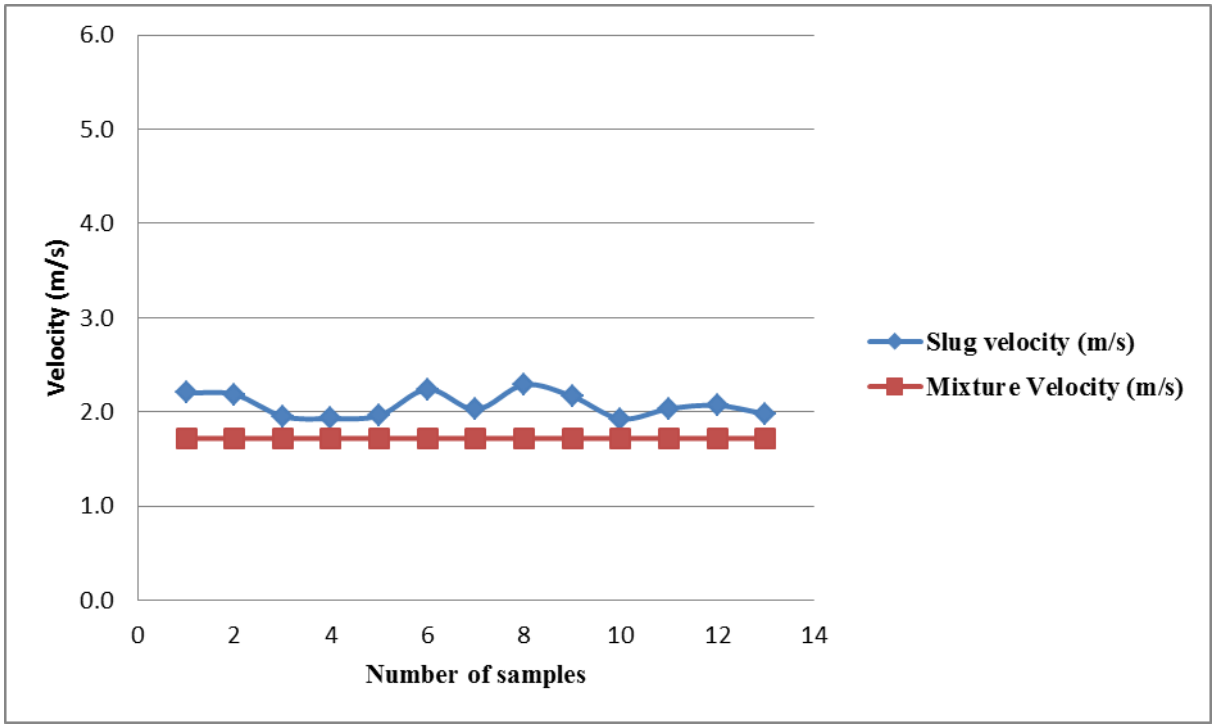

Figure 6-11 Measured slug velocity with mix velocity 0.7 V_{SL} and 1.02 V_{SG}

Table 6-4 Time delay and slug velocity calculation using flush ring waveguides

Superficial Liquid Velocity (V_{SL}) (m/s)	Superficial Gas Velocity (V_{SG}) (m/s)	Calculated Mixture Velocity (m/s)	Measured Slug Velocity (m/s)	% Difference Between Measured Slug and Calculated Mixture Velocities	Standard Deviation in slug velocity (m/s)
0.70	1.02	1.72	2.07	20.61%	0.13
0.70	1.52	2.22	2.65	19.2%	0.14
0.70	2.02	2.72	3.12	14.6%	0.13
0.70	2.52	3.22	3.77	17.0%	0.15
1.02	1.02	2.04	2.54	24.4%	0.11
1.02	1.52	2.54	3.00	18.0%	0.15
1.02	2.02	3.04	3.44	13.0%	0.17
1.02	2.52	3.54	4.01	13.3%	0.15
1.52	1.02	2.54	3.02	19.0%	0.15
1.52	1.52	3.04	3.52	15.8%	0.19
1.52	2.02	3.54	3.95	11.6%	0.13
1.52	2.52	4.04	4.41	9.1%	0.20
2.02	1.02	3.04	3.51	15.3%	0.17
2.02	1.52	3.54	3.99	12.6%	0.18
2.02	2.02	4.04	4.46	10.4%	0.19
2.02	2.52	4.54	5.00	10.2%	0.25

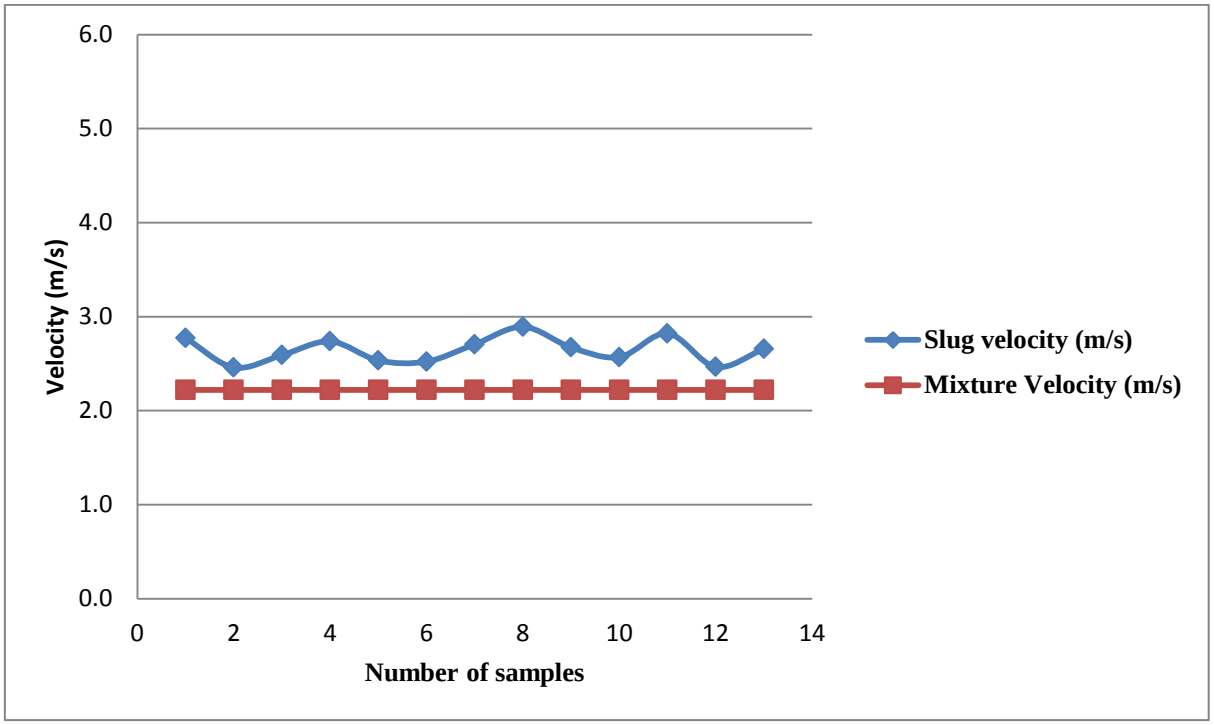

Figure 6-12 Measured slug velocity with mix velocity 0.7 V_{SL} and 1.52 V_{SG}

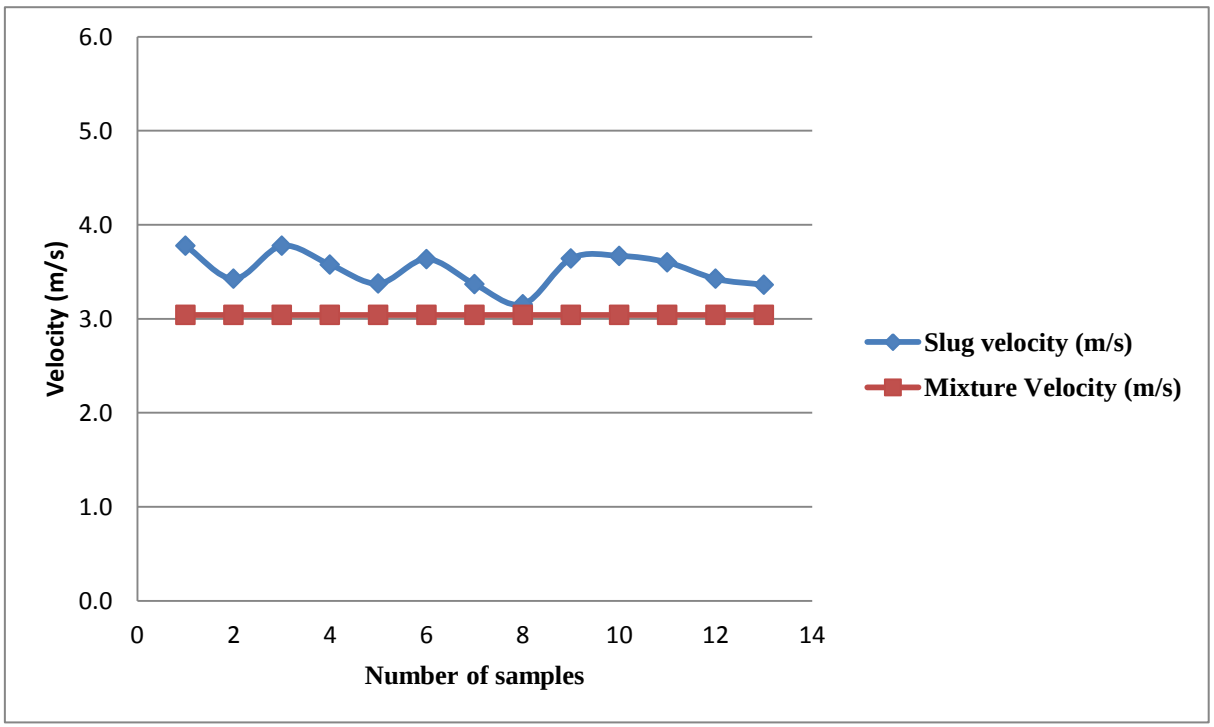

Figure 6-13 Measured slug velocity with mix velocity 1.52 V_{SL} and 1.52 V_{SG}

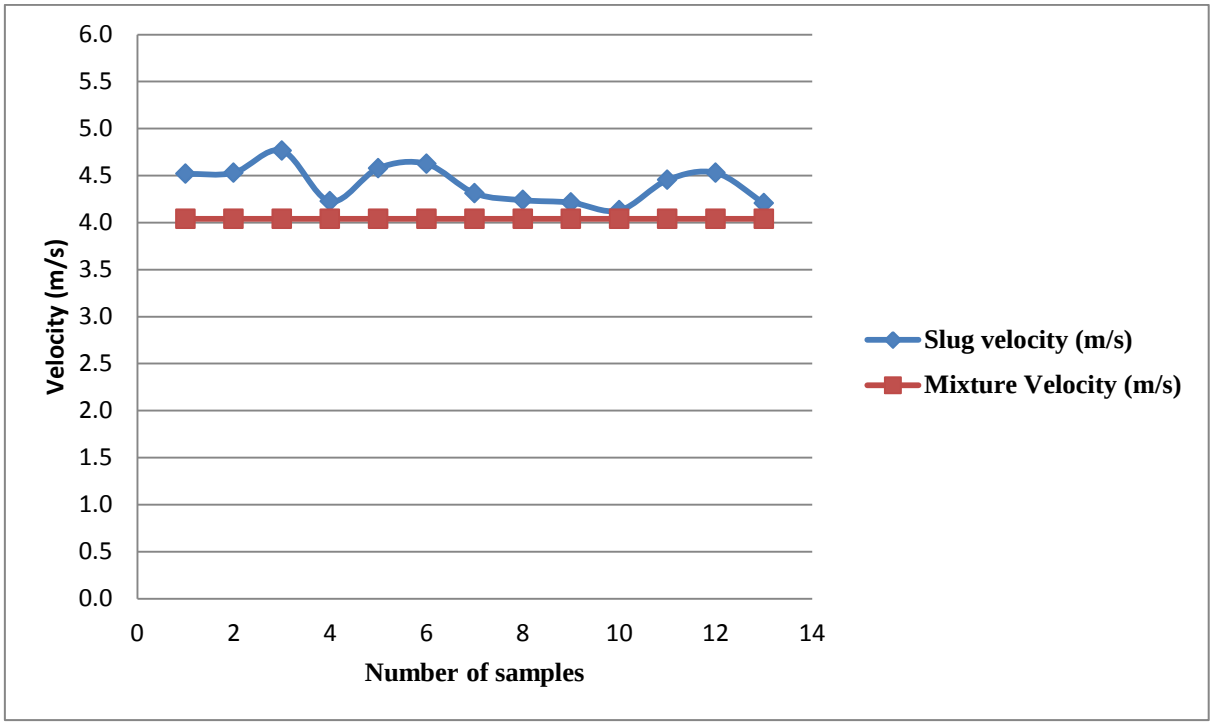

Figure 6-14 Measured slug velocity with mix velocity of 1.52 V_{SL} and 2.52 V_{SG}

6.1.3 Comparing the measured slug velocity by using M12 and flush-rings waveguides

By comparing Tables 6-1 and 6-3 the mean slug velocities using M12 and flush rings methods are μ_1 =3.89 m/s and μ_2=4.01 m/s respectively. The respective standard deviations are σ_1= 0.20 m/s and σ_2= 0.15 m/s. The sample size is 13 for both samples, $n_1=n_2=13$.

The T-test is a well-known and simple test first published in 1909 by W.M. Gossett. He published his work under the pseudonym “Student” so the common name for this test is “The Student t-test”. The null hypothesis is H_o : $\mu_1= \mu_2$ (there is no significant difference in the means) against H_1 : $\mu_1 \neq \mu_2$ (there is a significant difference between the means) (Walpole et al., 2011)

Using the standard formula, Equation 6-2, for combining the standard deviation of two sets of samples the standard deviation of the combined sample is found to be σ = 0.072 m/s.

$$\sigma = \sqrt{\left[{}^{[n_1\sigma_1^2 + n_2\sigma_2^2]}\Big/_{[(n_1 - 1) + (n_1 - 1)]} \right]} \qquad 6\text{-}2$$

Substituting the given data into Equation 6-3, the t value for the test, t-test, is 1.66.

$$t - test = \frac{|\mu_2 - \mu_1|}{\sigma\sqrt{({}^{1}/_{n_2} + {}^{1}/_{n_1})}} \qquad 6\text{-}3$$

Hence t-test =1.66, and the number of degrees of freedom is 24 (degrees of freedom of the system = $n_1 + n_2 - 2$).

Because it is unknown whether one mean is bigger or smaller than the other, the two-tailed test must be used. For the 5% confidence level (two tailed test) t-crit = 2.06 for 24 degrees of freedom (Murdoch and Barnes, 2008). Since t-test < t-crit, the result is not significant and H_o is accepted. The data suggests there was no significant difference between the mean velocities as found by the M12 method and the circumferential ring.

It is assumed:

(i) That the two tests were independently carried out, the results on one did not affect the other - this condition applies here.

(ii) That the distributions of measured velocities are Gaussian; since the thirteen samples were randomly selected from a large number of experimental results this can reasonably be taken to be the case here.

6.1.4 Comparison of Test Results with Results from other Methods

To validate slug velocities obtained using the AE technique, comparisons were made with measured slug velocities using the ultrasound transit time technique (USTT) and images from a High Speed Camera (HSC).

Measured slug velocities using the USTT were taken from the previous work on the same test rig facilities by Al-lababidi (2006) and compared with results obtained using the present AE method for the same superficial liquid and gas velocities as used by Al-lababidi.

In addition, and because of the limitation of the USTT technique with high gas void fraction, another set of higher values of V_{SG} (where the USTT does not work) were undertaken to compare the measured slug velocities obtained using AE and HSC. The facilities were set as shown in Figure 6-15, and the experiment carried out at different V_{SL} and V_{SG}. The results acquired by AE and simultaneously by the HSC were compared.

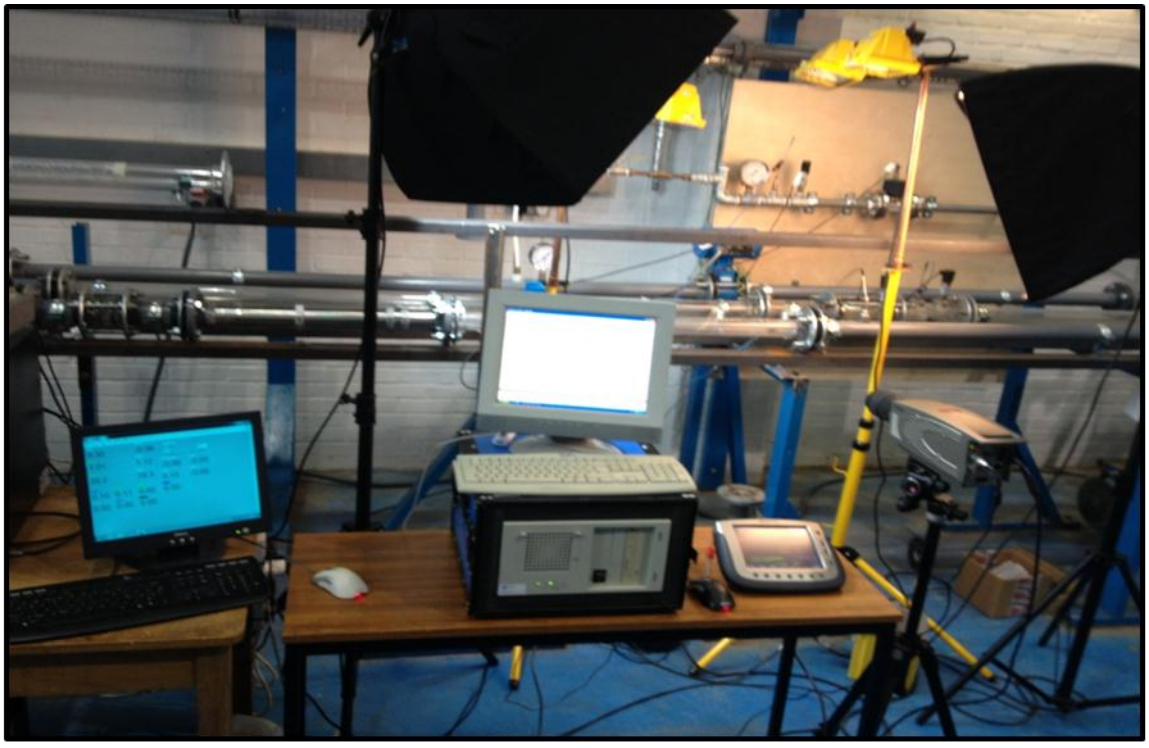

Figure 6-15 test-rig facilities set-up for validation

The different slug conditions under different superficial gas and liquid velocities are shown in Figure (6-16) which clearly shows that for high gas superficial velocity (greater than 2 m/s) the dominant phase in the front of the slug body is gas.

The acquired AE data was processed using MATLAB code (see Sections 6.1.1 and 6.1.2) to detect the presence of the slug, determine the time taken to travel from one detector to the second and then calculate the slug velocity. This was done for each V_{SL} and V_{SG}. The slug velocities obtained using HSC were calculated by determining the number of frames between the two marker points (21cm) to obtain the time difference. Slug velocity for each V_{SL} and V_{SG} was calculated using Equation (6-1). The slug velocity using USTT was taken from Al-lababidi (2006).

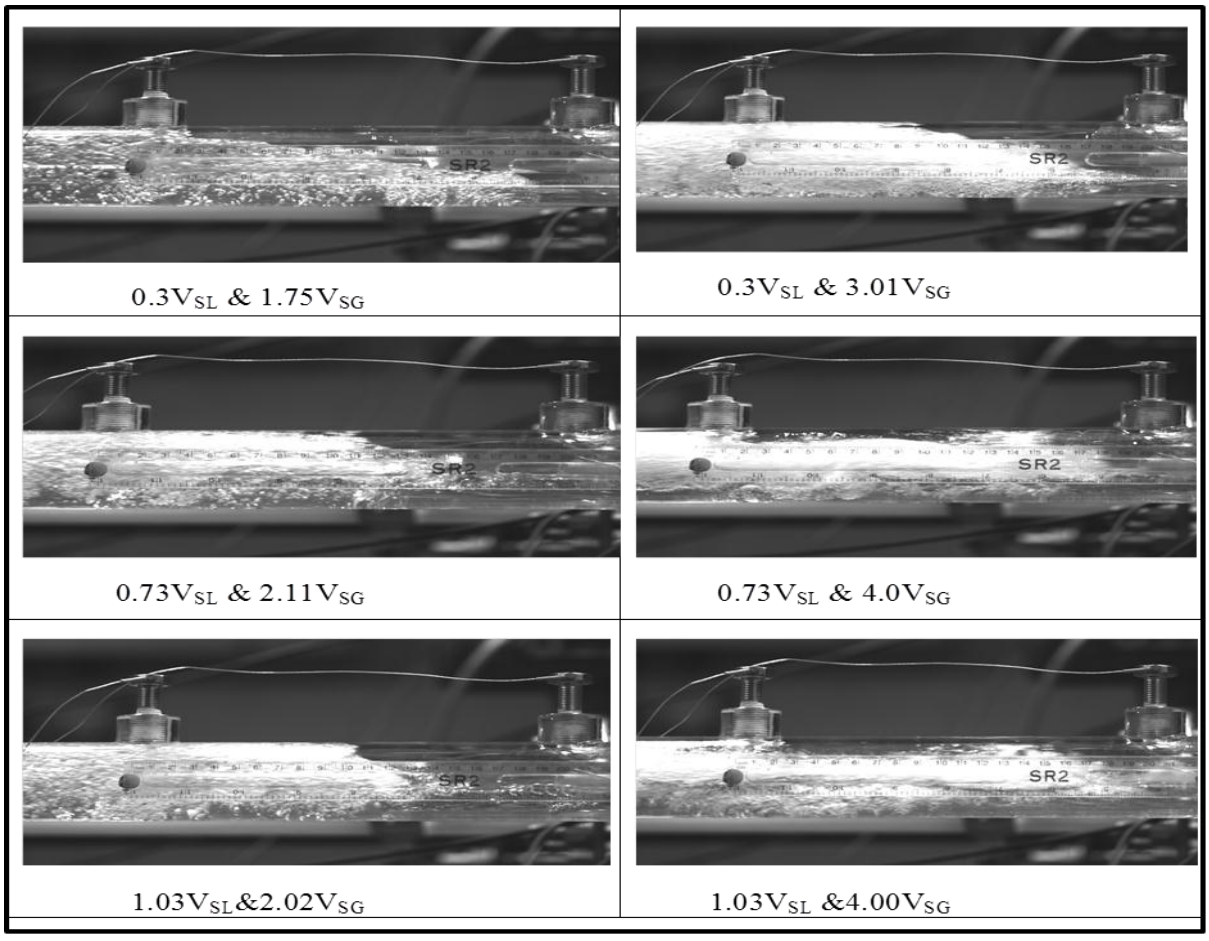

Figure 6-16 Two-phase slug flow images using HSC

Tables (6-5 to 6-9) show the measured slug velocities of two phase flow using AE, HSC and USTT. It can be seen that the three techniques give very similar results at low gas void fraction while USTT does not work at high gas void fraction due to the rapid attenuation ultrasonic waves under these conditions.

All three techniques show that the slug velocity is always higher than mixed flow velocity. Measured slug velocities using AE and HSC seem to be closer for most flow rates (V_{SL} and V_{SG}) compared to USTT, see Figures 6-17 to 6-20.

Table 6-5 Measured slug velocity at 0.3 V_{SL}

Superficial Liquid Velocity V_{SL} (M/s)	Superficial Gas Velocity V_{SG} (m/s)	GVF (%)	EL (Slug Liquid Hold-up)	Mixture Velocity (m/s)	Slug Velocity Using USTT (m/s)	Slug Velocity Using AE (m/s)	Slug Velocity Using HSC (m/s)
0.30	0.60	66.67	0.33	0.90	1.16	1.085	1.175
0.30	0.80	72.73	0.27	1.10	1.56	1.368	1.514
0.30	1.00	76.92	0.23	1.30	1.70	1.554	1.694
0.30	1.48	83.15	0.17	1.78	1.88	1.980	2.072
0.30	1.75	85.37	0.15	2.05	2.67	2.421	2.461
0.30	2.07	87.34	0.13	2.37	3.10	2.732	2.603
0.30	3.01	90.94	0.09	3.31	3.97	3.761	3.540
0.30	4.01	93.04	0.07	4.31	High Gas Ratio (US Attenuation)	4.678	4.820
0.30	5.50	94.83	0.05	5.80	High Gas Ratio (US Attenuation)	6.138	5.940
0.30	6.50	95.59	0.04	6.80	High Gas Ratio (US Attenuation)	7.258	6.428
0.30	7.50	96.15	0.04	7.80	High Gas Ratio (US Attenuation)	8.154	8.326

Table 6-6 Measured slug velocity at 0.5 V_{SL}

Superficial Liquid Velocity V_{SL} (M/s)	Superficial Gas Velocity V_{SG} (m/s)	GVF (%)	EL (Slug Liquid Hold-up)	Mixture Velocity (m/s)	Slug Velocity Using USTT (m/s)	Slug Velocity Using AE (m/s)	Slug Velocity Using HSC (m/s)
0.50	0.62	55.36	0.45	1.12	1.62	1.214	1.458
0.50	0.83	62.41	0.38	1.33	1.88	1.512	1.465
0.50	1.03	67.32	0.33	1.53	1.96	1.789	1.630
0.50	1.52	75.25	0.25	2.02	2.07	2.660	2.461
0.50	1.77	77.97	0.22	2.27	2.37	2.591	2.380
0.50	2.07	80.54	0.19	2.57	3.20	2.904	2.760
0.50	2.67	84.23	0.16	3.17	3.21	3.382	3.387
0.50	3.15	86.30	0.14	3.65	4.09	3.963	4.038
0.50	4.50	90.00	0.10	5.00	High Gas Ratio (US Attenuation)	5.457	5.000
0.50	5.50	91.67	0.08	6.00	High Gas Ratio (US Attenuation)	6.023	6.653
0.50	6.00	92.31	0.08	6.50	High Gas Ratio (US Attenuation)	7.185	6.802
0.50	6.50	92.86	0.07	7.00	High Gas Ratio (US Attenuation)	7.082	7.102
0.50	7.50	93.75	0.06	8.00	High Gas Ratio (US Attenuation)	8.160	8.304

Table 6-7 Measured slug velocity at 0.73 V_{SL}

Superficial Liquid Velocity V_{SL} (M/s)	Superficial Gas Velocity V_{SG} (m/s)	GVF (%)	EL (Slug Liquid Hold-up)	Mixture Velocity (m/s)	Slug Velocity Using USTT (m/s)	Slug Velocity Using AE (m/s)	Slug Velocity Using HSC (m/s)
0.73	0.63	46.32	0.54	1.36	1.73	1.739	1.759
0.73	0.84	53.50	0.46	1.57	1.96	1.846	1.800
0.73	1.05	58.99	0.41	1.78	2.18	2.117	1.886
0.73	1.26	63.32	0.37	1.99	2.56	2.282	2.234
0.73	1.54	67.84	0.32	2.27	2.65	2.663	2.440
0.73	1.76	70.68	0.29	2.49	2.90	2.719	2.580
0.73	2.11	74.30	0.26	2.84	3.46	3.178	3.380
0.73	2.47	77.19	0.23	3.20	4.74	3.578	3.968
0.73	2.95	80.16	0.20	3.68	4.91	3.891	4.022
0.73	3.15	81.19	0.19	3.88	High Gas Ratio (US Attenuation)	4.259	4.200
0.73	4.50	86.04	0.14	5.23	High Gas Ratio (US Attenuation)	5.489	5.625
0.73	5.50	88.28	0.12	6.23	High Gas Ratio (US Attenuation)	6.532	6.170
0.73	6.50	89.90	0.10	7.23	High Gas Ratio (US Attenuation)	7.329	7.875
0.73	7.50	91.13	0.09	8.23	High Gas Ratio (US Attenuation)	8.402	8.077

Table 6-8 Measured slug velocity at 0.93 V_{SL}

Superficial Liquid Velocity V_{SL} (M/s)	Superficial Gas Velocity V_{SG} (m/s)	GVF (%)	EL (Slug Liquid Hold-up)	Mixture Velocity (m/s)	Slug Velocity Using USTT (m/s)	Slug Velocity Using AE (m/s)	Slug Velocity Using HSC (m/s)
0.93	0.62	40.00	0.60	1.55	1.93	1.815	1.607
0.93	0.82	46.86	0.53	1.75	2.17	1.961	1.842
0.93	1.01	52.06	0.48	1.94	2.50	2.151	2.019
0.93	1.26	57.53	0.42	2.19	2.81	2.297	2.207
0.93	1.49	61.57	0.38	2.42	3.10	2.752	2.910
0.93	2.07	69.00	0.31	3.00	3.46	3.413	3.650
0.93	3.15	77.21	0.23	4.08	High Gas Ratio (US Attenuation)	4.538	4.565
0.93	4.50	82.87	0.17	5.43	High Gas Ratio (US Attenuation)	6.215	6.848
0.93	5.50	85.54	0.14	6.43	High Gas Ratio (US Attenuation)	7.044	7.159
0.93	6.50	87.48	0.13	7.43	High Gas Ratio (US Attenuation)	7.764	7.683
0.93	7.50	88.97	0.11	8.43	High Gas Ratio (US Attenuation)	8.632	8.513

Table 6-9 Measured slug velocity at 1.03V_{SL}

Superficial Liquid Velocity V_{SL} (M/s)	Superficial Gas Velocity V_{SG} (m/s)	GVF (%)	EL (Slug Liquid Hold-up)	Mixture Velocity (m/s)	Slug Velocity Using USTT (m/s)	Slug Velocity Using AE (m/s)	Slug Velocity Using HSC (m/s)
1.03	0.82	44.32	0.56	1.85	2.31	2.248	1.981
1.03	1.00	49.26	0.51	2.03	2.61	2.413	2.299
1.03	2.02	66.23	0.34	3.05	3.75	3.450	3.705
1.03	3.15	75.36	0.25	4.18	High Gas Ratio (US Attenuation)	4.816	4.846
1.03	3.50	77.26	0.23	4.53	High Gas Ratio (US Attenuation)	5.203	5.326
1.03	4.00	79.52	0.20	5.03	High Gas Ratio (US Attenuation)	5.413	5.557
1.03	4.50	81.37	0.19	5.53	High Gas Ratio (US Attenuation)	5.795	5.834
1.03	5.00	82.92	0.17	6.03	High Gas Ratio (US Attenuation)	6.483	6.875
1.03	5.50	84.23	0.16	6.53	High Gas Ratio (US Attenuation)	6.945	7.159
1.03	6.50	86.32	0.14	7.53	High Gas Ratio (US Attenuation)	7.544	7.683
1.03	7.50	87.92	0.12	8.53	High Gas Ratio (US Attenuation)	8.632	8.865

From Figures 6-17to 6-21, the measurements for the slug velocities using the high speed camera were in good general agreement with the slug velocities obtained using the AE technique. The difference between slug velocities using AE and HSC was in the range 1% to 10%. Using the transit time ultrasound technique, the measured velocity was in reasonable agreement with the measurements made with both AE and HCS over the flow range for which USTT was applicable. The range of applicability was 0.6 m/s to 2 m/s for VSG and 40% to 75% GVF in the slug body. However, and as reported by Al-lababidi (2006), the ultrasound signals are attenuated by the presence of the gas bubble in the slug body, resulting in failure of slug detection and slug velocity measurements.

For the AE technique and based on the experimental work, it is clear that this technique can continue to operate at high gas velocities typically above 2 m/s which corresponds to gas void fraction in the slug body of 95% or higher.

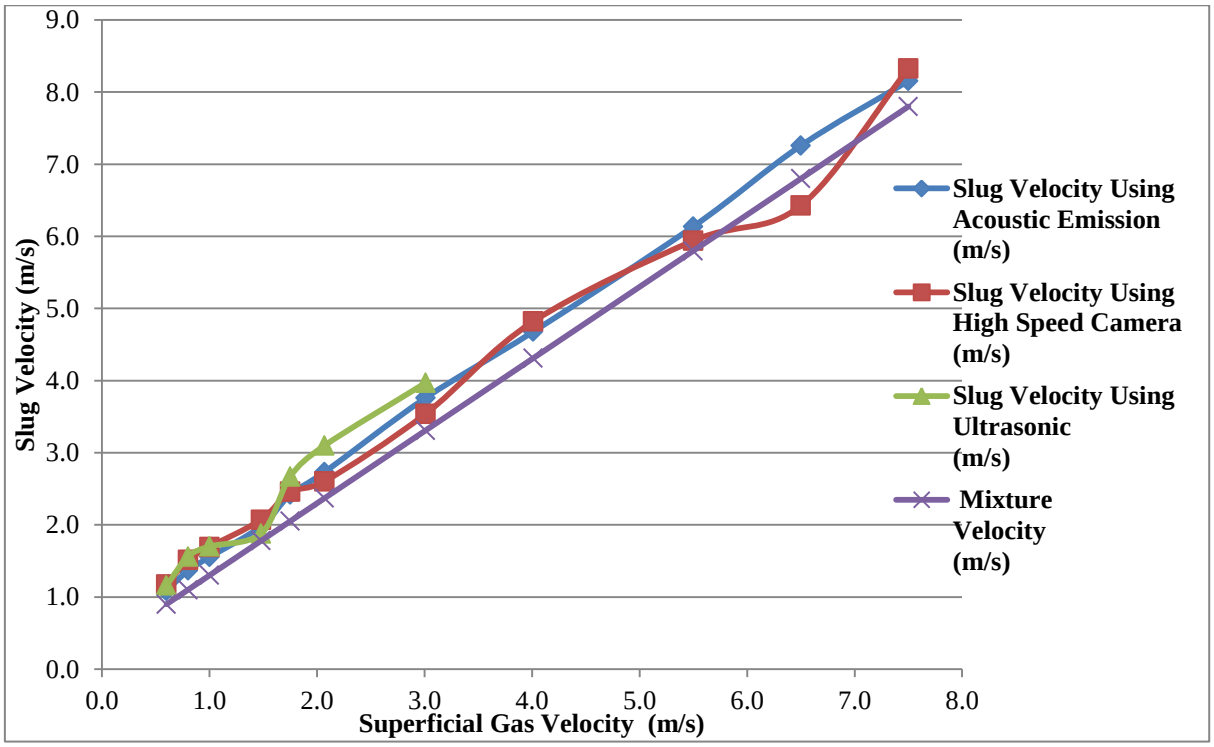

Figure 6-17 Comparative of slug velocity results at 0.30 V_{SL}

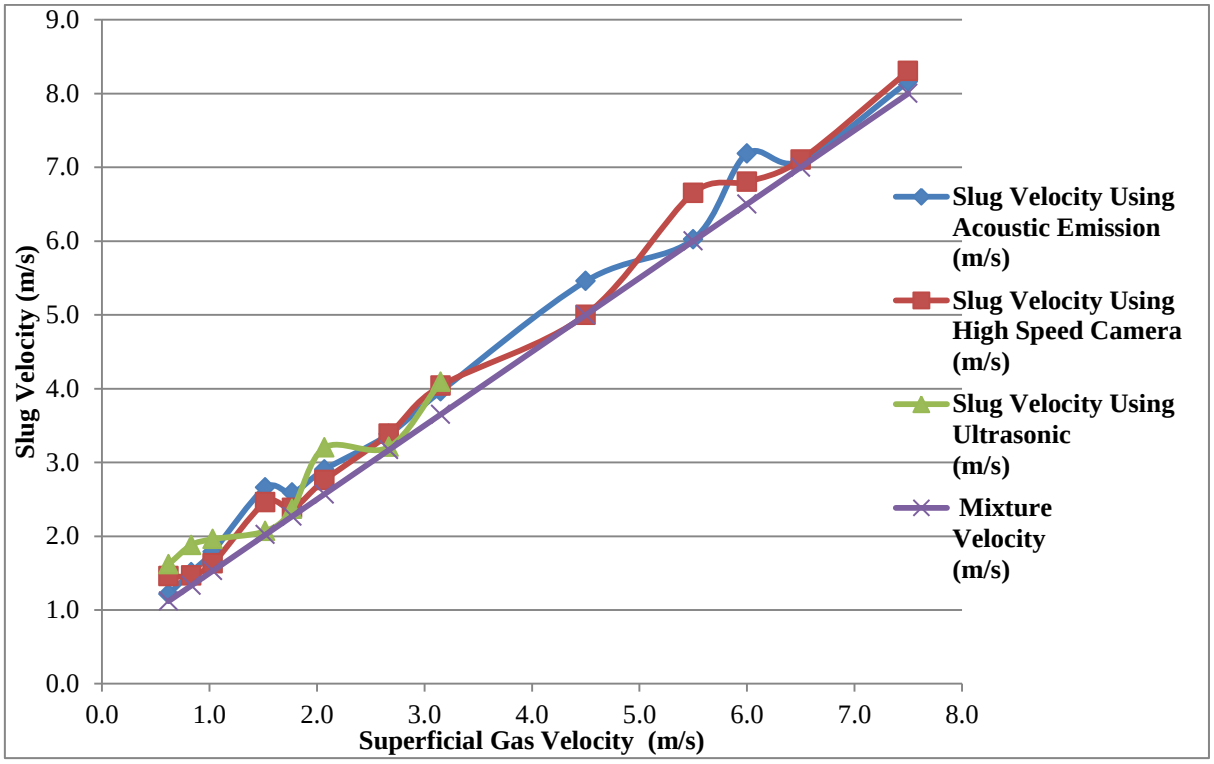

Figure 6-18 Comparative of slug velocity results at 0.50 V_{SL}

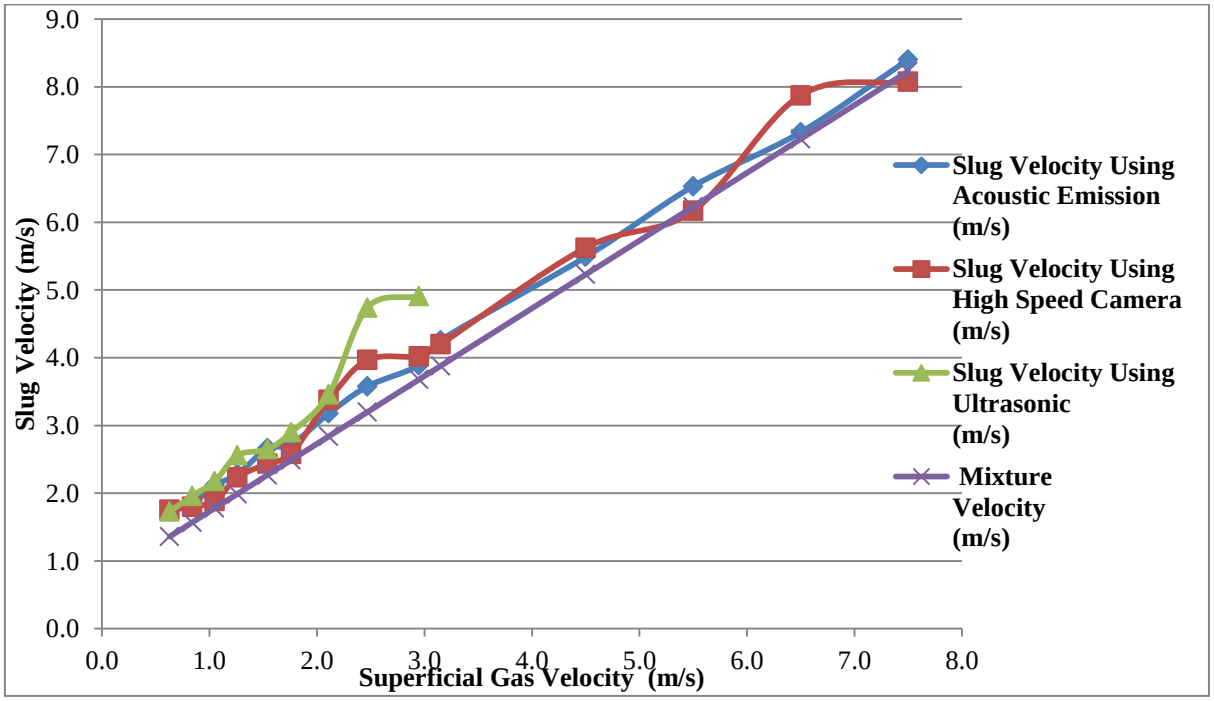

Figure 6-19 Comparative of slug velocity results at 0.73 V_{SL}

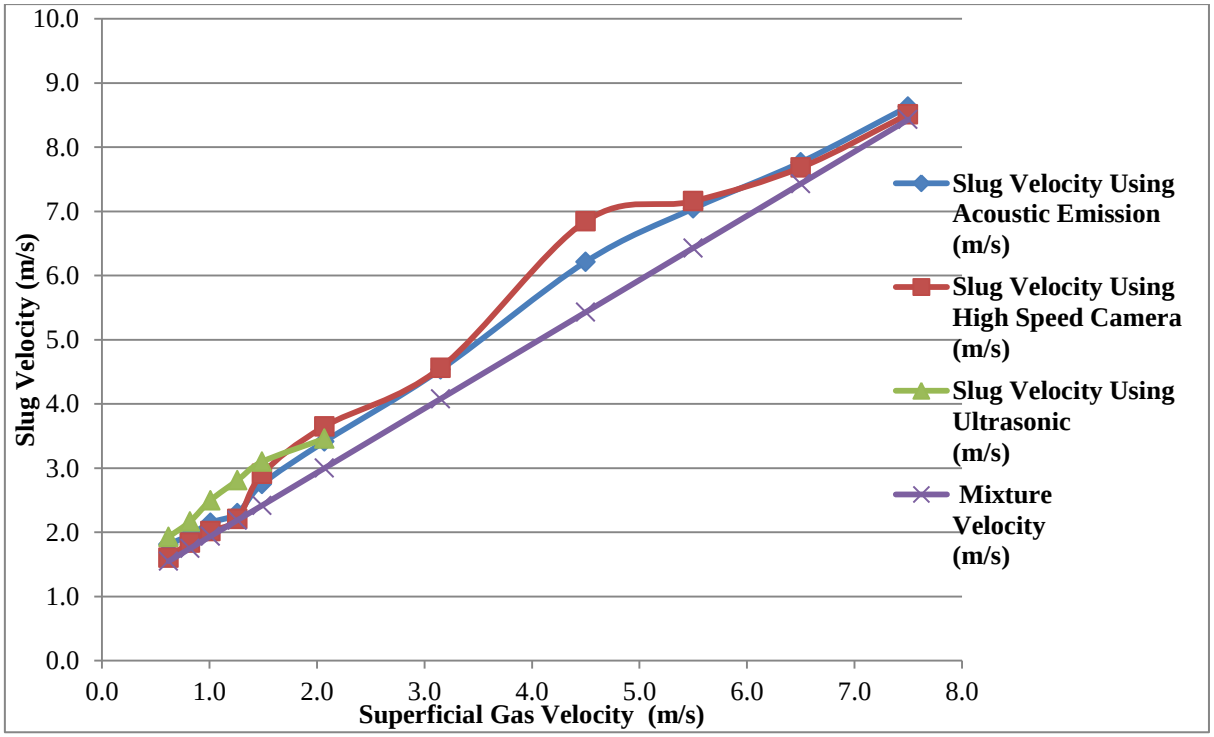

Figure 6-20 Comparative of slug velocity results at 0.93 V_{SL}

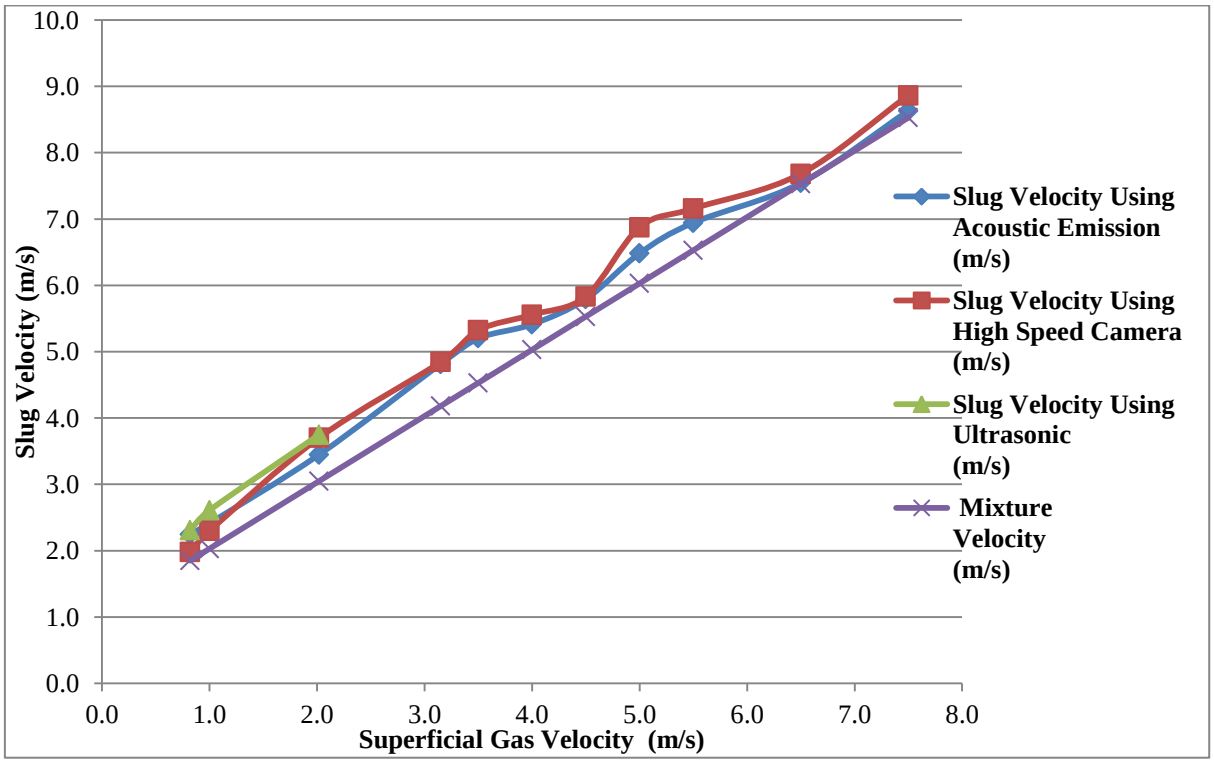

Figure 6-19 Comparative of slug velocity results at 1.03 V_{SL}

6.2 Flow regime recognition

Many tests were conducted to determine the optimum test-rig design for the detection of slugs in two phase flow and determination of slug velocity. The test-rig was used to investigate the capability of AE technology not only to determine slug flow velocity but also to recognise two phase flow regimes.

An AE Pico sensor was mounted on a waveguide (M12 hexagonal bolt) fitted onto the Perspex pipe section in a specifically designed housing as shown in Figure 6-22. This housing was constructed to allow for direct contact between the waveguide and the fluid passing inside the pipe. The AE system was programmed for a 32 dB threshold to avoid background noise and a 2 MHz sampling rate. The experiment was undertaken at different superficial gas (V_{SG}) and liquid (V_{SL}) velocities. The superficial velocities investigated ranged from (0-9.5) m/s V_{SG} and (0-6.3) m/s V_{SL}. AE signals of each pair of V_{SL} and V_{SG} simulation was recorded to be analysed afterward. It was observed that the captured AE signals of different V_{SL} and V_{SG} are distinguishable as shown in Figure 6-23.

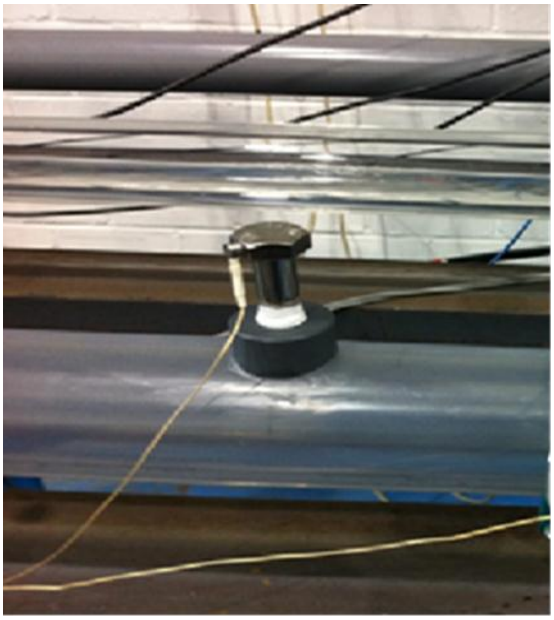

Figure 6-20 M12 waveguide and AE Pico sensor installation for two phase flow regime recognition

A total of 627 different tests were carried out to cover the whole range of superficial gas and liquid velocities that could be achieved by the available facilities. The experiment began with a fixed 0.1 m/s V_{SL} and increasing V_{SG} gradually from 0.0 m/s to 9.5 m/s in increments of 0.5 m/s. Superficial liquid velocity was increased in increments of 0.2 m/s and for each value of V_{SL} the same V_{SG} velocities were used.

The AE signals were captured for each run. It can be seen from Figure 6-23 that three different flow regimes were clearly distinguishable from the AE signals. A V_{SL} in the range 0.1-0.7 m/s accompanied by a gas velocity of less 1 m/s produced no AE signal; the flow was stratified flow, see Figure 6-23-A.

As the flow rates of both V_{SL} and V_{SG} increased, the flow generates AE energy as a result of bubble formation, oscillation and collapse. However, from about 0.3 m/s V_{SL} and 1.10 m/s V_{SG} slug flow appears, as shown in Figure 6-23-B.

When the liquid velocity increased to above about 3 m/s with superficial gas velocity above 0.5 m/s, a third regime (bubble flow) is generated, as shown in Figure 6-23-C.

The above conclusions were based on comparison of visual observation and changes in AE signal waveform. To prove that the AE waveform can, indeed, predict the flow regime the Kolmogorov–Smirnov (KS) test was used.

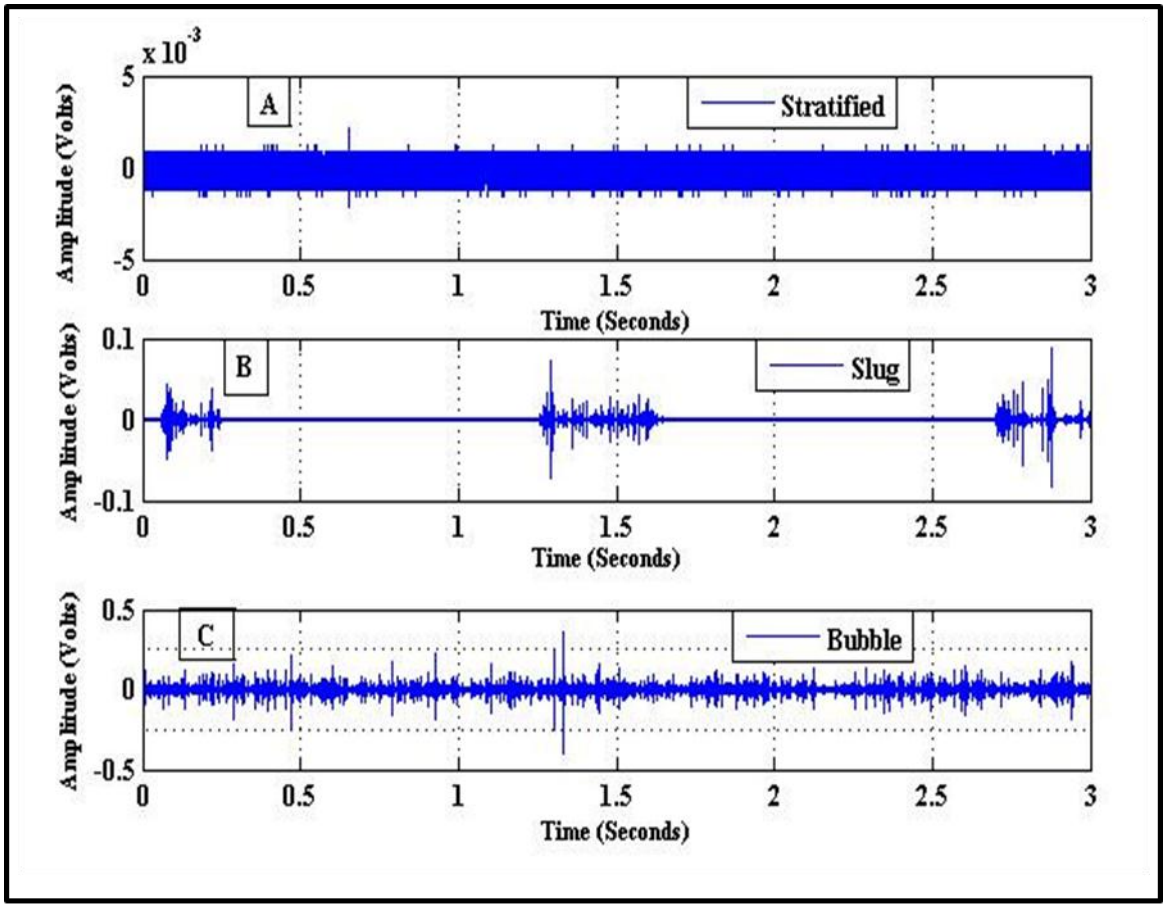

Figure 6-21 Original captured AE waveform signals

6.2.1 Kolmogorov–Smirnov test (KS-test)

The KS test is a simple but powerful tool which assesses goodness-of-fit. It is a statistical algorithm used to compare the distributions of the values in two data sets (X1 and X2) based on the null hypothesis that X1 and X2 have the same continuous distribution; that is H0: F1(X) =F2(X) for all (X).

The alternative hypothesis is that the data sets come from different distributions, that is H1: F1(X) ≠ F2(X) for all (X). The KS-statistic is obtained by calculating the distance (D) which is the maximum absolute difference between the cumulative density function (CDF) of X1 and X2 using Equation (6-2) (Chen et al., 2008):

$$D = \max_{-\infty \le x \le \infty} (|F_1(x) - F_2(x)|) \qquad 6\text{-}4$$

Where F1(X) is the proportion of X1 values less than or equal to x and F2(X) is the proportion of X2 values less than or equal to x.

If the result is H=1, it means the hypothesis that the two data sets have the same distribution and can be rejected at the 5% significance level. If the result is H= 0, it means the hypothesis that the two data sets have the same distribution and cannot be rejected at the 5% significance level. The p-value of KS-test is the probability of wrongly rejecting the null hypothesis if it is in fact true. It is equal to the significance level of the test for which the null hypothesis is rejected. The null hypothesis is unlikely to be true if p-value is small. The smaller it is, the more convincing is the rejection of the null hypothesis and the two data set distributions are different. I e H = 1 and H= 0 is rejected if the p-value is less than 5%. P-value is a strong indication of evidence to reject the null hypothesis (Chen et al., 2008).

6.2.3 Recognition of flow regime

The KS-test was employed to differentiate the three flow regimes quantitatively, see Table 6-10. The significant level (P-value) of the difference between AE waveform distributions is at the 5% significance level. Figures 6-24 to 6-27 present the overlying plots of the empirical cumulative density function (CDF) to visualize the difference of the AE waveform signals captured in this experiment.

Table 6-10 KS test distance and p-value for flow regime recognition

KS-parameters	Stratified/stratified	Stratified/slug	Stratified/bubble	Slug/bubble
H	1	1	1	1
P-value	1.9 %	0 %	0 %	0 %
D	0.002	0.5083	0.3547	0.3863

Figure 6-24 shows the stratified-stratified signals are almost identical but the hypothesis that the two are the same flows is rejected. The p-value is 1.9% for stratified flow arises from the maximum difference, D = 0.002 which is relatively small compared to the maximum distances found for the other signals. Figure 6-25 presents CDF plots for stratified and slug flows and these have D = 0.5083 and p-value of 0%, they can be clearly differentiated with a very high degree of confidence. Stratified and bubble signals are compared in Figure 6-26, D = 0.3457 and the p-value was 0%, they can be clearly differentiated with a very high degree of confidence. To make sure that KS test can differentiate between the three signals, slug and bubble signals are presented Figure 6-27. The maximum difference was 0.3863 and the p-value was 0%. This leads to the conclusion that flow regimes of two phase flow in horizontal pipes can be recognized by using a combination of AE technology and the Kolmogorov–Smirnov test.

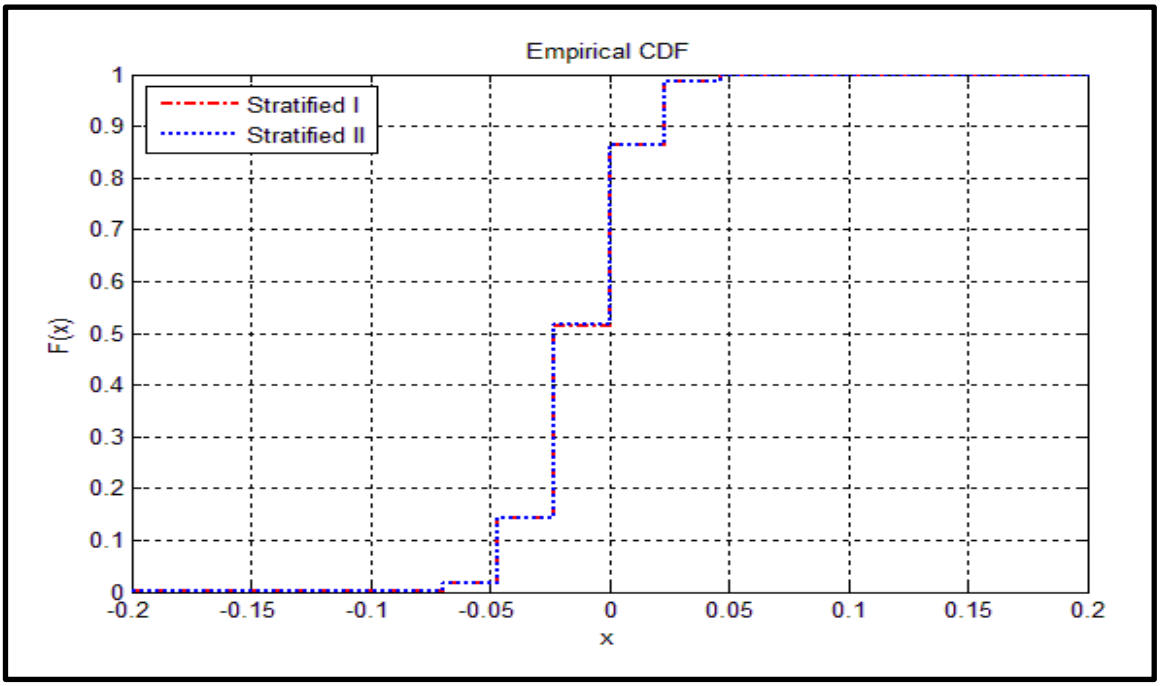

Figure 6-22 KS test CDF of stratified-stratified signals

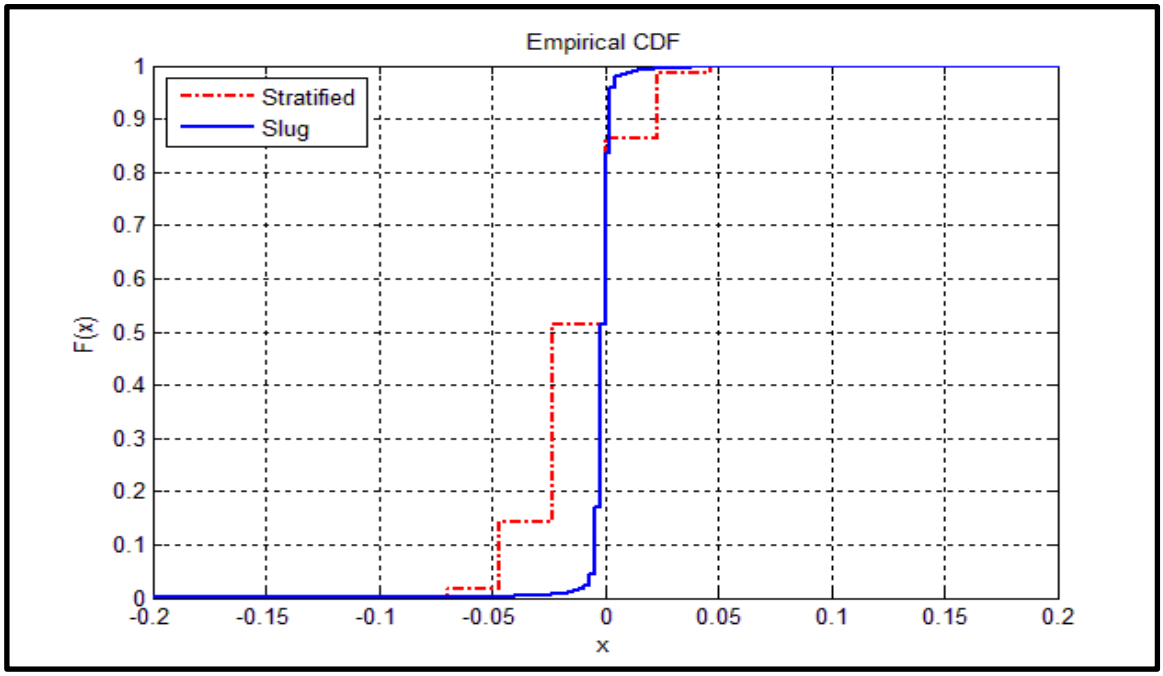

Figure 6-23 KS test CDF of stratified-slug signals

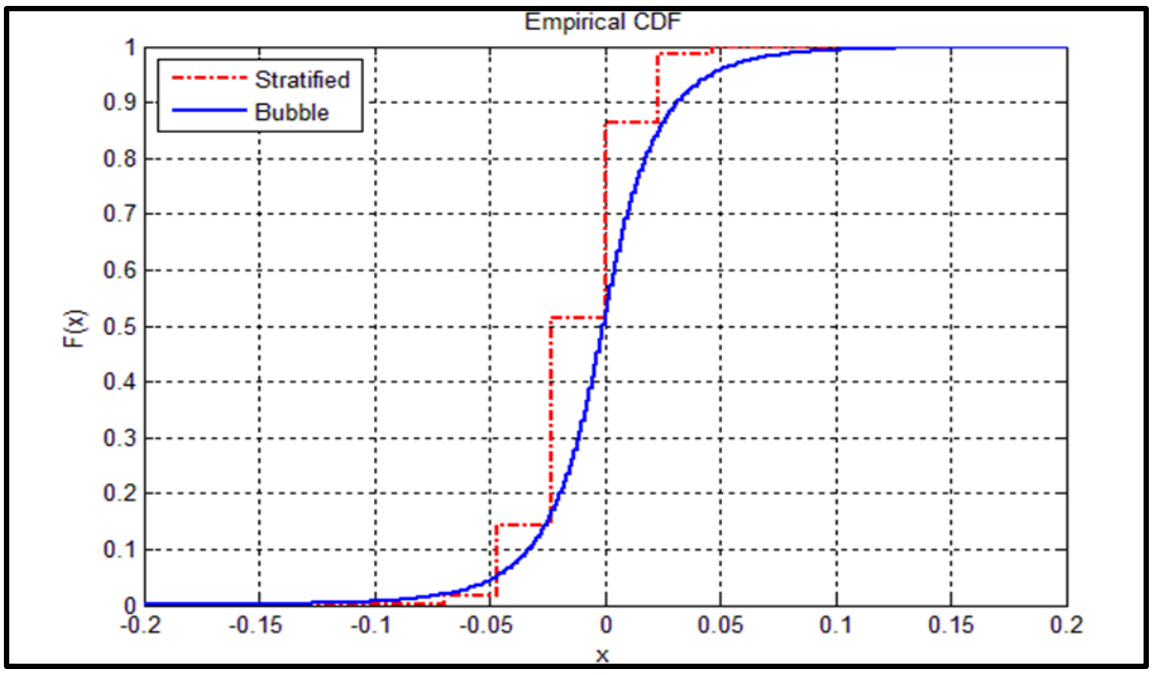

Figure 6-24 KS test CDF of stratified-bubble signals

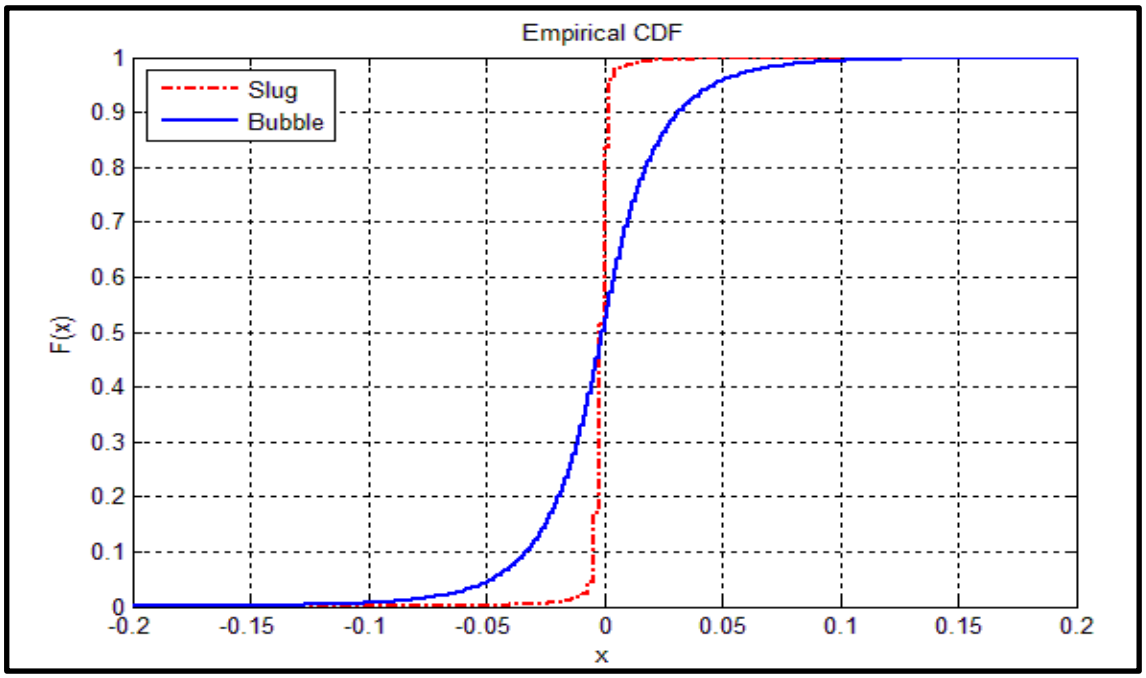

Figure 6-25 KS test CDF of slug-bubble signals

Chapter 7 Conclusions and recommendations for future work

7.1 Conclusions

7.1.1 Test-rig design and construction

The major objective of this study is investigating the capability of Acoustic Emission (AE) Technology to measure slug velocity and recognise flow regimes in two phase air/water flow in horizontal pipes. As measuring slug velocity was the most challenging objective this was the determining factor in the design of the test-rig, see Figure 5-1.

Five methods were used: two non-intrusive methods involving - mounting AE sensors directly on the exterior of the steel pipe section with and without clamps (two different clamps were used to attenuate upstream and downstream AE energy travelling through the steel); and three intrusive methods with the sensors mounted flush with the inner wall of the pipe - using 4 mm ID Prismatic cylinders as waveguides; M12 hexagonal bolts as waveguides, and circumferential rings as waveguides, see Figures 5-9, 5-12 and 5-14 respectively.

The experiment was run for ranges of superficial liquid (V_{SL}) and gas (V_{SG}) velocities that covered the slug flow regimes. The acquired data was collected and stored for analysis and review.

With the test rig, it is concluded that non-intrusive acoustic emission cannot detect and measure the slug velocity of two phase flow in horizontal pipes. The captured AE waveforms for each of the three non-intrusive approaches were so noisy that the start and end of each burst signal cannot be distinguished. There was reduction in noise amplitude when clamps type I and II were applied but not sufficient to allow useful measurements of the AE signals generated by the flow in the immediate vicinity of the sensors. The steel pipe acted as a conduit for the AE energy generated by the flow upstream, underneath and downstream of

the AE sensors. Thus the design of the test-rig had to be adapted to detect and measure the relevant AE signals when using a steel pipe.

The first of the intrusive methods to detect and measure the AE signal was the insertion of two 4 mm diameter Prismatic cylinder fitted onto the Perspex pipe section in a specially designed housing and used as an AE waveguide. The inner surface was flush with the pipe and this design attenuated the unwanted AE signal, detecting the presence of the slug as it travelled past the AE waveguide. The captured AE waveforms were significantly improved in terms of the clarity of the start and end of each burst signal which could be clearly determined, see Figure 5-11. The rise time of each burst signal was very short with a clearly distinguishable peak so that arrival time could be easily determined.

However, these AE waveguides have very small surface area and as the energy source is uncontrolled it may not release energy immediately underneath the AE sensor. Increasing the sensor area would improve detection of the slug front as it passed underneath the AE waveguides. Using M12 hexagonal bolts as waveguides was the second intrusive approach. The captured AE signal quality improved significantly in terms of high intensity burst signals, distinct peaks and sharper rise times so that the arrival time of each waveform burst signal could easily be identified.

To test whether further increase in contact area would further improve the AE signal, another experiment was undertaken. The AE waveguide was a circumferential steel ring mounted inside the Perspex pipe flush with the pipe wall. Two AE Pico sensors were mounted on the ring. Under identical test conditions as the previous tests, it is clear that the signal quality is superior to that of the previous tests, with distinct peaks and improved consistency in slug detection; compare Figures 5-13 and 5-16.

However, the rise time obtained with this method was not as fast as with either the Prismatic cylinder or M12 waveguide methods. This led to difficulties in determining the precise arrival time of the slug at each AE sensor. A possible

reason for loss of precision is that the ring performed a kind of attenuation AE energy, Detected emitted energy on the other side of circumference of the flush rings, opposite AE sensors, were attenuated due to traveling before being captured by AE sensors. Flush rings and M12 waveguides were used to investigate the possibility of measuring the slug velocity in two phase (gas/water) flow in horizontal pipes.

7.1.2 Slug velocity measurement

The M12 waveguide experiment was conducted at four different superficial liquid velocities, 0.70, 1.02, 1.52 and 2.02 m/s V_{SL}, and four superficial gas velocities 1.02, 1.52, 2.02 and 2.52 m/s V_{SG}, to cover the whole range of slug flow regimes. The data acquired from AE were analysed to determine the arrival time of each slug at each AE sensor. The measured slug velocity varied slightly for the same values of V_{SL} and V_{SG} because of the uncontrolled manner in which AE energy is released from the slug, minor variations in the liquid and gas flow rate as controlled by throttling valve and brass gate respectively, and perturbations in the flow dynamics. However, the average measured slug velocity at each V_{SL} and V_{SG} was always higher than mixture velocity by between 9% and 26%.

The flush ring waveguides intrusive method was also used to measure slug velocity in two phase flow under the same operating conditions. For the same reasons as with the M12 waveguides, there were some minor variations in slug velocities at constant V_{SL} and V_{SG}. It was found that the arrival time of the slugs was more difficult to detect compared to using M12 waveguides. It was again found that the average measured slug velocity at each V_{SL} and V_{SG} was always higher than mixture velocity by between 9% and 24%. This means that with flush rings AE waveguide there is no significant difference in the mean values compared to M12 waveguide intrusive method.

The M12 waveguide method is easy to implement and can be installed at any point on a pipeline. Also, the results obtained by M12 and flush rings show no significant difference in measured mean velocities. Thus the validation of the AE

results using a high speed camera (HSC) and Ultrasound Transit Time (USTT) was conducted using M12 AE waveguide intrusive methods.

Previous work measuring two phase slug velocity using USTT was carried out on the same facilities of the test rig. The AE method was used to measure slug velocity using the same V_{SL} and V_{SG} values as had been used for the USTT tests. The HSC was installed to film the slug flow simultaneously with the AE measurements. The results show good agreement among the three techniques at low superficial gas velocities where the USTT method is applicable. There is also good agreement between the HSC and AE results at up to 95% V_{SG} where USTT cannot operate. The differences between slug velocities measured with AE and HSC was in the range 1% to 10%.

These results confirm that in horizontal pipes Acoustic Emission technology has the capability of detecting the presence of slug flow, as shown in Figure 7-1 and measuring slug velocity in two phase flow that contain up to 95% GVF. Thus, AE can overcome the limitations of the USTT method as shown in Figure 7-2.

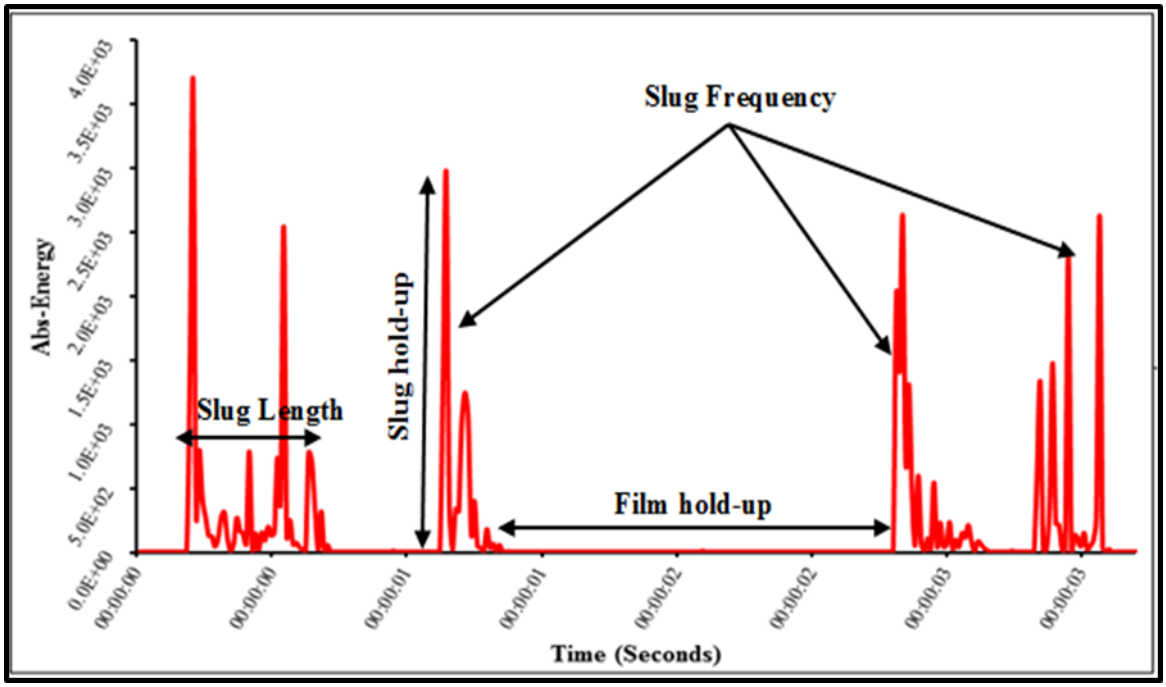

Figure 7-1Slug signal captured by Acoustic Emission probe

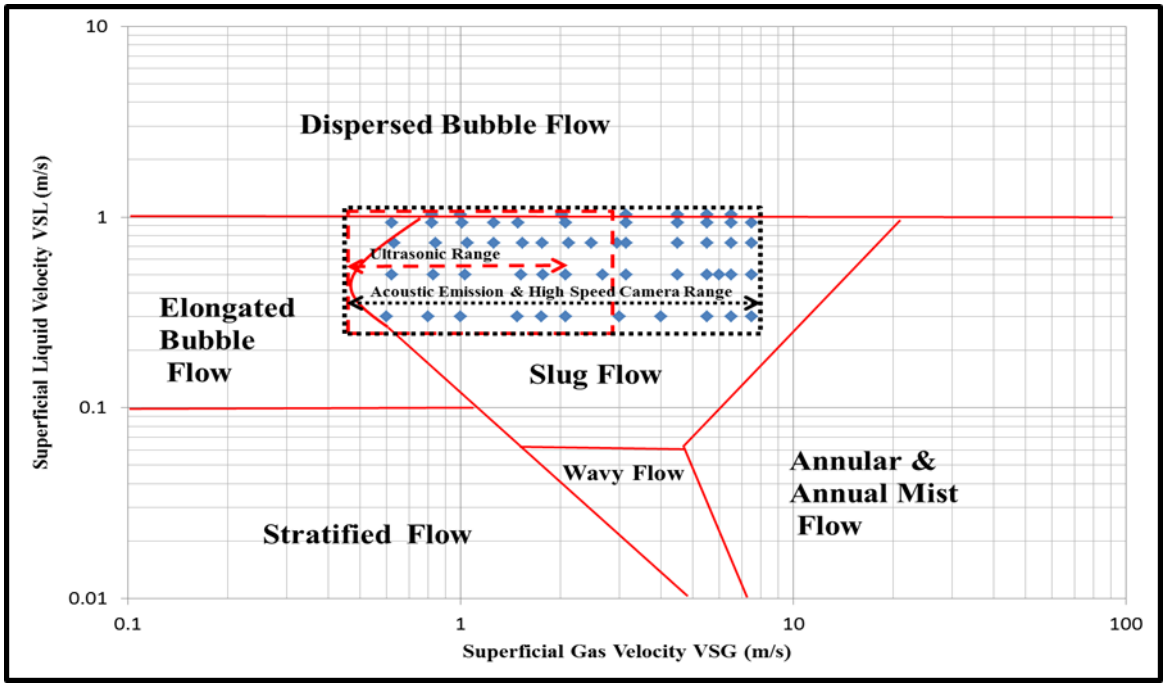

Figure 7-2 Two phase flow experimental campaigns map

7.1.3 Flow regime recognition

Two phase flow regime recognition was achieved by the using M12 AE waveguide intrusive method. A total of 627 different tests were undertaken covering the entire range of superficial gas and liquid velocities that can be achieved by the available facilities. From 0.0 to 6.5 m/s V_{SL} with an increment of 0.2 m/s and from 0.0 to 9.5 m/s V_{SG} with an increment of 0.5 m/s. For each V_{SL}, the whole range of V_{SG} flows was used. The AE signals for each run were captured and three different and easily distinguishable types of AE signal were detected associated with one of three flow regimes; stratified, slug and bubble flow. The gas flow rate limitation in this test-rig meant these were the only flow regimes possible. The Kolmogorov–Smirnov test was used to assess whether the three AE waveforms were quantitatively different. The result showed that applying the K-S test to the AE signals identifies the flow regime of two phase flow that travels through horizontal pipe whether it is stratified, slug or bubble regime.

In summary, it can be concluded that:

- Acoustic Emission technology is not suitable as a non-intrusive technique (simply mounting the AE sensors externally) for measuring the slug velocity in two phase flow in horizontal steel pipe.
- Acoustic Emission technology is not suitable as a non-intrusive technique (simply mounting the AE sensors externally) for measuring the slug velocity in two phase flow in horizontal steel pipe.
- Acoustic emission technology can successfully measure slug velocity in two phase flow horizontal pipes using intrusive methods. Area of contact between AE sensor and flow is important and it was found that using M12 hexagonal bolts mounted flush with the internal wall as waveguides gave good accuracy when measuring slug velocity. Circumferential steel rings mounted flush with the internal pipe wall also gave good accuracy when measuring slug velocity in two phase flow in horizontal Perspex pipes.
- Good agreement of slug velocity was between three different measurement methods, AE, HSC and USTT at low gas void fraction. There was also good agreement between slug velocities measured by AE and HSC at high gas void fraction (up to 95% GVF). The differences in slug velocities were typically less than 10%.
- Acoustic Emission Technology can differentiate two phase flow regimes in horizontal pipes.

It is conclude that Acoustic Emission Technology has the capability to contribute more to multiphase flow monitoring. In addition to the previous capability in the literature review (chapter III), this study provides an effective detection and measuring method for slug velocity and flow regime recognition in two phase flow in horizontal pipes.

7.2 Contribution to knowledge:

The major contribution to knowledge is the development of a new method to measure slug velocity and recognize flow regimes in two phase horizontal flow.

7.3 Recommendations for future work

The research work described in this thesis could be extended in particular by:

- Installing Teflon sections into the steel pipe to filter out unwanted AE energy travelling upstream and downstream in the steel pipe.
- Applying AE technology to the measurement of slug frequency in two phase flow.
- Investigating empirical correlation between two phase flow regimes and gas void fraction
- Improving the test rig by increasing air compressor capability to cover the four common flow regimes and further develop flow regime recognition using AE technology.

REFERENCES

Addali, A. (2010), Monitoring Gas Void Fraction in Two-phase Flow with Acoustic Emission (PhD thesis), Cranfield University, Cranfield University Library.

Ahmed, W. H. (2006), Capacitance sensors for void-fraction measurements and flow pattern identification in air–oil two-phase flow, IEEE Sensors Journal, vol. 6, pp. 1153 - 1163.

Ai, Q., Liu, C., Chen, X., He, P. and Wang, Y. (2010), Acoustic emission of fatigue crack in pressure pipe under cyclic pressure, Nuclear Engineering and Design, vol. 240, no. 10, pp. 3616 - 3620.

Ajbar, A., Al-Masry, W. and Ali, E. (2009), Prediction of flow regimes transitions in bubble columns using passive acoustic measurements, Chemical Engineering and Processing: Process Intensification, vol. 48, no. 1, pp. 101-110.

Albion, K., Briens, L., Briens, C. and Berruti, F. (2007), Flow regime determination in horizontal pneumatic transport of fine powders using non-intrusive acoustic probes, Powder Technology, vol. 172, no. 3, pp. 157-166.

Al-lababidi, S., Addali, A., Yeung, H. and Mba, D. (2009), Gas void fraction measurement in two-phase gas/liquid slug flow using acoustic emission, Journal of vibration and acoustics, vol. 131, no. 6, pp. 064501-11.

Al-Lababidi, S. (2006), Multiphase flow measurement in the slug regime using ultrasonic measurement techniques and slug closure model (PhD thesis), Cranfield University, Cranfield University Library.

Al-Masry, W. A., Ali, E. M. and Aqeel, Y. M. (2005), Determination of bubble characteristics in bubble columns using statistical analysis of acoustic sound measurements, Chemical Engineering Research and Design, vol. 83, no. 10, pp. 1196 -1207.

Al-Safran, E. (2009), Investigation and prediction of slug frequency in gas/liquid horizontal pipe flow, Journal of Petroleum Science and Engineering, vol. 69, no. 1–2, pp. 143-155.

Andreussi, P. and Bendiksen, K. (1989), An investigation of void fraction in liquid slugs for horizontal and inclined gas—liquid pipe flow, International Journal of Multiphase Flow, vol. 15, no. 6, pp. 937-946.

Bendiksen, H.; (1984), An experimental investigation of the motion of long bubbles in inclined tubes, International Journal of Multiphase Flow, Vol. 10, no. 4, pp. 467-483,

Bendjaballah, N., Dhaouadi, H., Poncin, S., Midoux, N., Hornut, J. and Wild, G. (1999), Hydrodynamics and flow regimes in external loop airlift reactors, Chemical Engineering Science, vol. 54, no. 21, pp. 5211-5221.

Bertani, C., De Salve, M. and and Malandrone, M. (2010), State-of-Art and selection of techniques in multiphase flow measurement, ENEA, no. Report RdS/2010/67.

Betteridge, D., Joshlin, M. T. and Lilley, T. (1981), Acoustic emissions from chemical reactions, Analytical Chemistry, vol. 53, no. 7, pp. 1064 -1073.

Bieberle, M., Fischer, F., Schleicher, E., Koch, D. a. M., H.J., Mayer, H. G. and Hampel, U. (2009), Experimental two-phase flow measurement using ultra-fast limited-angle-type electron beam X-ray computed tomography, Experiments in Fluids, vol. 47, no. 3, pp. 369 - 378.

Boyer, A., Duquenne, M. and Wild, G. (2002), Measuring techniques in gas-liquid and gas-liquid-solid reactors, Journal of Chemical Engineering Science, vol. 57, pp. 3185 - 3215.

Bratland, O. (2010), Pipe Flow 2, Multiphase Flow Assurance, Available at drbratland.com.

Camarasa, E., Viala, C., Poncin, S., Wild, G., Midouxa, N. and Bouillard, J. (1999), Influence of coalescence behaviour of the liquid and of gas sparging

on hydrodynamics and bubble characteristics in a bubble column, Chemical Engineering and Processing: Process Intensification, vol. 38, pp. 329 - 344.

Chatelier, le. (1923), La Métallographie. Recl. Trav. Chim. Pays-Bas, 42: 846–849. doi: 10.1002/recl.19230421006

Chen, H. X., Chua, P. S. K. and Lim, G. H. (2008), Fault degradation assessment of water hydraulic motor by impulse vibration signal with Wavelet Packet Analysis and Kolmogorov–Smirnov Test, Mechanical Systems and Signal Processing, vol. 22, no. 7, pp. 1670-1684.

Chen, L., Wood, S., Moore, S. and Nguyen, B. (2012), Acoustic Emission of Bubbly Flow and Its Size Distribution Spectrum, Proceedings of Acoustics 2012 - Fremantle, Australia, 21-23 November, .

Christopher, E. B. (2005), Fundamentals of Multiphase Flows, Cambridge University Press, UK.

Chunguo, J. and Qiuguo, B. (2009), Flow regime identification of gas/liquid two-phase flow in vertical pipe using RBF neural networks, Control and Decision Conference, 2009.CCDC '09. Chinese, pp. 5143.

Clayton, T. C. (ed.) (2005), Multiphase Flow Handbook, New Edition ed, CRC Press.

Colombo, S., Giannopoulos, A., Forde, M., Hasson, R. and Mulholland, J. (2005), Frequency response of different couplant materials for mounting transducers, In: Ndt & e international, vol. 38, no. 3, pp. 187--193.

Connor,T.(July17,2011),http://www.drtomoconnor.com/3760/3760lect03.htm (accessed November 25, 2011).

Costigan, G. and Whalley, P. B. (1997), Slug flow regime identification from dynamic void fraction measurements in vertical air-water flows, International Journal of Multiphase Flow, vol. 23, no. 2, pp. 263 - 282.

Crowther, T. G., Wade, A. P., Wentzell, P. D. and Gopal, R. (1991), Characterization of acoustic emission from an electrolysis cell, Analytica Chimica Acta, vol. 254, no. 1-2, pp. 223 - 234.

Czochralski, J. (1916), Metallographie des Zinns und die Theorie der Formänderung bildsamer Metalle, Metall und Erz, vol. 22, pp. 381-393.

Drouillard, T. F. (1996), A history of acoustic emission, Journal of AE, vol. 14, no. 1, pp. 1-34.

Duclos, J. B., Reuben, R. L. and Steel J. A. (2004), Study of Particle Impacts in Fluid Flow using Acoustic Emission, in: International Congress & Exhibition On Machine Tool Performance Monitoring, Vol. ISBN 0 – 954 1307 – 1 – 5, 2004, Heriot-Watt University, COMADEM, UK, pp. 566 -575.

Dukler, A. E. and and Hubbard, M. G. (1975), A model for gas-liquid slug flow in horizontal tubes, Industrial and Engineering Chemistry Fundamental, vol. 14, no. 4, pp. 337-347.

Dunegan, H. L. (2004), Location of Leaks in Pipes by Use of Acoustic Emission Modal Ratio Techniques , Dunegan Engineering Company Inc, URL www.deci.com.

Emerson, d. R. and Leonardo, G. J. (2005), A non-intrusive probe for bubble profile and velocity measurement in horizontal slug flows, Flow Measurement and Instrumentation, vol. 16, no. 4, pp. 229-239.

Envirocoustics. (2010), Testing Cryogenic Tank Walls with AE, available at: www.envirocoustics.gr (accessed July).

Fabre, J. and Line, A. (2010), Slug Flow, available at: http://www.thermopedia.com (accessed May/ 15).

Faia, P. M., Silva, R., Rasteiro, M. G., Garcia, F. A. P., Ferreira, A. R., Santos, M. J., Santos, J. B. and Coimbra, A. P. (2012), Imaging Particulate Two-Phase Flow in Liquid Suspensions with Electric Impedance

Tomography, Particulate Science and Technology, vol. 30, no. 4, pp. 329-342.

Fan, Z., Lusseyran, F. and and Hanratty, T. J. (1993), Initiation of slugs in horizontal gas-liquid flows, Journal of American Institute of Chemical Engineering, vol. 39, pp. 1741--1753.

Farrar, B., Samways, A. L., Ali, J. and Bruun, H. H. (1995), A computer-based hot-film technique for two-phase flow measurements, Measurement Science and Technology, vol. 6, no. 10, pp. 1528 –1537.

FlowMeters, c. (2010), Ultrasonic Flowmeters, available at: http://www.flowmeters.com/ufm/index.cfm?task=ultrasonic&TechFlash=transit%2Dtime%2Dulrasonic1%2Eswf (accessed April).

Foerster, F.; and Scheil, E.; (1936) Akustische Untersuchung der Bildungvon Marten-sitnadeln (Acoustic Study of the Formation of Martensile Needels). Zeitschrift fur Metallkunde 28(9), pp245-247.

Fusheng Zhang and Feng Dong (2010), A measurement method of slug flow velocity of gas-liquid two-phase flow in horizontal pipe, Instrumentation and Measurement Technology Conference (I2MTC), 2010 IEEE, pp. 250.

Ghosh, S., Pratihar, D. K., Maiti, B. and Das, P. K. (2012), Identification of flow regimes using conductivity probe signals and neural networks for counter-current gas–liquid two-phase flow, Chemical Engineering Science, vol. 84, no. 0, pp. 417-436.

Graham, B., Wallis, G. B. and Dobson, J. E. (1973), The onset of slugging in horizontal stratified air-water flow, International Journal of Multiphase Flow, vol. 1, no. 1, pp. 173 -193.

Gu, H. and Gue, L. (2008), Experimental Investigation of Slug Development on Horizontal Two-phase Flow, Chinese Journal of Chemical Engineering, vol. 16, no. 2, pp. 171-177.

Hauptmann, P., Hoppe, N. and Puttmer, A. (2002), Review Article Application of Ultrasonic Sensors in the Process Industry, Measurement Science and Technology, vol. 13, pp. 73-83.

Heindel, T. J. (2000), "Gas flow regime changes in a bubble column filled with a fibre suspension", The Canadian Journal of Chemical Engineering, vol. 78, no. 5, pp. 1017-- 1022.

Hellier, C. (2001), Handbook of nondestructive evaluation, McGraw-Hill, New York ; London.

Hervieu, E. and Junior, P. S. (1999), Direct Imaging of Two-Phase Flows by Electrical Impedance Measurements, 1st World Congress on Industrial Process Tomography, Buxton, Greater Manchester, April 14-17, .

Holroyd, T. J. (2000), The acoustic emission & ultrasonic monitoring handbook, Coxmoor, Oxford.

Hou, R., Hunt, A. and Williams , R. A. (1999), Acoustic Monitoring of pipeline flows: Particulate slurries, Powder Technology, vol. 106, no. 1-2, pp. 30- 36.

Huang, C., Lee, J., Schultz, W. W. and and Ceccio, S. L. (2003), Singularity image method for electrical impedance tomography of bubbly flows, Inverse Problems Journal, vol. 19, no. 4, pp. 919.

Hunziker, J. (2011), Acoustic Emission Sensing in Wireless Sensor Networks (Master Thesis thesis), Institut für Technische Informatik und Kommunikationsnetze, .

Husin, S. (2011), An Experimental Investigation into the Correlation between Acoustic Emission (AE) and Bubble Dynamics (PhD Thesis thesis), Cranfield University, UK.

Issa, R. (2009), Simulation of Intermittent Flow in Multiphase Oil and Gas Pipelines, Seventh International Conference on CFD in the Minerals and Process Industries (CSIRO), 9-11 December 2009, Melbourne, Australia.

Kaiser, J.; (1950), A study of acoustic phenomena in tensile tests. Dr.-Ing. dissertation, Technical University of Munich.

Kalicka, M. (2010), Acoustic Emission Signal Propagation through Welded Steel Bridge Joints, Proceedings of 10th ECNDT Conference, Extended abstract, Moscow, Russia, June, .

Kim, M. C., Kim, K. Y. and Kim, S. (2003), Two Phase Visualization by Electrical Impedance Tomography with Prior Information, Korean J. Chem. Eng., vol. 20, no. 4, pp. 601--608.

Kishore, M., Kumar, V., Meikap, B. C. and Chakraborty, S. (2010), Development of Soft Sensor to Identify Flow Regimes in Horizontal Pipe Using Digital Signal Processing Technique, Ind. Eng. Chem. Res., vol. 49, no. 6, pp. 3001-- 3010.

Kohn, D. (1995), Acoustic Emission and Non-destructive evaluation of Biomaterials and Tissues, 3rd ed, Critical reviews in Biomedical Engineering.

Kordyban, E. S. and Ranov, T. (1970), Mechanism of Slug Formation in Horizontal Two-Phase Flow, Journal of Basic Engineering, vol. 92, pp. 857-864.

Longuet-Higgins, M. S., Kerman, B. R. and Lunde, K. (1991), The release of air bubbles from an underwater nozzle, J. Fluid Mech., vol. 230, pp. 365–390.

Ma, Y., Chung, N., Pei, B. and Lin, W. (1991), Two simplified methods to determine void fractions for two-phase flow, Nuclear Technology, vol. 94, no. 1, pp. 124-133.

Manasseh, R. (2004), Passive acoustic analysis of complex bubbly flows, 16th International Congress of Chemical and Process Engineering, , pp. 22-26.

Manasseh, R., Riboux, G. and Risso, F. (2008), Sound generation on bubble coalescence following detachment, International Journal of Multiphase Flow, vol. 34, no. 10, pp. 938-949.

Mark, S., Zhi, Y., Lynn, G., Michael, L. J., Derek, L. and Benedict, N. (2009), SPRITE MRI of bubbly flow in a horizontal pipe, Journal of Magnetic Resonance, vol. 199, pp. 126-135.

Miller, R. K. and McIntire, P. (1987), Nondestructive testing handbook: volume 5 acoustic emission testing, 2nd ed, Asnt, S.l.

Mishima, K. and Ishii, M. (1980), Theoretical prediction of onset of horizontal slug flow, Journal of Fluids Engineering, Transactions of the ASME, vol. 102, pp. 441-445.

muravin (2010), available at: www.muravin.com (accessed July).

Muravin, B., (2009), Acoustic emissions science and technology, J. Building and Infrastructure Engineering of the Israeli Association of Engineers and Architects, pp. 10 pages.

Murdoch, J. and Barnes, J. (2008), Statistical Tables, Macmillan.

NDT-ed (2010), Modes of Sound Wave Propagation, available at: www.ndt-ed.org/EducationResources/CommunityCollege/Ultrasonics/Physics/modepropagation.htm (accessed June).

Nicol, R. S. and Davidson, J. F. (1988), Gas holdup in circulating bubble columns, Chemical Engineering Research and Design, vol. 68, no. 2, pp. 152–158.

Nydal, O. J., Pintus, S. and Andreussi, P. (1992), Statistical characterization of slug flow in horizontal pipes, International Journal of Multiphase Flow, vol. 18, no. 3, pp. 439-453.

OMEGA (2001), Flow & Level Measurement, A Technical Reference Series Brought by OMEGA, vol. 4.

OMEGA, (2010), Flow and Level Measurement, OMEGA.COM

PAC (2007), PCI-2 based AE system user's manual, Physical Acoustics Corporation, Princeton Junction.

Pandit, A. B., Varley, J., Thorpe, R. B. and Davidson, J. F. (1992), Measurement of Bubble Size Distribution: An Acoustic Technique, Chemical Engineering Science, vol. 47, no. 5, pp. 1079-1089.

Peterson, D. A., Tankin, R. S. and Bankoff, S. G. (1987), Bubble behaviour in a three-phase fluidized bed, International Journal of Multiphase Flow, vol. 13, no. 4, pp. 477-491.

Portevin, A. and Le Chatelier, M. A., (1923), Sur un Phenomene Observe lors de l'Essai de Traction d'Alliages en Cours de Transformation, Comptes Rendus, vol. 176, pp. 507-510.

Rahiman, M. H. F., Abdul Rahim, R. and Pusppanathan, J. (2010), Two Phase Flow Regime Identification by Ultrasonic Computerized Tomography, Sensors & Transducers Journal, vol. 216, no. 5, pp. 76-82.

Rasteiro, M. G., Silva, R., Garcia, F. A. P. and Faia, P. (2011), Electrical Tomography: a review of Configurations and Applications to Particulate Processes, KONA Powder and Particle Journal No.29.

Reinecke, N., Petritsch, G., Boddem, M. and Mewes, D. (1998), Tomographic imaging of the phase distribution in two-phase slug flow, International Journal of Multiphase Flow, vol. 24, no. 4, pp. 617-634.

Roberts, T. M. and Talebzadeh, M. (2003), Fatigue life predictionbased on crack propagation and acoustic emission count rates, Journal of Constructional Steel Research, vol. 59, no. 6, pp. 679-694.

Ruder, Z., Hanratty, P. H. and and Hanratty, T. J. (1989), Necessary conditions for the existence of stable slugs, International Journal of Multiphase Flow, vol. 15, no. 2, pp. 209-226.

Sanderson, M. L. and Yeung, H. (2002), "Guidelines for the use of ultrasonic non-invasive metering techniques ", Flow Measurement and Instrumentation, vol. 13, no. 4, pp. 125-142.

Sarfarazi, M. P. (1992), Acoustic emissions and damage constitutive characteristics of Paper, Atlanta, GA, Georgia Institute of Technology.

Shuib, H., Addali, A. and MBA, D. (2010a), Acoustic Emission of a Single Bubble Activities, Proceedings of the World Congress on Engineering 2010, Vol. II, June 30 - July 2, 2010, London, U.K.

Shuib, H., Addali, A. and MBA, D. (2010b), Acoustic Emission for monitoring tow-phase flow, 29th EWGAE 2010 conference, 8th to 10th September, Vienna, NDT, .

Storck, A., Latifi, M. A., Barthole, G., Laurent A. and Carpenter J.C. (1986), Electrochemical study of liquid–solid mass transfer in packed bed electrodes with upward and downward co-current gas–liquid flow, Journal of Applied Electrochemistry, vol. 16, pp. 947–963.

Stott, A. L., Green, R. G. and Seraji, K. (1985), Comparison of the use of internal and external electrodes for the measurement of the capacitance and conductance of fluids in pipes, Journal of Physics E: Scientific Instruments, vol. 18, pp. 587–592.

Strasberg, M. (1953), the pulsation frequency of non-spherical gas bubbles in liquid, Journal of the Acoustical Society of America, vol. 25, pp. 536–537.

Sun, L., Li, Y., Li, C., Wang, L. and Wu, J. (2010), Active defects detection and localization using acoustic emission method, Intelligent Control and Automation (WCICA), 2010 8th World Congress on, 7-9 July, pp. 5348.

Surgeon, M. and Wevers, M. (1999), Modal analysis of acoustic emission signals from CFRP laminates, NDT & E International, vol. 32, no. 6, pp. 311-322.

Taitel, Y. and Dukler, A. D. (1976a), A model for predicting flow regime transitions in horizontal and near horizontal gas–liquid flow, AIChE Journal, vol. 22, no. 1, pp. 47-55.

Taitel, Y. and Dukler, A. E. (1976b), A model for predicting flow regime transitions in horizontal and near horizontal gas-flow Engineering, American Institute of Chemical Engineering Journal, vol. 22, no. 1, pp. 47-55.

Tekna (ed.) (2005), Handbook of Multiphase Flow Metering, Rev. 2 ed.

Theobald, P., Zeqir, B. and Avison, J. (2012), Couplants and Their Influence on AE Sensor Sensitivity, National Physical Laboratory, Teddington, United Kingdom

Thiyagarajan, T. K., Dixit, N. S., Satyamurthy, P., Venkatramani, N. and and Rohatgi, V. K. (1991), Gamma-ray attenuation method for void fraction measurement in fluctuating two-phase liquid metal flows, Measurement Science and Technology, vol. 2, no. 1, pp. 69.

Thorn, R., Johansen, G. A. and and Hammer, E. A. (1999), Three-Phase Flow Measurement in the Offshore Oil Industry Is There a Place for Process Tomography?, In Proc. 1st World Congress on Industrial Process Tomography, Buxton, UK. April 14-17, 1999, .

Thorn, R., Johansen, G. A. and and Hjertaker, B. T. (2013), Three-phase flow measurement in the petroleum industry, Measurement Science and Technology, vol. 24, no. 1, pp. 012003.

Tjugum, S. A.; and Mihalca, R., (2009), X-ray based densitometer for multiphase flow measurements, The 27th international North Sea Flow Measurement Workshop, 20 – 23 October, Norway.

Upp, E. L. (2002), Fluid flow measurement: a practical guide to accurate flow measurement, 2nd ed, Gulf; Butterworth-Heinemann, Houston, Tex.; Oxford.

Utiger, M., Stuber, F., Duquenne, A., Delmas, H. and Guy, C. (1999), Local measurements for the study of external loop airlift hydrodynamics, Canadian Journal of Chemical Engineering, vol. 77, no. 2, pp. 375-382.

Vallen, D. I. H. (2002), AE Testing Fundamentals; Equipment and Applications, www.NDT.net, vol. 7, no. 09, pp. Visited on June 2010.

Vallen, S. (2012), Acoustic Emission Sensors Specification, Vallen Systeme GmbH.

Vial, C., Poncin, S., Wild, G. and Midoux, N. (2001), A simple method for regime identification and flow characterisation in bubble columns and airlift reactors, Chemical Engineering and Processing: Process Intensification, vol. 40, no. 2, pp. 135-151.

Walpole, R. E., Myers, R. H., Myers, S. L. and Ye, K. (2011), Probability & Statistics for Engineers & Scientists, 9th ed, Pearson Education, Inc., USA.

Yehuda, T. (1986), Stability of Severe Slugging, Int. J. Multiphase Flow, vol. 12, no. 2, pp. 203-217.

Yen, G. G. and Lu, H. (2002), Acoustic emission data assisted process monitoring, ISA transactions, vol. 41, no. 3, pp. 273-282.

Yu, Y. H. and Kim, S. D. (1991), Bubble properties and local liquid velocity in the radial direction of co-current gas-liquid flow, Chemical Engineering Science, vol. 46, no. 1, pp. 313-320.

Zhou, Y., Chen, F. and Sun, B. (2008), Identification Method of Gas-Liquid Two-phase Flow Regime Based on Image Multi-feature Fusion and Support Vector Machine, Chinese Journal of Chemical Engineering, vol. 16, no. 6, pp. 832-840.

APPENDICES

Appendix B

Table A-1Time delay and slug velocity calculation using M12 waveguide at 0.7 V_{SL} and 1.02 V_{SG}

Burst signals number	Mixture Velocity (m/s)	Time delay (s)	Slug velocity (m/s)
1	1.72	0.10501	1.905
2	1.72	0.11117	1.799
3	1.72	0.09493	2.107
4	1.72	0.08536	2.343
5	1.72	0.08723	2.293
6	1.72	0.08767	2.281
7	1.72	0.08976	2.228
8	1.72	0.08344	2.397
9	1.72	0.09559	2.092
10	1.72	0.10137	1.973
11	1.72	0.09701	2.062
12	1.72	0.08350	2.395
13	1.72	0.08492	2.355
Average of Slug Velocity SV (m/s)			2.17
Mixture flow velocity VM (m/s)			1.72
Standard deviation of SV (m/s)			0.20
% difference between SV and Vm (m/s)			26.25%

Table A-2 Time delay and slug velocity calculation using M12 waveguide at 0.7 V_{SL} and 1.52 V_{SG}

Burst signals number	Mixture Velocity (m/s)	Time delay (s)	Slug velocity (m/s)
1.00	2.22	0.07	3.07
2.00	2.22	0.07	2.74
3.00	2.22	0.08	2.63
4.00	2.22	0.07	3.01
5.00	2.22	0.07	2.77
6.00	2.22	0.08	2.60
7.00	2.22	0.07	2.96
8.00	2.22	0.07	2.99
9.00	2.22	0.07	2.89
10.00	2.22	0.08	2.57
11.00	2.22	0.09	2.29
12.00	2.22	0.08	2.51
13.00	2.22	0.08	2.49
Average of Slug Velocity SV (m/s)			2.73
Mixture flow velocity VM (m/s)			2.22
Standard deviation of SV (m/s)			0.24
% difference between SV and Vm (m/s)			23.06%

Table A-3 Time delay and slug velocity calculation using M12 waveguide at 0.7 V_{SL} and 2.02 V_{SG}

Burst signals number	Mixture Velocity (m/s)	Time delay (s)	Slug velocity (m/s)
1	2.72	0.05398	3.705
2	2.72	0.05918	3.380
3	2.72	0.05470	3.656
4	2.72	0.05671	3.527
5	2.72	0.05873	3.405
6	2.72	0.06161	3.246
7	2.72	0.06106	3.275
8	2.72	0.05928	3.374
9	2.72	0.06985	2.863
10	2.72	0.06028	3.318
11	2.72	0.07069	2.829
12	2.72	0.06386	3.132
13	2.72	0.07139	2.802
Average of Slug Velocity SV (m/s)			3.27
Mixture flow velocity VM (m/s)			2.72
Standard deviation of SV (m/s)			0.30
% difference between SV and Vm (m/s)			20.23%

Table A-4 Time delay and slug velocity calculation using M12 waveguide at 0.7 V_{SL} and 2.52 V_{SG}

Burst signals number	Mixture Velocity (m/s)	Time delay (s)	Slug velocity (m/s)
1	3.22	0.05115	3.910
2	3.22	0.05177	3.863
3	3.22	0.05136	3.894
4	3.22	0.05185	3.857
5	3.22	0.05556	3.600
6	3.22	0.05924	3.376
7	3.22	0.05487	3.645
8	3.22	0.05200	3.846
9	3.22	0.05406	3.700
10	3.22	0.04425	4.520
11	3.22	0.04701	4.255
12	3.22	0.05239	3.818
13	3.22	0.04894	4.086
Average of Slug Velocity SV (m/s)			3.8747
Mixture flow velocity VM (m/s)			3.22
Standard deviation of SV (m/s)			0.29
% difference between SV and Vm (m/s)			20.33%

Table A-5 Time delay and slug velocity calculation using M12 waveguide at 1.02 V_{SL} and 1.02 V_{SG}

Burst signals Number	Mixture Velocity (m/s)	Time delay (s)	Slug velocity (m/s)
1	2.04	0.08516	2.348
2	2.04	0.07819	2.558
3	2.04	0.08528	2.345
4	2.04	0.08594	2.327
5	2.04	0.08119	2.463
6	2.04	0.08021	2.493
7	2.04	0.08544	2.341
8	2.04	0.08224	2.432
9	2.04	0.07785	2.569
10	2.04	0.07623	2.624
11	2.04	0.07630	2.621
12	2.04	0.07870	2.541
13	2.04	0.08186	2.443
Average of Slug Velocity SV (m/s)			2.47
Mixture flow velocity VM (m/s)			2.04
Standard deviation of SV (m/s)			0.11
% difference between SV and Vm (m/s)			21.07%

Table A-6 Time delay and slug velocity calculation using M12 waveguide at 1.02 V_{SL} and 1.52 V_{SG}

Burst signals Number	Mixture Velocity (m/s)	Time delay (s)	Slug velocity (m/s)
1	2.54	0.06629	3.017
2	2.54	0.06813	2.936
3	2.54	0.07216	2.772
4	2.54	0.06536	3.060
5	2.54	0.06360	3.145
6	2.54	0.06359	3.145
7	2.54	0.06441	3.105
8	2.54	0.07015	2.851
9	2.54	0.06565	3.046
10	2.54	0.06996	2.859
11	2.54	0.06641	3.011
12	2.54	0.06665	3.001
13	2.54	0.06232	3.210
Average of Slug Velocity SV (m/s)			3.01
Mixture flow velocity VM (m/s)			2.54
Standard deviation of SV (m/s)			0.13
% difference between SV and Vm (m/s)			18.59%

Table A-7 Time delay and slug velocity calculation using M12 waveguide at 1.02 V_{SL} and 2.02 V_{SG}

Burst signals Number	Mixture Velocity (m/s)	Time delay (s)	Slug velocity (m/s)
1	3.04	0.06071	3.294
2	3.04	0.05431	3.683
3	3.04	0.06133	3.261
4	3.04	0.05753	3.477
5	3.04	0.05845	3.422
6	3.04	0.05577	3.586
7	3.04	0.05676	3.524
8	3.04	0.05836	3.427
9	3.04	0.05508	3.631
10	3.04	0.05910	3.384
11	3.04	0.06171	3.241
12	3.04	0.05814	3.440
13	3.04	0.05790	3.454
Average of Slug Velocity SV (m/s)			3.45
Mixture flow velocity VM (m/s)			3.04
Standard deviation of SV (m/s)			0.14
% difference between SV and Vm (m/s)			13.42%

Table A-8 Time delay and slug velocity calculation using M12 waveguide at 1.52 V_{SL} and 1.02 V_{SG}

Burst signals Number	Mixture Velocity (m/s)	Time delay (s)	Slug velocity (m/s)
1	2.54	0.06409	3.121
2	2.54	0.07040	2.841
3	2.54	0.06743	2.966
4	2.54	0.06608	3.027
5	2.54	0.07268	2.752
6	2.54	0.07048	2.838
7	2.54	0.07024	2.848
8	2.54	0.07139	2.802
9	2.54	0.07527	2.657
10	2.54	0.06440	3.106
11	2.54	0.06840	2.924
12	2.54	0.06070	3.295
13	2.54	0.06120	3.268
Average of Slug Velocity SV (m/s)			2.96
Mixture flow velocity VM (m/s)			2.54
Standard deviation of SV (m/s)			0.20
% difference between SV and Vm (m/s)			16.42%

Table A-9 Time delay and slug velocity calculation using M12 waveguide at 1.52 V_{SL} and 1.52 V_{SG}

Burst signals Number	Mixture Velocity (m/s)	Time delay (s)	Slug velocity (m/s)
1	3.04	0.06222	3.214
2	3.04	0.05499	3.637
3	3.04	0.05516	3.626
4	3.04	0.05546	3.606
5	3.04	0.06281	3.184
6	3.04	0.06120	3.268
7	3.04	0.05658	3.535
8	3.04	0.05359	3.732
9	3.04	0.05858	3.414
10	3.04	0.06495	3.079
11	3.04	0.05704	3.506
12	3.04	0.06183	3.235
13	3.04	0.06386	3.132
Average of Slug Velocity SV (m/s)			3.40
Mixture flow velocity VM (m/s)			3.04
Standard deviation of SV (m/s)			0.22
% difference between SV and Vm (m/s)			11.76%

Table A-10 Time delay and slug velocity calculation using M12 waveguide at 1.52 V_{SL} and 2.02 V_{SG}

Burst signals Number	Mixture Velocity (m/s)	Time delay (s)	Slug velocity (m/s)
1	3.54	0.05000	4.000
2	3.54	0.05353	3.736
3	3.54	0.04949	4.041
4	3.54	0.05314	3.763
5	3.54	0.05714	3.500
6	3.54	0.05193	3.851
7	3.54	0.05312	3.765
8	3.54	0.05464	3.661
9	3.54	0.04960	4.033
10	3.54	0.04975	4.020
11	3.54	0.05485	3.646
12	3.54	0.05535	3.614
13	3.54	0.05318	3.761
Average of Slug Velocity SV (m/s)			3.80
Mixture flow velocity VM (m/s)			3.54
Standard deviation of SV (m/s)			0.18
% difference between SV and Vm (m/s)			7.32%

Table A-11 Time delay and slug velocity calculation using M12 waveguide at 1.52 V_{SL} and 2.52 V_{SG}

Burst signals Number	Mixture Velocity (m/s)	Time delay (s)	Slug velocity (m/s)
1	4.04	0.04539	4.406
2	4.04	0.04059	4.928
3	4.04	0.04552	4.394
4	4.04	0.04658	4.294
5	4.04	0.04165	4.801
6	4.04	0.04226	4.733
7	4.04	0.04748	4.213
8	4.04	0.04443	4.501
9	4.04	0.04048	4.940
10	4.04	0.04573	4.373
11	4.04	0.04532	4.414
12	4.04	0.04226	4.733
13	4.04	0.04226	4.733
Average of Slug Velocity SV (m/s)			4.57
Mixture flow velocity VM (m/s)			4.04
Standard deviation of SV (m/s)			0.25
% difference between SV and Vm (m/s)			13.22%

Table A-12 Time delay and slug velocity calculation using M12 waveguide at 2.02 V_{SL} and1.02 V_{SG}

Burst signals Number	Mixture Velocity (m/s)	Time delay (s)	Slug velocity (m/s)
1	3.04	0.05684	3.519
2	3.04	0.05547	3.606
3	3.04	0.05873	3.405
4	3.04	0.06202	3.225
5	3.04	0.05754	3.476
6	3.04	0.05388	3.712
7	3.04	0.05790	3.454
8	3.04	0.05569	3.591
9	3.04	0.05214	3.836
10	3.04	0.05683	3.519
11	3.04	0.05272	3.794
12	3.04	0.05782	3.459
13	3.04	0.05504	3.634
Average of Slug Velocity SV (m/s)			3.56
Mixture flow velocity VM (m/s)			3.04
Standard deviation of SV (m/s)			0.17
% difference between SV and Vm (m/s)			16.98%

Table A-13 Time delay and slug velocity calculation using M12 waveguide at 2.02 V_{SL} and 1.52 V_{SG}

Burst signals Number	Mixture Velocity (m/s)	Time delay (s)	Slug velocity (m/s)
1	3.54	0.05251	3.809
2	3.54	0.04846	4.127
3	3.54	0.05203	3.844
4	3.54	0.05017	3.986
5	3.54	0.05066	3.948
6	3.54	0.04842	4.130
7	3.54	0.05273	3.793
8	3.54	0.04990	4.008
9	3.54	0.05324	3.757
10	3.54	0.05001	4.000
11	3.54	0.05209	3.839
12	3.54	0.05345	3.742
13	3.54	0.04958	4.034
Average of Slug Velocity SV (m/s)			3.92
Mixture flow velocity VM (m/s)			3.54
Standard deviation of SV (m/s)			0.13
% difference between SV and Vm (m/s)			10.86%

Table A-14 Time delay and slug velocity calculation using M12 waveguide at 2.02 V_{SL} and 2.02 V_{SG}

Burst signals Number	Mixture Velocity (m/s)	Time delay (s)	Slug velocity (m/s)
1	4.04	0.04118	4.857
2	4.04	0.04673	4.280
3	4.04	0.04587	4.360
4	4.04	0.04460	4.485
5	4.04	0.04727	4.231
6	4.04	0.04223	4.736
7	4.04	0.04310	4.640
8	4.04	0.04768	4.195
9	4.04	0.04489	4.455
10	4.04	0.04423	4.522
11	4.04	0.04834	4.138
12	4.04	0.04481	4.463
13	4.04	0.04276	4.678
Average of Slug Velocity SV (m/s)			4.46
Mixture flow velocity VM (m/s)			4.04
Standard deviation of SV (m/s)			0.22
% difference between SV and Vm (m/s)			10.51%

Table A-15 Time delay and slug velocity calculation using M12 waveguide at 2.02 V_{SL} and 2.52 V_{SG}

Burst signals Number	Mixture Velocity (m/s)	Time delay (s)	Slug velocity (m/s)
1	4.54	0.03805	5.256
2	4.54	0.04238	4.719
3	4.54	0.03903	5.124
4	4.54	0.04120	4.854
5	4.54	0.03823	5.232
6	4.54	0.04206	4.755
7	4.54	0.04233	4.725
8	4.54	0.04104	4.874
9	4.54	0.03796	5.269
10	4.54	0.03796	5.269
11	4.54	0.03919	5.103
12	4.54	0.04422	4.523
13	4.54	0.04088	4.892
Average of Slug Velocity SV (m/s)			4.97
Mixture flow velocity VM (m/s)			4.54
Standard deviation of SV (m/s)			0.25
% difference between SV and Vm (m/s)			9.45%

Appendix B

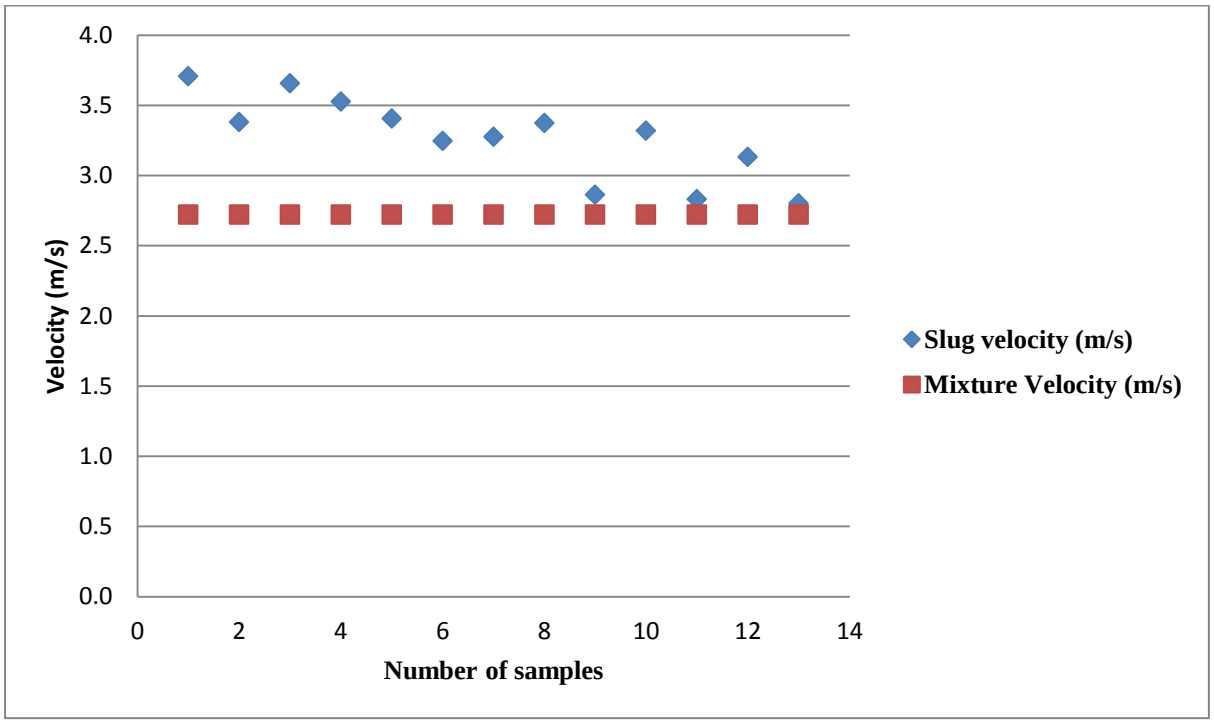

Figure B-1 Measured slug velocity and mixed flow velocity at 0.7 V_{SL} and 2.02 V_{SG}

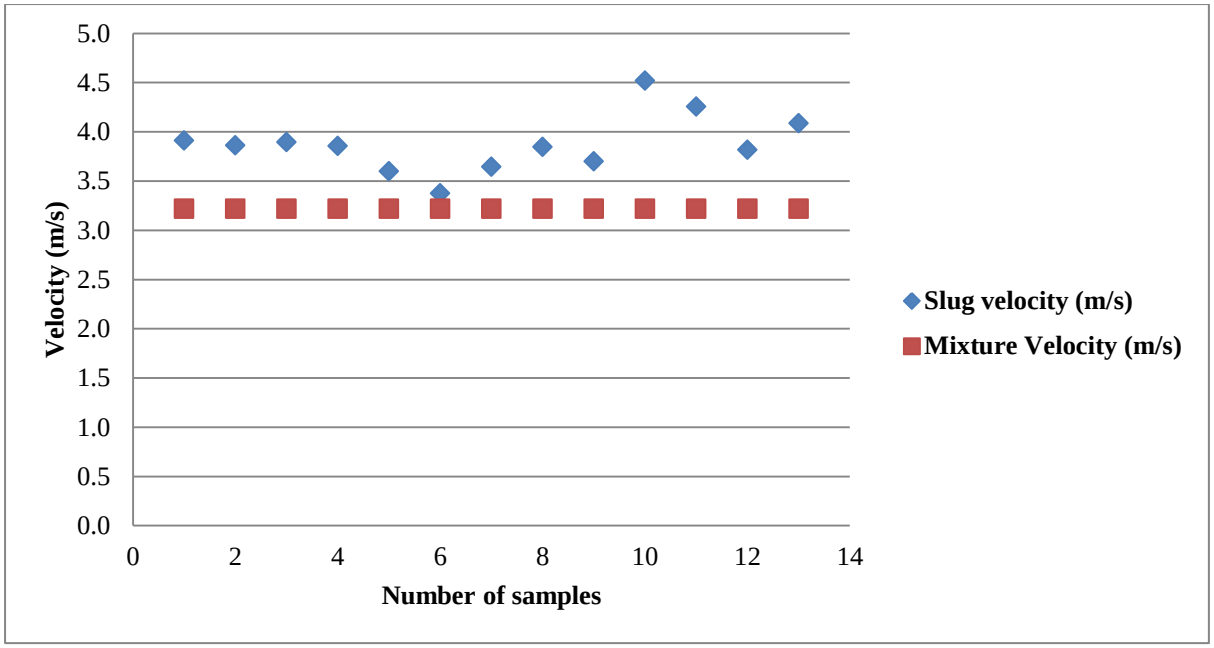

Figure B-2 Measured slug velocity and mixed flow velocity at 0.7 V_{SL} and 2.52 V_{SG}

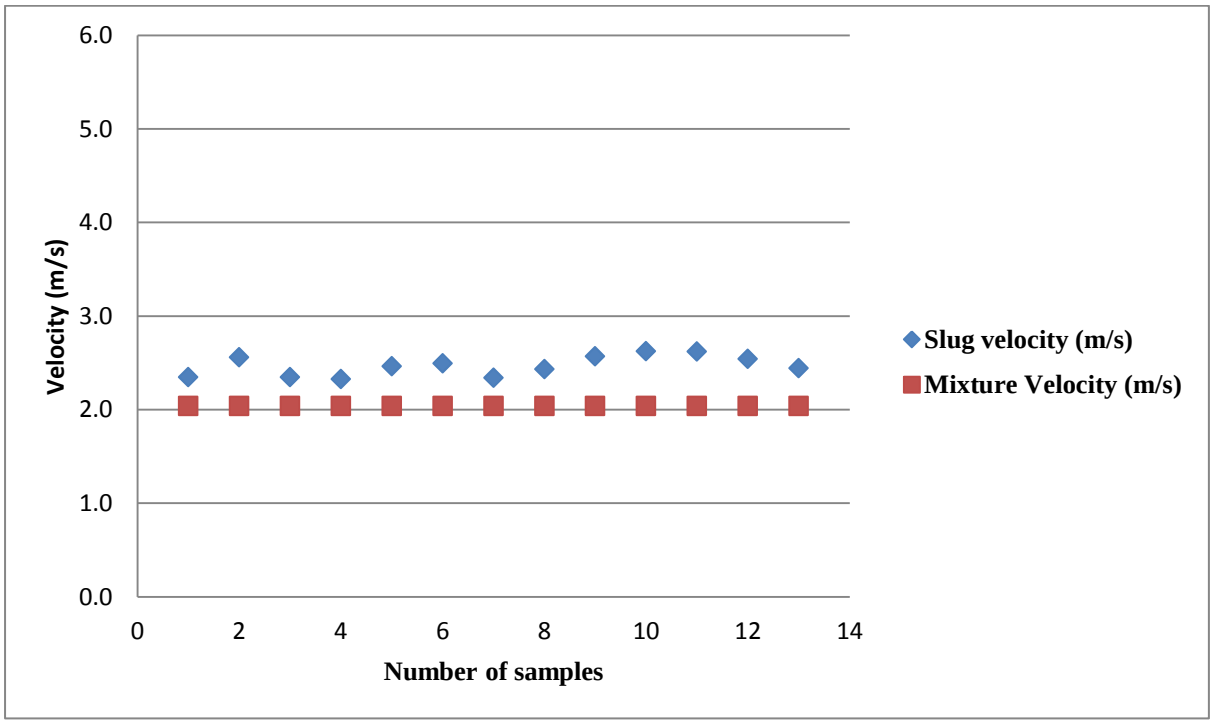

Figure B-3 Measured slug velocity and mixed flow velocity at 1.02 V_{SL} and 1.02 V_{SG}

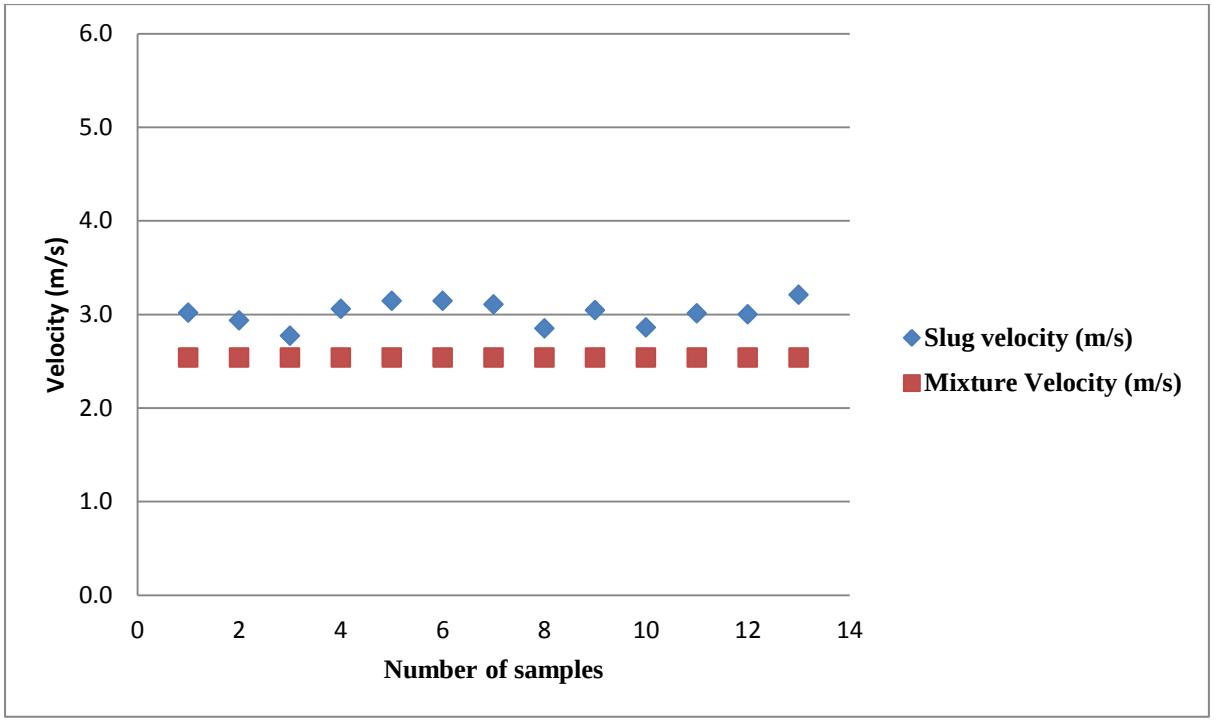

Figure B-4 Measured slug velocity and mixed flow velocity at 1.02 V_{SL} and 1.52 V_{SG}

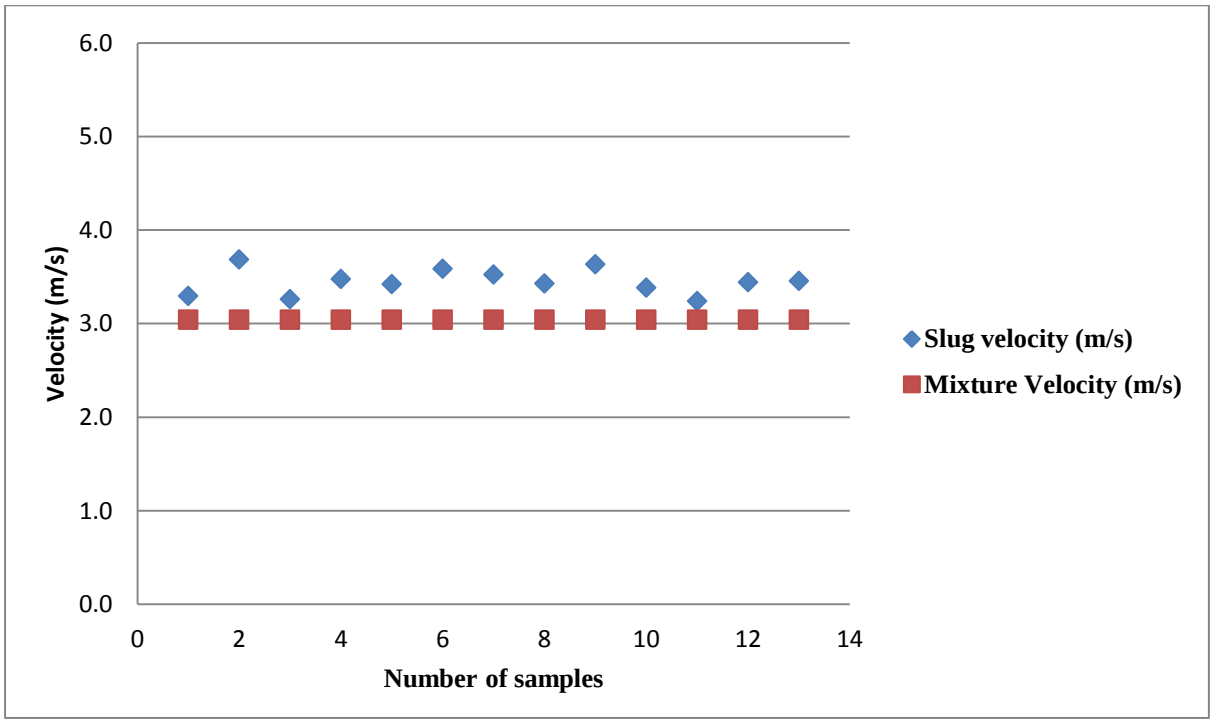

Figure B-5 Measured slug velocity and mixed flow velocity at 1.02 V_{SL} and 2.02 V_{SG}

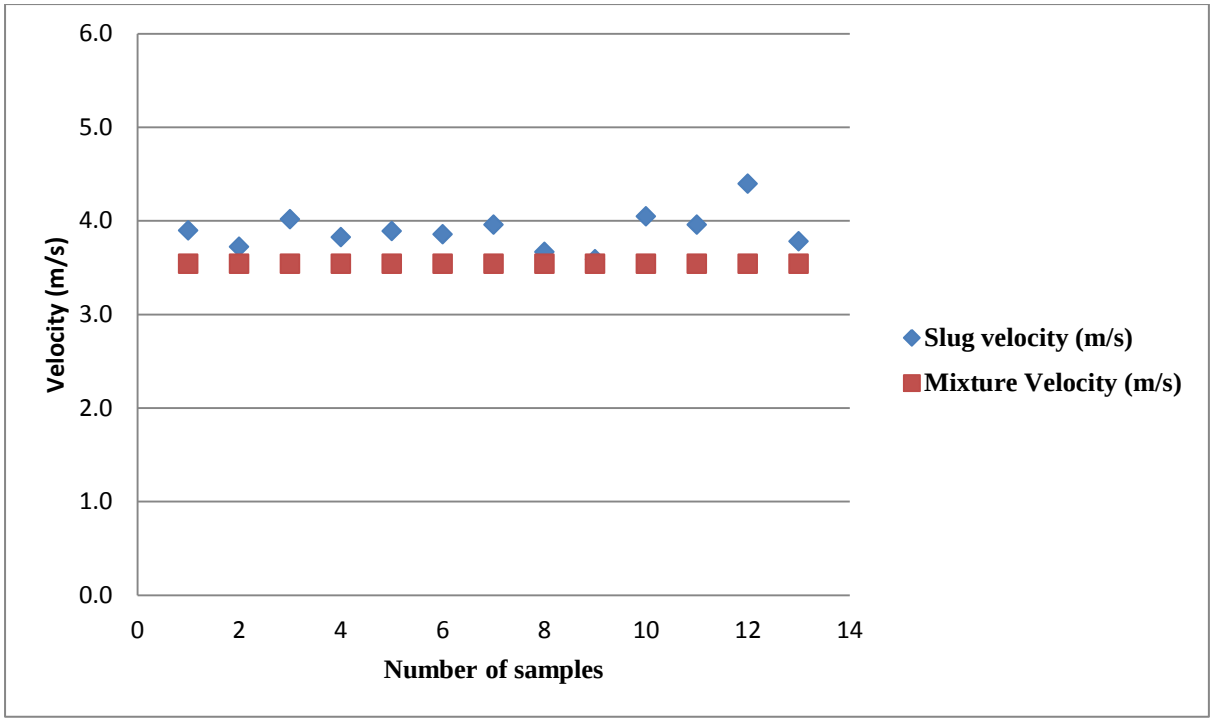

Figure B-6 Measured slug velocity and mixed flow velocity at 1.02 V_{SL} and 2.52 V_{SG}

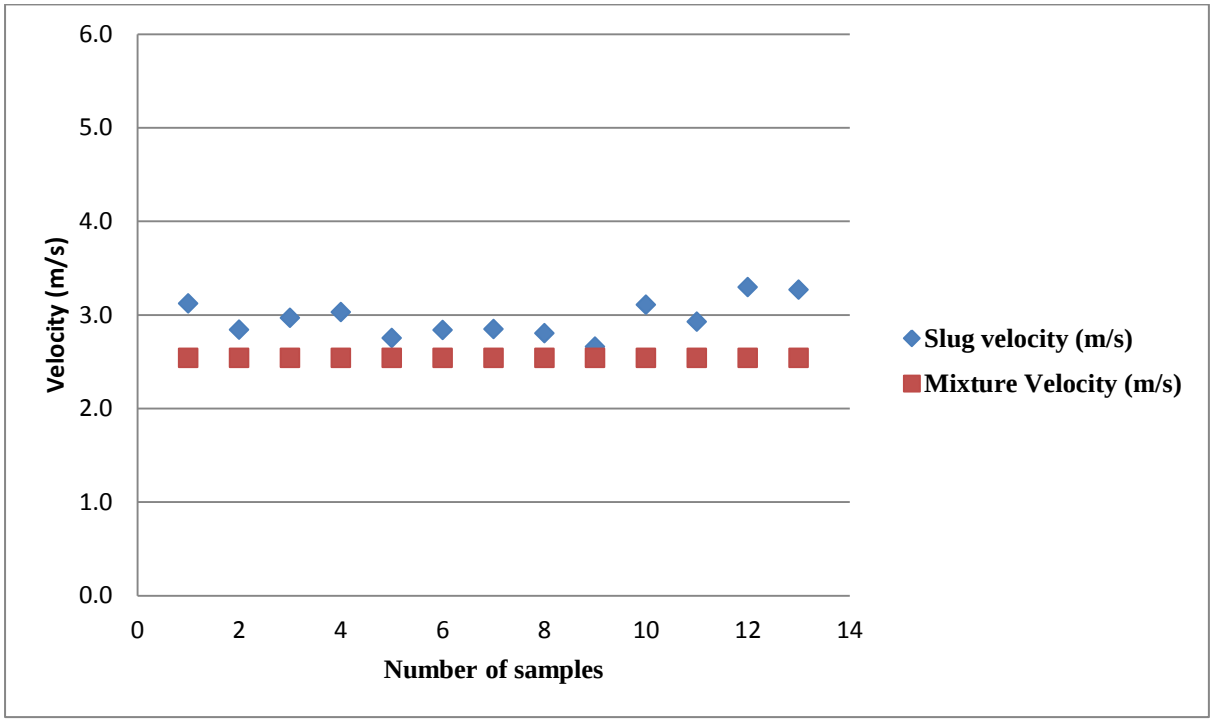

Figure B-7 Measured slug velocity and mixed flow velocity at 1.52 V_{SL} and 1.02 V_{SG}

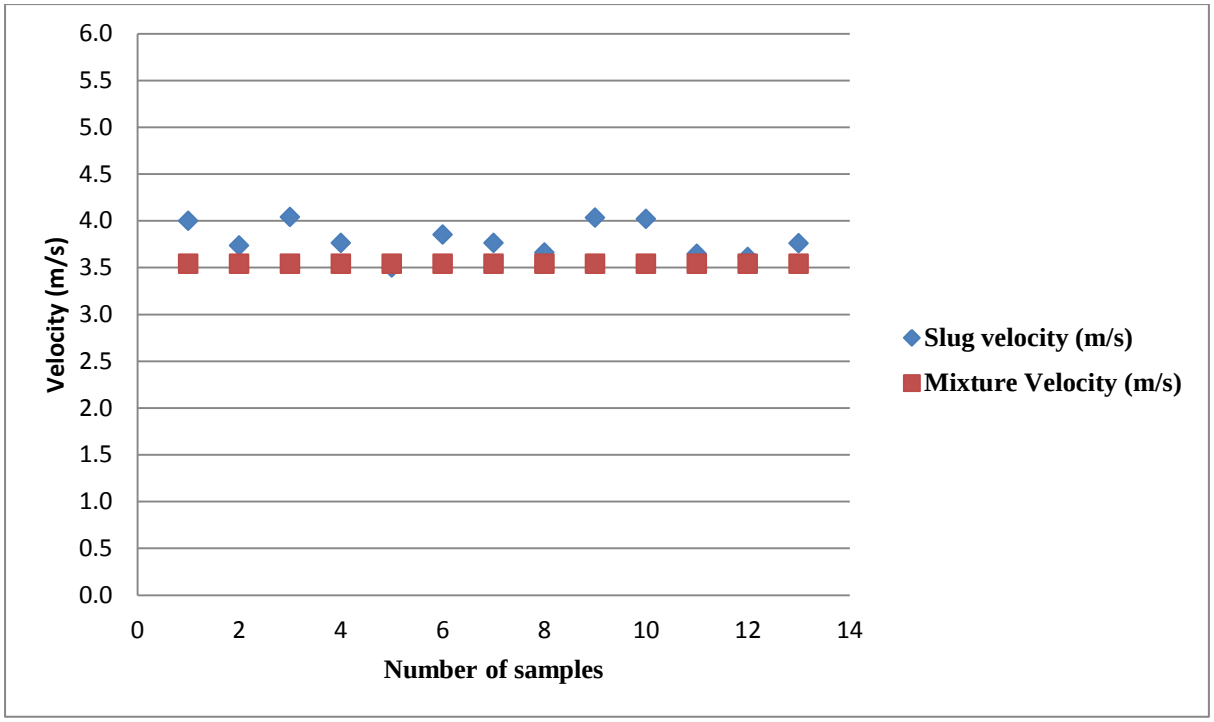

Figure B-8 Measured slug velocity and mixed flow velocity at 1.52 V_{SL} and 2.02 V_{SG}

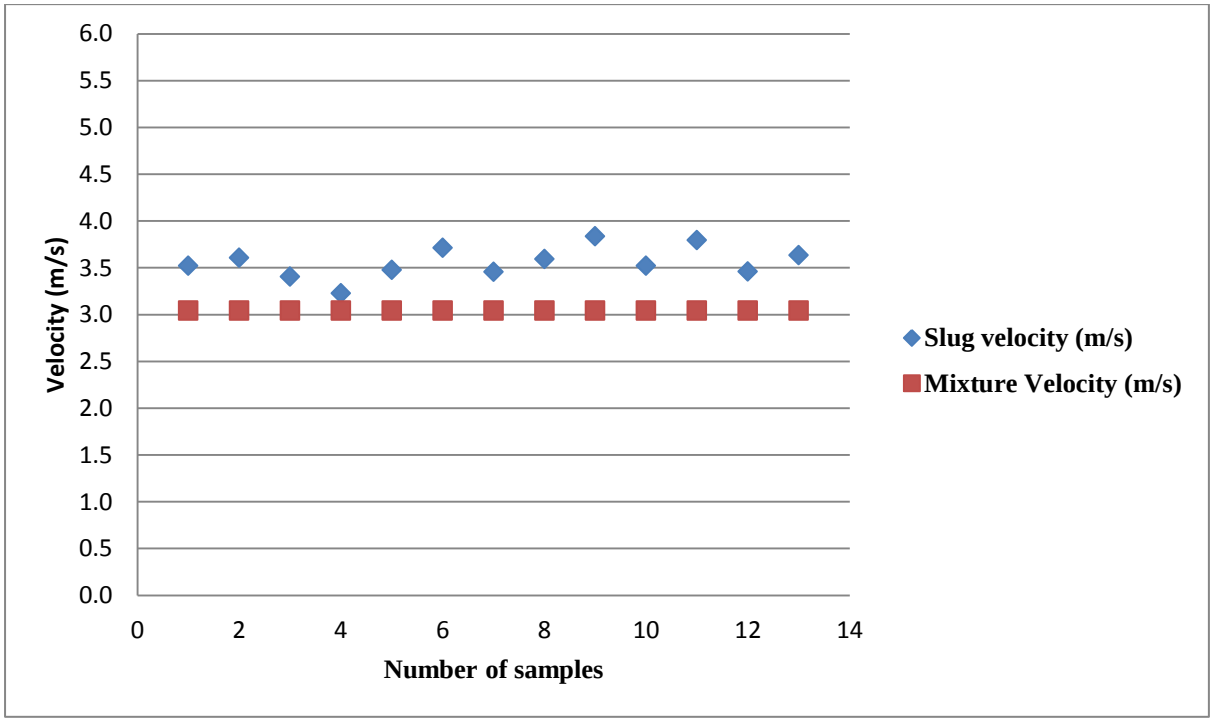

Figure B-9 Measured slug velocity and mixed flow velocity at 2.02 V_{SL} and 1.02 V_{SG}

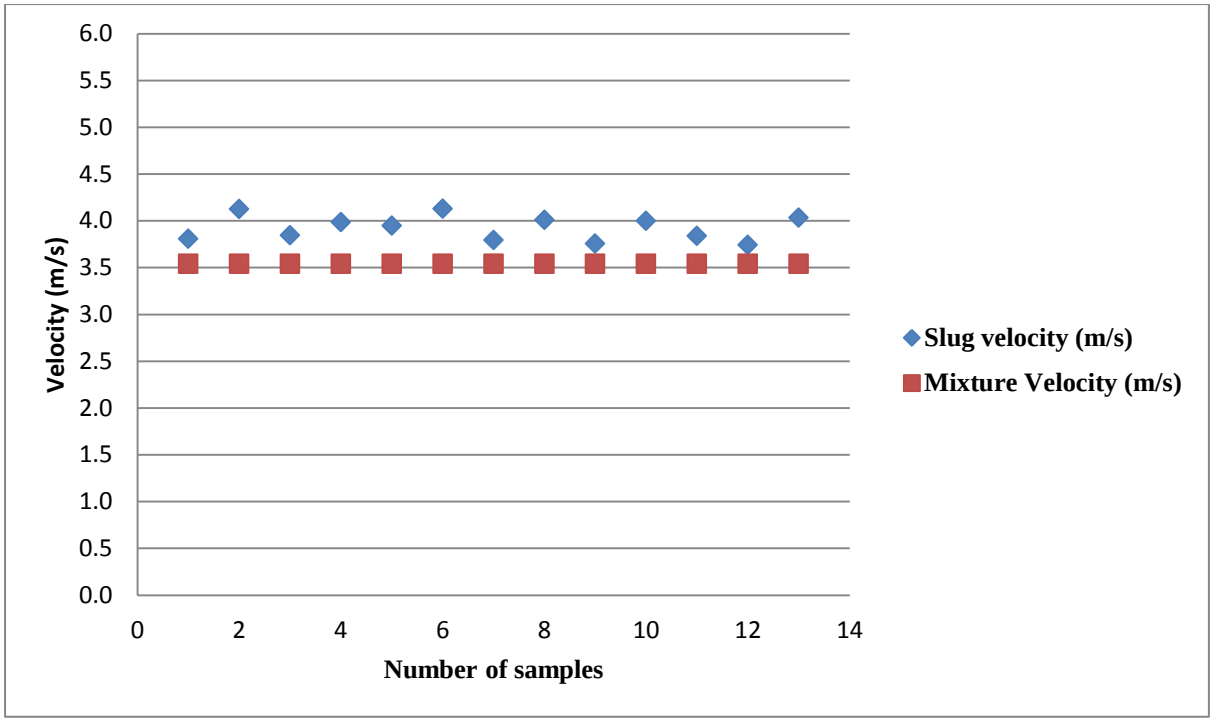

Figure B-10 Measured slug velocity and mixed flow velocity at 2.02 V_{SL} and 1.52 V_{SG}

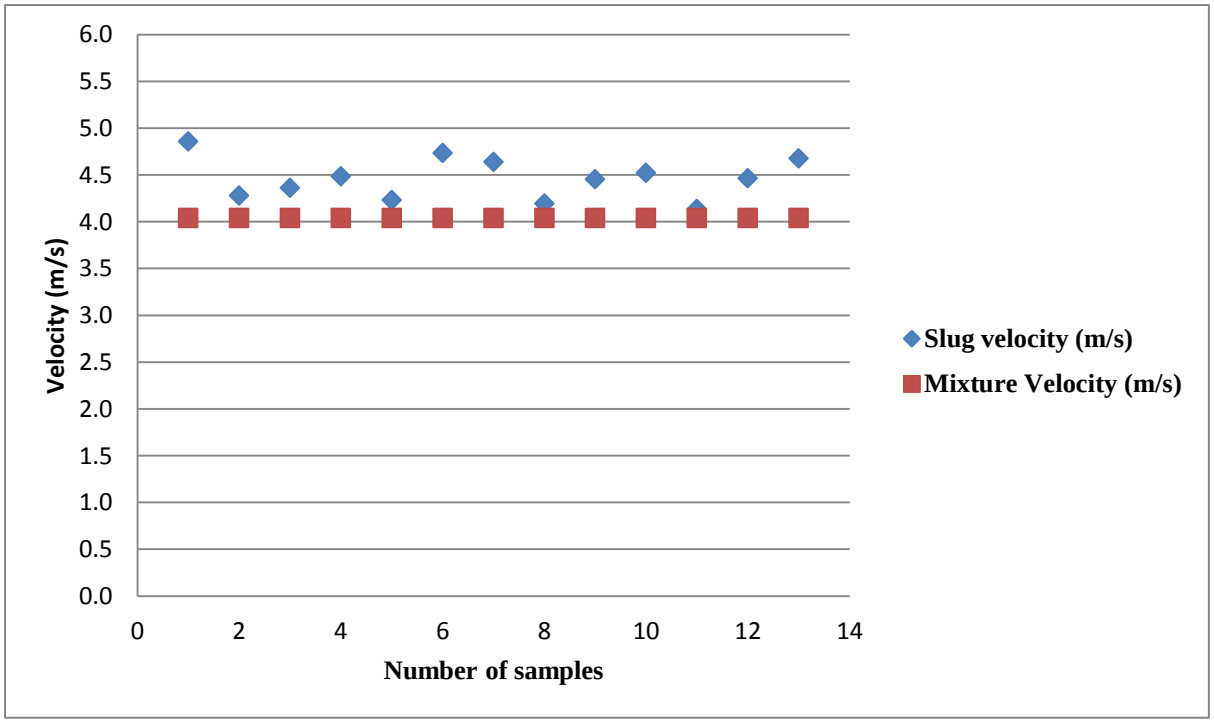

Figure B-11 Measured slug velocity and mixed flow velocity at 2.02 V_{SL} and 2.02 V_{SG}

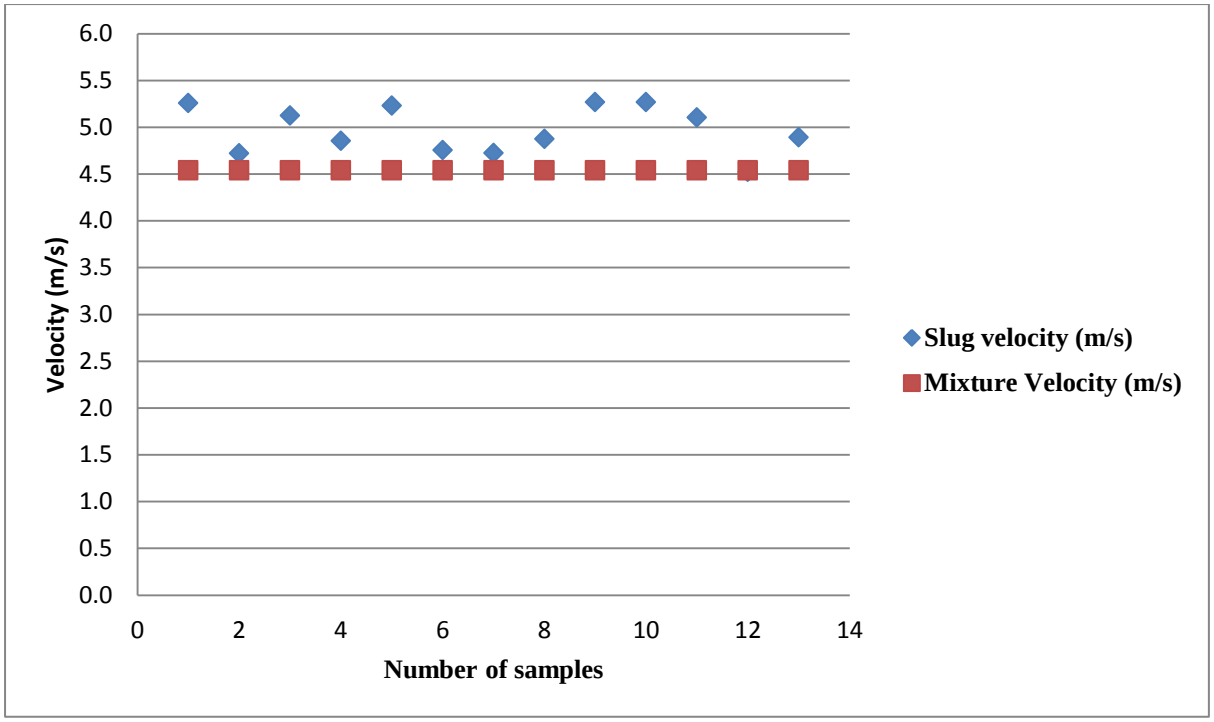

Figure B-12 Measured slug velocity and mixed flow velocity at 2.02 V_{SL} and 2.52 V_{SG}

Appendix C

Table C- 1 Time delay and slug velocity calculation using flush ring waveguides at 0.7 V_{SL} and 1.02 V_{SG}

Burst signals Number	Mixture Velocity (m/s)	Time delay (s)	Slug velocity (m/s)
1	1.72	0.0953373	2.203
2	1.72	0.0960658	2.186
3	1.72	0.107461	1.954
4	1.72	0.108822	1.930
5	1.72	0.106998	1.963
6	1.72	0.0937174	2.241
7	1.72	0.103567	2.028
8	1.72	0.0917509	2.289
9	1.72	0.0969989	2.165
10	1.72	0.108942	1.928
11	1.72	0.103208	2.035
12	1.72	0.101455	2.070
13	1.72	0.106168	1.978
Average of Slug Velocity SV (m/s)			2.07
Mixture flow velocity VM (m/s)			1.72
Standard deviation of SV (m/s)			0.127
% difference between SV and Vm (m/s)			20.61%

Table C- 2 Time delay and slug velocity calculation using flush ring waveguides at 0.7 V_{SL} and 1.52 V_{SG}

Burst signals Number	Mixture Velocity (m/s)	Time delay (s)	Slug velocity (m/s)
1	2.22	0.0757315	2.773
2	2.22	0.085377	2.460
3	2.22	0.0810754	2.590
4	2.22	0.0767398	2.737
5	2.22	0.0828823	2.534
6	2.22	0.0832862	2.521
7	2.22	0.0776186	2.706
8	2.22	0.0726249	2.892
9	2.22	0.0785708	2.673
10	2.22	0.0817443	2.569
11	2.22	0.0744349	2.821
12	2.22	0.085189	2.465
13	2.22	0.0790818	2.655
Average of Slug Velocity SV (m/s)			2.65
Mixture flow velocity VM (m/s)			2.22
Standard deviation of SV (m/s)			0.137
% difference between SV and Vm (m/s)			19.18%

Table C- 3 Time delay and slug velocity calculation using flush ring waveguides at 0.7 V_{SL} and 2.02 V_{SG}

Burst signals Number	Mixture Velocity (m/s)	Time delay (s)	Slug velocity (m/s)
1	2.72	0.0700508	2.998
2	2.72	0.0696875	3.013
3	2.72	0.069002	3.043
4	2.72	0.0653523	3.213
5	2.72	0.069673	3.014
6	2.72	0.0657393	3.194
7	2.72	0.07085	2.964
8	2.72	0.071881	2.921
9	2.72	0.0656545	3.199
10	2.72	0.0646028	3.251
11	2.72	0.063889	3.287
12	2.72	0.0649921	3.231
13	2.72	0.0660888	3.178
Average of Slug Velocity SV (m/s)			3.12
Mixture flow velocity VM (m/s)			2.72
Standard deviation of SV (m/s)			0.125
% difference between SV and Vm (m/s)			14.56%

Table C- 4 Time delay and slug velocity calculation using flush ring waveguides at 0.7 V_{SL} and 2.52 V_{SG}

Burst signals Number	Mixture Velocity (m/s)	Time delay (s)	Slug velocity (m/s)
1	3.22	0.0571636	3.674
2	3.22	0.0564443	3.720
3	3.22	0.0568588	3.693
4	3.22	0.0539618	3.892
5	3.22	0.0586666	3.580
6	3.22	0.0517114	4.061
7	3.22	0.0582708	3.604
8	3.22	0.056763	3.700
9	3.22	0.057913	3.626
10	3.22	0.0547815	3.833
11	3.22	0.0527487	3.981
12	3.22	0.0542753	3.869
13	3.22	0.0563595	3.726
Average of Slug Velocity SV (m/s)			3.77
Mixture flow velocity VM (m/s)			3.22
Standard deviation of SV (m/s)			0.149
% difference between SV and Vm (m/s)			16.96%

Table C- 5 Time delay and slug velocity calculation using flush ring waveguides at 1.02 V_{SL} and 1.02 V_{SG}

Burst signals Number	Mixture Velocity (m/s)	Time delay (s)	Slug velocity (m/s)
1	2.04	0.0817456	2.569
2	2.04	0.08427	2.492
3	2.04	0.083626	2.511
4	2.04	0.0886323	2.369
5	2.04	0.0818138	2.567
6	2.04	0.0749752	2.801
7	2.04	0.0779705	2.693
8	2.04	0.0849213	2.473
9	2.04	0.0877116	2.394
10	2.04	0.0844119	2.488
11	2.04	0.0814883	2.577
12	2.04	0.082536	2.544
13	2.04	0.0835968	2.512
Average of Slug Velocity SV (m/s)			2.54
Mixture flow velocity VM (m/s)			2.04
Standard deviation of SV (m/s)			0.114
% difference between SV and Vm (m/s)			24.40%

Table C- 6 Time delay and slug velocity calculation using flush ring waveguides at 1.02 V_{SL} and 1.52 V_{SG}

Burst signals Number	Mixture Velocity (m/s)	Time delay (s)	Slug velocity (m/s)
1	2.54	0.0687351	3.055
2	2.54	0.0751884	2.793
3	2.54	0.0754115	2.785
4	2.54	0.0676191	3.106
5	2.54	0.0673704	3.117
6	2.54	0.0704105	2.983
7	2.54	0.0642808	3.267
8	2.54	0.0710641	2.955
9	2.54	0.0738625	2.843
10	2.54	0.0664263	3.161
11	2.54	0.0690125	3.043
12	2.54	0.0703556	2.985
13	2.54	0.0727663	2.886
Average of Slug Velocity SV (m/s)			3.00
Mixture flow velocity VM (m/s)			2.54
Standard deviation of SV (m/s)			0.146
% difference between SV and Vm (m/s)			18.04%

Table C- 7 Time delay and slug velocity calculation using flush ring waveguides at 1.02 V_{SL} and 2.02 V_{SG}

Burst signals Number	Mixture Velocity (m/s)	Time delay (s)	Slug velocity (m/s)
1	3.04	0.0566591	3.706
2	3.04	0.059703	3.517
3	3.04	0.0598441	3.509
4	3.04	0.0616208	3.408
5	3.04	0.0624912	3.360
6	3.04	0.0671384	3.128
7	3.04	0.0616968	3.404
8	3.04	0.06378	3.293
9	3.04	0.0639285	3.285
10	3.04	0.0627651	3.346
11	3.04	0.055765	3.766
12	3.04	0.0605979	3.465
13	3.04	0.0605394	3.469
Average of Slug Velocity SV (m/s)			3.44
Mixture flow velocity VM (m/s)			3.04
Standard deviation of SV (m/s)			0.171
% difference between SV and Vm (m/s)			13.00%

Table C- 8 Time delay and slug velocity calculation using flush ring waveguides at 1.02 V_{SL} and 2.5 V_{SG}

Burst signals Number	Mixture Velocity (m/s)	Time delay (s)	Slug velocity (m/s)
1	3.54	0.0527384	3.982
2	3.54	0.0515261	4.076
3	3.54	0.0519823	4.040
4	3.54	0.0535305	3.923
5	3.54	0.052804	3.977
6	3.54	0.0569343	3.688
7	3.54	0.0494315	4.248
8	3.54	0.0507274	4.140
9	3.54	0.051453	4.081
10	3.54	0.051412	4.085
11	3.54	0.0530325	3.960
12	3.54	0.0508281	4.132
13	3.54	0.0552768	3.799
Average of Slug Velocity SV (m/s)			4.01
Mixture flow velocity VM (m/s)			3.54
Standard deviation of SV (m/s)			0.148
% difference between SV and Vm (m/s)			13.28%

Table C- 9 Time delay and slug velocity calculation using flush ring waveguides at 1.52 V_{SL} and 1.02 V_{SG}

Burst signals Number	Mixture Velocity (m/s)	Time delay (s)	Slug velocity (m/s)
1	2.54	0.0741998	2.830
2	2.54	0.075092	2.797
3	2.54	0.0662751	3.169
4	2.54	0.0656303	3.200
5	2.54	0.0691719	3.036
6	2.54	0.0684453	3.068
7	2.54	0.0721316	2.911
8	2.54	0.0656723	3.198
9	2.54	0.0703787	2.984
10	2.54	0.0665845	3.154
11	2.54	0.0733434	2.863
12	2.54	0.0658726	3.188
13	2.54	0.0722178	2.908
Average of Slug Velocity SV (m/s)			3.02
Mixture flow velocity VM (m/s)			2.54
Standard deviation of SV (m/s)			0.150
% difference between SV and Vm (m/s)			19.03%

Table C- 10 Time delay and slug velocity calculation using flush ring waveguides at 1.52 V_{SL} and 1.52 V_{SG}

Burst signals Number	Mixture Velocity (m/s)	Time delay (s)	Slug velocity (m/s)
1	3.04	0.05561037	3.776
2	3.04	0.061312	3.425
3	3.04	0.0556254	3.775
4	3.04	0.0587273	3.576
5	3.04	0.0622379	3.374
6	3.04	0.0577745	3.635
7	3.04	0.0623698	3.367
8	3.04	0.0665597	3.155
9	3.04	0.0576825	3.641
10	3.04	0.0572344	3.669
11	3.04	0.0583325	3.600
12	3.04	0.0613278	3.424
13	3.04	0.0624721	3.362
Average of Slug Velocity SV (m/s)			3.52
Mixture flow velocity VM (m/s)			3.04
Standard deviation of SV (m/s)			0.185
% difference between SV and Vm (m/s)			15.84%

Table C- 11 Time delay and slug velocity calculation using flush ring waveguides at 1.52 V_{SL} and 2.02 V_{SG}

Burst signals Number	Mixture Velocity (m/s)	Time delay (s)	Slug velocity (m/s)
1	3.54	0.052114	4.030
2	3.54	0.0536274	3.916
3	3.54	0.0553276	3.796
4	3.54	0.0548355	3.830
5	3.54	0.0516377	4.067
6	3.54	0.0500951	4.192
7	3.54	0.0525395	3.997
8	3.54	0.055544	3.781
9	3.54	0.0558309	3.761
10	3.54	0.0528732	3.972
11	3.54	0.0524892	4.001
12	3.54	0.053045	3.959
13	3.54	0.051941	4.043
Average of Slug Velocity SV (m/s)			3.95
Mixture flow velocity VM (m/s)			3.54
Standard deviation of SV (m/s)			0.128
% difference between SV and Vm (m/s)			11.57%

Table C- 12 Time delay and slug velocity calculation using flush ring waveguides at 2.02 V_{SL} and 1.02 V_{SG}

Burst signals Number	Mixture Velocity (m/s)	Time delay (s)	Slug velocity (m/s)
1	3.04	0.0628119	3.343
2	3.04	0.0559354	3.754
3	3.04	0.060369	3.479
4	3.04	0.063663	3.299
5	3.04	0.0570575	3.680
6	3.04	0.0582938	3.602
7	3.04	0.0636918	3.297
8	3.04	0.0574248	3.657
9	3.04	0.0618451	3.396
10	3.04	0.0587552	3.574
11	3.04	0.0568072	3.697
12	3.04	0.0636469	3.299
13	3.04	0.0599378	3.504
Average of Slug Velocity SV (m/s)			3.51
Mixture flow velocity VM (m/s)			3.04
Standard deviation of SV (m/s)			0.167
% difference between SV and Vm (m/s)			15.34%

Table C- 13 Time delay and slug velocity calculation using flush ring waveguides at 2.02 V_{SL} and 1.52 V_{SG}

Burst signals Number	Mixture Velocity (m/s)	Time delay (s)	Slug velocity (m/s)
1	3.54	0.05559	3.778
2	3.54	0.05397	3.891
3	3.54	0.05563	3.775
4	3.54	0.05456	3.849
5	3.54	0.05071	4.141
6	3.54	0.05338	3.934
7	3.54	0.05050	4.159
8	3.54	0.05172	4.061
9	3.54	0.05029	4.175
10	3.54	0.05067	4.145
11	3.54	0.04931	4.259
12	3.54	0.05389	3.897
13	3.54	0.05574	3.768
Average of Slug Velocity SV (m/s)			3.99
Mixture flow velocity VM (m/s)			3.54
Standard deviation of SV (m/s)			0.175
% difference between SV and Vm (m/s)			12.63%

Table C- 14 Time delay and slug velocity calculation using flush ring waveguides at 2.02 V_{SL} and 2.02 V_{SG}

Burst signals Number	Mixture Velocity (m/s)	Time delay (s)	Slug velocity (m/s)
1	4.04	0.04617	4.549
2	4.04	0.04435	4.735
3	4.04	0.04523	4.643
4	4.04	0.04860	4.321
5	4.04	0.04628	4.537
6	4.04	0.04787	4.387
7	4.04	0.04797	4.378
8	4.04	0.04685	4.482
9	4.04	0.04721	4.449
10	4.04	0.04772	4.401
11	4.04	0.04797	4.378
12	4.04	0.04838	4.341
13	4.04	0.04800	4.375
Average of Slug Velocity SV (m/s)			4.46
Mixture flow velocity VM (m/s)			4.04
Standard deviation of SV (m/s)			0.125
% difference between SV and Vm (m/s)			10.39%

Table C- 15 Time delay and slug velocity calculation using flush ring waveguides at 2.02 V_{SL} and 2.52 V_{SG}

Burst signals Number	Mixture Velocity (m/s)	Time delay (s)	Slug velocity (m/s)
1	4.54	0.04384	4.791
2	4.54	0.04241	4.952
3	4.54	0.04236	4.957
4	4.54	0.04026	5.217
5	4.54	0.04352	4.826
6	4.54	0.03934	5.338
7	4.54	0.04248	4.944
8	4.54	0.04482	4.685
9	4.54	0.04107	5.114
10	4.54	0.04260	4.930
11	4.54	0.04299	4.885
12	4.54	0.04017	5.228
13	4.54	0.04061	5.171
Average of Slug Velocity SV (m/s)			5.00
Mixture flow velocity VM (m/s)			4.54
Standard deviation of SV (m/s)			0.195
% difference between SV and Vm (m/s)			10.19%

Appendix D

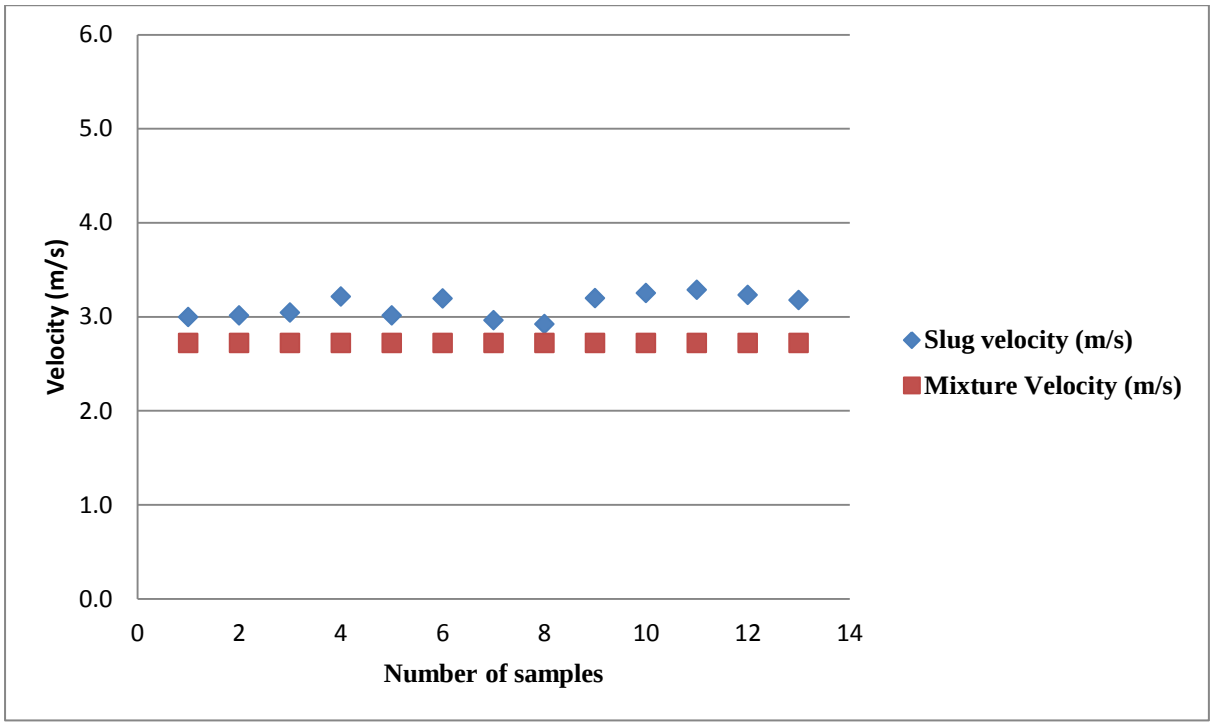

Figure D-1 Measured slug velocity with mix velocity 0.7 V_{SL} and 2.02 V_{SG}

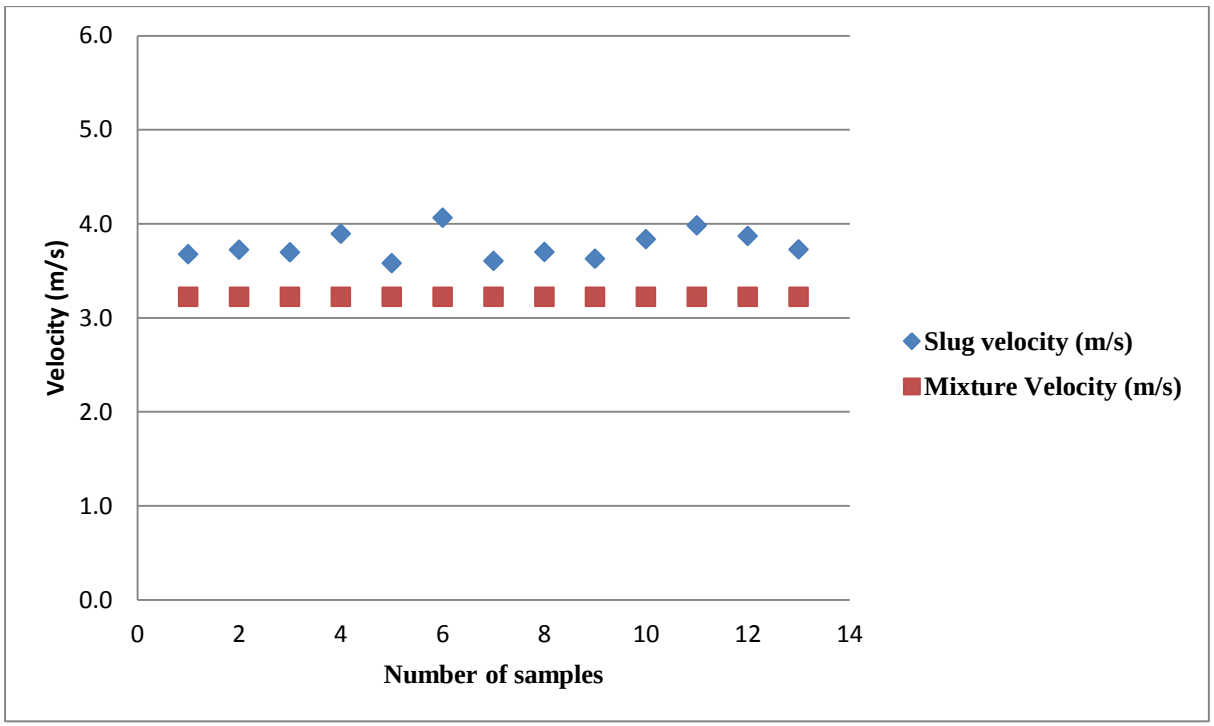

Figure D-2 Measured slug velocity with mix velocity 0.7 V_{SL} and 2.52 V_{SG}

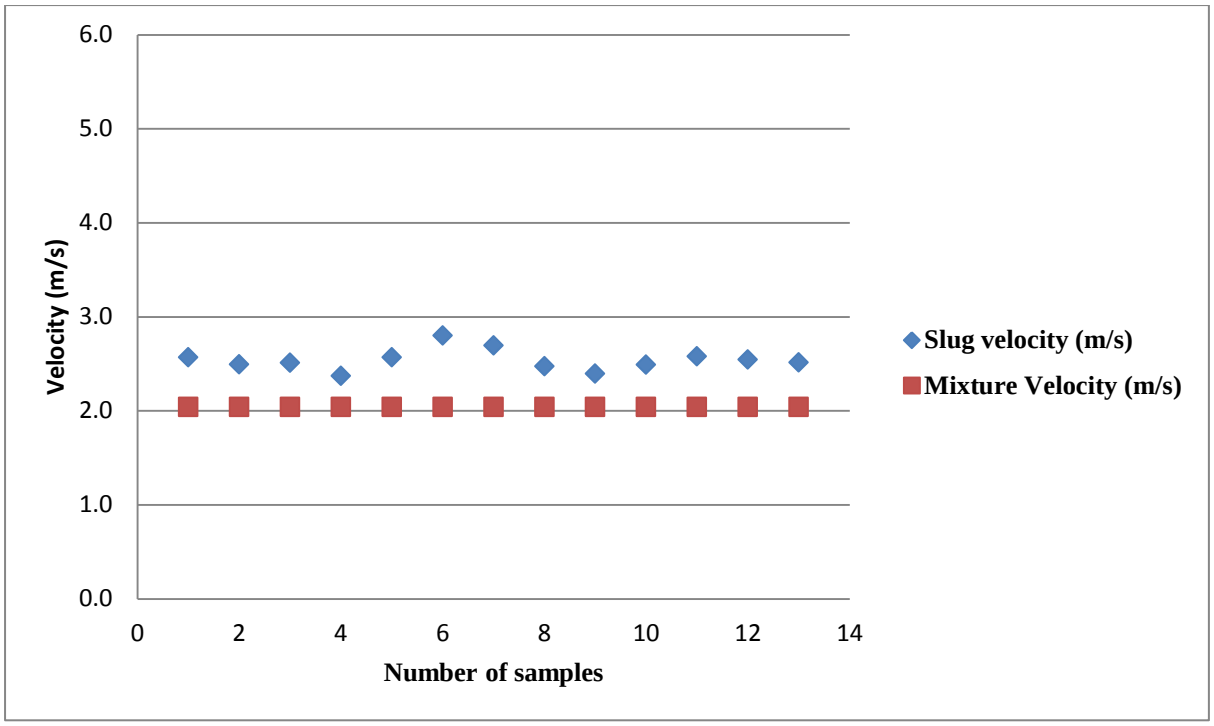

Figure D-3 Measured slug velocity with mix velocity 1.02 V_{SL} and 1.02 V_{SG}

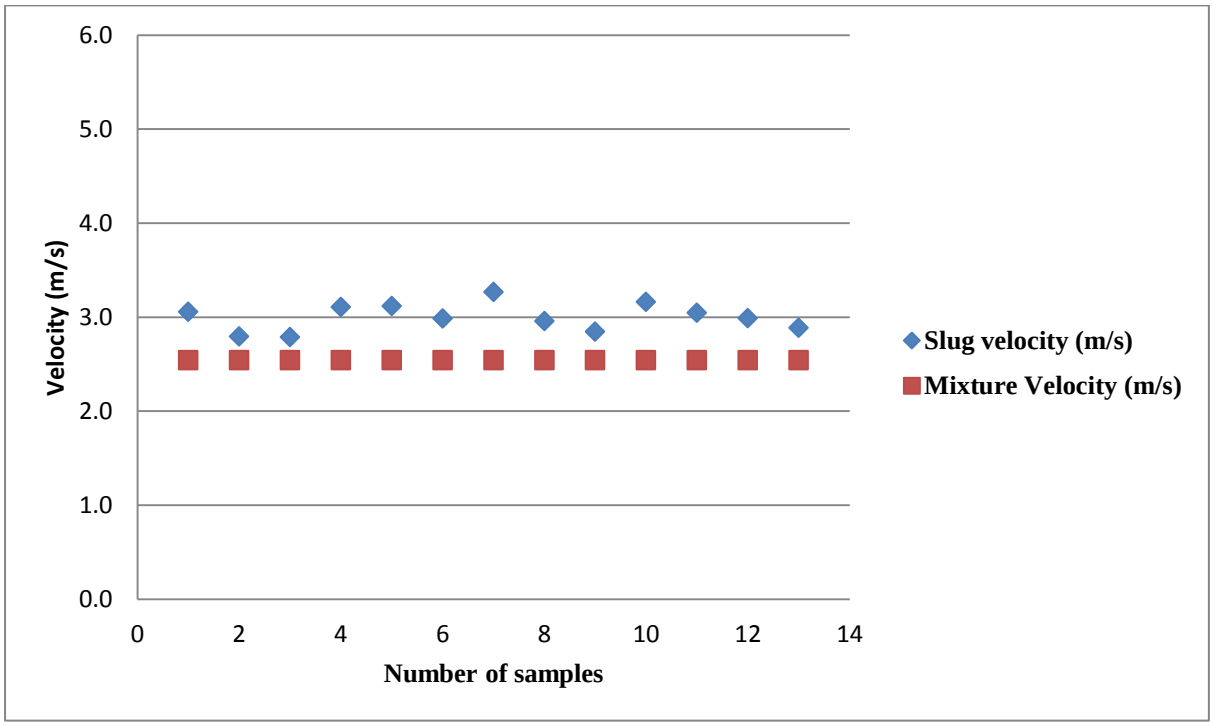

Figure D-4 Measured slug velocity with mix velocity 1.02 V_{SL} and 1.02 V_{SG}

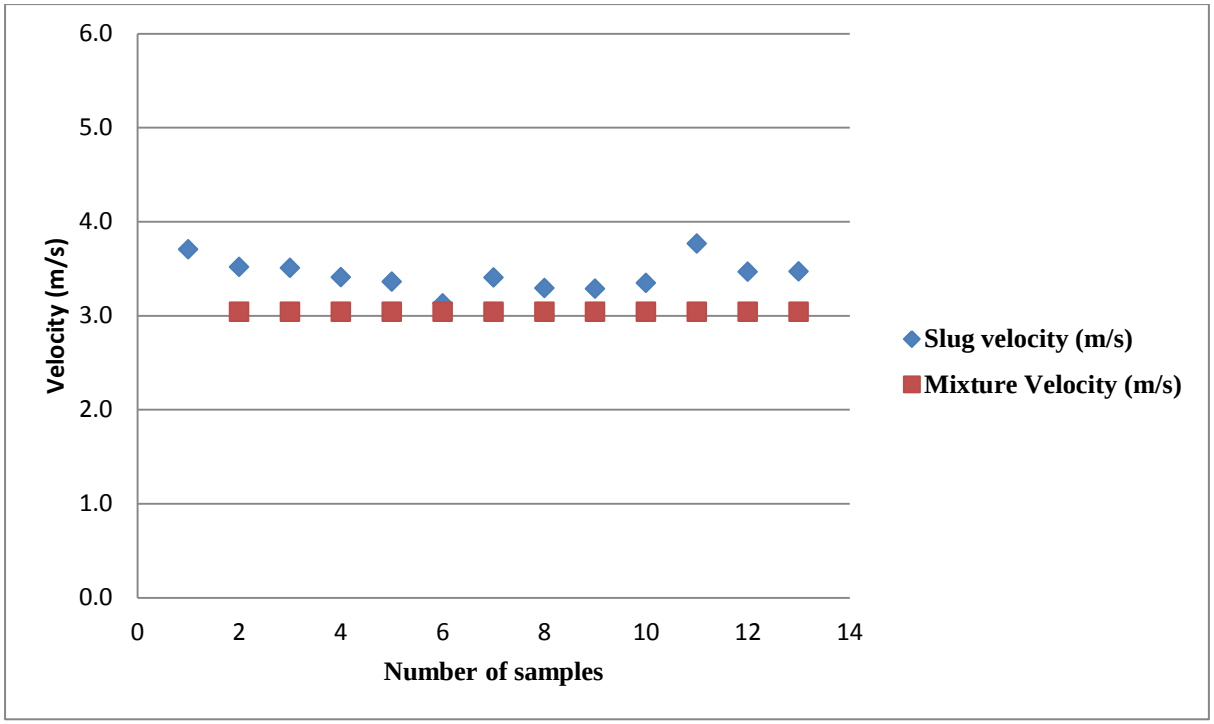

Figure D-5 Measured slug velocity with mix velocity 1.02 V_{SL} and 2.02 V_{SG}

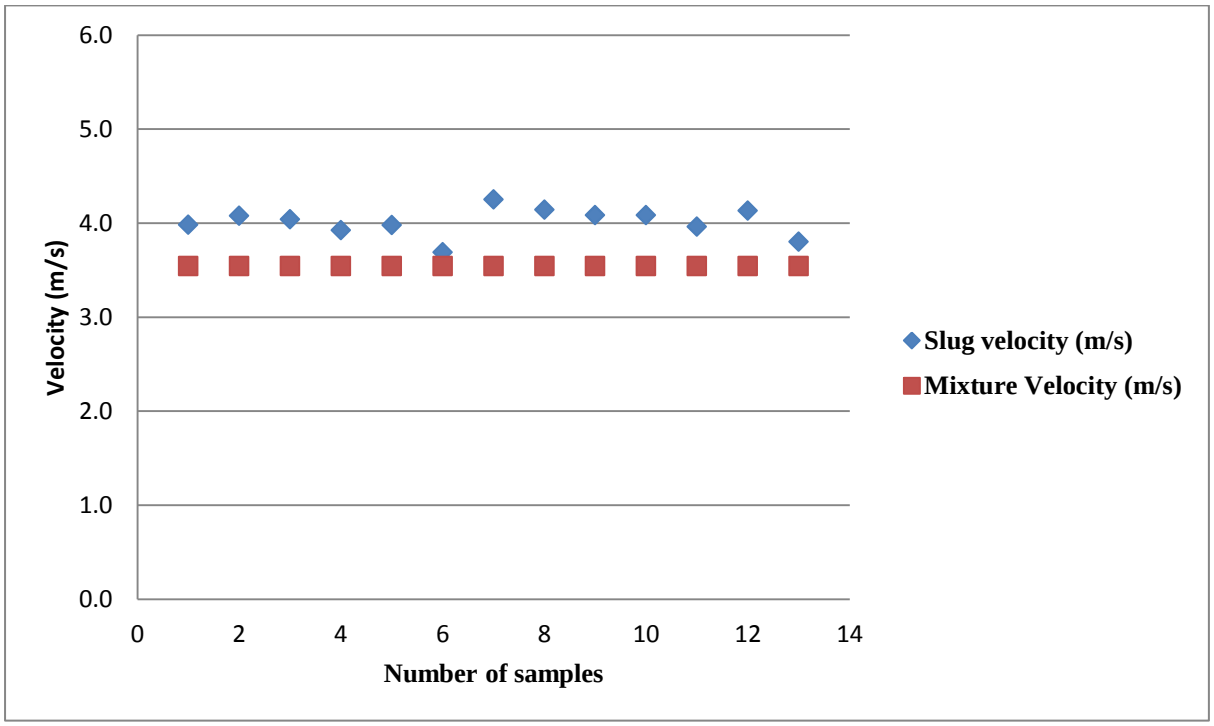

Figure D-6 Measured slug velocity with mix velocity 1.02 V_{SL} and 2.52V_{SG}

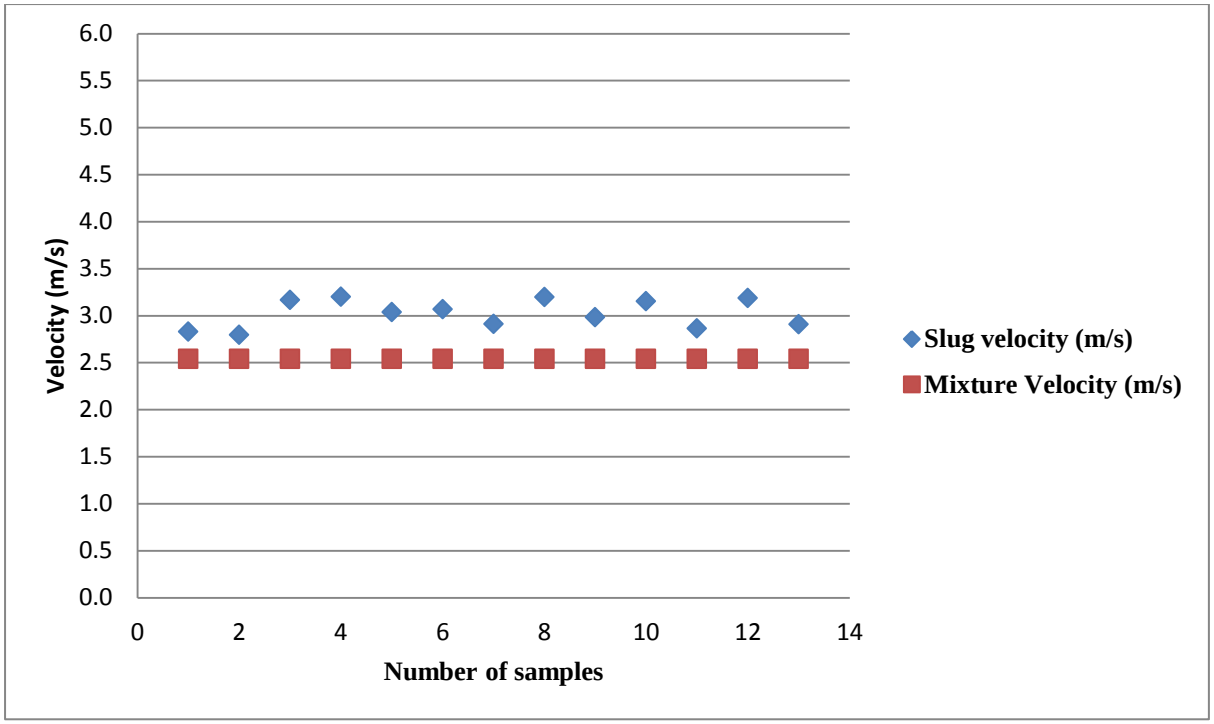

Figure D-7 Measured slug velocity with mix velocity 1.52 V_{SL} and 1.02V_{SG}

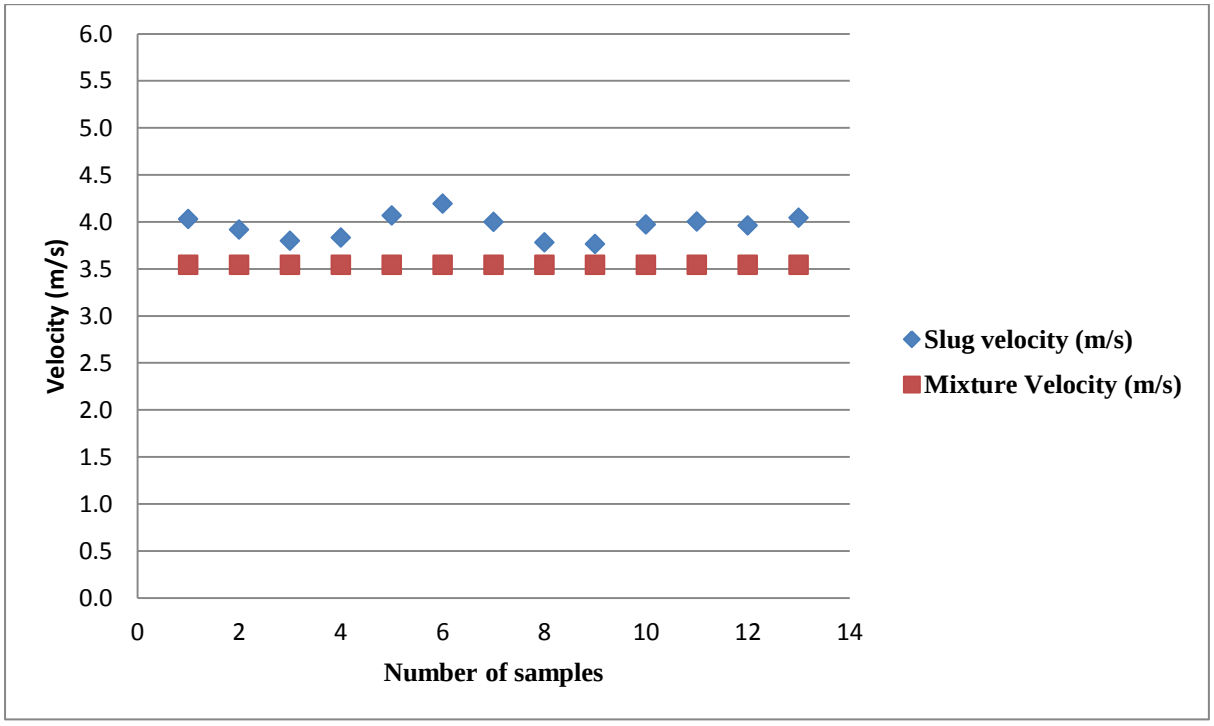

Figure D-8 Measured slug velocity with mix velocity 1.52 V_{SL} and 2.02V_{SG}

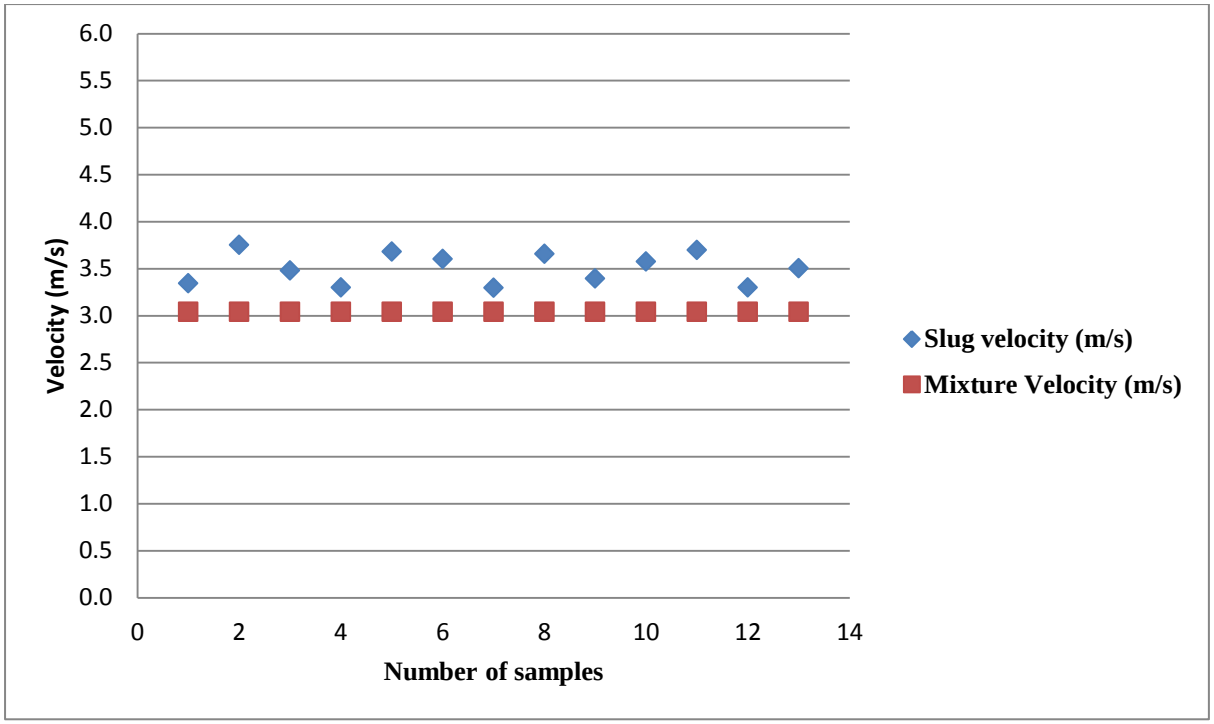

Figure D-9 Measured slug velocity with mix velocity 2.02 V_{SL} and 1.02V_{SG}

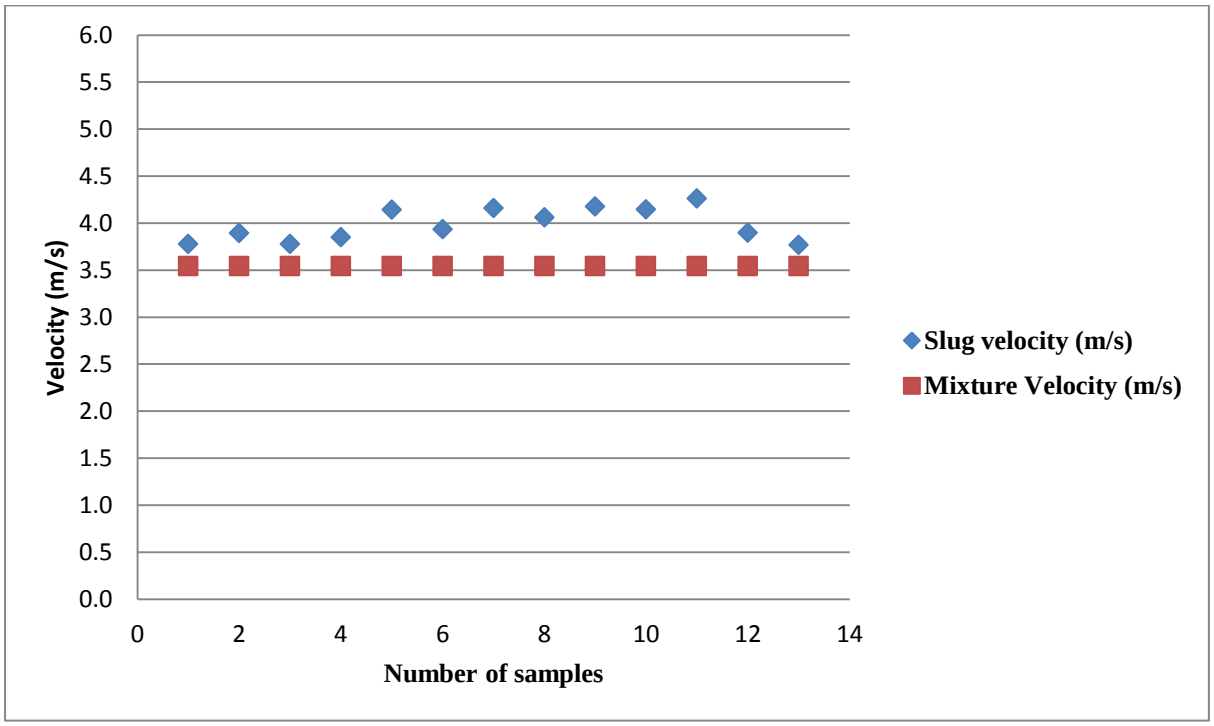

Figure D-10 Measured slug velocity with mix velocity 2.02 V_{SL} and 1.52V_{SG}

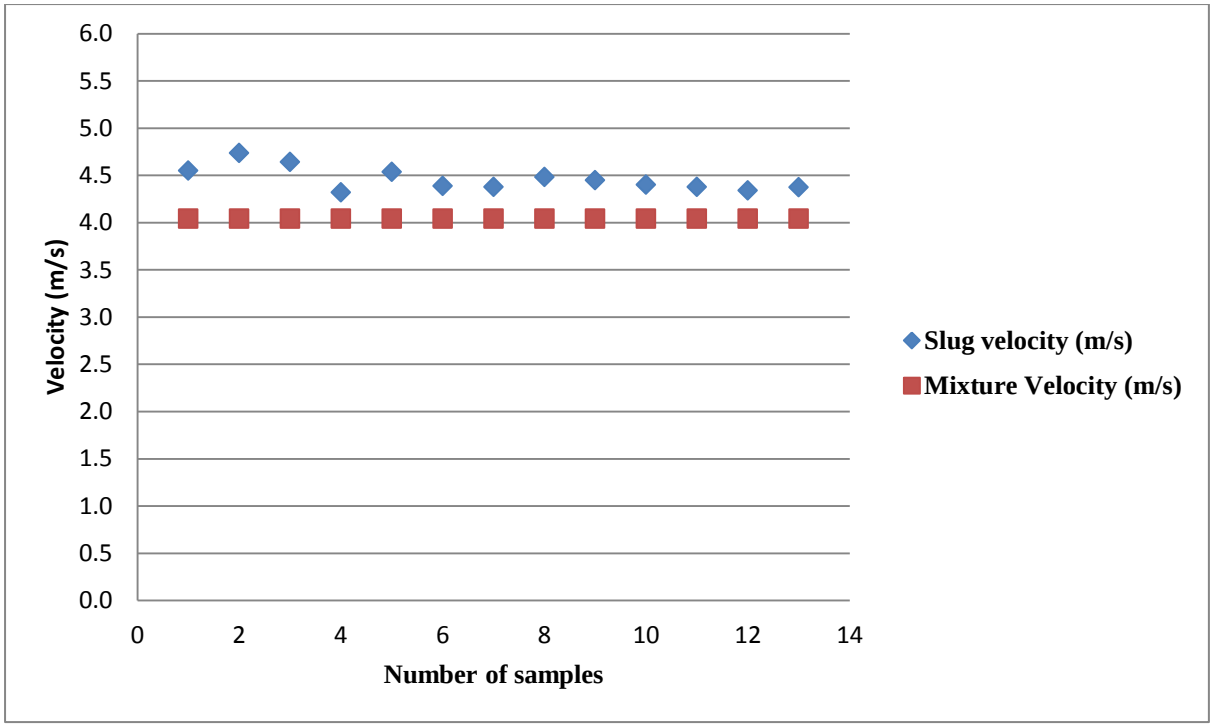

Figure D-11 Measured slug velocity with mix velocity 2.02 V_{SL} and 2.02V_{SG}

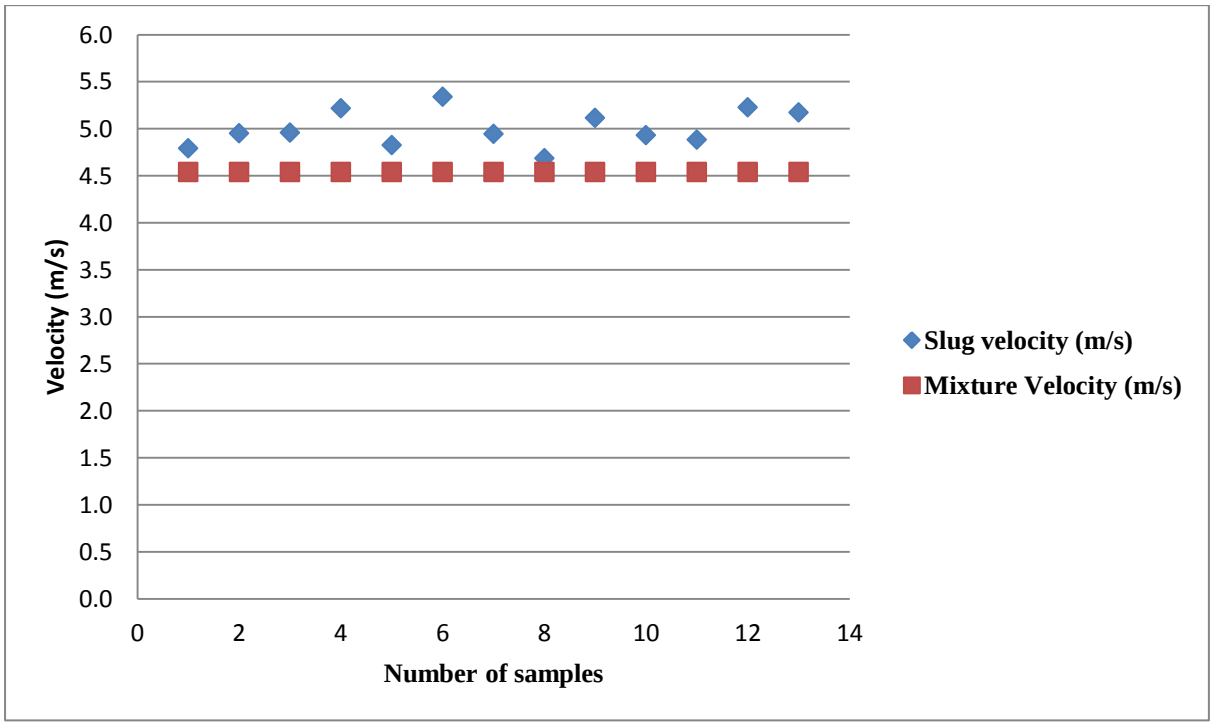

Figure D-12 Measured slug velocity with mix velocity 2.02 V_{SL} and 2.52V_{SG}